日中笹川医学奨学金制度(学位取得コース)中間報告書
研究者用

第44期　　　研究者番号：　G4405　　　作成日：2023年3月10日

氏名	陈 曹杰	CHEN CAOJIE	性別	M	生年月日　1984/01/23
所属機関(役職)	慶應義塾大学医学部(大学院生)				
研究先(指導教官)	慶應義塾大学医学部形成外科学教室(貴志 和生　教授)				
研究テーマ	YAPはEngrailed-1 / mTOR軸を調節して、創傷治癒におけるオートファジーを促進します YAP regulates the Engrailed-1/mTOR axis to promote autophagy in wound healing				
専攻種別	論文博士		□	課程博士	☑

1．研究概要(1)

Abstract

Goal: Wound repair dysfunction is a major worldwide public health problem. Autophagy has been reported to have a significant correlation with wound healing. Yes-associated protein (YAP) is closely related to wound healing, while the role of YAP in regulating autophagy during wound healing needs to be further probed.

Approach:Conduct research using comparable methods.

Materials and methods: A full-thickness excisional wounds (8 mm) in mice was created to construct in vivo wound model. HE staining was employed to examine formation of the epidermis and dermis at the wound. The mRNA and protein expressions were assessed using RT-qPCR, western blot and IHC. The viability, proliferation and migration of fibroblast were examined using MTT assay and wound healing assay.

Results: We found that the autophagy inhibitor (3-MA) accelerated wound closure in vivo. Loss-of-function experiments subsequently revealed that YAP knockdown led to accelerated wound closure in vivo and increased fibroblast cell proliferation and migration as well as reduced autophagy. In addition, our results revealed that YAP could positively regulate En1 expression in fibroblasts. En1 knockdown promoted the proliferation and migration of fibroblasts, meanwhile resulted in increased mTOR level and reduced autophagy.

Discussion: Skin injury is a common event after accidental trauma . Delayed wound healing has always been an important health problem worldwide, especially among diabetic patients and the elderly . Wound healing is a complicated process, the specific mechanism of wound healing has not been fully understood. In the current study, it was found that autophagy inhibition promoted wound closure in vivo. We subsequently investigated the regulatory mechanisms of autophagy during wound healing in vitro, our results revealed that YAP promote autophagy in wound healing by regulating the En1/mTOR axis, providing potential therapeutic target for wound healing dysfunction.

Autophagy refers to a catabolic process which removes unwanted components via lysosomal degradation pathways. The function of autophagy in tissue regeneration is intriguing. A previous study revealed that advanced glycation end-products resulted in refractory wounds through autophagy activation . In addition, it was observed that the autophagy inhibitor accelerated wound healing in normal mice or diabetic wounds . Herein, we also observed that 3-MA treatment could accelerate wound closure in vivo. However, studies on autophagy in wound healing also found that autophagy activation promotes wound healing . Autophagy is a dynamic process in wound healing. Thus, autophagy has a dual role in regulating wound healing and can determine different clinical outcomes depending on the tissue or cell in which it occurs. Although the current research on autophagy in skin wound healing has achieved some results, the dual role of autophagy requires further in-depth studies to confirm its potential clinical efficacy.

As widely described, YAP, as a transcriptional coactivator of the Hippo signaling, plays a critical role in skin wound repair . As proof, ectopic expression of activated YAP mutants or deregulation of upstream regulators of YAP localization resulted in an uncontrolled epidermal injury response . More importantly, it was also previously reported that verteporfin (YAP inhibitor) or YAP knockdown could promote wound regeneration with restoration of skin attachment, ultrastructure and mechanical strength . It's suggested that YAP is a risking factor affecting wound healing, while the function of YAP in regulating autophagy during wound healing is still unclear. Loss-of-function experiments revealed that YAP knockdown resulted in accelerated wound closure in vivo as well as reduced autophagy in wounds. Consistently, YAP silencing promoted the proliferation and migration of fibroblasts, whereas its knockdown inhibited autophagy. Therefore, we came to the conclusion that YAP knockdown accelerated wound healing in vitro and in vivo by suppressing autophagy. As previously described, YAP inhibition promoted wound regeneration by suppressing En1 activation , indicating that En1 might function as the target of YAP in regulating wound healing. En1-history-naive fibroblasts and present scarring abilities . Herein, we observed that En1 was remarkably upregulated in wound tissues of patients with skin defect. In addition, it was found that YAP could positively regulate En1 expression in fibroblasts. As expected, En1 knockdown promoted the proliferation and migration of fibroblasts. mTOR, a serine/threonine kinase, is a master regulator of autophagy . mTOR activation results in inhibition of autophagy . Our results revealed that En1 knockdown led to increased mTOR level and reduced autophagy in fibroblasts. Collectively, YAP knockdown increased mTOR level by inhibiting En1 expression, thereby repressing autophagy during wound healing.

Taken together, YAP knockdown repressed autophagy in wound healing by regulating the En1/mTOR axis. Our research provided a hopeful strategy for wound repair dysfunction.

References：
1. Singer, A.J. and R.A. Clark, Cutaneous wound healing. N Engl J Med, 1999. 341(10): p. 738-46.
2. Eming, S.A., P. Martin, and M. Tomic-Canic, Wound repair and regeneration: mechanisms, signaling, and translation. Sci Transl Med, 2014. 6(265): p. 265sr6.
3. Reed, B.R. and R.A. Clark, Cutaneous tissue repair: practical implications of current knowledge. II. J Am Acad Dermatol, 1985. 13(6): p. 919-41.
4. Brem, H. and M. Tomic-Canic, Cellular and molecular basis of wound healing in diabetes. J Clin Invest, 2007. 117(5): p. 1219-22.
5. Klionsky, D.J., Autophagy: from phenomenology to molecular understanding in less than a decade. Nat Rev Mol Cell Biol, 2007. 8(11): p. 931-7.
6. Ren, H., et al., Autophagy and skin wound healing. Burns Trauma, 2022. 10: p. tkac003.
7. Gao, Y., et al., Autophagy inhibition facilitates wound closure partially dependent on the YAP/IL-33 signaling in a mouse model of skin wound healing. Faseb j, 2021. 35(10): p. e21920.
8. Dey, A., X. Varelas, and K.L. Guan, Targeting the Hippo pathway in cancer, fibrosis, wound healing and regenerative medicine. Nat Rev Drug Discov, 2020. 19(7): p. 480-494.
9. Wei, F., et al., Plasma endothelial cells-derived extracellular vesicles promote wound healing in diabetes through YAP and the PI3K/Akt/mTOR pathway. Aging (Albany NY), 2020. 12(12): p. 12002-12018.
10. Mascharak, S., et al., Preventing Engrailed-1 activation in fibroblasts yields wound regeneration without scarring. Science, 2021. 372(6540).
11. Izquierdo, C., et al., Long-term impact of temozolomide on 1p/19q-codeleted low-grade glioma growth kinetics. J Neurooncol, 2018. 136(3): p. 533-539.
12. Györfi, A.H., et al., Engrailed 1 coordinates cytoskeletal reorganization to induce myofibroblast differentiation. J Exp Med, 2021. 218(9).
13. Huo, J.F. and X.B. Chen, Long noncoding RNA growth arrest-specific 5 facilitates glioma cell sensitivity to cisplatin by suppressing excessive autophagy in an mTOR-dependent manner. J Cell Biochem, 2019. 120(4): p. 6127-6136.
14. Nordströma, U., et al., Progressive nigrostriatal terminal dysfunction and degeneration in the engrailed1 heterozygous mouse model of Parkinson's disease. Neurobiol Dis, 2015. 73: p. 70-82.
15. Qiang, L., et al., Epidermal SIRT1 regulates inflammation, cell migration, and wound healing. Sci Rep, 2017. 7(1): p. 14110.
16. Spiekstra, S.W., et al., Wound-healing factors secreted by epidermal keratinocytes and dermal fibroblasts in skin substitutes. Wound Repair Regen, 2007. 15(5): p. 708-17.
17. van Zanten, M.C., et al., The Lymphatic Response to Injury with Soft-Tissue Reconstruction in High-Energy Open Tibial Fractures of the Lower Extremity. Plast Reconstr Surg, 2017. 139(2): p. 483-491.
18. Ban, E., et al., Accelerated wound healing in diabetic mice by miRNA-497 and its anti-inflammatory activity. Biomed Pharmacother, 2020. 121: p. 109613.
19. Guo, Y., et al., AGEs Induced Autophagy Impairs Cutaneous Wound Healing via Stimulating Macrophage Polarization to M1 in Diabetes. Sci Rep, 2016. 6: p. 36416.
20. Wang, F., et al., Bafilomycin A1 Accelerates Chronic Refractory Wound Healing in db/db Mice. Biomed Res Int, 2020. 2020: p. 6265701.
21. Lawrence, J. and R. Nho, The Role of the Mammalian Target of Rapamycin (mTOR) in Pulmonary Fibrosis. Int J Mol Sci, 2018. 19(3).
22. Qiang, L., et al., Keratinocyte autophagy enables the activation of keratinocytes and fibroblastsand facilitates wound healing. Autophagy, 2021. 17(9): p. 2128-2143.
23. Schlegelmilch, K., et al., Yap1 acts downstream of α-catenin to control epidermal proliferation. Cell, 2011. 144(5): p. 782-95.
24. Silvis, M.R., et al., α-catenin is a tumor suppressor that controls cell accumulation by regulating the localization and activity of the transcriptional coactivator Yap1. Sci Signal, 2011. 4(174): p. ra33.
25. Jiang, D., et al., Two succeeding fibroblastic lineages drive dermal development and the transition from regeneration to scarring. Nat Cell Biol, 2018. 20(4): p. 422-431.
26. Kim, Y.C. and K.L. Guan, mTOR: a pharmacologic target for autophagy regulation. J Clin Invest, 2015. 125(1): p. 25-32.

2．執筆論文　Publication of thesis　※記載した論文を添付してください。Attach all of the papers listed below.

<table>
<tr>
<td>論文名 1
Title</td>
<td colspan="8">Single-Cell RNA-seq Analysis Reveals Cellular Functional Heterogeneity in Dermis Between Fibrotic and Regenerative Wound Healing Fates</td>
</tr>
<tr>
<td rowspan="2">掲載誌名
Published journal</td>
<td colspan="8">Frontiers in immunology</td>
</tr>
<tr>
<td>2022 年　5　月</td>
<td colspan="2">2022　　巻（号）</td>
<td colspan="2">頁　〜　　　頁</td>
<td>言語
Language</td>
<td colspan="2">English</td>
</tr>
<tr>
<td>第1著者名
First author</td>
<td colspan="2">Caojie Chen</td>
<td>第2著者名
Second author</td>
<td colspan="2">Hiroki Kajita</td>
<td>第3著者名
Third author</td>
<td colspan="2">Kento Takaya</td>
</tr>
<tr>
<td>その他著者名
Other authors</td>
<td colspan="8">Noriko Aramaki-Hattori , Shigeki Sakai , Toru Asou , Kazuo Kishi</td>
</tr>
<tr>
<td>論文名 2
Title</td>
<td colspan="8">Screening of Autophagy-Related Prognostic Genes in Metastatic Skin Melanoma</td>
</tr>
<tr>
<td rowspan="2">掲載誌名
Published journal</td>
<td colspan="8">Disease markers</td>
</tr>
<tr>
<td>2022 年　1　月</td>
<td colspan="2">2022　　巻（号）</td>
<td colspan="2">頁　〜　　　頁</td>
<td>言語
Language</td>
<td colspan="2">English</td>
</tr>
<tr>
<td>第1著者名
First author</td>
<td colspan="2">Caojie Chen</td>
<td>第2著者名
Second author</td>
<td colspan="2">Hiroki Kajita</td>
<td>第3著者名
Third author</td>
<td colspan="2">Noriko Aramaki-Hattori</td>
</tr>
<tr>
<td>その他著者名
Other authors</td>
<td colspan="8">Shigeki Sakai and Kazuo Kishi</td>
</tr>
<tr>
<td>論文名 3
Title</td>
<td colspan="8"></td>
</tr>
<tr>
<td rowspan="2">掲載誌名
Published journal</td>
<td colspan="8"></td>
</tr>
<tr>
<td>年　　　月</td>
<td colspan="2">巻（号）</td>
<td colspan="2">頁　〜　　　頁</td>
<td>言語
Language</td>
<td colspan="2"></td>
</tr>
<tr>
<td>第1著者名
First author</td>
<td colspan="2"></td>
<td>第2著者名
Second author</td>
<td colspan="2"></td>
<td>第3著者名
Third author</td>
<td colspan="2"></td>
</tr>
<tr>
<td>その他著者名
Other authors</td>
<td colspan="8"></td>
</tr>
<tr>
<td>論文名 4
Title</td>
<td colspan="8"></td>
</tr>
<tr>
<td rowspan="2">掲載誌名
Published journal</td>
<td colspan="8"></td>
</tr>
<tr>
<td>年　　　月</td>
<td colspan="2">巻（号）</td>
<td colspan="2">頁　〜　　　頁</td>
<td>言語
Language</td>
<td colspan="2"></td>
</tr>
<tr>
<td>第1著者名
First author</td>
<td colspan="2"></td>
<td>第2著者名
Second author</td>
<td colspan="2"></td>
<td>第3著者名
Third author</td>
<td colspan="2"></td>
</tr>
<tr>
<td>その他著者名
Other authors</td>
<td colspan="8"></td>
</tr>
<tr>
<td>論文名 5
Title</td>
<td colspan="8"></td>
</tr>
<tr>
<td rowspan="2">掲載誌名
Published journal</td>
<td colspan="8"></td>
</tr>
<tr>
<td>年　　　月</td>
<td colspan="2">巻（号）</td>
<td colspan="2">頁　〜　　　頁</td>
<td>言語
Language</td>
<td colspan="2"></td>
</tr>
<tr>
<td>第1著者名
First author</td>
<td colspan="2"></td>
<td>第2著者名
Second author</td>
<td colspan="2"></td>
<td>第3著者名
Third author</td>
<td colspan="2"></td>
</tr>
<tr>
<td>その他著者名
Other authors</td>
<td colspan="8"></td>
</tr>
</table>

3．学会発表　Conference presentation　※筆頭演者として総会・国際学会を含む主な学会で発表したものを記載してください

※Describe your presentation as the principal presenter in major academic meetings including general meetings or international meetin

学会名 Conference	第30回日本形成外科学会基礎学術集会
演　題 Topic	オートファジーと創傷治癒の関係
開催日 date	2021　年　10　月　7　日　　開催地 venue　東京
形式　method	☑　口頭発表 Oral　□　ポスター発表 Poster　言語 Language　☑　日本語　□　英語　□　中国語
共同演者名 Co-presenter	
学会名 Conference	第50回日本創傷治癒学会
演　題 Topic	オートファジーと創傷治癒の関係
開催日 date	2020　年　11　月　9　日　　開催地 venue　web開催
形式　method	☑　口頭発表 Oral　□　ポスター発表 Poster　言語 Language　□　日本語　☑　英語　□　中国語
共同演者名 Co-presenter	
学会名 Conference	
演　題 Topic	
開催日 date	年　　月　　日　　開催地 venue
形式　method	□　口頭発表 Oral　□　ポスター発表 Poster　言語 Language　□　日本語　☑　英語　□　中国語
共同演者名 Co-presenter	
学会名 Conference	
演　題 Topic	
開催日 date	2021　年　10　月　7　日　　開催地 venue　東京
形式　method	□　口頭発表 Oral　□　ポスター発表 Poster　言語 Language　□　日本語　□　英語　□　中国語
共同演者名 Co-presenter	

4．受賞（研究業績）　Award (Research achievement)

名　称 Award name				
	国名 Country		受賞年 Year of award	年　　月
名　称 Award name				
	国名 Country		受賞年 Year of award	年　　月

5．本研究テーマに関わる他の研究助成金受給 Other research grants concerned with your resarch theme

受給実績 Receipt record	□ 有　　■ 無			
助成機関名称 Funding agency				
助成金名称 Grant name				
受給期間 Supported period	年　　　　月 ～		年　　　　月	
受給額 Amount received	円			
受給実績 Receipt record	□ 有　　■ 無			
助成機関名称 Funding agency				
助成金名称 Grant name				
受給期間 Supported period	年　　　　月 ～		年　　　　月	
受給額 Amount received	円			

6．他の奨学金受給 Another awarded scholarship

受給実績 Receipt record	□ 有　　■ 無			
助成機関名称 Funding agency				
奨学金名称 Scholarship name				
受給期間 Supported period	年　　　　月 ～		年　　　　月	
受給額 Amount received	円			

7．研究活動に関する報道発表 Press release concerned with your research activities

※記載した記事を添付してください。Attach a copy of the article described below

報道発表 Press release	□ 有　　■ 無	発表年月日 Date of release	
発表機関 Released medium			
発表形式 Release method	・新聞　・雑誌　・Web site　・記者発表　・その他（　　　　　　　　　　　）		
発表タイトル Released title			

8．本研究テーマに関する特許出願予定 Patent application concerned with your research theme

出願予定 Scheduled	□ 有　　■ 無	出願国 Application	
出願内容（概要） Application contents			

9．その他 Others

指導責任者（記名）　貴志和生

Check for updates

Single-Cell RNA-seq Analysis Reveals Cellular Functional Heterogeneity in Dermis Between Fibrotic and Regenerative Wound Healing Fates

Cao-Jie Chen[1], Hiroki Kajita[1], Kento Takaya[1], Noriko Aramaki-Hattori[1], Shigeki Sakai[1], Toru Asou[2]* and Kazuo Kishi[1]*

[1] Department of Plastic and Reconstructive Surgery, Keio University School of Medicine, Tokyo, Japan, [2] Department of Plastic Surgery, Tokyo Cosmetic Surgery Clinic, Tokyo, Japan

Background: Fibrotic scars are common in both human and mouse skin wounds. However, wound-induced hair neogenesis in the murine wounding models often results in regenerative repair response. Herein, we aimed to uncover cellular functional heterogeneity in dermis between fibrotic and regenerative wound healing fates.

Methods: The expression matrix of single-cell RNA sequencing (scRNA-seq) data of fibrotic and regenerative wound dermal cells was filtered, normalized, and scaled; underwent principal components analysis; and further analyzed by Uniform Manifold Approximation and Projection (UMAP) for dimension reduction with the Seurat package. Cell types were annotated, and cell–cell communications were analyzed. The core cell population myofibroblast was identified and the biological functions of ligand and receptor genes between myofibroblast and macrophage were evaluated. Specific genes between fibrotic and regenerative myofibroblast and macrophage were identified. Temporal dynamics of myofibroblast and macrophage were reconstructed with the Monocle tool.

Results: Across dermal cells, there were six cell types, namely, EN1-negative myofibroblasts, EN1-positive myofibroblasts, hematopoietic cells, macrophages, pericytes, and endothelial cells. Ligand and receptor genes between myofibroblasts and macrophages mainly modulated cell proliferation and migration, tube development, and the TGF-β pathway. Specific genes that were differentially expressed in fibrotic compared to regenerative myofibroblasts or macrophages were separately identified. Specific genes between fibrotic and regenerative myofibroblasts were involved in the mRNA metabolic process and organelle organization. Specific genes between fibrotic and regenerative macrophages participated in regulating immunity and phagocytosis. We then observed the underlying evolution of myofibroblasts or macrophages.

Conclusion: Collectively, our findings reveal that myofibroblasts and macrophages may alter the skin wound healing fate through modulating critical signaling pathways.

Keywords: skin wound healing, fibrosis, regeneration, myofibroblast, macrophage, single-cell RNA sequencing

INTRODUCTION

The skin is the organ with the largest surface area in the human body that provides an efficient protective barrier against mechanical injury, microbial pathogens, and trauma (1). The skin's immune system is divided into two structural compartments: epidermis and dermis, both of which contain a plethora of immunocompetent cell types (2). The epidermis is home to the main skin-resident immune cells, Langerhans cells, and melanocytes. Meanwhile, immune-specialized cells like dendritic cells, macrophages, and T cells reside in the dermis (3). The communications within immune populations and the skin environment are critical to the effectiveness of the skin immune system (4). Wound healing is a complex process in the human body, where numerous cell populations with different functions are involved in the stages of hemostasis, inflammatory response, growth, re-epithelialization, and remodeling (5). It is essential to repair the skin after damage (6). Skin wound healing involves three primary phases: inflammation, re-epithelialization, and tissue remodeling (7). Nevertheless, effective therapeutic strategies of accelerating healing and decreasing scarring remain lacking. Single-cell RNA sequencing (scRNA-seq) technology has emerged as an indispensable tool for elucidating cellular phenotype and functional heterogeneity (8). Deciphering the role of each cell type and interactions within cells is of importance to understand the mechanism of normal wound closure (9). Alterations in the microenvironment may influence cellular recruitment or activation, resulting in damaged states of wound healing. ScRNA-seq can be applied for deciphering the cellular changes in chronic wounds and hypertrophic scarring, thereby promoting the development of more effective therapeutic solutions for healing wounds (10). Moreover, in-depth understanding of the differences between fibrotic and regenerative wound healing fates is a prerequisite for developing more effective therapeutic interventions (2). Here, the purpose of this study was to reveal cellular functional heterogeneity in the dermis between fibrotic and regenerative wound healing fates.

MATERIALS AND METHODS

Acquisition of scRNA-seq Profiles

10× genomics scRNA-seq data of regenerative [GSM4213633; large full-thickness excision (1 cm^2) allows *de novo* follicle regeneration] and fibrotic (GSM4213632; large wounds lead to hairless scars) wound-induced hair neogenesis (WIHN) wounds of adult 6- or 7-week-old C57Bl/6j mice were curated from the Gene Expression Omnibus (GEO) repository (https://www.ncbi.nlm.nih.gov/gds/). The accession number was GSE141814 (11). Regenerative wounds were defined as hair neogenesis, decreased contraction, decreased Wnt and TGF-β signaling activity, and decreased collagen production, while fibrotic wounds were defined as decreased hair neogenesis, increased contraction, increased Wnt and TGF-β signaling activity, and increased collagen production. This dataset was based on the platform of GPL21103 Illumina HiSeq 4000 (*Mus musculus*).

Quality Control

The DropletUtils package (v 3.13) was adopted to read unique molecular identifiers (UMI) count matrix, identify cells from empty droplets, remove barcode-swapped pseudo-cells, and downsample the count matrix (12). The calculateQCMetrics function of the Scater package was used for counting the expression of genes in cells (13). Cells with proportions of mitochondrial genes ≤ 10% and ribosomal genes ≥ 10% were determined for further analysis.

Data Preprocessing and Principal Component Analysis

The expression matrix was normalized with the NormalizeData function of the Seurat package (14). The top 2,000 highly variable genes were screened by the FindVariableFeatures function. Then, expression data were linearly scaled utilizing the ScaleData function. Finally, principal component analysis (PCA) was performed with the RunPCA function based on the 2,000 genes.

Cell Cluster and Annotation

The principal components with large standard deviations were selected. Then, cell clustering analysis was performed using the FindNeighbors and FindClusters function of the Seurat package. With the RunUMAP function, Uniform Manifold Approximation and Projection (UMAP) was carried out for dimension reduction. Cell types were annotated on the basis of the known marker genes.

Identification of Novel Marker Genes

To calculate the differentially expressed genes between each cluster and all other cells, the FindAllMarkers function of the Seurat package was used and novel marker genes were identified according to the following criteria: |log fold change (FC)| ≥ 0.1, the minimum expression ratio of cell population = 0.25, and *p*-value ≤ 0.05.

Ligand–Receptor Network Analysis

Based on the ligand–receptor pairs from the previous literature (15), the relationship pairs of receptors and ligands were analyzed based on the marker genes of various cells. Then, a cell–cell communication network was conducted and visualized with the Cytoscape software (16). The core cell population was identified according to the largest number of receptor–ligand pairs in the network. Moreover, the receptor and ligand genes were extracted.

Function Enrichment Analysis

Function enrichment analysis of the indicated genes was carried out utilizing the clusterProfiler package, including Gene Ontology (GO) and Kyoto Encyclopedia of Genes and Genomes (KEGG) pathway analysis (17). GO categories contain biological process, cellular component, and molecular function. Terms with *p* < 0.05 were considered significantly enriched.

Protein–Protein Interaction Analysis

The Search Tool for the Retrieval of Interacting Genes (STRING) database (version 11.0; https://string-db.org/) was utilized for

exploring the functional interactions between marker gene-encoded proteins (18). Then, PPI networks were constructed and the top 20 hub genes were identified.

Pseudotime Analysis

Pseudotime analysis was carried out with the Monocle 3 tool (19). Firstly, genes that were expressed in at least 5% of the cells were selected. Then, the reduceDimension function was utilized to perform dimensionality reduction analysis, followed by cell cluster with the clusterCells function. Afterwards, the differentialGeneTest function was adopted to determine candidate genes with differences between the clusters with $p < 0.05$. The dimensionality reduction analysis of the cells was carried out using the DDRTree approach and the reduceDimension function based on the candidate genes. Through the orderCells function, the cells along the quasi-chronological trajectory were sorted and visualized.

Gene Set Variation Analysis

The single-sample gene set enrichment analysis (ssGSEA) function of the Gene Set Variation Analysis (GSVA) package was utilized for comparisons of the differences in GO and KEGG terms between groups (20).

Isolation and Culture of Fibroblasts

C57BL/6 male mice (8–10 weeks old; Sankyo) were used for fibroblast isolation. Briefly, mice were sacrificed by cervical dislocation. The trunk skin was separated in the ultra-clean bench, immersed in 75% ethanol for disinfection, and then cut into small pieces. Blood was removed by rinsing with PBS buffer and transferred evenly to cell culture dishes. DMEM complete medium (Wako) was added to submerge the tissue block that was placed in a constant temperature incubator to fully cultivate. After 24 h, DMEM complete medium was added, which was replaced every 3 days. The mouse skin fibroblasts were purified by the differential adhesion method and were used for subsequent experiments. Our study was approved by the Animal Ethics Committee of Keio University School of Medicine [12090(5)].

Transfection

Using the TransIT-TKO Transfection Reagent (Mirus), siRNA-Engrailed-1 (horizon) and siRNA-control were transfected into fibroblasts in a constant-temperature incubator. Forty-eight hours later, the knockdown effect of siRNA was confirmed by real-time quantitative polymerase-chain reaction (RT-qPCR).

RT-qPCR

Total RNA was extracted from fibroblasts using the Isogen reagent (Nippon Gene) following the manufacturer's instructions. cDNA synthesis was achieved based on the cDNA Synthesis System (Bio-Rad). RT-qPCR was carried out utilizing SYBR Qpcr Mix (Toyobo) on a 7500 Real-Time PCR system (Applied Biosystems). The primer sequences were as follows: EN1, 5'-ACACAACCCTGCGATCC TACT-3'(forward) and 5'-GGACGGTCCGAATAGCGTG-3' (reverse); ACTB, 5'-GGC TGTATTCCCCTCCATCG-3'(forward) and 5'-CCAGTTGGTAACAATGCCATGT-3' (reverse). The relative expressions were calculated with the $2^{-\Delta\Delta Ct}$ method.

Wound Healing Assay

Fibroblasts were plated onto a 6-well plate (about 3×10^5 cells/well). When the confluence reached 100%, the fibroblast monolayer was scratched with a 1000-µl pipette tip. Additionally, detached fibroblasts were removed with serum-free medium. At 0 h and 24 h, the wounded area was photographed.

Statistical Analysis

All statistical analysis was performed using the R language (version 3.6.1) and R Bioconductor packages. $p < 0.05$ indicated statistical significance.

RESULTS

## Quality Control of scRNA-seq Data of Fibrotic and Regenerative Wound Dermal Cells

Herein, we collected scRNA data of dermal cells from large skin wounds on day 18 with two distinct healing fates (fibrosis: GSM4213632 or regeneration: GSM4213633) from the GSE141814 dataset. Before analysis, we presented quality control of scRNA data. Barcode rank plots separately depicted the distribution of barcodes in total UMI count for fibrotic and regenerative wound dermal cells (**Supplementary Figures 1A, B**). Knee and inflection points in the barcode rank plots indicated the transition of the total UMI count distribution, which reflected the difference between empty droplets and cell droplets. After filtrating empty droplets, we counted the expression of genes in each cell (**Supplementary Figures 1C, D**). Afterwards, we filtrated out cells with proportions of mitochondrial genes > 10% and ribosomal genes < 10% (**Supplementary Figures 1E, F**).

Cell Cluster of Fibrotic and Regenerative Wound Dermal Cells

After normalizing scRNA data, we screened the top 2,000 highly variable genes across fibrotic and regenerative wound dermal cells (**Figure 1A**). Then, scRNA data were linearly scaled and analyzed by dimensionality reduction with PCA. Here, we screened the top two principal components for subsequent analysis (**Figure 1B**). PCA results uncovered the prominent difference between fibrotic and regenerative wound dermal cells (**Figure 1C**). According to the elbow point, we identified the optimal principal components as 8 (**Figure 1D**). Heatmaps depicted the top 20 marker genes in each principal component (**Figure 1E**). With the UMAP method, dermal cells were clustered into 15 clusters (**Figure 1F**). The top ten marker genes of each cell cluster are presented in **Figure 1G**.

Identification of Cell Types and Their Marker Genes Across Fibrotic and Regenerative Wound Dermal Cells

This study attempted to identify cell types across fibrotic and regenerative wound dermal cells. Based on the known marker genes, six cell types were annotated, as follows: EN1-negative

FIGURE 1 | Cell cluster of fibrotic and regenerative wound dermal cells. **(A)** The top 2,000 highly variable genes across fibrotic and regenerative wound dermal cells according to standard deviation. Red dots meant highly variable genes. The top ten highly variable genes were marked. **(B)** Two of the most principal components according to standard deviation. **(C)** PCA plots of wound dermal cells between fibrotic (fib) and regenerative (reg) conditions. Reference atlas was colored by tissue of origin (fibrotic and regenerative wounds). **(D)** Determination of the optimal principal components through elbow plot. **(E)** Heatmaps showing the top 20 marker genes in each principal component. **(F)** Cell cluster based on the screened principal components. **(G)** Heatmap showing the expression patterns of the top ten marker genes in each cell cluster.

myofibroblasts (n = 6,392), EN1-positive myofibroblasts (n = 2,219), hematopoietic cells (n = 3,774), macrophages (n = 1,461), pericytes (n = 1,493), and endothelial cells (n = 303; **Figure 2A**). **Table 1** lists the cell ratio of each cell type. In particular, we noticed the differences in ratios of EN1-negative and -positive myofibroblasts between fibrotic and regenerative wound dermal cells (**Figure 2B**). With |logFC| ≥ 0.1, the minimum expression ratio of cell population = 0.25, and p-value ≤ 0.05, we identified novel marker genes in each cell type (**Supplementary Table 1**). The top ten marker genes in each cell type were visualized, as follows: EN1-negative myofibroblasts (Aebp1, Col1a1, Col1a2, Col3a1, Col8a1, Dcn, Eln, Mfap2, Mfap4, and Sparc),

hematopoietic cells (AW112010, Cd3d, Cd3g, Cd52, Hcst, Ltb, Ptprcap, Rac2, Srgn, and Trbc2), macrophages (Apoe, C1qb, Ccl9, Cd74, Ctss, Fcer1g, H2-Eb1, Lyz2, Ms4a6c, and Tyrobp), pericytes (Acta2, Col4a1, Col4a2, Gm13889, Higd1b, Myl9, Mylk, Rgs5, Sparcl1, and Tagln), EN1-positive myofibroblasts (Birc5, Pclaf, Stnm1, Ube2c, Hist1h2ap, Col5a3, Cks2, Aqp1, Tnfaip6, and Timp1), and endothelia cells (Egfl7, Cldn5, Cdh5, Ramp2, Ecscr, Pecam1, Cd200, Ltbp4, Aqp1, and Hist1h2ap) (**Figure 2C**). Furthermore, we detected the expression levels of the known marker genes that were used for annotating cell types, as follows: endothelial cells (Cldn5, Pecam1, and Cd74), EN1-negative and -positive myofibroblasts (En1, Col1a1, Dcn, Sfrp4,
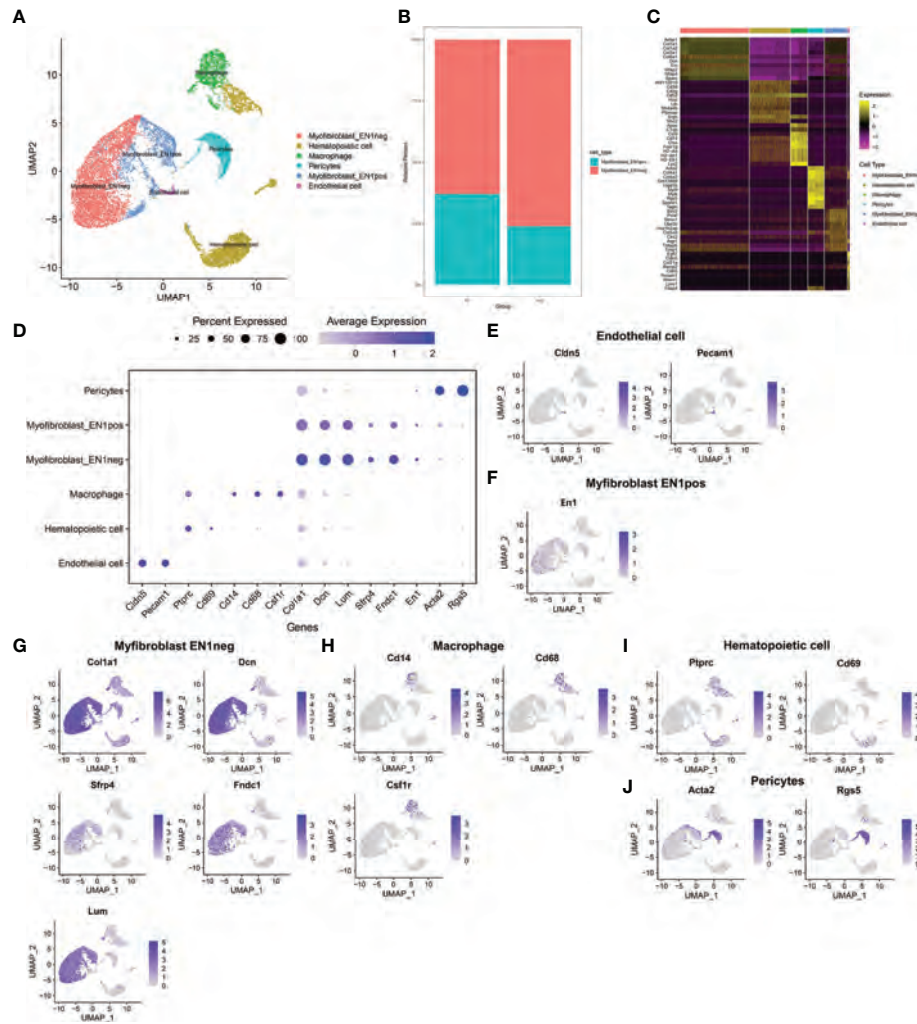
FIGURE 2 | Identification of cell types and their marker genes across fibrotic and regenerative wound dermal cells. (A) UMAP plots showing cell types identified by marker genes. Each cell type was colored by a unique color. (B) The cell ratio of EN1-negative and -positive myofibroblasts among fibrotic and regenerative wound dermal cells. (C) Heatmap visualizing cell-type-specific gene expression patterns. Each column represented the average expression after cells were grouped. (D) Integrated analysis showing marker genes across cell types. The size of each circle reflected the percentage of cells in each cell type where the gene was detected, and the color shadow reflected the average expression level within each cell type. (E–J) UMAP plots of expression of the marker genes for endothelial cells, EN1-negative and -positive myofibroblasts, macrophages, hematopoietic cells, and pericytes.

TABLE 1 | Cell ratio of each cell type.

Cell type	Group	Count	Total	Ratio
Endothelial cell	Fibrotic	76	5,130	0.014815
Endothelial cell	Regenerative	112	10,512	0.010654
EN1-negative myofibroblasts	Fibrotic	772	5,130	0.150487
EN1-negative myofibroblasts	Regenerative	5,620	10,512	0.534627
EN1-positive myofibroblasts	Fibrotic	454	5,130	0.088499
EN1-positive myofibroblasts	Regenerative	1,765	10,512	0.167903
Hematopoietic cell	Fibrotic	2,439	5,130	0.475439
Hematopoietic cell	Regenerative	1,335	10,512	0.126998
Macrophage	Fibrotic	725	5,130	0.141326
Macrophage	Regenerative	851	10,512	0.080955
Pericytes	Fibrotic	664	5,130	0.129435
Pericytes	Regenerative	829	10,512	0.078862

Fndc1, and Lum), macrophages (Cd14, Cd68, and Csf1r), and hematopoietic cells (Ptprc, Cd69, Acta2, and Rgs5) (**Figures 2D–J**).

Cell–Cell Interactions Based on Ligand–Receptor Interactions

Wound healing is a complex process that necessitates the collaborative efforts of diverse cell lineages (21). Cell-to-cell communications across diverse cell types thoroughly govern appropriate functions of metazoans as well as widely rely on interactions between secreted ligands and cell-surface receptors. Based on the marker genes, ligand–receptor interactions were matched. The number of ligands/receptors for myofibroblasts, pericytes, endothelial cells, macrophages, and hematopoietic cells

was 114, 91, 32, 28 and 17, respectively (**Figure 3A**). According to the number of intercellular receptor–ligand pairs, we screened out myofibroblasts as the core cell population.

Biological Functions of Ligand and Receptor Genes Between Myofibroblasts and Macrophages

We further evaluated the biological functions of ligand and receptor genes between myofibroblasts and macrophages. Our results demonstrated that ligand and receptor genes between myofibroblasts and macrophages were mainly involved in tube morphogenesis and development, regulation of cell migration, and motility (**Figure 3B**). Moreover, we found that the TGF-β signaling pathway was markedly enriched by these

FIGURE 3 | Cell–cell interactions and biological functions of ligand and receptor genes between myofibroblasts and macrophages. **(A)** The network of ligand–receptor-mediated multicellular signaling. The arrow pointed to the recipient cell, and the number on the line indicated the number of receptor–ligand pairs. **(B)** GO enrichment results of ligand and receptor genes between myofibroblasts and macrophages. **(C)** KEGG pathways enriched by ligand and receptor genes between myofibroblasts and macrophages. **(D)** RT-qPCR for the mRNA expressions of EN1 in fibroblasts transfected with siRNA of EN1. **(E, F)** Wound healing assay for the migration of EN1-knockdown fibroblasts. Bar, 20 μm. ***$p < 0.001$.

ligand and receptor genes between myofibroblasts and macrophages (**Figure 3C**).

Knockdown of EN1 Facilitates Fibroblast Migration

We further verified the effects of EN1 on the migration of fibroblasts. Firstly, siRNA against EN1 was designed and transected into fibroblasts. RT-qPCR demonstrated that EN1 mRNA expression was distinctly reduced following siRNA-EN1 transfection (**Figure 3D**). According to wound healing results, EN1-knockout fibroblasts displayed significantly enhanced migration capacity (**Figures 3E, F**). Hence, EN1 suppression enabled to facilitate fibroblast migration.

Identification of Specific Genes Between Fibrotic and Regenerative Myofibroblasts and Their Biological Functions

With the cutoffs of |FC| > 1.2 and p < 0.05, we identified 546 up- and 481 downregulated specific genes in regenerative compared to fibrotic myofibroblasts (**Figures 4A–C**). **Table 2** lists the first 20 up- and downregulated specific genes between regenerative and fibrotic myofibroblasts. As depicted in **Figure 4D**, we observed that the specific genes markedly participated in

collagen-containing extracellular matrix, posttranscriptional regulation of gene expression, positive regulation of cell migration, mRNA metabolic process, and apoptotic signaling pathway. Moreover, ribosome and thermogenesis were prominently enriched by the specific genes (**Figure 4E**).

Identification of Specific Genes Between Fibrotic and Regenerative Macrophages and Their Biological Functions

With the cutoffs of |FC| > 1.2 and p < 0.05, we found that 100 specific genes were significantly upregulated while 197 specific genes were significantly downregulated in regenerative compared to fibrotic macrophages (**Figures 5A–C**). **Table 3** lists the first 20 up- and downregulated specific genes between fibrotic and regenerative macrophages. GO enrichment analysis uncovered that the specific genes were markedly involved in the negative regulation of programmed cell death, the regulation of cell migration, innate immune response and apoptotic signaling pathway, collagen-containing extracellular matrix, the positive regulation of T cell activation, and response to interferon γ (**Figure 5D**). Moreover, we observed that antigen processing and presentation, pathways in cancer, phagosome, ribosome, and tuberculosis were prominently enriched by the specific genes (**Figure 5E**).

FIGURE 4 | Identification of specific genes between fibrotic and regenerative myofibroblasts and their biological functions. **(A, B)** Scatter plots and volcano diagram for the up- and downregulated specific genes in regenerative (reg) compared to fibrotic (fib) myofibroblasts. Red dots meant upregulated genes while blue dots meant downregulated genes. **(C)** Heatmap visualizing the expression patterns of the specific genes in fibrotic and regenerative myofibroblasts. Yellow represented upregulation and purple represented downregulation. **(D)** GO enrichment results of specific genes that were abnormally expressed between fibrotic and regenerative myofibroblasts. **(E)** KEGG pathways involved in specific genes that were abnormally expressed between fibrotic and regenerative myofibroblasts.

TABLE 2 | The first 20 up- and downregulated specific genes between fibrotic and regenerative myofibroblasts.

Gene	log2FC	p-value	Q-value	Regenerative	Fibrotic
Rplp0	0.870992	0	0	5.166991	4.295999
Ifitm2	0.843781	1.12E–173	1.94E–169	3.837826	2.994046
Mfap5	0.826158	5.93E–128	1.03E–123	4.591184	3.765026
Lgals1	0.820706	4.86E–284	8.43E–280	6.19352	5.372813
Hist1h2bc	0.81979	4.50E–90	7.81E–86	2.042755	1.222965
Serf2	0.805752	1.37E–310	2.39E–306	4.973459	4.167707
Rpl35	0.801322	0	0	5.164454	4.363133
Rps5	0.795055	5.07E–274	8.79E–270	4.725084	3.930029
Basp1	0.794315	1.55E–93	2.69E–89	2.268422	1.474106
Rpl6	0.792999	4.84E–266	8.40E–262	4.489802	3.696803
Ybx1	0.791379	6.39E–117	1.11E–112	2.98192	2.19054
Rps19	0.790084	0	0	5.198609	4.408525
Ost4	0.782118	2.55E–123	4.42E–119	3.079057	2.296939
Rpl29	0.780779	1.14E–175	1.98E–171	3.875578	3.094799
H19	0.767949	8.58E–45	1.49E–40	3.185378	2.417429
Rps11	0.763653	3.10E–260	5.37E–256	4.655295	3.891641
Rpl15	0.760256	2.28E–207	3.96E–203	4.262648	3.502392
Ift20	0.758	1.47E–93	2.55E–89	2.397842	1.639842
Ssr4	0.745387	2.11E–101	3.67E–97	2.89302	2.147633
Ubb	0.744921	1.14E–144	1.97E–140	4.529784	3.784862
mt-Nd4l	–2.08112	0	0	0.883721	2.964844
mt-Atp6	–1.85976	0	0	5.349053	7.20881
Hspa1b	–1.85125	4.49E–209	7.79E–205	0.611879	2.463132
mt-Co2	–1.84169	0	0	4.106449	5.948142
AC160336.1	–1.81875	4.98E–104	8.63E–100	0.763221	2.58197
Hspa1a	–1.79337	2.08E–164	3.61E–160	1.385872	3.179244
mt-Nd4	–1.60147	3.51E–321	6.08E–317	3.543676	5.145146
mt-Nd5	–1.59322	2.78E–221	4.83E–217	1.144946	2.738165
mt-Cytb	–1.57454	0	0	4.565919	6.140456
Igfbp2	–1.4162	1.28E–20	2.21E–16	2.045862	3.462061
mt-Nd3	–1.41514	1.13E–177	1.96E–173	1.403288	2.818428
mt-Nd1	–1.4142	4.61E–280	8.00E–276	4.509633	5.923829
mt-Co3	–1.39259	1.24E–268	2.15E–264	5.529273	6.921861
mt-Co1	–1.35374	1.30E–265	2.26E–261	5.598606	6.952347
mt-Nd2	–1.32088	1.81E–190	3.14E–186	2.765453	4.086338
Gm26917	–1.31863	7.03E–191	1.22E–186	0.653702	1.972335
Cd74	–1.15624	2.79E–193	4.84E–189	0.624805	1.781046
Lars2	–0.96874	2.21E–146	3.83E–142	0.232192	1.200933
Luc7l2	–0.91132	1.16E–98	2.01E–94	1.18695	2.098275
Hspg2	–0.90368	3.60E–128	6.24E–124	2.381196	3.284878

PPI Network Analysis of Specific Genes Between Fibrotic and Regenerative Myofibroblasts or Macrophages

With the STRING tool, we probed the interactions between myofibroblast- or macrophage-specific gene-encoded proteins. In **Figure 6A**, there were 616 nodes in the PPI network of myofibroblasts, reflecting the close interactions of myofibroblast-specific gene-encoded proteins. According to degree, the top 20 nodes were identified as hub genes, including Rps27a, Rps11, Rps23, Rps3, Rps5, Rps15a, Rps6, Rps9, Rps13, Rps14, Rps25, Rps3a1, Rps27, Rps8, Rps19, Rps28, Rps7, Rpl8, Rps18, Rpl26, Rpl32, and Rps16, indicating that the above genes were the core of the network. **Figure 6B** depicts the interactions between macrophage-specific gene-encoded proteins. The 20 hub genes were as follows: Uba52, Rps9, Gnb2l1, Rpl27, Rpl38, Rps13, Rps15a, Fau, Rpl18, Rpl30, Rpl35a, Rpl7, Rplp2, Rps24, Rpl13a, Rpl4, Rps10, Rps12, Rps27rt, and Rps2. The above genes deserve in-depth explorations.

Reconstruction of the Temporal Dynamics of Myofibroblast and Macrophage

To investigate the underlying evolution among myofibroblasts and macrophages, this study adopted the Monocle tool to reveal a pseudotemporal ordering for the similarity of cell clusters with developmental lineages. For myofibroblasts, the results clearly demonstrated the uniform development of myofibroblasts from cluster 6 to cluster 10 (**Figure 7A**). The trends of pseudotime-dependent genes along the pseudo-timeline were divided into six cell clusters of myofibroblasts with diverse expression dynamics. Furthermore, we observed that macrophage under fibrotic conditions was in the beginning position of the differentiation process and was sequentially transformed into macrophage under regenerative conditions (**Figure 7B**).

GSVA Between Clusters 6 and 10 of Fibrotic and Regenerative Myofibroblasts

According to the results of pseudotime analysis of myofibroblasts, we carried out GSVA between the initially differentiated cluster 6
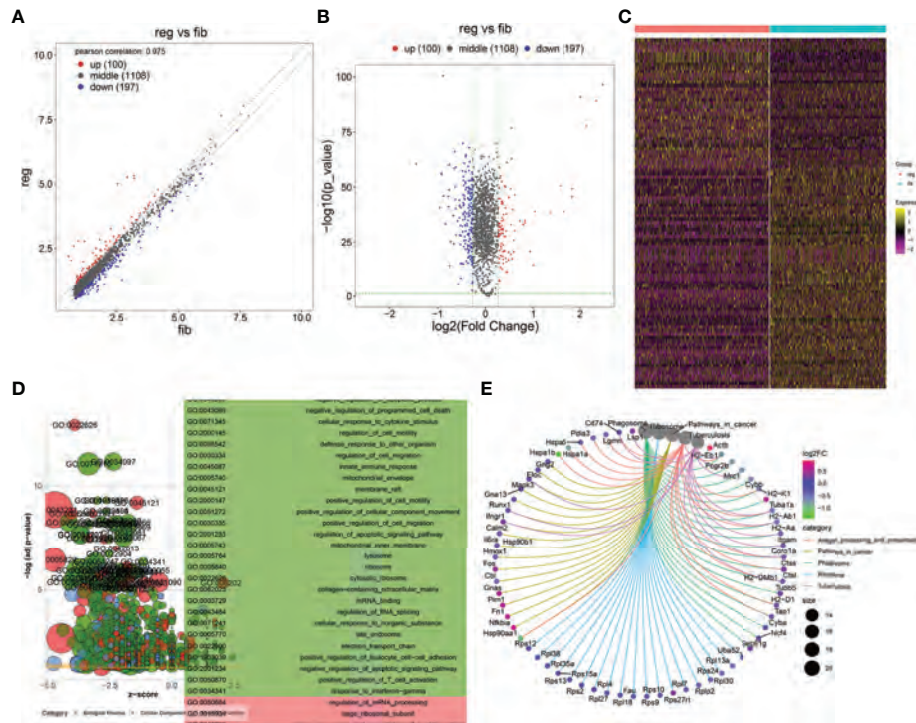
FIGURE 5 | Identification of specific genes between fibrotic and regenerative macrophages and their biological functions. **(A, B)** Scatter plots and volcano diagram showing the up- and downregulated specific genes in regenerative (reg) compared to fibrotic (fib) macrophages. Red dots meant upregulated genes while blue dots meant downregulated genes. **(C)** Heatmap visualizing the expression patterns of the specific genes in fibrotic and regenerative macrophages. Yellow represented upregulation and purple represented downregulation. **(D)** GO enrichment results of specific genes that were abnormally expressed between fibrotic and regenerative macrophages. **(E)** KEGG pathways involved in specific genes that were abnormally expressed between fibrotic and regenerative macrophages.

and the final differentiated cluster 10. Compared with cluster 10 of myofibroblasts in fibrotic and regenerative dermal cells, biological processes such as the metabolic process significantly activated cluster 6 of myofibroblasts in fibrotic and regenerative dermal cells (**Figure 8A**). As depicted in **Figure 8B**, we noticed the prominent activation of cellular components such as mitochondria in cluster 6 of fibrotic and regenerative myofibroblasts in comparison to those in cluster 10. Moreover, we observed that fibrotic and regenerative myofibroblasts in cluster 6 had significantly activated molecular functions like oxidoreductase activity compared with fibrotic and regenerative myofibroblasts in cluster 10 (**Figure 8C**). We also compared the differences in KEGG pathways between clusters. Diverse signaling pathways like metabolic pathways, RNA transport, spliceosome, thermogenesis, oxidative phosphorylation, carbon metabolism, ribosome, cell cycle, protein processing in the endoplasmic reticulum, and biosynthesis of amino acids were prominently activated in fibrotic and regenerative myofibroblasts in cluster 6 compared to those in cluster 10 (**Figure 8D**).

GSVA Between Fibrotic and Regenerative Macrophages

GSVA was also presented between fibrotic and regenerative macrophages. In **Figure 9A**, we determined that biological processes such as the metabolic process and immune response

were markedly activated in fibrotic macrophages compared to regenerative macrophages. The significantly activated cellular components such as the spliceosomal complex, catalytic complex, ribonucleoprotein complex, nuclear lumen, nucleoplasm, nucleolus, cytosol, nucleus, catalytic step 2 spliceosome, chromosome, and protein-containing complex were found in fibrotic macrophages compared with regenerative macrophages (**Figure 9B**). As shown in **Figure 9C**, we investigated the marked activation of molecular functions like RNA binding, ATP binding, mRNA binding, adenyl ribonucleotide binding, adenyl nucleotide binding, drug binding, nucleic acid binding, heterocyclic compound binding, organic cyclic compound binding, and ATPase activity in fibrotic macrophages in comparison to regenerative macrophages. Moreover, our results showed that KEGG pathways such as spliceosome, NOD-like receptor signaling pathway, Fc gamma R-mediated phagocytosis, antigen processing and presentation, endocytosis, necroptosis, and natural killer cell-mediated cytotoxicity displayed marked activation in fibrotic macrophages compared to regenerative macrophages (**Figure 9D**).

DISCUSSION

Skin wound healing involves complicated coordinated interactions within cells. Through scRNA-seq data, this study identified six cell

TABLE 3 | The first 20 up- and downregulated specific genes between fibrotic and regenerative macrophages.

Gene name	log2FC	p-value	Q-value	Regenerative	Fibrotic
Sparc	2.474022	3.60E−97	6.24E−93	5.010571	2.536548
Col1a1	2.33817	6.49E−90	1.13E−85	5.266303	2.928133
Col1a2	2.13485	3.01E−78	5.21E−74	5.327119	3.192269
Col3a1	2.005563	1.16E−91	2.01E−87	5.223726	3.218163
Dcn	1.836106	2.30E−46	3.98E−42	2.785851	0.949745
Bgn	1.83586	5.99E−50	1.04E−45	2.600128	0.764269
Fstl1	1.648779	1.28E−39	2.22E−35	2.200177	0.551399
Postn	1.572566	2.54E−51	4.40E−47	2.775437	1.202871
Mfap5	1.370976	2.18E−39	3.79E−35	2.023966	0.65299
Hbb-bs	1.031846	1.21E−39	2.10E−35	2.844128	1.812282
Cxcl2	1.004274	2.60E−15	4.51E−11	3.268016	2.263742
Actb	0.934603	1.46E−21	2.53E−17	7.663418	6.728815
Klf2	0.828223	1.34E−34	2.33E−30	2.497856	1.669632
Timp2	0.824526	1.09E−35	1.89E−31	1.978589	1.154062
Neat1	0.789153	1.13E−33	1.96E−29	2.328203	1.53905
Nfkbia	0.718421	2.88E−35	4.99E−31	2.761737	2.043317
Lgals1	0.61418	3.23E−47	5.60E−43	4.783109	4.168928
Fn1	0.610899	5.21E−31	9.03E−27	3.726565	3.115666
Pim1	0.59329	1.34E−26	2.32E−22	2.966403	2.373113
Cd63	0.592092	2.84E−21	4.92E−17	2.447508	1.855417
Hspa1b	−1.44863	2.08E−61	3.60E−57	1.266466	2.715092
Hsp90aa1	−0.957	1.59E−41	2.76E−37	2.518111	3.475109
Gm26917	−0.91834	3.81E−57	6.61E−53	0.782974	1.701314
Gm42418	−0.91626	1.85E−56	3.20E−52	1.082872	1.999131
Tpt1	−0.89005	3.21E−101	5.57E−97	4.517284	5.40733
mt-Nd5	−0.87923	1.13E−46	1.96E−42	0.858755	1.737986
Hspa1a	−0.83491	4.80E−34	8.32E−30	3.320621	4.155527
mt-Co2	−0.78506	1.59E−46	2.76E−42	3.967573	4.752638
mt-Atp6	−0.77046	5.82E−42	1.01E−37	4.934988	5.70545
Mycbp2	−0.75645	1.65E−49	2.86E−45	0.967289	1.723739
H2-Eb1	−0.75235	6.73E−15	1.17E−10	5.220528	5.972878
Fcgr2b	−0.75221	7.44E−61	1.29E−56	1.801335	2.553547
Mrc1	−0.72837	6.62E−26	1.15E−21	1.012111	1.740482
mt-Nd4l	−0.67023	7.15E−38	1.24E−33	0.682842	1.35307
AC160336.1	−0.65981	5.00E−25	8.66E−21	1.805651	2.465465
Prkcd	−0.6507	2.95E−59	5.12E−55	1.387319	2.038016
Cybb	−0.64225	8.79E−67	1.52E−62	1.99459	2.636836
Tgfbi	−0.63629	6.10E−51	1.06E−46	2.746255	3.382547
H2-K1	−0.62809	3.72E−45	6.44E−41	2.787025	3.415118
Ier5	−0.61724	5.52E−41	9.58E−37	2.037704	2.654947
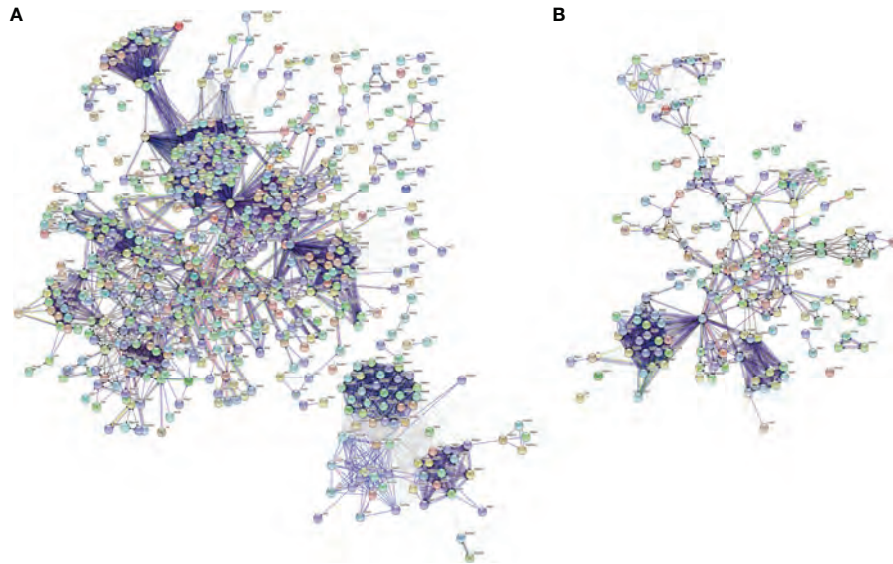
FIGURE 6 | PPI network analysis of specific genes between fibrotic and regenerative myofibroblasts or macrophages. **(A)** The PPI network of specific genes between fibrotic and regenerative myofibroblasts. **(B)** The PPI network of specific genes between fibrotic and regenerative macrophages.
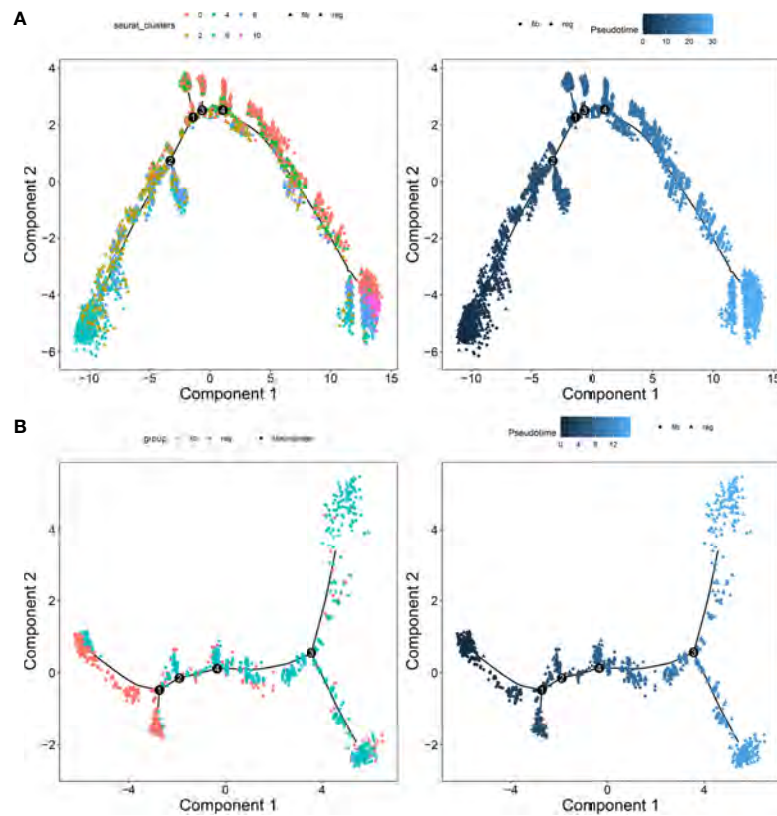
FIGURE 7 | Pseudotime ordering of myofibroblasts and macrophages. **(A)** Myofibroblasts and **(B)** macrophages. Each dot represented one cell and each branch represented one cell state. The left plot was labeled with cell states and the right plot was labeled with developmental time.
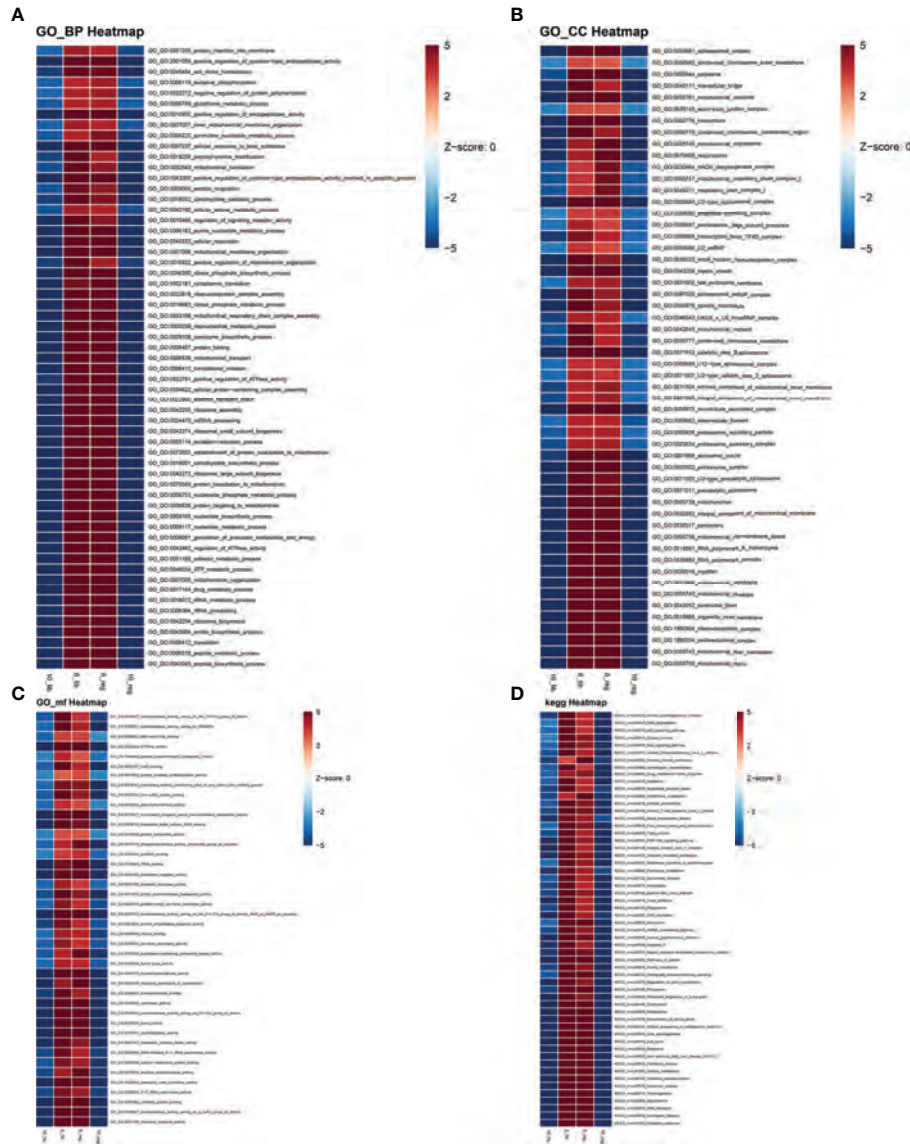
FIGURE 8 | GSVA between clusters 6 and 10 of fibrotic and regenerative myofibroblasts. **(A–D)** Heatmaps showing the differences in activation of biological processes, cellular components, molecular functions, and KEGG pathways between clusters 6 and 10 of fibrotic (fib) and regenerative (reg) myofibroblasts.

populations, namely, EN1-negative myofibroblasts, EN1-positive myofibroblasts, hematopoietic cells, macrophages, pericytes, and endothelial cells, across the dermis. Evidence suggests that EN1-positive fibroblasts are known to function in scarring, and EN1-negative fibroblasts yield wound regeneration. Thus, we used EN1 as a marker to divide the subgroups. Dynamic cellular events after skin injury rely on bidirectional cell–cell communications against effective wound healing (22). Our results demonstrated the cross-talks between myofibroblasts, hematopoietic cells, macrophages, pericytes, and endothelial cells in the dermis based on the ligand–receptor interactions. As per previous studies, CX3CR1 may mediate the recruitment of bone marrow-derived monocytes or macrophages in skin wound healing, thereby releasing profibrotic

as well as angiogenic mediators (23). Moreover, macrophages support proliferation and heterogeneity of myofibroblasts in skin repair (24). Serum endothelial cell-derived extracellular vesicles facilitate diabetic wound healing *via* enhancing myofibroblast proliferation and decreasing senescence (25). Intradermal adipocytes modulate the recruitment of myofibroblasts in skin wound healing (26). Fibroblasts promote NG^{2+} pericyte populations in murine skin development as well as repair (27). On the basis of the above lines of evidence, there were remarkable interplays between diverse cell types during dermis progression. According to the number of ligands and receptors, we identified myofibroblasts as the core cell population. Our function enrichment analyses uncovered that the ligand and receptor
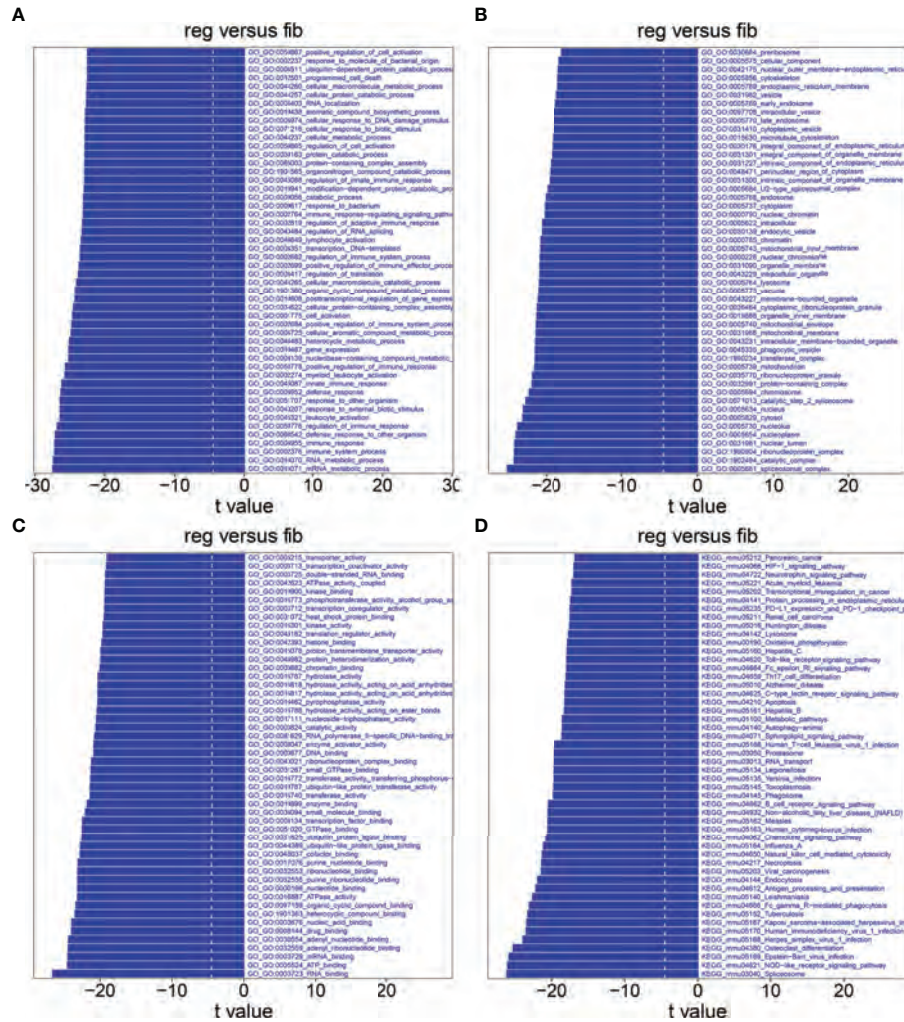
FIGURE 9 | GSVA between fibrotic and regenerative macrophages. **(A–D)** Heatmaps visualizing the differences in activation of biological processes, cellular components, molecular functions, and KEGG pathways between fibrotic (fib) and regenerative (reg) macrophages.

genes between myofibroblasts and macrophages were mainly involved in regulating cell proliferation and migration, tube development, and the TGF-β pathway. The TGF-β signaling pathway plays an important role in the formation of collagen in fibroblasts and myofibroblasts (28). Cytokine TGF-β may induce dermal dendritic cells to express IL-31, thereby activating sensory neurons as well as stimulating wound itching during skin would healing (29). Hence, targeting the TGF-β pathway is the promising therapeutic intervention to reduce abnormal skin scar formation.

To explore the differences in molecular mechanisms involving myofibroblasts between fibrotic and regenerative wound healing fates, we identified 546 up- and 481 downregulated specific genes in regenerative compared to fibrotic myofibroblasts. This revealed the heterogeneity of myofibroblasts between fibrotic and regenerative wound healing. Our GO and KEGG enrichment analysis uncovered the key biological functions involving the specific genes between fibrotic and regenerative myofibroblasts. As a result, these specific genes between fibrotic and regenerative myofibroblasts prominently participated in the mRNA metabolic process and organelle organization. Extracellular matrix of connective tissues is synthesized by myofibroblasts that play a critical role in sustaining the structural integrity of various tissues (30).

Skin wound macrophage is an important regulator of skin repair, and its dysfunction may cause chronic and non-healing skin wounds (31). Further analysis identified that 100 specific genes were significantly upregulated while 197 specific genes were significantly downregulated in regenerative compared to fibrotic macrophages. Functional enrichment analysis uncovered that these specific genes between fibrotic and regenerative macrophages primarily participated in regulating inflammatory response, immunity, and phagocytosis. Immunity is the most important function of the skin, which can prevent harmful exposure from the external and internal environment (32).

Furthermore, late wound macrophage phagocytosis of the Wnt inhibitor may induce chronic Wnt activity during fibrotic skin healing (11). Collectively, our findings revealed that the heterogeneity of myofibroblasts or macrophages might determine wound healing fate as regenerative or fibrotic.

CONCLUSION

Taken together, this study uncovered cellular functional heterogeneity in dermis between fibrotic and regenerative wound healing fates. Moreover, myofibroblasts and macrophages may change the skin wound healing fates by modulating critical signaling pathways. Therefore, our data provided an insight into the development of more effective therapeutic interventions for improving healing fates.

DATA AVAILABILITY STATEMENT

The datasets presented in this study can be found in online repositories. The names of the repository/repositories and accession number(s) can be found at: https://www.ncbi.nlm.nih.gov/, GSM4213633; https://www.ncbi.nlm.nih.gov/, GSM4213632; https://www.ncbi.nlm.nih.gov/, GSE141814.

ETHICS STATEMENT

Ethical review and approval were not required for the study on human participants in accordance with the local legislation and institutional requirements. Written informed consent for participation was not required for this study in accordance with the national legislation and the institutional requirements. The animal study was reviewed and approved by Keio University

School of Medicine. Written informed consent was not obtained from the individual(s) for the publication of any potentially identifiable images or data included in this article.

AUTHOR CONTRIBUTIONS

C-JC, HK, and KT: conception or design of the work. C-JC, HK, KT, NA-H, SS, TA, and KK: acquisition, analysis, or interpretation of data. C-JC, HK, KT, NA-H, SS, TA, and KK: drafting the manuscript or revising it critically for important intellectual content. All authors contributed to the article and approved the submitted version.

FUNDING

SUPPLEMENTARY MATERIAL

The Supplementary Material for this article can be found online at: https://www.frontiersin.org/articles/10.3389/fimmu.2022.875407/full#supplementary-material

Supplementary Figure 1 | Quality control of scRNA-seq data of fibrotic and regenerative wound dermal cells. **(A, B)** Barcode rank plots separately showing the detected knee and inflection points for fibrotic and regenerative wound dermal cells. **(C, D)** The expression of all genes, ribosomal genes, and mitochondrial genes in each cell was shown for fibrotic and regenerative wound dermal cells. **(E, F)** The proportions of mitochondrial and ribosomal genes expressed in each cell were counted for fibrotic and regenerative wound dermal cells.

Supplementary Table 1 | The list of novel marker genes identified in each cell type.

REFERENCES

1. Rajesh A, Stuart G, Real N, Tschirley A, Ahn J, Wise L, et al. Skin Antigen-Presenting Cells and Wound Healing: New Knowledge Gained and Challenges Encountered Using Mouse Depletion Models. *Immunology* (2021) 163(1):98–104. doi: 10.1111/imm.13311
2. Griffin DR, Archang MM, Kuan C-H, Weaver WM, Weinstein JS, Feng AC, et al. Activating an Adaptive Immune Response From a Hydrogel Scaffold Imparts Regenerative Wound Healing. *Nat Mater* (2021) 20(4):560–9. doi: 10.1038/s41563-020-00844-w
3. Yamaguchi K, Kanno E, Tanno H, Sasaki A, Kitai Y, Miura T, et al. Distinct Roles for Dectin-1 and Dectin-2 in Skin Wound Healing and Neutrophilic Inflammatory Responses. *J Invest Dermatol* (2021) 141(1):164–76.e8. doi: 10.1016/j.jid.2020.04.030
4. Chen T-Y, Wen T-K, Dai N-T, Hsu S-H. Cryogel/hydrogel Biomaterials and Acupuncture Combined to Promote Diabetic Skin Wound Healing Through Immunomodulation. *Biomaterials* (2021) 269:120608. doi: 10.1016/j.biomaterials.2020.120608
5. Rodrigues M, Kosaric N, Bonham CA, Gurtner GC. Wound Healing: A Cellular Perspective. *Physiol Rev* (2019) 99(1):665–706. doi: 10.1152/physrev.00067.2017

6. Aragona M, Dekoninck S, Rulands S, Lenglez S, Mascré G, Simons BD, et al. Defining Stem Cell Dynamics and Migration During Wound Healing in Mouse Skin Epidermis. *Nat Commun* (2017) 8:14684. doi: 10.1038/ncomms14684
7. Govindaraju P, Todd L, Shetye S, Monslow J, Puré E. CD44-Dependent Inflammation, Fibrogenesis, and Collagenolysis Regulates Extracellular Matrix Remodeling and Tensile Strength During Cutaneous Wound Healing. *Matrix Biol* (2019) 75–6:314–30. doi: 10.1016/j.matbio.2018.06.004
8. Haensel D, Jin S, Sun P, Cinco R, Dragan M, Nguyen Q, et al. Defining Epidermal Basal Cell States During Skin Homeostasis and Wound Healing Using Single-Cell Transcriptomics. *Cell Rep* (2020) 30(11):3932–47.e6. doi: 10.1016/j.celrep.2020.02.091
9. Theocharidis G, Baltzis D, Roustit M, Tellechea A, Dangwal S, Khetani RS, et al. Integrated Skin Transcriptomics and Serum Multiplex Assays Reveal Novel Mechanisms of Wound Healing in Diabetic Foot Ulcers. *Diabetes* (2020) 69(10):2157–69. doi: 10.2337/db20-0188
10. Guerrero-Juarez CF, Dedhia PH, Jin S, Ruiz-Vega R, Ma D, Liu Y, et al. Single-Cell Analysis Reveals Fibroblast Heterogeneity and Myeloid-Derived Adipocyte Progenitors in Murine Skin Wounds. *Nat Commun* (2019) 10(1):650. doi: 10.1038/s41467-018-08247-x
11. Gay D, Ghinatti G, Guerrero-Juarez CF, Ferrer RA, Ferri F, Lim CH, et al. Phagocytosis of Wnt Inhibitor SFRP4 by Late Wound Macrophages Drives

Chronic Wnt Activity for Fibrotic Skin Healing. *Sci Adv* (2020) 6(12): eaay3704. doi: 10.1126/sciadv.aay3704

12. Lun ATL, Riesenfeld S, Andrews T, Dao TP, Gomes T, Marioni JC. EmptyDrops: Distinguishing Cells From Empty Droplets in Droplet-Based Single-Cell RNA Sequencing Data. *Genome Biol* (2019) 20(1):63. doi: 10.1186/s13059-019-1662-y

13. McCarthy DJ, Campbell KR, Lun ATL, Wills QF. Scater: Pre-Processing, Quality Control, Normalization and Visualization of Single-Cell RNA-Seq Data in R. *Bioinformatics* (2017) 33(8):1179–86. doi: 10.1093/bioinformatics/btw777

14. Butler A, Hoffman P, Smibert P, Papalexi E, Satija R. Integrating Single-Cell Transcriptomic Data Across Different Conditions, Technologies, and Species. *Nat Biotechnol* (2018) 36(5):411–20. doi: 10.1038/nbt.4096

15. Ramilowski JA, Goldberg T, Harshbarger J, Kloppmann E, Lizio M, Satagopam VP, et al. A Draft Network of Ligand-Receptor-Mediated Multicellular Signalling in Human. *Nat Commun* (2015) 6:7866. doi: 10.1038/ncomms8866

16. Doncheva NT, Morris JH, Gorodkin J, Jensen LJ. Cytoscape StringApp: Network Analysis and Visualization of Proteomics Data. *J Proteome Res* (2019) 18(2):623–32. doi: 10.1021/acs.jproteome.8b00702

17. Yu G, Wang L-G, Han Y, He Q-Y. Clusterprofiler: An R Package for Comparing Biological Themes Among Gene Clusters. *OMICS* (2012) 16 (5):284–7. doi: 10.1089/omi.2011.0118

18. Szklarczyk D, Gable AL, Lyon D, Junge A, Wyder S, Huerta-Cepas J, et al. STRING V11: Protein-Protein Association Networks With Increased Coverage, Supporting Functional Discovery in Genome-Wide Experimental Datasets. *Nucleic Acids Res* (2019) 47(D1):D607–13. doi: 10.1093/nar/gky1131

19. Cao J, Spielmann M, Qiu X, Huang X, Ibrahim DM, Hill AJ, et al. The Single-Cell Transcriptional Landscape of Mammalian Organogenesis. *Nature* (2019) 566(7745):496–502. doi: 10.1038/s41586-019-0969-x

20. Hänzelmann S, Castelo R, Guinney J. GSVA: Gene Set Variation Analysis for Microarray and RNA-Seq Data. *BMC Bioinf* (2013) 14:7. doi: 10.1186/1471-2105-14-7

21. Sorkin M, Huber AK, Hwang C, Carson WF4, Menon R, Li J, et al. Regulation of Heterotopic Ossification by Monocytes in a Mouse Model of Aberrant Wound Healing. *Nat Commun* (2020) 11(1):722. doi: 10.1038/s41467-019-14172-4

22. Zhou X, Brown BA, Siegel AP, El Masry MS, Zeng X, Song W, et al. Exosome-Mediated Crosstalk Between Keratinocytes and Macrophages in Cutaneous Wound Healing. *ACS Nano* (2020) 14(10):12732–48. doi: 10.1021/acsnano.0c03064

23. Ishida Y, Gao J-L, Murphy PM. Chemokine Receptor CX3CR1 Mediates Skin Wound Healing by Promoting Macrophage and Fibroblast Accumulation and Function. *J Immunol* (2008) 180(1):569–79. doi: 10.4049/jimmunol.180.1.569

24. Shook BA, Wasko RR, Rivera-Gonzalez GC, Salazar-Gatzimas E, López-Giráldez F, Dash BC, et al. Myofibroblast Proliferation and Heterogeneity are Supported by Macrophages During Skin Repair. *Science* (2018) 362(6417). doi: 10.1126/science.aar2971

25. Wei F, Wang A, Wang Q, Han W, Rong R, Wang L, et al. Plasma Endothelial Cells-Derived Extracellular Vesicles Promote Wound Healing in Diabetes Through YAP and the PI3K/Akt/mTOR Pathway. *Aging (Albany NY)* (2020) 12(12):12002–18. doi: 10.18632/aging.103366

26. Schmidt BA, Horsley V. Intradermal Adipocytes Mediate Fibroblast Recruitment During Skin Wound Healing. *Development* (2013) 140 (7):1517–27. doi: 10.1242/dev.087593

27. Goss G, Rognoni E, Salameti V, Watt FM. Distinct Fibroblast Lineages Give Rise to NG2+ Pericyte Populations in Mouse Skin Development and Repair. *Front Cell Dev Biol* (2021) 9:675080. doi: 10.3389/fcell.2021.675080

28. Zhang T, Wang X-F, Wang Z-C, Lou D, Fang Q-Q, Hu Y-Y, et al. Current Potential Therapeutic Strategies Targeting the TGF-β/Smad Signaling Pathway To Attenuate Keloid and Hypertrophic Scar Formation. *BioMed Pharmacother* (2020) 129:110287. doi: 10.1016/j.biopha.2020.110287

29. Xu J, Zanvit P, Hu L, Tseng P-Y, Liu N, Wang F, et al. The Cytokine TGF-β Induces Interleukin-31 Expression From Dermal Dendritic Cells to Activate Sensory Neurons and Stimulate Wound Itching. *Immunity* (2020) 53(2):371–83.e5. doi: 10.1016/j.immuni.2020.06.023

30. Lynch MD, Watt FM. Fibroblast Heterogeneity: Implications for Human Disease. *J Clin Invest* (2018) 128(1):26–35. doi: 10.1172/JCI93555

31. Chen H, Shi R, Luo B, Yang X, Qiu L, Xiong J, et al. Macrophage Peroxisome Proliferator-Activated Receptor γ Deficiency Delays Skin Wound Healing Through Impairing Apoptotic Cell Clearance in Mice. *Cell Death Dis* (2015) 6 (1):e1597. doi: 10.1038/cddis.2014.544

32. Matejuk A. Skin Immunity. *Arch Immunol Ther Exp (Warsz)* (2018) 66(1):45–54. doi: 10.1007/s00005-017-0477-3

Research Article

Screening of Autophagy-Related Prognostic Genes in Metastatic Skin Melanoma

Cao-Jie Chen, Hiroki Kajita, Noriko Aramaki-Hattori, Shigeki Sakai ⓘ, and Kazuo Kishi ⓘ

Department of Plastic and Reconstructive Surgery, Keio University School of Medicine, Tokyo 160-8582, Japan

Correspondence should be addressed to Shigeki Sakai; shigekis@keio.jp and Kazuo Kishi; kkishi@a7.keio.jp

Cutaneous melanoma refers to a common skin tumor that is dangerous to health with a great risk of metastasis. Previous researches reported that autophagy is associated with the progression of cutaneous melanoma. Nevertheless, the role played by genes with a relation to autophagy (ARG) in the prediction of the course of metastatic cutaneous melanoma is still largely unknown. We observed that thirteen ARGs showed relations to overall survival (OS) in the Cox regression investigation based on a single variate. We developed 2-gene signature, which stratified metastatic cutaneous melanoma cases to groups at great and small risks. Cases suffering from metastatic cutaneous melanoma in the group at great risks had power OS compared with cases at small risks. The risk score, T phase, N phase, and age were proved to be individual factors in terms of the prediction of OS. Besides, the risk scores identified by the two ARGs were significantly correlated with metastatic cutaneous melanoma. Receiver operating characteristic (ROC) curve analysis demonstrated accurate predicting performance exhibited by the 2-gene signature. We also found that the immunization and stromal scores achieved by the group based on large risks were higher compared with those achieved by the group based on small risks. The metastatic cutaneous melanoma cases achieving the score based on small risks acquired greater expression of immune checkpoint molecules as compared with the high-risk group. In conclusion, the 2-ARG gene signature indicated a novel prognostic indicator for prognosis prediction of metastatic cutaneous melanoma, which served as an important tool for guiding the clinical treatment of cutaneous melanoma.

1. Introduction

Cutaneous melanoma refers to one type of skin malignant tumor exhibiting high malignancy and ineffective prediction of disease courses [1, 2]. Occult onset and easy invasion and metastasis are important clinical features of cutaneous melanoma [3]. According to the statistics, cutaneous melanoma's incidence in China rose to about 3-5% [4]. Although cutaneous melanoma's incidence within China and other Asian countries is relatively low compared with those in Europe and America, cutaneous melanoma's incidence within China is increasing rapidly [5]. Once cutaneous melanoma cases have distant metastasis, they are diagnosed as advanced or metastatic cm, so the survival time of cutaneous melanoma cases is often short [6]. In the current treatment strategies of metastatic cutaneous melanoma, targeted therapy and immunotherapy play an important role. Metastatic tumor surgery and radiotherapy can also be used selectively [7].

Due to the high metastasis rate of cutaneous melanoma, it is necessary to find a new prognosis model to provide theoretical guidance for the treatment of metastatic cutaneous melanoma.

Autophagy is a process in which cytoplasmic components, or organelles are encapsulated and transported to lysosomes for degradation by forming double membrane autophagosomes [8, 9]. Autophagy can be induced by DNA damage, chemical drugs, ion irradiation, reactive oxygen species, and abnormal growth of tumor cells [10]. According to existing works, autophagy refers to a barrier against malignant transformation of carcinoma cells [11, 12]. Some major oncogenes, such as mTOR and Akt, are considered to be negative regulators of autophagy [13, 14]. According to considerable works, mutant tumor suppressors such as PTEN and TSC1/2 can activate autophagy [15]. It is controversial whether autophagy has a tumor promoting or antitumor effect on the occurrence and development of

cancer. At present, according to some studies, autophagy impacts tumor inhibition in the early stage of cancer, but it plays a role in promoting cancer in the formed tumor and contributes to the generation of drug resistance of cancer cells [16, 17]. Therefore, autophagy is considered to help promote the survival of cancer cells in the advanced phase. At present, there are few comprehensive studies on exploring autophagy-relevant genes within the disease course prediction and immunotherapy of metastatic cutaneous melanoma.

Here, we obtained RNA-seq and clinic information regarding cutaneous melanoma cases from The Cancer Genome Atlas (TCGA) database. By several bioinformatics investigations, a multigene signature of ARG was constructed. Relationships of risk model and clinicopathological features of metastatic cutaneous melanoma were confirmed. Then, we carried out Cox regression investigations based on single and multiple variates for the identification of individual factors for the OS of metastatic cutaneous melanoma. A nomogram containing independent prognostic factors was built using "rms" package. We carried out GSVA for exploring the biological processes and pathways involved in the groups based on great and small risks. Furthermore, the analysis was conducted on the landscape of immune infiltration and the expression of immune checkpoint molecules in metastatic cutaneous melanoma. This work might provide a new idea for prognosis and immunotherapy of later phase metastasis melanoma.

2. Material and Method

2.1. Data Acquisition and Preprocessing. We retrieved the RNA-seq and clinic data regarding the cases with cutaneous melanoma according to The Cancer Genome Atlas (TCGA) cohort (https://portal.gdc.cancer.gov/), which contained 103 primary and 367 metastatic cancer cases. Totally, 232 ARGs were acquired in the Human Autophagy Database (http://autophagy.lu/).

2.2. Differentially Expressed Analysis. For screening the gene that achieves different expressions (DEGs) in the metastatic and primary carcinoma samples, the "limma" package was used with regulated P value < 0.05 as well as |log 2 (fold change) | >0.5 [18]. The expression of Top100 genes that achieved different expressions between the metastatic and primary carcinoma samples was shown in a heat map. Then, the DEGs were overlapped with the ARGs to obtain the ARGs that achieved different expressions (DE-ARGs), which were chosen to conduct the subsequent investigation.

2.3. Development and Verification of the Prognostic Signature in relation to Autophagy. Subsequently, metastatic cutaneous melanoma cases indiscriminately fell to the test set ($n = 93$) and the training set ($n = 217$) at 3 : 7. To explore whether each DE-ARG is related to overall survival (OS), we performed Cox regression investigation based on a single variate in the training set. The DE-ARGs with the P value < 0.05 were identified, followed by the subsequent analysis based on Cox regression investigation based on multiple variates to obtain the best risk model. In the Cox regression investigation based on multiple variates, this study applied the stepwise regression function and set the "direction" as "both."

Based on the risk model, the score of risk of the respective metastatic cutaneous melanoma case was obtained by: risk score = $(\beta 1\, G\, 1 + \beta 2\, G\, 2 + \beta 3\, G\, 3 + \cdots + \beta n\, G\, n)$. In the calculated formula, β stands the coefficient of gene, and G stands the expression level of each gene. The metastatic cutaneous melanoma cases were then stratified into the group based on small risks and group based on large risk in accordance with the mean value of risk score. Furthermore, the OS of these groups was compared using the Kaplan-Meier (K-M) approach on the basis of the log-rank test. In addition, using "survivalROC" R package, we obtained the curves of receiver operating characteristic (ROC) of 1, 3, and 5 years [19]. To be specific, we obtained the area under the curve (AUC) for assessing the risk model's effectiveness. The model of risk was further verified based on the test set.

2.4. Functional Enrichment Analysis. According to the gene sets files, we carried out GSVA (PMID: 23323831) for the exploration of the potential biology process and pathways most relevant to groups based on large risk and small risk of metastatic cutaneous melanoma cases. Using the "gsva" package of R software, we carried out a single sample gene set enrichment investigation (ssGSEA) for calculating infiltrating immune cells' proportion in cases with metastatic cutaneous melanoma [20].

2.5. Evaluation of Immune Microenvironment. We implemented "ESTIMATE" R package for obtaining the immunization and stromal scores of metastatic cutaneous melanoma cases within TCGA database [21]. Furthermore, the expressions of immunization checkpoint molecules were examined in the metastatic cutaneous melanoma samples.

2.6. Statistical Analysis. We carried out the statistical investigations with R software (Version 3.5.3). We investigated various groups' OS on the basis of K-M investigation and compared OS by the log-rank test. Cox regression investigations based on single and multiple variates were applied to investigate the individual prognostic factors for OS. The nomogram containing clinicopathological features was constructed by "rms" package. The differences between two groups were compared using Wilcox.test. Differences were considered statistically significant when $P < 0.05$.

3. Result

3.1. Identification of Autophagy-Related Genes with Different Expressions (DE-ARGs) in Metastatic Cutaneous Melanoma. To seek the ARGs in relations to the disease course prediction of cutaneous melanoma, we first analyzed the DEGs between the primary and metastatic cancer samples of TCGA database using "limma" package. Under the threshold of regulated P value < 0.05 as well as |log 2 (fold change) | >0.5, we identified 886 DEGs in total, covering 554 significantly upregulated and 332 significantly decreased genes within metastatic cancer samples in comparison with the primary cancer samples (Figure 1(a)). Figure 1(b) reveals the expression of Top100 DEGs between the primary and metastatic cancer samples of the TCGA database. Furthermore, we combined the 886 DEGs with 222 ARGs, obtaining

Significant

● Down

● Not

● Up
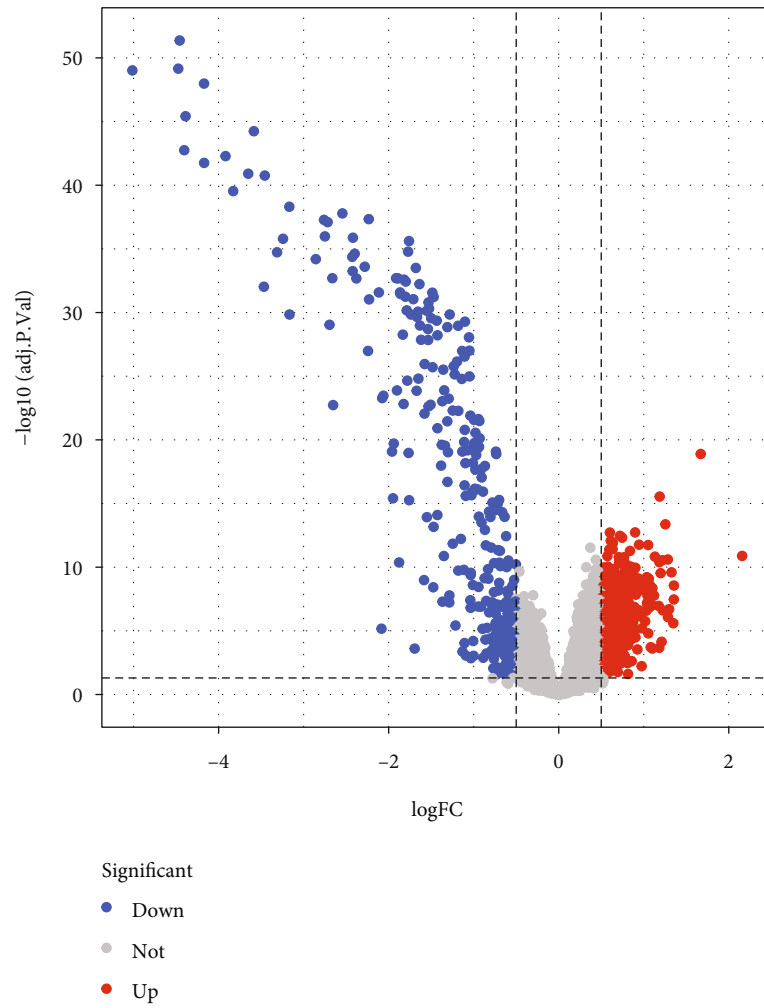
(a)

Figure 1: Continued.

(b)

(c)
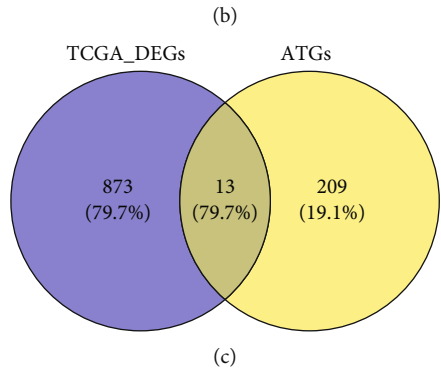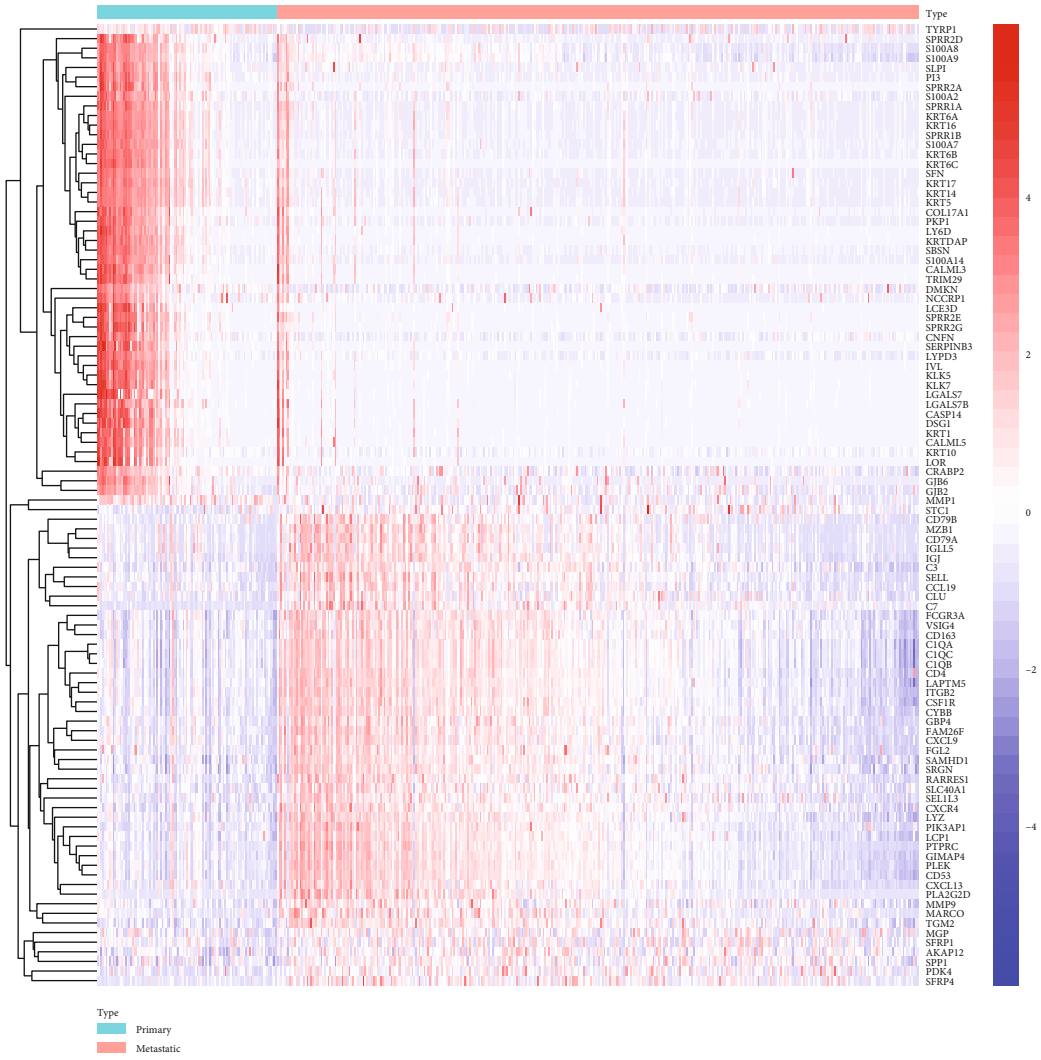
FIGURE 1: Identification of DE-ARGs in metastatic cutaneous melanoma. (a) Volcano plot of DEGs, including 554 significantly upregulated and 332 significantly downregulated genes were identified in metastatic cancer samples compared to the primary cancer samples. Threshold: |log 2 (fold change) | >0.5 and adjusted P value < 0.05. Blue dot for downregulated genes; red dot for upregulated genes. (b) The expression of Top100 DEGs between the primary and metastatic cancer samples of TCGA database. (c) Venn plot for combination of 886 DEGs (blue circle) and 222 ARGs (yellow circle), obtaining 13 DE-ARGs.

13 DE-ARGs, to carry out the following investigation (Figure 1(c)).

3.2. Establishment and Validation of the Prognostic Signature in relation to Autophagy. For more specifically assessing

whether the DE-ARGs are related to the survival of metastatic cutaneous melanoma cases, the Cox regression investigation based on single variate was performed within the training set (Figure 2(a)). The result indicated that two genes had significant relations to the metastatic cutaneous

(a)

(b)

(c)

(d)

(e)
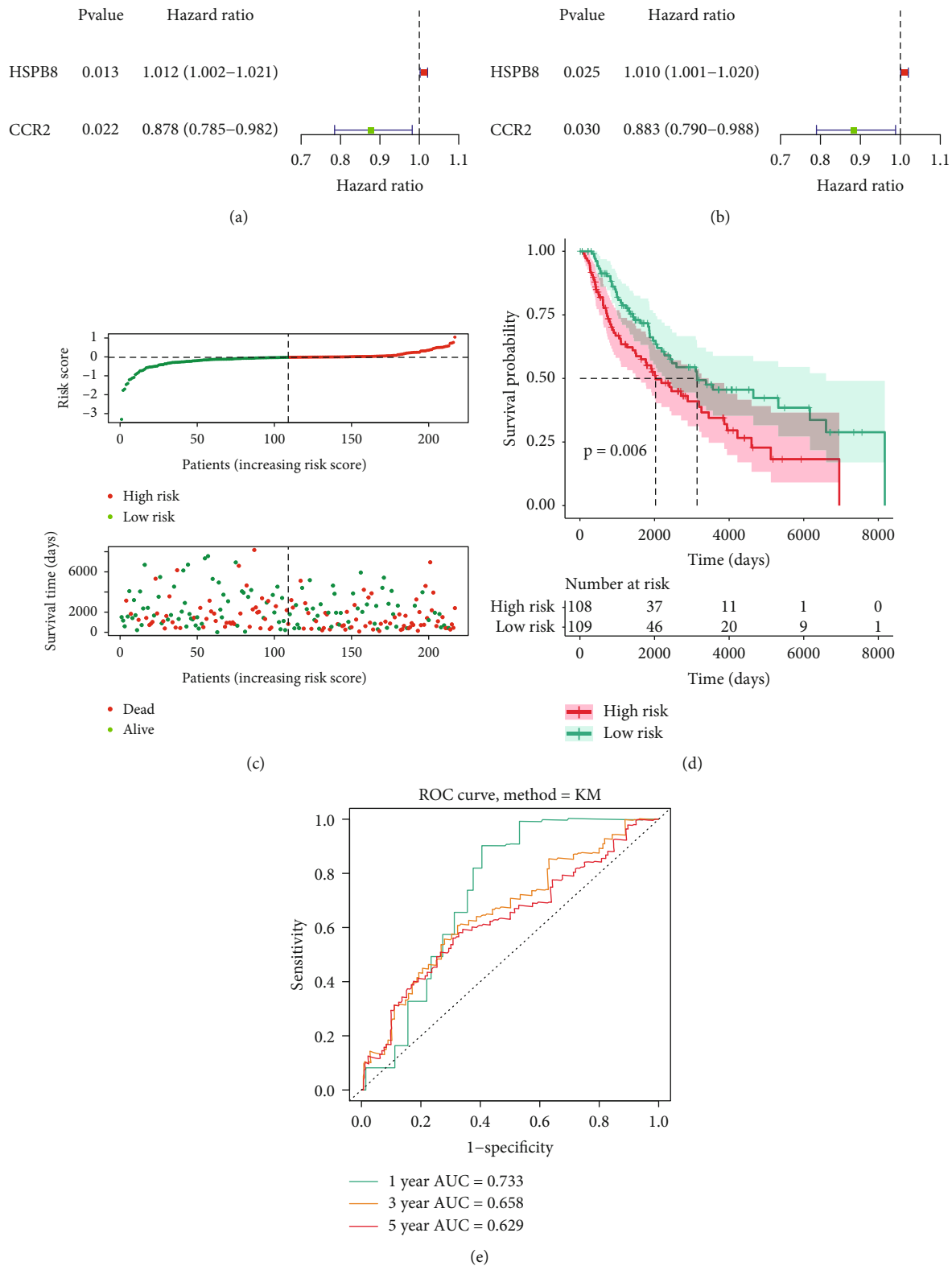
FIGURE 2: Training set for establishment of the autophagy-related prognostic signature. (a) The univariate Cox regression analysis for HSPB8, CCR2 with the survival of metastatic cutaneous melanoma in the training set. (b) The multivariate Cox regression analysis for combination of HSPB8 and CCR2 with the survival of metastatic cutaneous melanoma in the training set. (c) The distribution of patient risk scores and survival status in the training set. (d) The K-M survival analysis of the metastatic cutaneous melanoma patients between high-risk score and low-risk patients in overall survival. Red line for high risk; green line for low risk. (e) The time-dependent ROC curve and AUC values of 1-, 3-, and 5-year OS in the training set.

(a)

(b)

ROC curve, method = KM

1 year AUC = 0.711
3 year AUC = 0.627
5 year AUC = 0.683

(c)
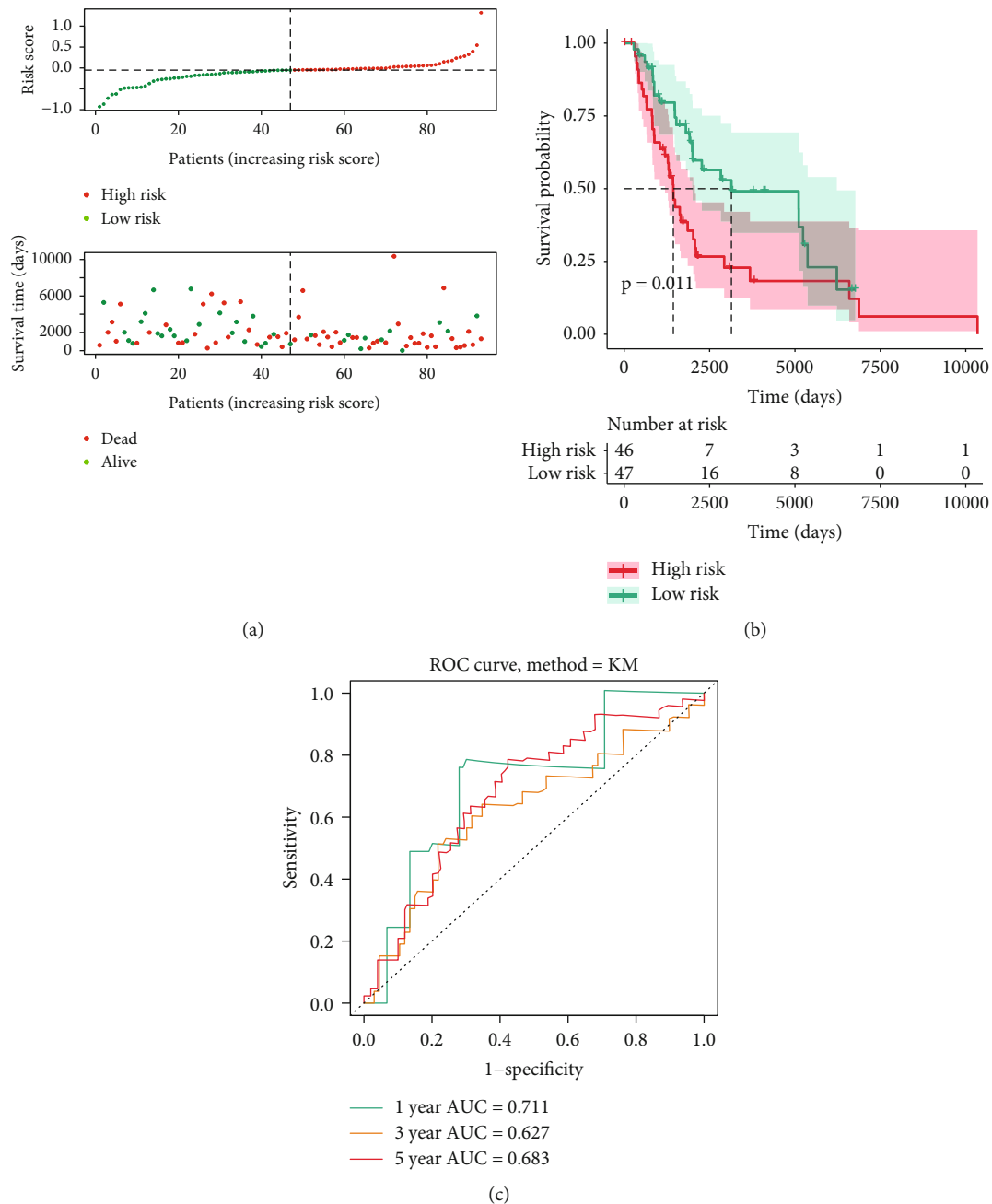
FIGURE 3: Validation set for the autophagy-related prognostic signature. (a) The distribution of patient risk scores and survival status in the validation set. (b) The K-M survival analysis of the metastatic cutaneous melanoma patients between high-risk score and low-risk patients in overall survival. Red line for high risk; green line for low risk. (c) The time-dependent ROC curve and AUC values of 1-, 3-, and 5-year OS in the validation set.

melanoma cases' OS ($P < 0.05$), of which HSPB8 was a risk factor (HR > 1), and CCR2 was a protective factor (HR < 1) in metastatic cutaneous melanoma. Then, we reported a 2-gene signature based on the Cox regression investigation based on multiple variates (Figure 2(b)). Two ARGs and their corresponding coefficients were utilized for determining the score of risk of the respective metastatic cutaneous melanoma case. The calculated equation in terms of the score of risk is presented as $0.0103 \times$ (expression value of HSPB8) + $(−0.124) \times$ (expression value of CCR2) within the training and test sets. Figure 2(c) illustrates the distributions

of case risk scores and survivals. The K-M survival investigation revealed that the metastatic cutaneous melanoma cases with high-risk scores had a significantly poorer OS in comparison with that of cases based on small risks (Figure 2(c), $P < 0.05$). Besides, according to the ROC depending on time, the AUC of 1-, 3-, and 5-year OS reached 0.733, 0.658, and 0.629, separately (Figure 2(e)). Lastly, we verified the 2-ARGs prognosis signature with the use of OS information according to the test set, complying with the results of the training set (Figures 3(a)–3(c)), in which AUC of 1-, 3-, and 5-year OS reached 0.711, 0.627, and 0.683, separately.

(a)

(b)

(c)
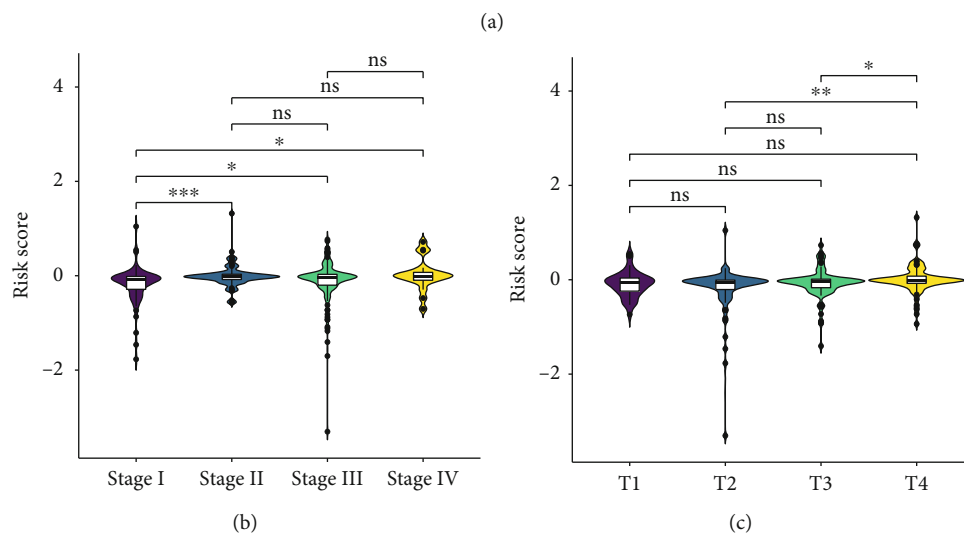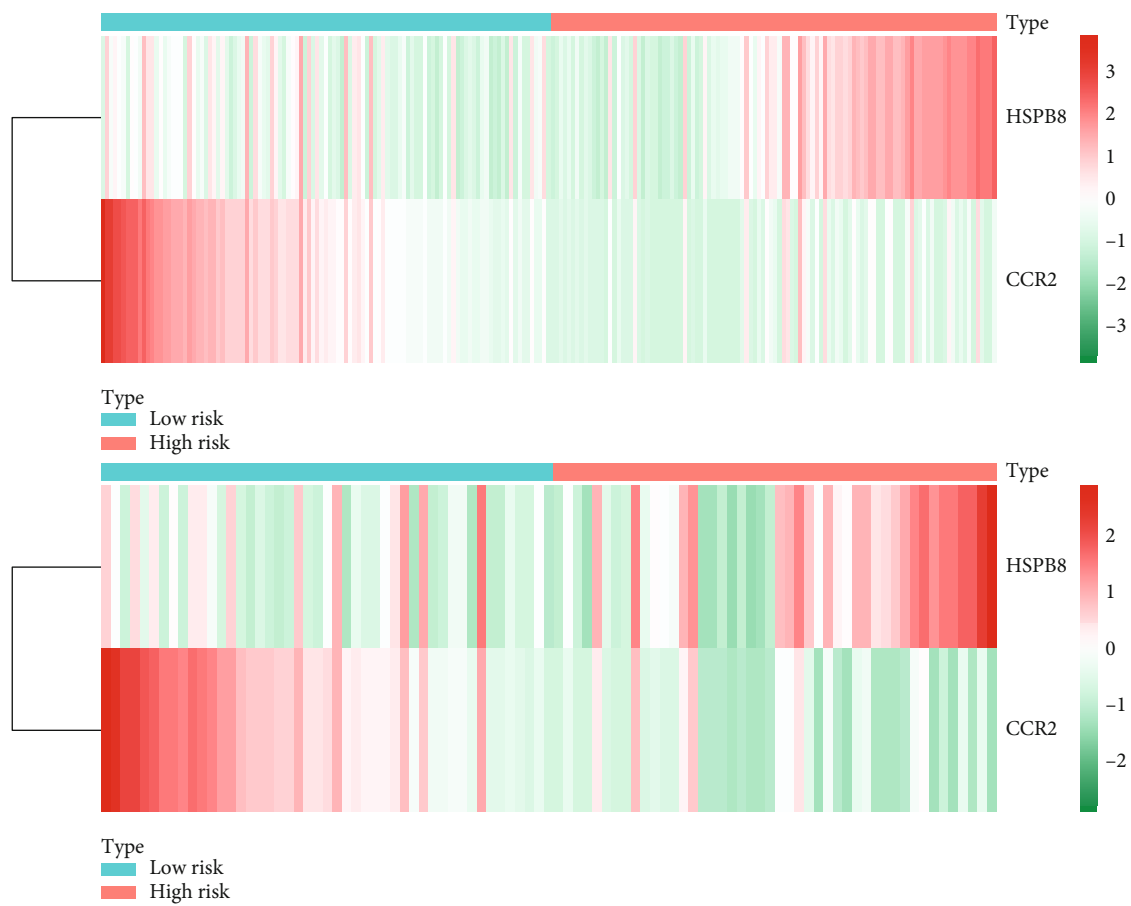
Figure 4: Continued.
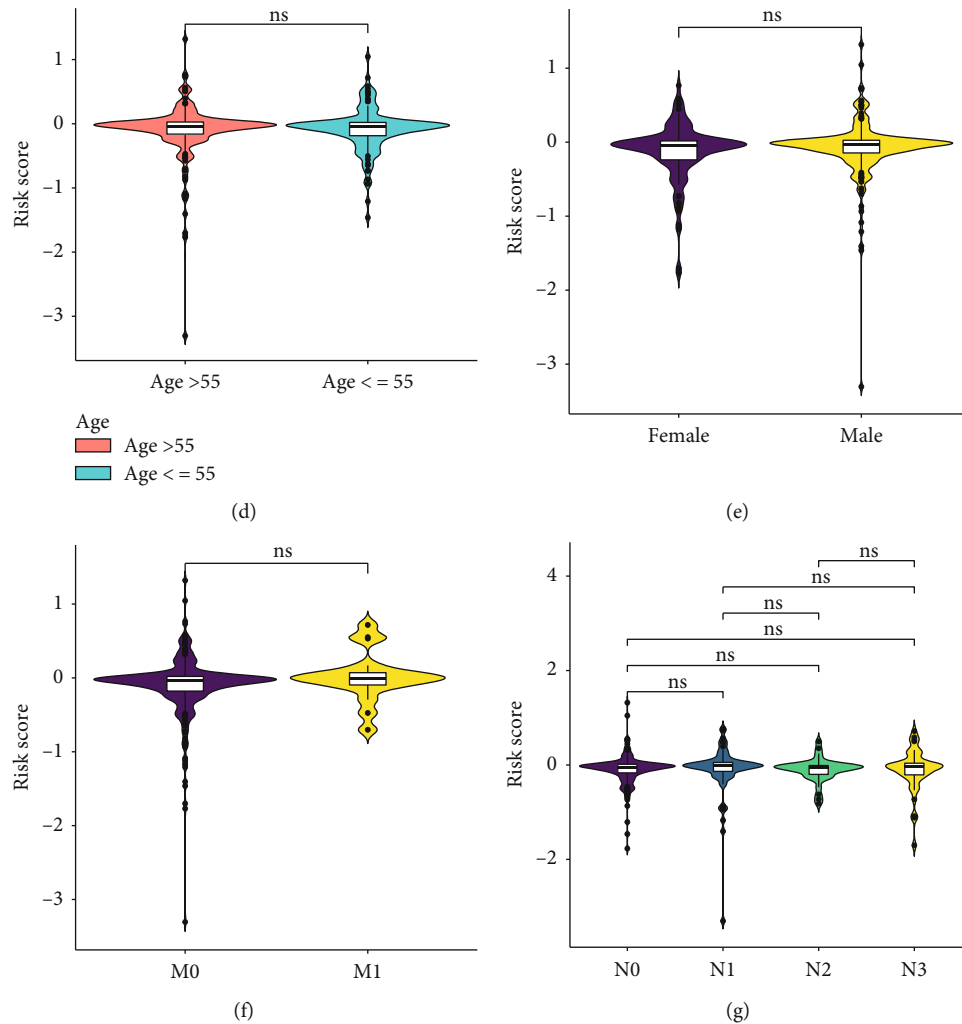
FIGURE 4: The associations between the risk score and the clinicopathological features in patients with metastatic cutaneous melanoma. (a) The expression of the two screened ARGs between the low- and high-risk samples in the TCGA dataset are displayed by heatmaps. Left: training set; right: validation set. Red for high risk; blue line for Low risk. (b)–(g) Violin plot for the associations between the risk score and clinicopathological features, involved with stage and T stage, age, gender, M, and N stage, respectively. ns: no significance; *: $P < 0.05$; **: $P < 0.01$; ***: $P < 0.001$.

Taken together, all the results suggested the reliable predicting performance exhibited by the prognosis signature constructed by the two ARGs.

3.3. The Associations between the Risk Score and the Clinicopathological Features in Cases with Metastatic Cutaneous Melanoma. The expression of the two screened ARGs of the small- and great-risk samples within the TCGA dataset is illustrated by heatmaps (Figure 4(a)). We observed differences with statistical significance in these groups within the training and test sets. To further investigate the associations of the risk scores and clinicopathology characteristics, this study quantitatively analyzed the risk score in metastatic cutaneous melanoma (Figures 4(b)–4(g)). As a result, the risk scores and the survival probability were both significantly different in these groups with the TCGA dataset compartmentalized by Phase and T phase. However, the risk scores were no significant differences in these groups divided by age, gender, M, and N phase. Moreover, the survival

probability was significantly different in these groups classified by age and N phase.

By the same taken, we performed the stratified survival investigation on the clinicopathological features. According to Figure 5(a), greater risk scores showed relations to lower survival according to male cases, whereas female cases showed an insignificant difference. Furthermore, high-risk score noticeably caused a poorer OS in metastatic cutaneous melanoma cases with Phase I-II, Phase III-IV (Figure 5(b)), M0, N0, and N1, whereas it was not found to be risk factors in terms of metastatic cutaneous melanoma cases with phase M1 (Figures 5(c) and 5(d)). The results demonstrated that the risk scores identified by two ARGs were significantly correlated with metastatic cutaneous melanoma.

3.4. Individual Prognosis Value Achieved by the 2-Gene Signature within Metastatic Cutaneous Melanoma. To further demonstrate whether this risk score acted as an individual factor in terms of the prediction of the course of

(a)

(b)
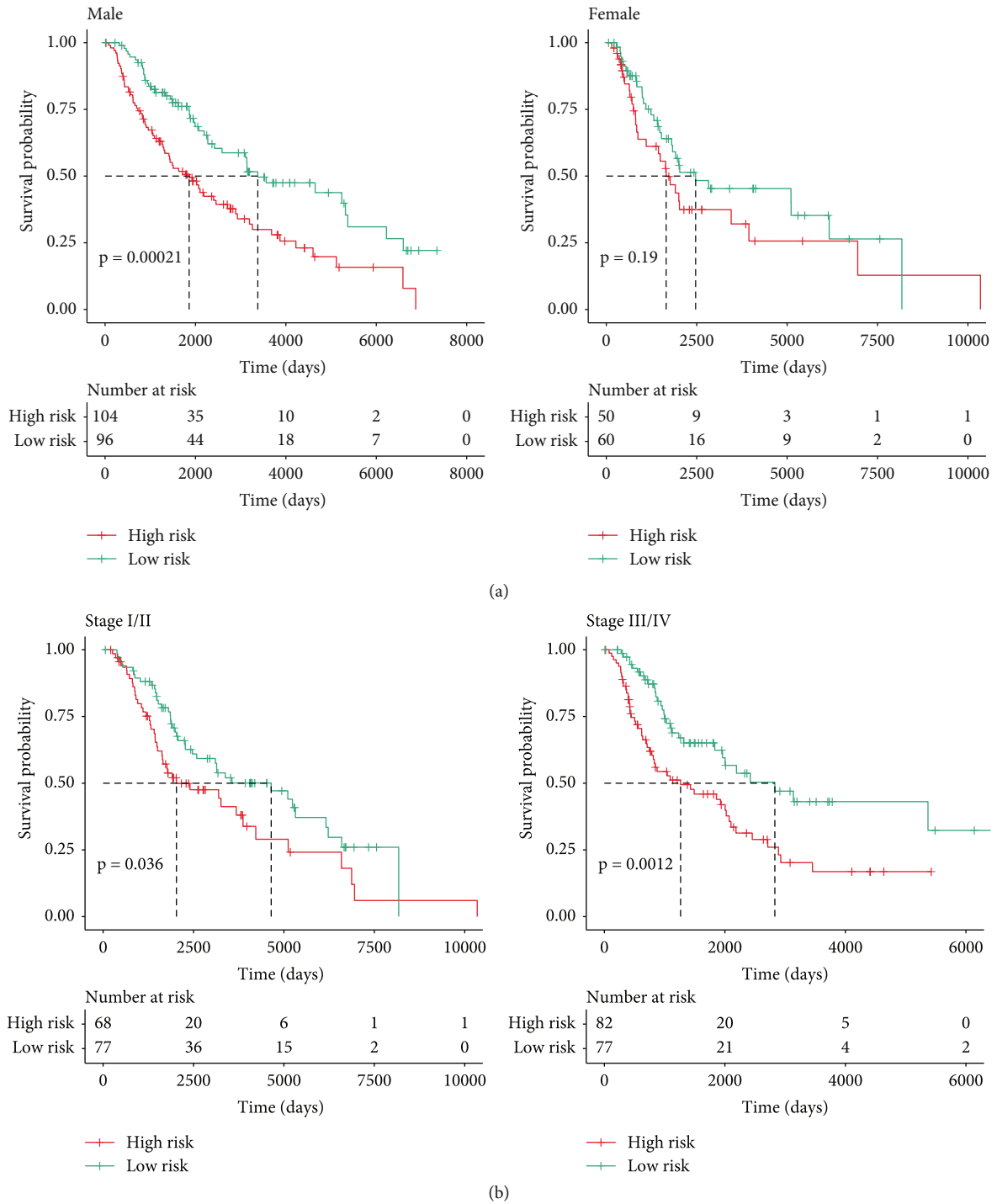
FIGURE 5: Continued.

(c)

(d)
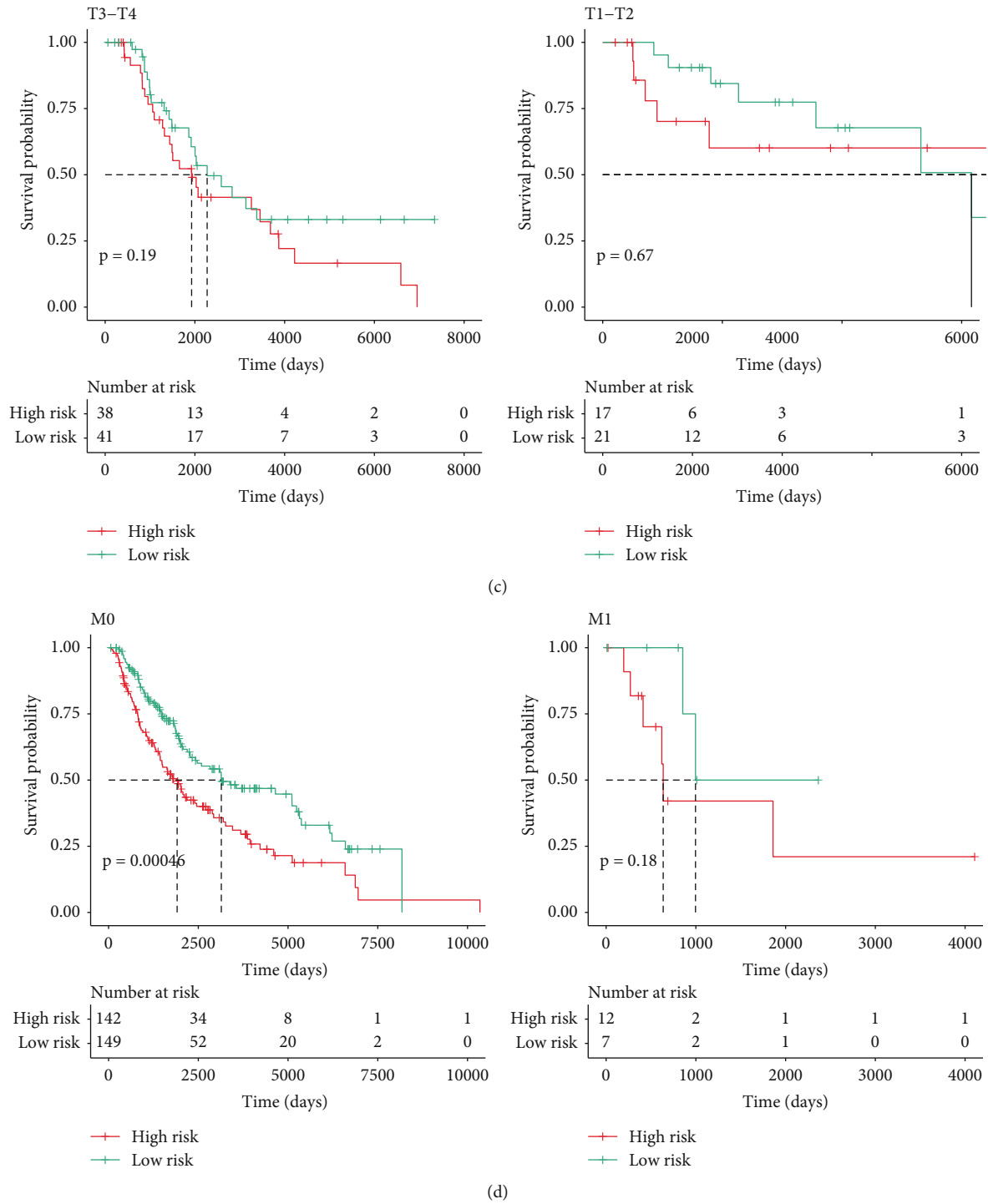
FIGURE 5: The survival analysis between the risk score and the stratified clinicopathological features in patients with metastatic cutaneous melanoma. (a)–(d) The K-M survival analysis of the metastatic cutaneous melanoma patients between high-risk score had and low-risk patients in overall survival, involved with stage I-II, stage III-IV, M0, M1, N0, and N1, respectively; red line for high risk; green line for low risk.

metastatic cutaneous melanoma according to the clinico-pathology characteristics of age, gender, T phase, N phase, M phase, and Pathological Phase. The result of univariate Cox regression investigations indicated that the risk score, age, pathologic phase, T phase, and N phase showed notice-able relations to the prediction of the course of metastatic

cutaneous melanoma (Figure 6(b), $P < 0.05$). Based on these significant clinicopathological features, we further performed Cox regression investigation based on multiple variates. As revealed from the result, the risk score, T phase, N phase, and age are significantly correlated with the OS (Figure 6(b), $P < 0.05$).

	Pvalue	Hazard ratio
Age	<0.001	1.023 (1.012–1.034)
Gender	0.999	1.000 (0.723–1.383)
Pathologic_stage	<0.001	1.341 (1.132–1.587)
Pathologic_t	<0.001	1.216 (1.099–1.346)
Pathologic_m	0.065	1.965 (0.960–4.022)
Pathologic_n	<0.001	1.297 (1.142–1.474)
Risk score	<0.001	2.492 (1.540–4.032)

Hazard ratio

(a)

	Pvalue	Hazard ratio
Age	<0.001	1.018 (1.007–1.029)
Pathologic_stage	0.180	1.143 (0.940–1.389)
Pathologic_t	0.010	1.145 (1.033–1.269)
Pathologic_n	0.008	1.214 (1.051–1.402)
Risk score	<0.001	2.455 (1.519–3.968)

Hazard ratio

(b)

FIGURE 6: Independent prognostic value of the 2-gene signature in metastatic cutaneous melanoma. (a) The result of univariate Cox regression between the risk score and clinicopathological features of age, gender, T stage, N stage, M stage, and pathological stage. (b) The result of multivariate Cox regression between the risk score and clinicopathological features of age, gender, T stage, N stage, M stage, and pathological stage.

3.5. Development and Evaluation of the Nomogram for OS in Metastatic Cutaneous Melanoma. Then, we established the nomogram using the five clinicopathological features including risk score, age, pathologic phase, T phase, and N phase (Figure 7(a)). The accurate prediction efficiency of 1-year survival and 3-year survival in the TCGA database was investigated by the calibration curve (Figure 7(b)). Moreover, according to the analysis in terms of decision curve (DCA), the risk model with the addition of clinicopathological features showed better net benefit than the risk only model (Figure 7(c)), which suggested the ability of the nomogram in the accurate prediction of the prognosis of metastatic cutaneous melanoma cases.

3.6. Functional Analyses in the TCGA Database. Furthermore, GSVA was performed for elucidating the biology process and channels related to the risk score. According to Figure 8(a), many immune-related GO terms, including GO_TOLL_LIKE_ RECEPTOR_7_SIGNALING_PATHWAY, GO_REGULA-TION_OF_NATURAL_KILLER_CELL_MEDIATED_IMMU-NITY, GO_NATURAL_KILLER_CELL_CHEMOTAXIS, GO_ T_CELL_ACTIVATION_VIA_T_CELL_RECEPTOR_CON-TACT_WITH_ANTIGEN_BOUND_TO_MHC_MOLECULE _ON_ANTIGEN_PRESENTING_CELL, and GO_POSITIVE_ REGULATION_OF_TYPE_2_IMMUNE_RESPONSE, showed enrichment within the groups with the score based on small risks. Besides, the KEGG pathway analyses also indicated the KEGG_INTESTINAL_IMMUNE_NETWORK_

FOR_IGA_PRODUCTION, KEGG_PRIMARY _IMMUNODEFICIENCY, KEGG_ANTIGEN_PROCESS-ING_AND_PRESENTATION, KEGG_AUTOIMMUNE_ THYROID_DISEASE, KEGG_GRAFT_VERSUS_HOST_DIS-EASE, KEGG_ALLOGRAFT_REJECTION, and KEGG_ TYPE_I_DIABETES_MELLITUS were enriched in high-risk groups (Figure 8(b)), further suggesting that these prognostic genes might participate in the progression of cutaneous melanoma metastasis.

3.7. The Landscape of Immune Infiltration within Metastatic Cutaneous Melanoma. With the use of the ESTIMATE, the content of stromal and immunization cells within metastatic cutaneous melanoma tumor tissues was calculated. We found that the immunization and stromal scores achieved by the group based on great risks exceeded those achieved by the group based on low risks (Figures 9(a) and 9(b), $P < 0.05$). Moreover, we analyzed the ESTIMATE of the two groups and obtained the same trends (Figure 9(c), $P < 0.05$). To investigate relations of the score of risk and immunization state, this study determined the enrichment score of immunization gene sets. Interestingly, the score of Th1 cells, TFH, Tem, Tcm, T helper cells, T cells, pDC NK CD56dim cells, neutrophils, mast cells, macrophages, iDC, iDC, eosinophils, DC, cytotoxic cells, CD8 T cells, B cells, aDC, Th17 cells, Th2 cells, and TReg showed noticeable distinctions in the groups based on small and great risks in the TCGA group (all $P < 0.05$, Figure 9(d)). Accordingly, the immune

(a)

(b)

(c)
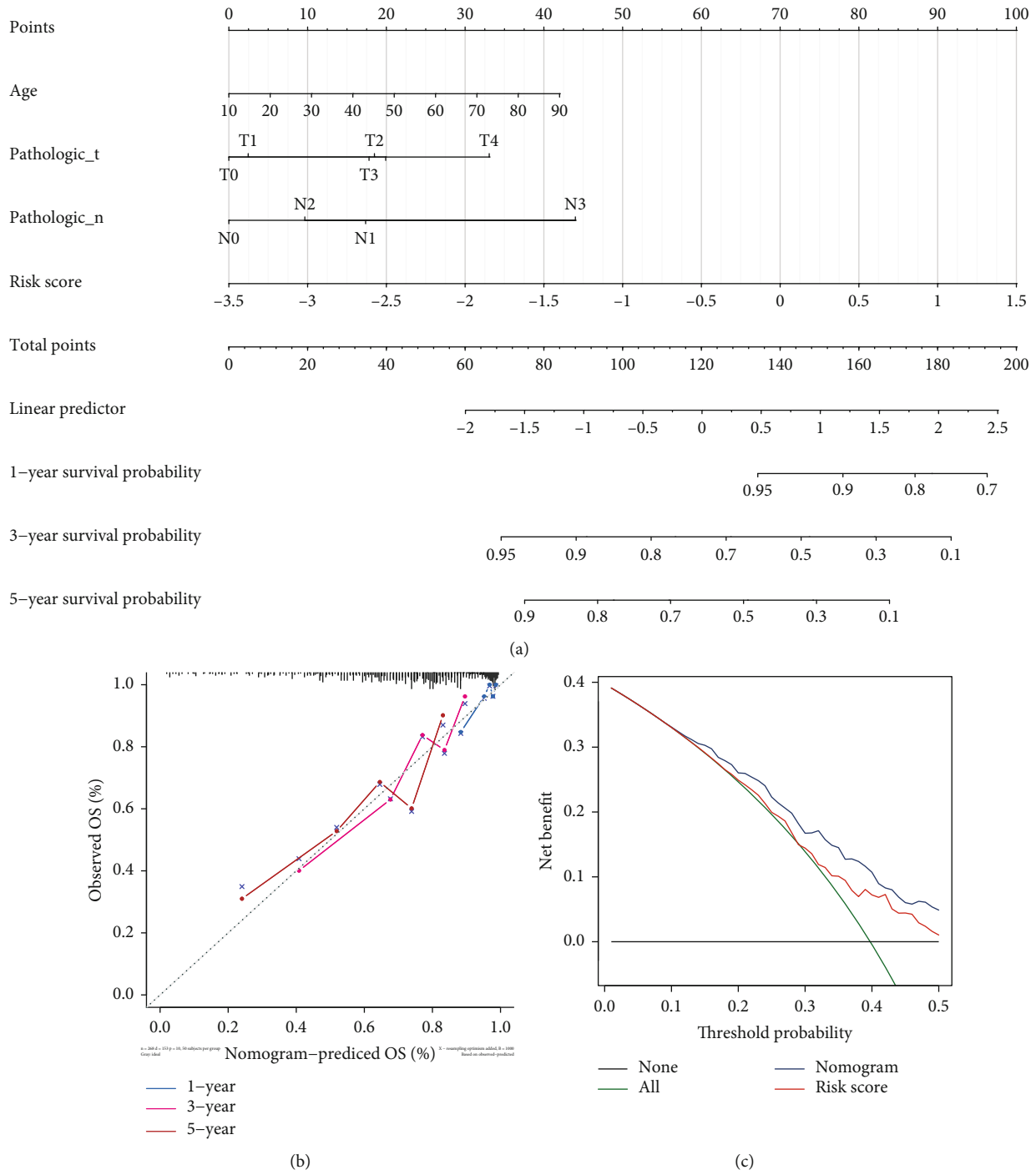
FIGURE 7: Clinical prediction model of clinicopathological features for OS in metastatic cutaneous melanoma. (a) The nomogram plot using the five clinicopathological features including risk score, age, pathologic stage, T stage, and N stage to predict the OS. (b) The calibration curve for accurate prediction efficiency of 1-, 3-, and 5- year survival in the TCGA database. (c) The decision curve analysis (DCA) compared the risk model with the addition of clinicopathological features by net benefit.

infiltration in metastatic cutaneous melanoma may act as targets for immunotherapy and may have potential clinical implications.

3.8. *The Expressions of Immune Checkpoint Molecules.* Programmed cell death receptor ligand 1 (PD-L1) and blocking programmed cell death 1 receptor (PD-1) have been a spe-

cial interest in developing antibodies for a subset of cancer cases (PMID: 31488176). Therefore, immune checkpoint proteins have diverse clinical implications in the immunotherapy of cancers. We then investigated any potential relation of the score of risk and the expressions achieved by immunization checkpoint molecules. According to Figure 10, the metastatic cutaneous melanoma cases

(a)

(b)
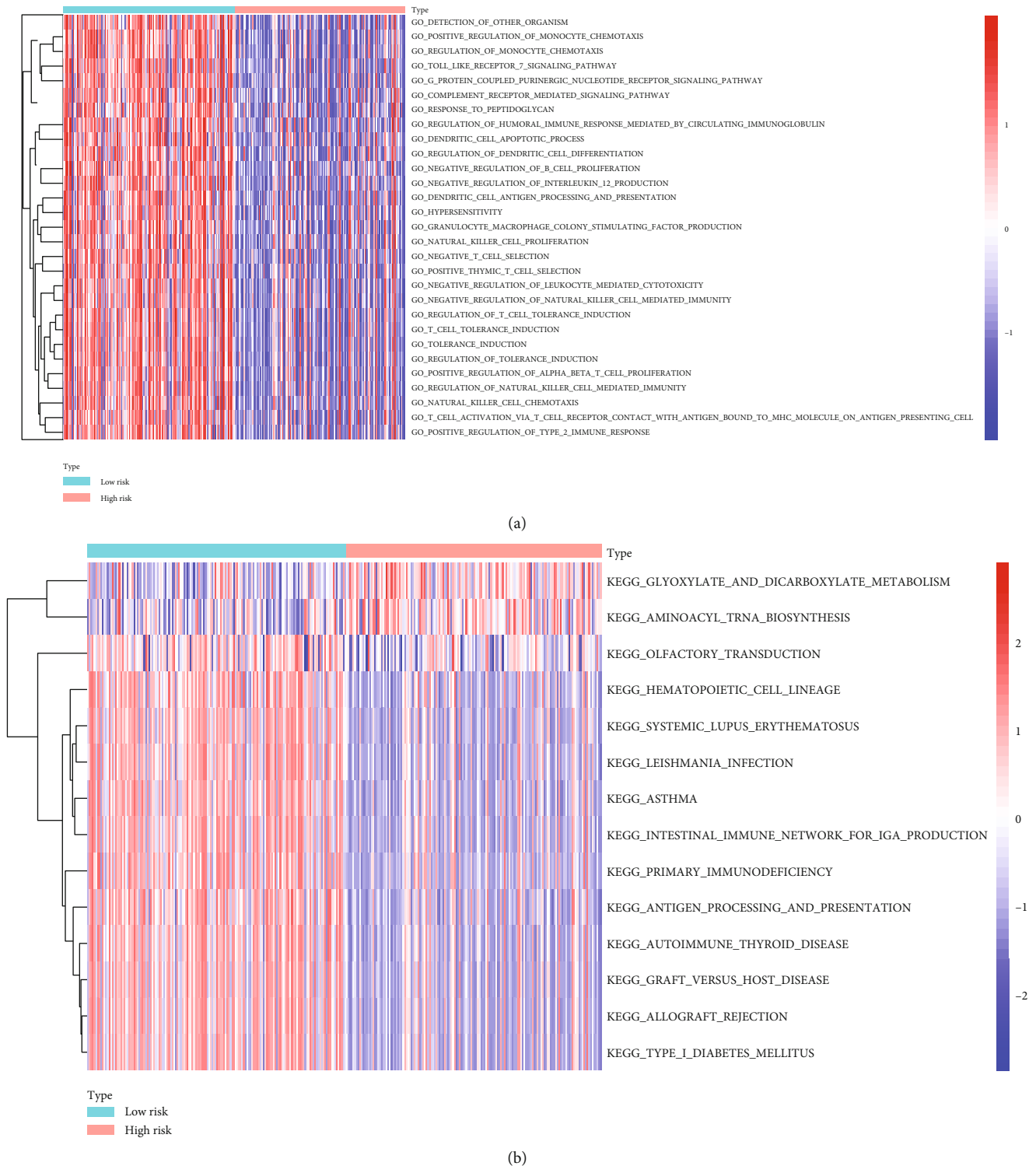
FIGURE 8: The result of functional analyses in the TCGA database. (a) GSVA analysis to elucidate the biological processes and pathways related to the risk score for GO Terms. (b) GSVA analysis to elucidate the biological processes and pathways related to the risk score for KEGG terms.

achieving low-risk score had greater expression of immune checkpoint molecules than the high-risk group. Accordingly, the low-risk cases suffering from metastatic cutaneous melanoma might have a more promising treatment to respond for immunotherapies.

4. Discussion

Autophagy and autophagy-related genes play an important role in metastatic cutaneous melanoma. Ryabaya et al. reported that autophagy inhibitor integration chloroquine
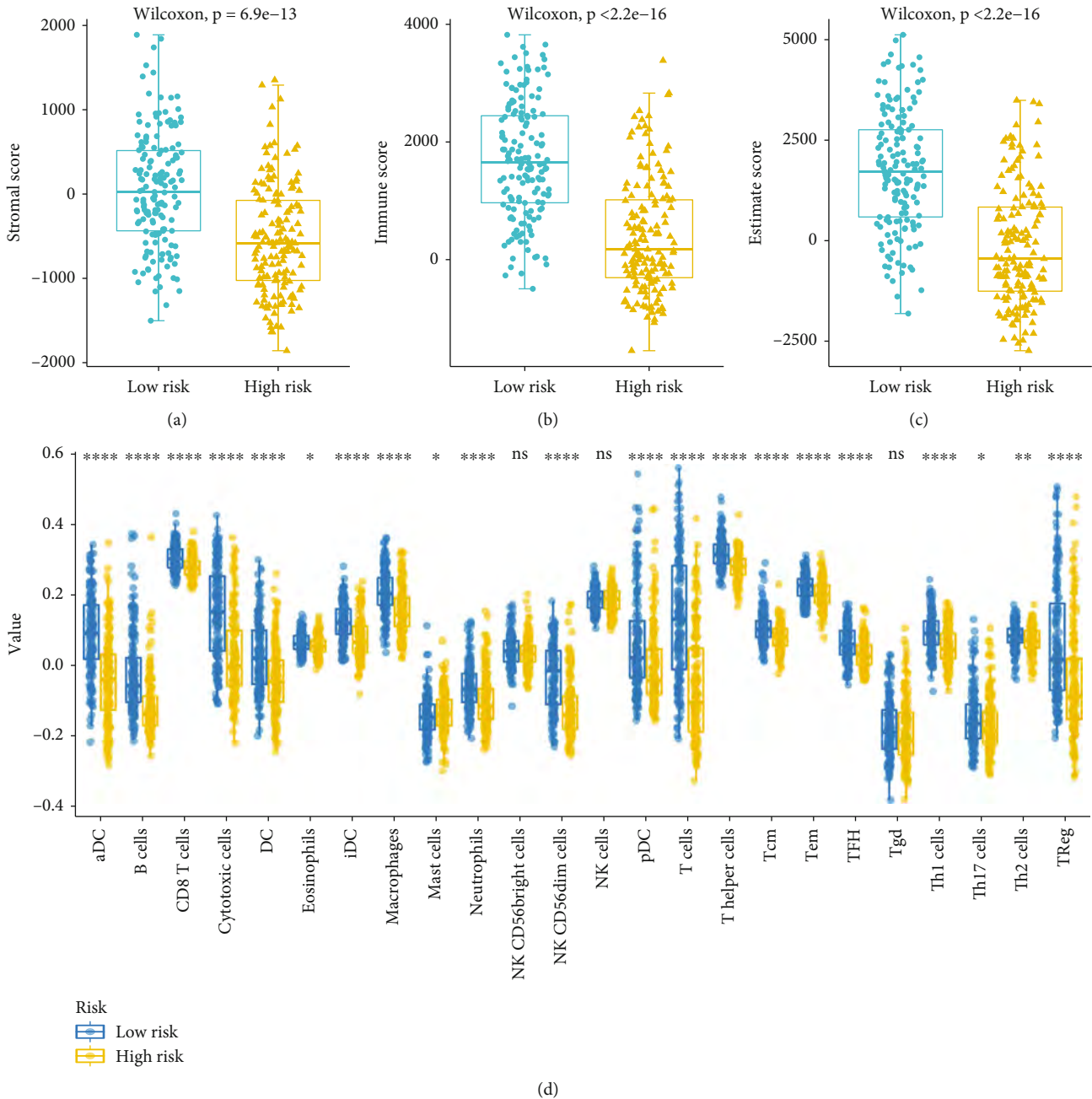
FIGURE 9: The landscape of immune infiltration in metastatic cutaneous melanoma. (a) ESTIMATE algorithm result of stromal score in metastatic cutaneous melanoma tumor between low risk and high risk. (b) ESTIMATE algorithm result of immune score in metastatic cutaneous melanoma tumor between low risk and high risk. (c) ESTIMATE score in metastatic cutaneous melanoma tumor between low risk and high risk. (d) The correlation between the risk score and immune status, aDC, B cells, CD8 T cells, cytotoxic cells, DC, eosinophils, iDC, macrophages, mast cells, neutrophils, NK CD56dim cells, pDC, T cells, T helper cells, Tcm, Tem, TFH, Th1 cells, Th17 cells, Th2 cells, and Treg between the low-risk and high-risk groups in the TCGA cohort. ns: no significance; ∗: $P < 0.05$; ∗∗: $P < 0.01$; ∗∗∗: $P < 0.001$.

or LY294002 and TMZ could enhance the cytotoxicity of alkylating agents on human melanoma cell lines [22]. Zhang et al. investigated that CX-F9, a novel Ribosomal S6 Kinase 2 (RSK2) inhibitor, could significantly suppress the proliferation, invasion, and autophagy of melanoma in vitro and in vivo [23]. In the present study, thirteen ARGs showed correlations to OS in the Cox regression investigation based on a single variate. A 2-gene signature was developed, which

stratified metastatic cutaneous melanoma cases into the groups based on great and small risks. Cases with metastatic cutaneous melanoma in the high-risk group had worse OS than that of the group based on small risks. The risk score, T phase, N phase, and age were proved to be individual factors for predicting OS. Besides, the risk scores identified by the two ARGs were significantly correlated with metastatic cutaneous melanoma. Receiver operating characteristic
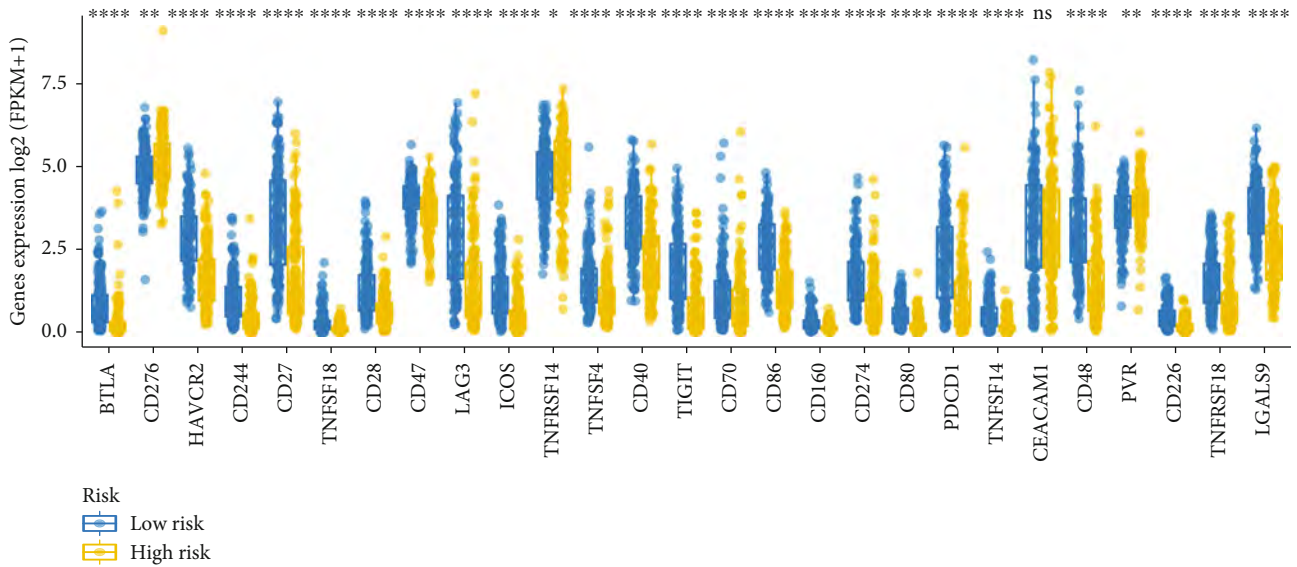
FIGURE 10: The expression of immune checkpoint molecules and the correlation between immune checkpoint molecules and risk score in the TCGA cohort. ns: no significance; ∗: $P < 0.05$; ∗∗: $P < 0.01$; ∗∗∗: $P < 0.001$.

(ROC) curve analysis demonstrated accurate predictive performance of the 2-gene signature. Functional enrichment analysis indicated that immune-related biological processes and channels were significantly enriched. The infiltrating immune cell content was different between the two risk groups. We also found that the immune scores and stromal scores of the high-risk group were higher compared with that of group based on low risks. The metastatic cutaneous melanoma cases achieving low-risk scores had greater expression of immune checkpoint molecules as compared with the high-risk group.

Although autophagy-related genes play a crucial role in some diseases, there is no comprehensive study on the prognosis and immunotherapy of autophagy-related genes in cases suffering from metastatic cutaneous melanoma. This study reports for the first time the role of autophagy-related genes in the prognosis and immunotherapy of cases with metastatic cutaneous melanoma. The risk models of HspB8 and CCR2 were established by univariate Cox and multivariate Cox analysis. HspB8 acts as an oncogene in several cancers. Shen et al. reported that HSPB8 promoted cancer cell growth by activating the ERK-CREB pathway and predicted a poor prognosis in gastric cancer cases [24]. The expression of HSPB8 is investigated to correlate with breast cancer progression [25]. In addition, HSPB8 is responsible for the rug resistance of breast cancer cells. The mTOR inhibitor (AZD8055) could inhibit the tamoxifen resistance in breast cancer cells by suppressing the expression of HSPB8 [26]. Several studies have shown that CCR2 acts as a novel biomarker in metastatic cutaneous melanoma [27, 28]. Furthermore, Zhang et al. demonstrated that Toll-like receptors 7 and 8 expression correlated with the expression of immune biomarkers (CCR2, CCR5, CCL3, and CCL5) and positively predicted the clinical outcome of cases with melanoma [29]. This work is the first time to stratify cases with metastatic cutaneous melanoma based on autophagy-

related genes, which provides new insights for predicting the efficacy of immunotherapy and possible differentiation targets.

We further performed functional analyses of ARGs in the TCGA database. The results of GSVA elucidated that autophagy-related genes may be closely related to tumor immunity. For example, the ARGs were enriched in GO_TOLL_LIKE_RECEPTOR_7_SIGNALING_PATHWAY, GO_NATURAL_KILLER_CELL_CHEMOTAXIS, and GO_POSITIVE_REGULATION_OF_TYPE_2_IMMUNE_RESPONSE. These pathways are associated with the tumor immunity of melanoma [30–32]. The KEGG pathway analyses also indicated the KEGG_INTESTINAL_IMMUNE_NETWORK_FOR_IGA_PRODUCTION, KEGG_PRIMARY_IMMUNODEFICIENCY, KEGG_ANTIGEN_PROCESSING_AND_PRESENTATION, KEGG_AUTOIMMUNE_THYROID_DISEASE, KEGG_GRAFT_VERSUS_HOST_DISEASE, KEGG_ALLOGRAFT_REJECTION, and KEGG_TYPE_I_DIABETES_MELLITUS were enriched in high-risk groups. These pathways participated in the process of immune escape in cutaneous melanoma metastasis [33, 34]. The results revealed that these prognostic genes might participate in the progression of cutaneous melanoma metastasis.

Since the discovery of immune checkpoint proteins, the development of antibodies against programmed cell death receptor-1 (PD-1) and programmed cell death receptor ligand-1 (PD-L1) has aroused special interest in the treatment of some cancer cases [35, 36]. PD-1 signal carries out the negative regulation of T cell-mediated immune response, which is one of the mechanisms of tumor escaping antigen-specific T cell immune response [37]. It facilitates tumor development and progression by improving the survival rate of tumor cells [38]. In this context, PD-1 signaling is a valuable new and effective target for cancer immunotherapy. Javed et al. reported that significant differences existed in PD-L1 expression between metastatic uveal melanoma and

metastatic cutaneous melanoma. The higher PD-L1 expression was observed in metastatic cutaneous melanoma [39]. This work reported that the expressions achieved by the mentioned key immune checkpoints increased in the group based on small risks. The key immune checkpoints including BTLA, CD86, CD244, and PDCD1 are recognized as predictors of sentinel lymph node metastasis in cutaneous melanoma [40, 41]. Our results indicated that the low-risk cases with metastatic cutaneous melanoma might have a more promising treatment to respond for immunotherapies.

In conclusion, the 2-ARG gene signature indicates a novel prognostic indicator for prognosis prediction of metastatic cutaneous melanoma, which served as an important tool for guiding the clinical treatment of cutaneous melanoma.

Data Availability

The datasets used and analyzed during the current study are available from the corresponding author on reasonable request.

Ethical Approval

Ethical approval is not necessary.

Conflicts of Interest

The authors declare that there is no conflict of interest regarding the publication of this paper.

Authors' Contributions

Cao-Jie Chen, Shigeki Sakai, and Kazuo Kishi conceived and designed the study. Cao-Jie Chen, Hiroki Kajita, and Noriko Aramaki-Hattori did bioinformatics analysis and wrote the manuscript. Shigeki Sakai and Noriko Aramaki-Hattori had supervised this project and contributed to writing and revision of the manuscript. All authors contributed to the article and approved the submitted version.

References

[1] R. I. Hartman and J. Y. Lin, "Cutaneous Melanoma–A Review in Detection, Staging, and Management," *Hematology/Oncology Clinics of North America*, vol. 33, no. 1, pp. 25–38, 2019.

[2] D. Coricovac, C. Dehelean, E. A. Moaca et al., "Cutaneous melanoma-a long road from experimental models to clinical outcome: a review," *International Journal of Molecular Sciences*, vol. 19, no. 6, p. 1566, 2018.

[3] J. Read, K. A. Wadt, and N. K. Hayward, "Melanoma genetics," *Journal of Medical Genetics*, vol. 53, no. 1, pp. 1–14, 2016.

[4] K. W. Nassar and A. C. Tan, "The mutational landscape of mucosal melanoma," *Seminars in Cancer Biology*, vol. 61, pp. 139–148, 2020.

[5] B. Tang, Z. Chi, and J. Guo, "Toripalimab for the treatment of melanoma," *Expert Opinion on Biological Therapy*, vol. 20, no. 8, pp. 863–869, 2020.

[6] P. Gorayski, B. Burmeister, and M. Foote, "Radiotherapy for cutaneous melanoma: current and future applications," *Future Oncology*, vol. 11, no. 3, pp. 525–534, 2015.

[7] S. A. Weiss, D. Hanniford, E. Hernando, and I. Osman, "Revisiting determinants of prognosis in cutaneous melanoma," *Cancer*, vol. 121, no. 23, pp. 4108–4123, 2015.

[8] N. Mizushima and M. Komatsu, "Autophagy: renovation of cells and tissues," *Cell*, vol. 147, no. 4, pp. 728–741, 2011.

[9] F. Nazio, M. Bordi, V. Cianfanelli, F. Locatelli, and F. Cecconi, "Autophagy and cancer stem cells: molecular mechanisms and therapeutic applications," *Cell Death and Differentiation*, vol. 26, no. 4, pp. 690–702, 2019.

[10] B. Levine and G. Kroemer, "Biological functions of autophagy genes: a disease perspective," *Cell*, vol. 176, no. 1-2, pp. 11–42, 2019.

[11] A. V. Onorati, M. Dyczynski, R. Ojha, and R. K. Amaravadi, "Targeting autophagy in cancer," *Cancer*, vol. 124, no. 16, pp. 3307–3318, 2018.

[12] C. G. Towers, B. E. Fitzwalter, D. Regan et al., "Cancer cells upregulate NRF2 signaling to adapt to autophagy inhibition," *Developmental Cell*, vol. 50, no. 6, pp. 690–703.e6, 2019.

[13] Z. Cheng, "The FoxO-autophagy axis in health and disease," *Trends in Endocrinology and Metabolism*, vol. 30, no. 9, pp. 658–671, 2019.

[14] P. Boya, F. Reggiori, and P. Codogno, "Emerging regulation and functions of autophagy," *Nature Cell Biology*, vol. 15, no. 7, pp. 713–720, 2013.

[15] H. Xiang, J. Zhang, C. Lin, L. Zhang, B. Liu, and L. Ouyang, "Targeting autophagy-related protein kinases for potential therapeutic purpose," *Acta Pharmaceutica Sinica B*, vol. 10, no. 4, pp. 569–581, 2020.

[16] R. K. Amaravadi, A. C. Kimmelman, and J. Debnath, "Targeting autophagy in cancer: recent advances and future directions," *Cancer Discovery*, vol. 9, no. 9, pp. 1167–1181, 2019.

[17] D. Glick, S. Barth, and K. F. Macleod, "Autophagy: cellular and molecular mechanisms," *The Journal of Pathology*, vol. 221, no. 1, pp. 3–12, 2010.

[18] M. E. Ritchie, B. Phipson, D. Wu et al., "Limma powers differential expression analyses for RNA-sequencing and microarray studies," *Nucleic Acids Research*, vol. 43, no. 7, article e47, 2015.

[19] P. Lin, R. Q. He, F. C. Ma et al., "Systematic analysis of survival-associated alternative splicing signatures in gastrointestinal pan-adenocarcinomas," *eBioMedicine*, vol. 34, pp. 46–60, 2018.

[20] S. Hänzelmann, R. Castelo, and J. Guinney, "GSVA: gene set variation analysis for microarray and RNA-seq data," *BMC Bioinformatics*, vol. 14, no. 1, p. 7, 2013.

[21] O. O. Yavorska and S. Burgess, "MendelianRandomization: an R package for performing Mendelian randomization analyses using summarized data," *International Journal of Epidemiology*, vol. 46, no. 6, pp. 1734–1739, 2017.

[22] O. O. Ryabaya, A. N. Inshakov, A. V. Egorova et al., "Autophagy inhibitors chloroquine and LY294002 enhance temozolomide cytotoxicity on cutaneous melanoma cell lines in vitro," *Anti-Cancer Drugs*, vol. 28, no. 3, pp. 307–315, 2017.

[23] X. Zhang, L. Cai, S. Zhao et al., "CX-F9, a novel RSK2 inhibitor, suppresses cutaneous melanoma cells proliferation and metastasis through regulating autophagy," *Biochemical Pharmacology*, vol. 168, pp. 14–25, 2019.

[24] J. Shen, M. Li, and L. Min, "HSPB8 promotes cancer cell growth by activating the ERK-CREB pathway and is indicative of a poor prognosis in gastric cancer patients," *Oncology Reports*, vol. 39, no. 6, pp. 2978–2986, 2018.

[25] J. J. Shi, S. M. Chen, C. L. Guo, Y. X. Li, J. Ding, and L. H. Meng, "The mTOR inhibitor AZD8055 overcomes tamoxifen resistance in breast cancer cells by down-regulating HSPB8," *Acta Pharmacologica Sinica*, vol. 39, no. 8, pp. 1338–1346, 2018.

[26] S. M. Chen, C. L. Guo, J. J. Shi et al., "HSP90 inhibitor AUY922 abrogates up-regulation of RTKs by mTOR inhibitor AZD8055 and potentiates its antiproliferative activity in human breast cancer," *International Journal of Cancer*, vol. 135, no. 10, pp. 2462–2474, 2014.

[27] M. M. Tu, H. A. Abdel-Hafiz, R. T. Jones et al., "Inhibition of the CCL2 receptor, CCR2, enhances tumor response to immune checkpoint therapy," *Commun Biol*, vol. 3, no. 1, p. 720, 2020.

[28] S. F. Ngiow, D. A. Knight, A. Ribas, G. A. McArthur, and M. J. Smyth, "BRAF-targeted therapy and immune responses to melanoma," *Oncoimmunology*, vol. 2, no. 6, article e24462, 2013.

[29] M. Zhang, Z. Yan, J. Wang, and X. Yao, "Toll-like receptors 7 and 8 expression correlates with the expression of immune biomarkers and positively predicts the clinical outcome of patients with melanoma," *Oncotargets and Therapy*, vol. - Volume 10, pp. 4339–4346, 2017.

[30] M. Rathore, C. Girard, M. Ohanna et al., "Cancer cell-derived long pentraxin 3 (PTX3) promotes melanoma migration through a toll-like receptor 4 (TLR4)/NF-κB signaling pathway," *Oncogene*, vol. 38, no. 30, pp. 5873–5889, 2019.

[31] J. Kim, J. S. Kim, H. K. Lee et al., "CXCR3-deficient natural killer cells fail to migrate to B16F10 melanoma cells," *International Immunopharmacology*, vol. 63, pp. 66–73, 2018.

[32] R. Fang, H. Hara, S. Sakai et al., "Type I interferon signaling regulates activation of the absent in melanoma 2 inflammasome during Streptococcus pneumoniae infection," *Infection and Immunity*, vol. 82, no. 6, pp. 2310–2317, 2014.

[33] L. Huang, H. Chen, Y. Xu, J. Chen, Z. Liu, and Q. Xu, "Correlation of tumor-infiltrating immune cells of melanoma with overall survival by immunogenomic analysis," *Cancer Medicine*, vol. 9, no. 22, pp. 8444–8456, 2020.

[34] G. Kamińska-Winciorek, B. Cybulska-Stopa, I. Lugowska, M. Ziobro, and P. Rutkowski, "Principles of prophylactic and therapeutic management of skin toxicity during treatment with checkpoint inhibitors," *Advances in Dermatology and Allergology/Postępy Dermatologii i Alergologii*, vol. 36, no. 4, pp. 382–391, 2019.

[35] F. Schütz, S. Stefanovic, L. Mayer, A. von Au, C. Domschke, and C. Sohn, "PD-1/PD-L1 pathway in breast cancer," *Oncology Research and Treatment*, vol. 40, no. 5, pp. 294–297, 2017.

[36] F. K. Dermani, P. Samadi, G. Rahmani, A. K. Kohlan, and R. Najafi, "PD-1/PD-L1 immune checkpoint: potential target for cancer therapy," *Journal of Cellular Physiology*, vol. 234, no. 2, pp. 1313–1325, 2019.

[37] J. H. Cha, L. C. Chan, C. W. Li, J. L. Hsu, and M. C. Hung, "Mechanisms controlling PD-L1 expression in cancer," *Molecular Cell*, vol. 76, no. 3, pp. 359–370, 2019.

[38] A. Rotte, "Combination of CTLA-4 and PD-1 blockers for treatment of cancer," *Journal of Experimental & Clinical Cancer Research*, vol. 38, no. 1, p. 255, 2019.

[39] A. Javed, D. Arguello, C. Johnston et al., "PD-L1 expression in tumor metastasis is different between uveal melanoma and cutaneous melanoma," *Immunotherapy*, vol. 9, no. 16, pp. 1323–1330, 2017.

[40] D. M. Barrios, M. H. Do, G. S. Phillips et al., "Immune checkpoint inhibitors to treat cutaneous malignancies," *Journal of the American Academy of Dermatology*, vol. 83, no. 5, pp. 1239–1253, 2020.

[41] U. Sahin, P. Oehm, E. Derhovanessian et al., "An RNA vaccine drives immunity in checkpoint-inhibitor-treated melanoma," *Nature*, vol. 585, no. 7823, pp. 107–112, 2020.

日中笹川医学奨学金制度（学位取得コース）中間評価書
論文博士：指導教官用

第 44 期　　研究者番号：G4406　　　　　　　　　　作成日 ：2023 年 3 月 10 日

氏　名	趙　宏波	ZHAO HONGBO	性別	M	生年月日	1980/10/11
所属機関（役職）	中国医学科学院腫瘍医院深圳医院胸外科（副主任医師）					
研究先（指導教官）	東海大学医学部消化器外科上部消化管グループ（小柳 和夫　教授）					
研究テーマ	食道癌術後縫合不全に対する ICG 蛍光イメージング法の有用性の検討 To investigate the value of Indocyanine Green Fluorescence Imaging (ICGFI) in preventing postoperative anastomotic leakage after esophagectomy					
専攻種別	☑論文博士			□課程博士		

研究者評価（指導教官記入欄）

成績状況	㊵ 良 可 不可	取得単位数
		取得単位数／取得すべき単位総数
学生本人が行った研究の概要	標記研究内容に関して、患者データの取得を行った。それに先立ち、当院規定の電子カルテ操作方法の研修を受け、実際に患者データへのアクセス方法を習得した。食道がん手術に立ち会い、実際の手技を習得した。論文博士の取得のために、当院の語学審査を受験し合格した。	
総合評価	【良かった点】 東海大学で研究に当たり、環境に柔軟に適応した。 教室の医師、臨床研修中の学生、秘書さんなどと、良好な人間関係を構築できた。 共著者として論文執筆に携わった。 【改善すべき点】 特になし 【今後の展望】 研究内容の結果を解析して、論文執筆を行う。 学位取得のための準備を行う。	
学位取得見込	来年度中の審査にむけて準備を進める	

評価者（指導教官名）　小柳　和夫

第44期　　　　　研究者番号： G4406　　　　　作成日：2023年3月6日

氏名	赵 宏波	ZHAO HONGBO	性別	M	生年月日　1980/10/11

所属機関(役職)	中国医学科学院腫瘤医院深圳医院胸外科(副主任医師)

研究先(指導教官)	東海大学医学部消化器外科上部消化管グループ(小柳 和夫　教授)

研究テーマ	食道癌術後縫合不全に対するICG蛍光イメージング法の有用性の検討 To investigate the value of Indocyanine Green Fluorescence Imaging (ICGFI) in preventing postoperative anastomotic leakage after esophagectomy

専攻種別	論文博士	☑	課程博士	☐

1．研究概要(1)

1）目的(Goal)
To investigate the value of Indocyanine Green fluorescence imaging in preventing postoperative anastomotic leakage after esophagectomy.

2）戦略(Approach)
Esophageal cancer is a common and deadly cancer, with esophageal squamous cell carcinoma being the most prevalent type globally. Presently, surgical resection remains a critical component of potentially curative treatment of cancer of the esophagus. However, esophagectomy accompanies with highly morbidity and mortality. Anastomotic fistula is the most common and serious complication after esophagectomy, and the most important factor that leads to long hospital stay and perioperative deaths. The rate of anastomotic leakage reportedly ranges from 6.2% to 27%. There are many factors affecting anastomotic leakage after operation, including blood supply around the anastomotic stoma, tension around the anastomotic stoma and contamination around the anastomotic stoma during operation.

It is widely accepted among surgeons that sufficient blood supply to the esophagus and the site of anastomosis is a crucial factor for successful healing after surgery.

Further elaborating on the topic of blood supply around the anastomotic site after esophageal cancer surgery, it is necessary to consider the blood supply to the gastric conduit and residual esophagus. In the case of cervical anastomosis, the blood supply to the cervical esophagus is generally supplied by the inferior thyroid artery and is relatively stable. Therefore, the quality of blood supply around the anastomotic site is primarily evaluated based on the blood supply to the top of the gastric conduit. When evaluating the quality of organ blood supply, both arterial input and venous output must be considered as they are interdependent and indispensable. If arterial input is poor or venous output is compromised, both can impact the organ's blood circulation. Therefore, when assessing the blood circulation of the gastric conduit after esophageal cancer surgery, attention should not only be given to arterial input via the right gastroepiploic artery but also to ensuring venous output is preserved. In the traditional process of creating a gastric conduit, a vertical incision is made along the lesser curvature of the stomach, starting at a point 5 centimeters from the pylorus. However, a new technique has been employed in our center since 2021, whereby the incision is made on the lesser curvature at the point where the right and left gastric veins converge, and the cutting angle is adjusted to form a blunt angle with the stomach wall towards the proximal end. The purpose of this technique is to preserve the right gastric vein and blood circulation of the gastric body to the greatest extent possible, thereby improving the blood supply to the gastric conduit and reducing the risk of anastomotic leakage.

In recent years, indocyanine green (ICG) fluorescence imaging has emerged as a valuable technique for mapping blood perfusion in the gastrointestinal tract, particularly in cases where a sufficient blood supply is crucial, such as in esophageal surgery. By using ICG fluorescence imaging, surgeons can confirm the adequacy of blood supply at the border and determine the optimal anastomotic site. As previously reported, we have utilized indocyanine green (ICG) imaging to visually assess the blood supply of the gastric conduit and anastomotic site. Furthermore, we have implemented quantitative technological improvements to evaluate the blood supply of the gastric conduit and anastomotic site.

3）材料と方法（Materials and methods）

We conducted a retrospective study between December 2018 and September 2021, which enrolled 249 patients with esophageal cancer who underwent esophagectomy at Tokai University Hospital. During the surgical procedures, we employed the indocyanine green (ICG) fluorescence imaging technique and quantitatively processed the data for all the patients above. Based on the improvement in the modified sleeve gastrectomy technique, which was implemented in 2021 in our center, the patients were divided into two groups.

The cancer stage was determined based on the 8th edition of the International Union Against Cancer TNM Classification of Malignant Tumors. The study was conducted in accordance with the guidelines established by the Institutional Review Board for Clinical Research of the Tokai University School of Medicine, and all patients provided informed consent for the operative procedures and ICG fluorescence imaging study.

Correlations with categorizable variables were evaluated using a chi-square test and the Fisher exact test, while those with continuous variables were evaluated using the Mann-Whitney U test. The Student's t-test or Welch t-test was used to compare the number of dissected LNs after checking for equal variances using the Levene test. The statistical examinations were performed using SPSS 21.0 (IBM SPSS, New York, USA). All tests were two-sided, and p values < 0.05 were considered to indicate statistical significance.

4）実験結果（Results）&5考察（Discussion）

Our research results are currently being discussed and interpreted. As we analyze the data, we are working to understand the implications and draw meaningful conclusions. We are committed to ensuring that our interpretation of the findings is accurate and relevant, and will continue to review and refine our conclusions as necessary.

6）参考文献（References）

1) Rooijens, Pgm P , Smaal, et al. VASCULAR ANATOMY OF THE STOMACH RELATED TO THE CONSTRUCTION OF A SUFFICIENTLY NOURISHED GASTRIC TUBE.[J]. European Journal of Morphology, 2003.

2) Uhlenhopp D J , Then E O , Sunkara T , et al. Epidemiology of esophageal cancer: update in global trends, etiology and risk factors[J]. Clinical Journal of Gastroenterology, 2020, 13(6).

3) Koyanagi, Kazuo, Ozawa, et al. Blood flow speed of the gastric conduit assessed by indocyanine green fluorescence New predictive evaluation of anastomotic leakage after esophagectomy.

4) Sitia L , Sevieri M , Bonizzi A , et al. Development of Tumor-Targeted Indocyanine Green-Loaded Ferritin Nanoparticles for Intraoperative Detection of Cancers[J]. ACS Omega, 2020, 5(21):12035-12045.

5) Ikeda Y, Niimi M, Kan S, et al. Clinical signifcance of tissue blood fow during esophagectomy by laser Doppler fowmetry. J Thorac Cardiovasc Surg. 2001;122:1101-6.

6) Koyanagi, et al. Association between indocyanine green fluorescence blood flow speed in the gastric conduit wall and superior mesenteric artery calcification: predictive significance for anastomotic leakage after esophagectomy[J]. Esophagus, 2021, 18(2):248-257.

7) Koyanagi, et al. Indocyanine green fluorescence imaging for evaluating blood flow in the reconstructed conduit after esophageal cancer surgery[J]. 2021.

8) Settembre N , Labrousse M , Magnan P E , et al. Surgical anatomy of the right gastro-omental artery: a study on 100 cadaver dissections[J]. Anatomia Clinica, 2018, 40(4):1-8.

9) Kodai T , Masahiko M , Akira S , et al. Anatomical and surgical evaluation of gastroepiploic artery[J]. Okajimas Folia Anat Jpn, 2016, 92(3.4):49-52.

10) Takeda F R , Cecconello I , Ph. D , et al. Anatomic study of gastric vascularization and its relationship to cervical gastroplasty[J]. Journal of Gastrointestinal Surgery, 2005, 9(1):132-137.

11) Rino Y , Yukawa N , Sato T , et al. Visualization of blood supply route to the reconstructed stomach by indocyanine green fluorescence imaging during esophagectomy[J]. BMC Medical Imaging, 2014, 14(1):18.

12) Takeda F R , Cecconello I , Ph. D , et al. Anatomic study of gastric vascularization and its relationship to cervical gastroplasty[J]. Journal of Gastrointestinal Surgery, 2005, 9(1):132-137.

13) Rino Y , Yukawa N , Sato T , et al. Visualization of blood supply route to the reconstructed stomach by indocyanine green fluorescence imaging during esophagectomy[J]. BMC Medical Imaging, 2014, 14(1):18.

14) Jansen SM, de Bruin DM, van Berge Henegouwen MI, et al. Optical techniques for perfusion monitoring of the gastric tube after esophagectomy: a review of technologies and thresholds. Dis Esophagus 2018;31.

15) Zehetner J, DeMeester SR, Alicuben ET, et al. Intraoperative Assessment of Perfusion of the Gastric Graft and Correlation With Anastomotic Leaks After Esophagectomy. Ann Surg 2015;262:74-8.

16) Dalton BGA, Ali AA, Crandall M, et al. Near infrared perfusion assessment of gastric conduit during minimally invasive Ivor Lewis esophagectomy. Am J Surg 2018;216:524-7.

17) Murawa D, Hünerbein M, Spychata A, et al. Indocyanine green angiography for evaluation of gastric conduit perfusion during esophagectomy-frst experience. Acta Chir Belg. 2012;112:275-80.

18) acheco PE, Hill SM, Henriques SM, et al. The novel use of intraoperative laser-induced fuorescence of indocyanine green tissue angiography for evaluation of the gastric conduit in esophageal reconstructive surgery. Am J Surg. 2013;205:349-53.

2．執筆論文　Publication of thesis　※記載した論文を添付してください。Attach all of the papers listed below.

論文名 1 Title	Usefulness of three-dimensional thoracoscope for prone position thoracoscopic esophagectomy improves mediastinal lymph node dissection and prognosis for esophageal cancer.					
掲載誌名 Published journal	Full consideration for publication in Annals of Gastroenterological Surgery.					
	年　　　　月	巻（号）	頁　〜　頁		言語 Language	English
第1著者名 First author	Kohei Kanamori&Kazuo Koyanagi	第2著者名 Second author	Soji Ozawa	第3著者名 Third author		Junya Oguma
その他著者名 Other authors	Akihito Kazuno,Yamato Ninomiya,Tadashi Higuchi,Kentaro Yatabe,Miho Yamamoto,Kohei Tajima,Yoshiaki Shoji,Hongbo Zhao					
論文名 2 Title	Perioperative outcomes of neoadjuvant chemotherapy plus camrelizumab compared with chemotherapy alone and chemoradiotherapy for locally advanced esophageal squamous cell cancer.					
掲載誌名 Published journal	Frontiers in Immunology					
	2023　年　2　月	14　巻（号）	頁　〜　頁		言語 Language	English
第1著者名 First author	Hongbo Zhao&Baihua Zhang	第2著者名 Second author	Xun Wu	第3著者名 Third author		Lianghui Gong
その他著者名 Other authors	Desong Yang,Xu Li,Xiaoyan Chen,Jigang Li,Wenxiang Wang,Jie Wu,and Qin Xiao					
論文名 3 Title						
掲載誌名 Published journal						
	年　　　　月	巻（号）	頁　〜　頁		言語 Language	
第1著者名 First author		第2著者名 Second author		第3著者名 Third author		
その他著者名 Other authors						
論文名 4 Title						
掲載誌名 Published journal						
	年　　　　月	巻（号）	頁　〜　頁		言語 Language	
第1著者名 First author		第2著者名 Second author		第3著者名 Third author		
その他著者名 Other authors						
論文名 5 Title						
掲載誌名 Published journal						
	年　　　　月	巻（号）	頁　〜　頁		言語 Language	
第1著者名 First author		第2著者名 Second author		第3著者名 Third author		
その他著者名 Other authors						

3. 学会発表 Conference presentation ※筆頭演者として総会・国際学会を含む主な学会で発表したものを記載してください

※Describe your presentation as the principal presenter in major academic meetings including general meetings or international meetin

学会名 Conference	Chinese Anti-Cancer Association			
演 題 Topic	Personal experience introduction of single-port thoracoscopic pulmonary sleeve resection.			
開催日 date	2022 年 10 月 27 日	開催地 venue	Online	
形式 method	☑ 口頭発表 Oral □ ポスター発表 Poster	言語 Language	□ 日本語 □ 英語 ☑ 中国語	
共同演者名 Co-presenter				
学会名 Conference	Chinese Medical Association			
演 題 Topic	The role of neoadjuvant immunotherapy in the treatment of esophageal cancer.			
開催日 date	2023 年 2 月 19 日	開催地 venue	Online	
形式 method	☑ 口頭発表 Oral □ ポスター発表 Poster	言語 Language	□ 日本語 □ 英語 ☑ 中国語	
共同演者名 Co-presenter				
学会名 Conference				
演 題 Topic				
開催日 date	年 月 日	開催地 venue		
形式 method	□ 口頭発表 Oral □ ポスター発表 Poster	言語 Language	□ 日本語 □ 英語 □ 中国語	
共同演者名 Co-presenter				
学会名 Conference				
演 題 Topic				
開催日 date	年 月 日	開催地 venue		
形式 method	□ 口頭発表 Oral □ ポスター発表 Poster	言語 Language	□ 日本語 □ 英語 □ 中国語	
共同演者名 Co-presenter				

4. 受賞（研究業績） Award（Research achievement）

名 称 Award name				受賞年 Year of award	年 月
	国名 Country				
名 称 Award name				受賞年 Year of award	年 月
	国名 Country				

5. 本研究テーマに関わる他の研究助成金受給 Other research grants concerned with your resarch theme

受給実績 Receipt record	□ 有　　■ 無				
助成機関名称 Funding agency					
助成金名称 Grant name					
受給期間 Supported period	年　　　　月 ～		年　　　　月		
受給額 Amount received	円				
受給実績 Receipt record	□ 有　　■ 無				
助成機関名称 Funding agency					
助成金名称 Grant name					
受給期間 Supported period	年　　　　月 ～		年　　　　月		
受給額 Amount received	円				

6. 他の奨学金受給 Another awarded scholarship

受給実績 Receipt record	□ 有　　■ 無			
助成機関名称 Funding agency				
奨学金名称 Scholarship name				
受給期間 Supported period	年　　　　月 ～		年　　　　月	
受給額 Amount received	円			

7. 研究活動に関する報道発表 Press release concerned with your research activities

※記載した記事を添付してください。Attach a copy of the article described below

報道発表 Press release	□ 有　　■ 無	発表年月日 Date of release	
発表機関 Released medium			
発表形式 Release method	・新聞　・雑誌　・Web site　・記者発表　・その他(　　　　　　　　　)		
発表タイトル Released title			

8. 本研究テーマに関する特許出願予定 Patent application concerned with your research theme

出願予定 Scheduled	□ 有　　■ 無	出願国 Application	
出願内容(概要) Application contents			

9. その他 Others

指導責任者(記名)　　　小柳　和夫

*CORRESPONDENCE
Jie Wu
✉ wujie@hnca.org.cn
Qin Xiao
✉ xiaoqin2501@hnca.org.cn

†These authors have contributed
equally to this work and share
first authorship

Perioperative outcomes of neoadjuvant chemotherapy plus camrelizumab compared with chemotherapy alone and chemoradiotherapy for locally advanced esophageal squamous cell cancer

Baihua Zhang[1†], Hongbo Zhao[2†], Xun Wu[1], Lianghui Gong[1], Desong Yang[1], Xu Li[1], Xiaoyan Chen[3], Jigang Li[3], Wenxiang Wang[1], Jie Wu[1*] and Qin Xiao[4*]

[1]The Second Department of Thoracic Surgery, Hunan Clinical Medical Research Center of Accurate Diagnosis and Treatment for Esophageal Carcinoma, Hunan Cancer Hospital and The Affiliated Cancer Hospital of Xiangya School of Medicine, Central South University, Changsha, China, [2]Department of Thoracic Surgery, National Cancer Center/National Clinical Research Center for Cancer/Cancer Hospital and Shenzhen Hospital, Chinese Academy of Medical Sciences and Peking Union Medical College, Shenzhen, China, [3]Department of Pathology, Hunan Cancer Hospital and The Affiliated Cancer Hospital of Xiangya School of Medicine, Central South University, Changsha, China, [4]Key Laboratory of Translational Radiation Oncology, Hunan Province, The First Department of Thoracic Radiation Oncology, Hunan Cancer Hospital, The Affiliated Cancer Hospital of Xiangya School of Medicine, Central South University, Changsha, Hunan, China

Purpose: Neoadjuvant chemoimmunotherapy (nCIT) is becoming a new therapeutic frontier for resectable esophageal squamous cell carcinoma (ESCC); however, crucial details and technical know-how regarding surgical techniques and the perioperative challenges following nCIT remain poorly understood. The study investigated and compared the advantages and disadvantages of esophagectomy following nCIT with neoadjuvant chemotherapy (nCT) and chemoradiotherapy (nCRT).

Methods: We retrospectively analyzed data of patients initially diagnosed with resectable ESCC at clinical stage T2-4N+ and received neoadjuvant therapy followed by esophagectomy at the Hunan Cancer Hospital between October 2014 and February 2021. Patients were divided into three groups according to neoadjuvant treatment: (i) nCIT; (ii) nCT; and (iii) nCRT.

Results: There were 34 patients in the nCIT group, 97 in the nCT group, and 31 in the nCRT group. Compared with nCT, nCIT followed by esophagectomy achieved higher pathological complete response (pCR; 29.0% versus 4.1%, p<0.001) and major pathological response (MPR; 52.9% versus 16.5%, p<0.001) rates, more resected lymph nodes during surgery (25.06 ± 7.62 versus 20.64 ± 9.68, p=0.009), less intraoperative blood loss (200.00 ± 73.86 versus 266.49 ± 176.29 mL, p=0.035), and comparable results in other perioperative parameters. Compared with nCRT, nCIT achieved similar pCR (29.0% versus 25.8%) and MPR (52.9% versus 51.6%, p=0.862) rates, with significantly more lymph nodes resected

during surgery (25.06 ± 7.62 versus 16.94 ± 7.24, p<0.001), shorter operation time (267.79 ± 50.67 versus 306.32 ± 79.92 min, p=0.022), less intraoperative blood loss (200.00 ± 73.86 versus 264.53 ± 139.76 mL, p=0.022), and fewer ICU admissions after surgery (29.4% versus 80.6%, p<0.001). Regarding perioperative adverse events and complications, no significant statistical differences were detected between the nCIT and the nCT or nCRT groups. The 3-year overall survival rate after nCIT was 73.3%, slightly higher than 46.1% after nCT and 39.7% after nCRT, with no statistically significant differences (p=0.883).

Conclusions: This clinical analysis showed that nCIT is safe and feasible, with satisfactory pCR and MPR rates. Esophagectomy following nCIT has several perioperative advantages over nCT and nCRT, with comparable perioperative morbidity and mortality. The long-term survival benefits after nCIT still requires further investigation.

Introduction

In 2020, esophageal carcinoma was the seventh most prevalent cancer and sixth leading cause of cancer-related death worldwide (1). The predominant esophageal cancer subtype in Asia is esophageal squamous cell carcinoma (ESCC) (2). ESCC accounts for over 84% of newly diagnosed esophageal cancers annually (3, 4). Surgical resection remains the gold standard for patients with locally advanced resectable ESCC. However, studies have shown that local recurrence and distant metastasis occur in approximately 33% of patients who receive surgery alone (5, 6). Thus, ESCC treatment is challenging and requires a multidisciplinary approach to improve the surgical therapeutic effect in locally advanced resectable disease.

Following the launch of a new era in immunotherapy (including programmed cell death-ligand 1 [PD-L1] and programmed cell death protein-1 [PD-1] inhibitors), further exploration of neoadjuvant immunotherapy alone or combined with chemotherapy or chemoradiotherapy is expected to further improve the therapeutic effect in locally advanced resectable ESCC. In a recent systematic review including 27 phase 2 or 3 clinical trials with 815 patients, the pooled pathological complete response (pCR) rate was 32.4% in ESCC after neoadjuvant chemoimmunotherapy(nCIT), with the pooled incidence of treatment-related severe adverse events of 26.9% (7). Zhu et al. reported that neoadjuvant immunochemoradiotherapy could not improve the pCR rate than neoadjuvant chemoradiotherapy (nCRT) for ESCC, but significantly increased the risk of severe adverse events (8). Another multicenter retrospective study that included 370 ESCC patients showed that the pCR rates of mono-immunotherapy, nCIT, and nCRT plus immunotherapy were 12.1%, 25.5%, and 42.3%, respectively (9). Hence, neoadjuvant PD-1/PD-L1 inhibitors in combination with chemotherapy or chemoradiotherapy are becoming a new therapeutic frontier for resectable ESCC with promising clinical outcomes. However, long-term follow-up are warranted to validate the survival benefits of nCIT or nCRT plus immunotherapy.

Camrelizumab is a PD-1 inhibitor produced in China by Jiangsu Hengrui Pharmaceuticals Co, Ltd. (Lianyungang, China). The ESCORT-1st study showed that first-line camrelizumab plus chemotherapy could achieve better disease control and long-term survival in advanced ESCC than chemotherapy alone (10). Several prospective phase-II clinical trials have also demonstrated that after neoadjuvant chemotherapy plus camrelizumab (nCIT) for ESCC, pCR rates ranged from 24.1% to 42.5%, with major pathological response (MPR) rates of between 45% and 68.8% (11–14). However, these sample sizes were small, and only a few studies reported survival results. Additionally, crucial details and technical know-how regarding the surgical techniques and perioperative challenges following nCIT are still poorly understood.

In the present study, we retrospectively reviewed the perioperative outcomes of esophagectomy following nCIT to compare it with surgery after nCT and nCRT. This study aimed to investigate the potential advantages and disadvantages of esophagectomy after nCIT.

Patients and methods

Inclusion and exclusion criteria

This is a retrospective, single-center, observational study. Patients initially diagnosed with resectable ESCC at clinical stages T2-4N+ (American Joint Committee on Cancer, 8th edition) and received neoadjuvant therapy followed by curative-intent surgery between October 2014 and February 2021 at the Hunan Cancer Hospital were recruited. The Eastern Cooperative Oncology Group's performance status of all patients was 0 or 1. Patients were included on the basis of the following criteria; (1): only squamous cell carcinoma components; (2); thoracic ESCC; (3); patients who received neoadjuvant chemotherapy (nCT), nCIT (only camrelizumab), or nCRT followed by esophagectomy; and (4) the

chemotherapy regimens only consisted of paclitaxel and platinum. The exclusion criteria were as follows; (1): pathological non-squamous cell carcinoma components; (2); patients with unresectable primary tumors, more than seven lymph node metastases (N3), or distant metastasis (M1) before neoadjuvant treatment; (3); patients with previous cancer type(s) or other concurrent malignant tumors; (4); patients that received other forms of treatment before surgery; and (5) incomplete medical records.

All clinical data were obtained from medical records and retrospectively analyzed. This study was conducted per the Declaration of Helsinki (as revised in 2013). The Ethics Committee of Hunan Cancer Hospital approved this study (No. 2022097), and patients' written informed consent was obtained.

Neoadjuvant treatment modalities

Patients were retrospectively divided into three groups according to the neoadjuvant treatment modality they received; (1): the nCT group, including patients who received one to four cycles of paclitaxel combined with platinum chemotherapy (21 days per cycle); (2); the nCIT group, including patients who received conventional chemotherapy (1–4 cycles of paclitaxel and platinum) and camrelizumab (200 mg) on the first day of each cycle; and (3) the nCRT group, including patients who received concurrent chemotherapy (1–4 cycles of paclitaxel and platinum) and radiotherapy (6-MV X-ray, 39.6–45.0 Gy/1.8–2.0 Gy/f) before esophagectomy.

Surgery and adjuvant therapy

Generally, patients would receive a tumor re-evaluation within 2 to 6 weeks after the last neoadjuvant treatment cycle. Following multidisciplinary discussion, a curative-intent surgical resection was immediately performed when the tumor was considered operable. Overall, esophagectomy with the stomach as the esophageal substitute and cervical or thoracic anastomosis were performed in all patients, while experienced surgeons regularly conducted a standard 2-field lymphadenectomy. Cervical lymphadenectomy (3-field) was performed only when lymph node metastasis was suspected in the neck region.

Adjuvant treatments were then performed on the basis of pathological tumor stage and each patient's recovery condition. After multidisciplinary discussion, postoperative chemoradiotherapy or chemotherapy alone might be recommended for patients with ypN + or palliative resection. In the nCIT group, adjuvant therapy with camrelizumab might be recommended for 1 year after surgery.

Outcome measures and follow-up

As reported in previous studies (15, 16), pCR was defined as no viable tumor cells in the resected specimen. In contrast, MPR was defined as <10% viable residual tumor cells detected in the specimen. Pathological responses were evaluated independently by two

experienced pathologists. Treatment-related adverse events (TRAEs) were graded as per the National Cancer Institute Common Terminology Criteria for Adverse Events (CTCAE) version 5.0. Weight loss at initial diagnosis was defined as weight loss detected within six months before the diagnosis of ESCC. Operation time was calculated from incision to wound closure.

Radiographic evaluations were conducted every 3 months for the first 2 years after surgery, and then every 6 months thereafter. Whenever recurrence was suspected, rebiopsy and/or 18F-FDG positron emission tomography-computed tomography (PET-CT) or both were performed to identify the possible recurrence.

Statistical analysis

The primary endpoint was the MPR rate, and the secondary endpoints were the pCR, perioperative morbidity, and 3-year OS rates. OS was defined as the time (in months) from surgery to the date of death or the last follow-up. Survival analyses were calculated and compared using Kaplan–Meier curves and the log-rank test.

Differences in clinicopathological features between groups were calculated using the chi-square (χ^2) test or t-test. SPSS software 23.0 (IBM Corp., Armonk, NY, USA) was used to perform all statistical analyses. A p-value <0.05 (two-sided) was considered to be statistically significant.

Results

Overview of patient cohorts

Between October 2014 and February 2021, 194 patients were screened for eligibility. Eventually, 162 patients were enrolled for further analysis (34 patients in the nCIT group, 97 in the nCT group, and 31 in the nCRT group) (Figure 1). All 162 patients in the study finished one to four cycles of neoadjuvant therapy. As summarized in Table 1, the enrolled patients in the nCIT group have a mean age of 60.68 ± 7.44 years old and predominantly consisted of males (91.2%), which were consistent with the nCT and nCRT groups. No significant differences were detected between the nCIT and the nCT or nCRT groups in other baseline characteristics, including cigarette consumption, alcohol abuse, weight loss at initial diagnosis, body mass index, tumor location, tumor length, cN, and pathological differentiation. However, the cT4 percentage in the nCIT group was 35.3%, which was significantly higher than in the nCT group (16.5%, p=0.021) but comparable to that in the nCRT group (19.4%, p=0.238).

Perioperative outcomes

All patients successfully received esophagectomy and most achieved radical resection with no significant statistical differences (Table 2). The time interval between final neoadjuvant therapy and surgery in the nCIT group was 35.91 ± 6.76 days, which was significantly longer than in the nCT group (32.70 ± 7.56 days, p=0.024) but shorter than in the nCRT group (41.87 ± 10.60 days,
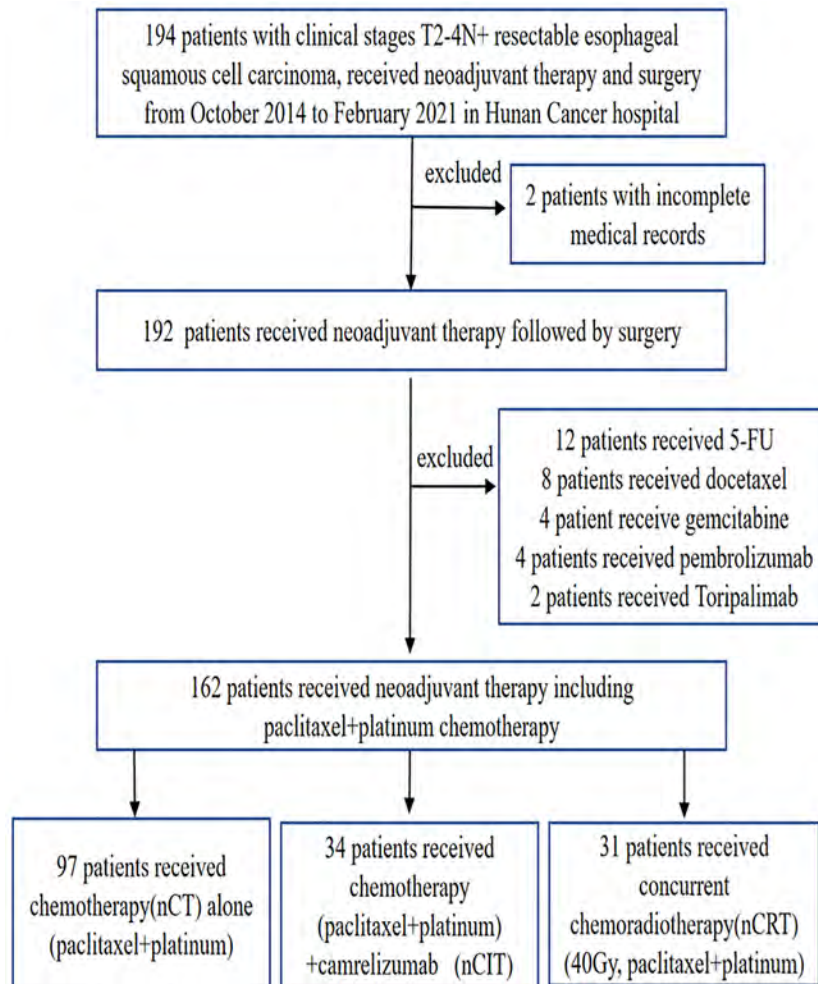
FIGURE 1
Patient selection flowchart.

p=0.010). Patients in the nCIT group (267.79 ± 50.67 min) required a shorter operation time than those in the nCRT group (306.32 ± 79.92 min, p=0.022). Meanwhile, no significant difference was detected between the nCIT and nCT groups (291.40 ± 71.48 min, p=0.078). Additionally, intraoperative blood loss in the nCIT group (200.00 ± 73.86 mL) was less than in the nCT (266.49 ± 176.29 mL, p=0.035) and nCRT (264.53 ± 139.76 mL, p=0.022) groups. Notably, 2-field lymphadenectomy was the principal method for lymph node resection in all groups. However, the average number of resected lymph nodes in the nCIT group (25.06 ± 7.62) was significantly higher than in the other two groups (p=0.009, p<0.001, respectively).

Three-incisional esophagectomy with anastomosis in the neck was the principal surgery in all three groups. As summarized in Table 2, no significant differences were detected between the groups in the total drainage after operation, duration of chest tube, and hospital stay after surgery. The frequency of ICU stay after surgery in the nCIT group (29.4%) was comparable with that in the nCT group (32.0%, p=0.783) but significantly lower than in the nCRT group (80.6%, p<0.001).

Pathological efficacy

In the pathological analysis after surgery, MPR was observed in 18 patients in the nCIT group (52.9%), including nine primary tumor pCRs (26.4%) (8 T0N0 [23.5%], 1 T0N+ [2.9%]), and nine patients (26.5%) had 1% to 10% viable residual tumor cells detected in the specimens. In the nCT group, MPR was achieved in 16 patients (16.5%), including four primary tumor pCRs (4.1%) (3 T0N0 [3.1%], 1 T0N+ [1.0%]), which was significantly lower than in the nCIT group (p<0.001). In the nCRT group, 16 patients (51.6%) achieved MPR, including eight primary tumor pCRs (25.8%) (7 T0N0 [22.6%], 1 T0N+ [3.2%]), which was similar to the nCIT group (p=0.862).

Accordingly, the ypT0-2 percentage in the nCIT group (67.6%) was also significantly higher than in the nCT group (39.2%, p=0.004) but similar to the nCRT group (58.1%, p=0.424). No significant differences were detected between the groups for other pathological parameters including ypN stage, ypTNM stage, positive lymph node number, and lymphovascular invasion (LVI), or perineural invasion. After surgery, approximately half of the patients received adjuvant

TABLE 1 Clinical characteristics for ESCC patients received neoadjuvant therapy.

Variables	nCIT (n=34)	nCT (n=97)	P value	nCIT (n=34)	nCRT (n=31)	P value
Age						
Mean ± SD[a], y	60.68 ± 7.44	60.08 ± 7.78	0.699	60.68 ± 7.44	57.23 ± 6.79	0.056
Gender						
Male	31 (91.2)	94 (96.9)	0.169	31 (91.2)	30 (96.8)	0.348
Female	3 (8.8)	3 (3.1)		3 (8.8)	1 (3.2)	
Cigarette consumption						
Former/current	30 (88.2)	86 (88.7)	0.947	30 (88.2)	27 (87.1)	0.889
No	4 (11.8)	11 (11.3)		4 (11.8)	4 (12.9)	
Alcohol abuse						
Former/current	28 (82.4)	78 (80.4)	0.804	28 (82.4)	29 (93.5)	0.170
No	6 (17.6)	19 (19.6)		6 (17.6)	2 (6.5)	
Weight loss at initial diagnosis						
Yes	21 (61.8)	50 (51.5)	0.303	21 (61.8)	15 (48.4)	0.279
No	13 (38.2)	47 (48.5)		13 (38.2)	16 (51.6)	
BMI index						
Mean ± SD [a]	21.82 ± 2.74	21.35 ± 3.17	0.442	21.82 ± 2.74	21.77 ± 1.91	0.932
Tumor location						
Upper thoracic	3 (8.8)	10 (10.3)	0.642	3 (8.8)	4 (12.9)	0.169
Middle thoracic	11 (32.4)	39 (40.2)		11 (32.4)	16 (51.6)	
Lower thoracic	20 (58.8)	48 (49.5)		20 (58.8)	11 (35.5)	
Tumor length before treatment						
Mean ± SD [a], cm	5.36 ± 1.81	5.11 ± 1.89	0.512	5.36 ± 1.81	5.21 ± 1.72	0.736
cT						
T2/3	22 (64.7)	81 (83.5)	0.021	22 (64.7)	25 (80.6)	0.151
T4	12 (35.3)	16 (16.5)		12 (35.3)	6 (19.4)	
cN						
N1	17 (50.0)	59 (60.8)	0.271	17 (50.0)	11 (35.5)	0.238
N2	17 (50.0)	38 (39.2)		17 (50.0)	20 (64.5)	
Pathological differentiation						
Poor/moderate	27 (79.4)	70 (72.2)	0.407	27 (79.4)	27 (87.1)	0.409
Well	7 (20.6)	27 (27.8)		7 (20.6)	4 (12.9)	

[a]Variables were described by mean (x) and standard deviation (s).

ESCC, esophageal squamous cell carcinoma; cT, clinical T stage before treatment; cN, clinical N stage before treatment; nCT, neoadjuvant chemotherapy; nCIT, neoadjuvant chemotherapy plus Camrelizumab; nCRT, neoadjuvant chemoradiotherapy.

therapy, with no statistically significant difference observed among the three groups.

Perioperative adverse events and complications

The adverse events related to neoadjuvant therapy are summarized in Table 3. The frequency of adverse events in the nCIT group was 47.1%, which was comparable with the nCT and nCRT groups. Regarding CTCAE grade, the frequency of severe adverse events (grade III/IV) in the nCIT group was 25.0%, which was similar to the 16.2% and 41.1% in the nCT and nCRT groups, respectively. No deaths related to neoadjuvant therapy (CTCAE grade V) were observed in any group. As to the adverse event types, myelosuppression and erythra were the principal events in the nCIT group, which was different from that of myelosuppression and gastrointestinal react in the nCT group (p=0.002).

TABLE 2 The perioperative outcomes of esophagectomy after neoadjuvant therapy.

Variables	nCIT (n=34)	nCT (n=97)	P value	nCIT (n=34)	nCRT (n=31)	P value
Interval days
x ± s [a](day)	35.91 ± 6.76	32.70 ± 7.56	0.024	35.91 ± 6.76	41.87 ± 10.60	0.010
Surgical radicality
Radical	33 (97.1)	89 (91.8)	0.293	33 (97.1)	29 (93.5)	0.500
Palliative	1 (2.9)	8 (8.2)		1 (2.9)	2 (6.5)	
Operation time
x ± s [a](min)	267.79 ± 50.67	291.40 ± 71.48	0.078	267.79 ± 50.67	306.32 ± 79.92	0.022
Intraoperative blood loss
x ± s [a](ml)	200.00 ± 73.86	266.49 ± 176.29	0.035	200.00 ± 73.86	264.53 ± 139.76	0.022
Extent of lymph node resection
2-field	34 (100.0)	96 (99.0)	0.552	34 (100.0)	30 (96.8)	0.291
3-field	0	1 (1.0)		0	1 (3.2)	
Resected lymph nodes number
x ± s [a]	25.06 ± 7.62	20.64 ± 9.68	0.009	25.06 ± 7.62	16.94 ± 7.24	< 0.001
Anastomosis position
Neck	33 (97.1)	90 (92.8)	0.370	33 (97.1)	26 (83.9)	0.067
Thoracic	1 (2.9)	7 (7.2)		1 (2.9)	5 (16.1)	
Total drainage after operation
x ± s [a](ml)	1925.29 ± 2239.05	2476.25 ± 3335.70	0.285	1925.29 ± 2239.05	3664.35 ± 6581.08	0.151
Duration of chest tube
x ± s [a](day)	8.00 ± 4.70	8.78 ± 3.47	0.378	8.00 ± 4.70	11.42 ± 19.98	0.336
ICU stay after surgery
Yes	10 (29.4)	31 (32.0)	0.783	10 (29.4)	25 (80.6)	< 0.001
No	24 (70.6)	66 (68.0)		24 (70.6)	6 (19.4)	
Hospital stays after surgery
x ± s [a](day)	12.76 ± 7.30	12.27 ± 4.71	0.713	12.76 ± 7.30	15.65 ± 19.38	0.423
Pathological response
MPR	18 (52.9)	16 (16.5)	< 0.001	18 (52.9)	16 (51.6)	0.862
PR	9 (26.5)	48 (49.5)		9 (26.5)	7 (22.6)	
SD/PD	7 (20.6)	33 (34.0)		7 (20.6)	8 (25.8)	
ypT stage
T0-2	23 (67.6)	38 (39.2)	0.004	23 (67.6)	18 (58.1)	0.424
T3-4	11 (32.4)	59 (60.8)		11 (32.4)	13 (41.9)	
ypN stage
N-	20 (58.8)	45 (46.4)	0.212	20 (58.8)	18 (58.1)	0.951
N+	14 (41.2)	52 (53.6)		14 (41.2)	13 (41.9)	
ypTNM stage

(Continued)

TABLE 2   Continued

Variables	nCIT (n=34)	nCT (n=97)	P value	nCIT (n=34)	nCRT (n=31)	P value
0-II	22 (64.7)	45 (46.4)	0.179	22 (64.7)	20 (64.5)	0.839
III	9 (26.5)	41 (42.3)		9 (26.5)	7 (22.6)	
IVA	3 (8.8)	11 (11.3)		3 (8.8)	4 (12.9)	
Positive lymph nodes number						
x ± s [a]	1.32 ± 2.43	1.51 ± 2.36	0.707	1.32 ± 2.43	1.06 ± 1.98	0.642
LVI/perineural invasion						
Yes	6 (17.6)	14 (14.4)	0.654	6 (17.6)	2 (6.5)	0.170
No	28 (82.4)	83 (85.6)		28 (82.4)	29 (93.5)	
Adjuvant therapy						
Yes	20 (58.8)	46 (47.4)	0.253	20 (58.8)	15 (48.4)	0.399
No	14 (41.2)	51 (52.6)		14 (41.2)	16 (51.6)	

[a]Variabls were described by mean (x) and standard deviation (s).
nCIT, neoadjuvant chemotherapy plus Camrelizumab; nCT, neoadjuvant chemotherapy; nCRT, neoadjuvant chemoradiotherapy; Interval days, interval days between final neoadjuvant therapy and surgery; ypT, pathological T stage after neoadjuvant therapy; ypN, pathological N stage after neoadjuvant therapy; ypTNM, pathological TNM stage after neoadjuvant therapy; ICU, intensive care unit; LVI, lymphovascular invasion; MPR, major pathological response; PR, partial response; SD, stable disease; PD, progressive disease.

Postoperative complications related to surgery within 30 days occurred in 17 patients (50.0%) in the nCIT group, approximately 37 patients (38.1%) in the nCT group, and 13 patients (41.9%, p=0.227) in the nCRT group (p=0.515) (Table 4). The principal complications included pulmonary complications, anastomotic leakage, hoarseness, and cardiac complications, and these were unrelated to the neoadjuvant therapeutic modality. One patient in the nCIT group received a reoperation within 30 days due to diaphragmatic hernia and chyle, four patients in the nCT group due to anastomotic leakage or tracheostomy, and one patient in the nCRT group due to intrathoracic anastomotic leakage.

Only one patient suffered from sudden death, which was 11 days after surgery, and the patient was in the nCT group. The 90-day mortality rate was 8.8% in the nCIT group, and 7.2% in the nCT group (p=0.761), while no deaths within 90 days were observed in the

TABLE 3   The adverse events of neoadjuvant therapy.

Variables	nCIT (n=34)	nCT (n=97)	P value	nCIT (n=34)	nCRT (n=31)	P value
Adverse events						
Yes	16 (47.1)	37 (38.1)	0.362	16 (47.1)	17 (54.8)	0.531
No	18 (52.9)	60 (61.9)		18 (52.9)	14 (45.2)	
CTCAE grade						
Any grade	N=16	N=37		N=16	N=17	
I	6 (37.5)	15 (40.5)	0.765	6 (37.5)	4 (23.5)	0.596
II	6 (37.5)	16 (43.2)	0.877	6 (37.5)	6 (35.3)	0.859
III	2 (12.5)	3 (8.1)	0.465	2 (12.5)	4 (23.5)	0.329
IV	2 (12.5)	3 (8.1)	0.465	2 (12.5)	3 (17.6)	0.566
V	0	0		0	0	
Adverse event types						
Myelosuppression	7 (43.8)	18 (48.6)	0.002	7 (43.8)	12 (70.6)	0.129
Erythra	7 (43.8)	1 (2.7)		7 (43.8)	1 (5.9)	
Hepatic dysfunction	1 (6.3)	4 (10.8)		1 (6.3)	1 (5.9)	
Gastrointestinal react	1 (6.3)	12 (32.4)		1 (6.3)	2 (11.8)	
Renal dysfunction	0	2 (5.49)		0	1 (5.9)	

nCT, neoadjuvant chemotherapy; nCIT, neoadjuvant chemotherapy plus Camrelizumab; nCRT, neoadjuvant chemoradiotherapy; CTCAE, Common Terminology Criteria for Adverse Events (version 5.0).

TABLE 4   Perioperative complications within 30 days after surgery and mortality.

Variables	nCIT (n=34)	nCT (n=97)	*P* value	nCIT (n=34)	nCRT (n=31)	*P* value
Postoperative complications						
Yes	17 (50.0)	37 (38.1)	0.227	17 (50.0)	13 (41.9)	0.515
No	17 (50.0)	58 (61.9)		17 (50.0)	18 (58.1)	
Complication types	n=17	n=37		n=17	n=13	
Hoarseness	2 (11.8)	6 (16.2)		2 (11.8)	1 (7.7)	
Pulmonary complications	7 (41.7)	10 (27.0)		7 (41.7)	3 (23.1)	
Cardiac complications	2 (11.8)	1 (2.7)		2 (11.8)	2 (15.4)	
Chyle	1 (5.9)	3 (8.1)		1 (5.9)	0	
Anastomotic leakage	2 (11.8)	8 (21.6)		2 (11.8)	4 (30.8)	
Gastric and intestinal complications	1 (5.9)	3 (8.1)		1 (5.9)	0	
Other complications	2 (11.8)	6 (16.2)		2 (11.8)	3 (23.1)	
Reoperation in 30 days						
No	33 (97.1)	93 (95.9)	0.757	33 (97.1)	30 (96.8)	0.947
Yes	1 (2.9)	4 (4.1)		1 (2.9)	1 (3.2)	
30-day mortality						
No	34 (100.0)	96 (99.0)	0.552	34 (100.0)	31 (100.0)	1.000
Yes	0	1 (1.0)		0	0	
90-day mortality						
No	31 (91.2)	90 (92.8)	0.761	31 (91.2)	31 (100.0)	0.09
Yes	3 (8.8)	7 (7.2)		3 (8.8)	0	

nCT, neoadjuvant chemotherapy; nCIT, neoadjuvant chemotherapy plus Camrelizumab; nCRT, neoadjuvant chemoradiotherapy.

nCRT group. No statistically significant difference was found between the nCIT and nCRT groups (*p*=0.09).

Overall survival and analysis of prognostic factors

Until July 30, 2022, the median follow-up of the entire cohort was 20.45 months, with a range of 0.36 to 84.76 months. In the nCIT group, the 1- and 3-year OS rates were 82.4% and 73.3%, respectively, which were not significantly different from the nCT group (77.3% and 46.1%, respectively) and the nCRT group (83.9% and 39.7%, respectively) (Figure 2A, *p*=0.883). Furthermore, the 3-year OS for patients who achieved MPR was 68.7%, which was significantly higher than 46.3% for partial responders and 23.8% for those with stable/progressive disease (Figure 2B, *p*<0.001). Patients who achieved radical esophagectomy attained a much better 3-year OS rate than those who achieved palliative surgery (49.7% versus 0%, Figure 2C, *p*<0.001). In the analysis of postoperative pathological stage, patients with stage ypN- achieved a 3-year OS of 60.6%, which was longer than the 29.0% for patients with ypN+ (Figure 2D, *p*<0.001). Further analysis showed that patients with earlier ypT0-2 and yp0-II staged disease also had better long-term survival rates (Figures 2E, F, *p*<0.001).

Interestingly, the 3-year OS rate of patients with weight loss at initial diagnosis was 38.7%, which was significantly shorter than the 55.8% for patients without weight loss (*p*=0.032). Additionally, the 3-year OS for patients without LVI/perineural invasion was 48.3%, which was longer than the 33.8% for patients with LVI/perineural invasion (*p*=0.022). However, age, sex, body mass index, tumor length at initial diagnosis, tumor location, pathological differentiation, and adjuvant systemic therapy were not significantly correlated with OS in univariate Cox analysis (Table 5).

In the multivariate analysis, which included significant factors identified by univariate analysis, only surgical radicality (hazard ratio [HR]: 5.882, 95% confidence interval [CI]: 2.799–12.359, *p*<0.001), pathological response (HR: 1.493, 95% CI: 1.040–2.143, *p*=0.030), and ypN stage (HR: 2.100, 95% CI: 1.245–3.542, *p*=0.005) were found to be independent prognostic factors for OS other than neoadjuvant modality (Table 5).

Discussion

This study described potential intraoperative technical challenges after nCIT and compared them with other neoadjuvant treatment modalities including nCT and nCRT. Compared with nCT, nCIT followed by esophagectomy achieved higher pCR and MPR rates,
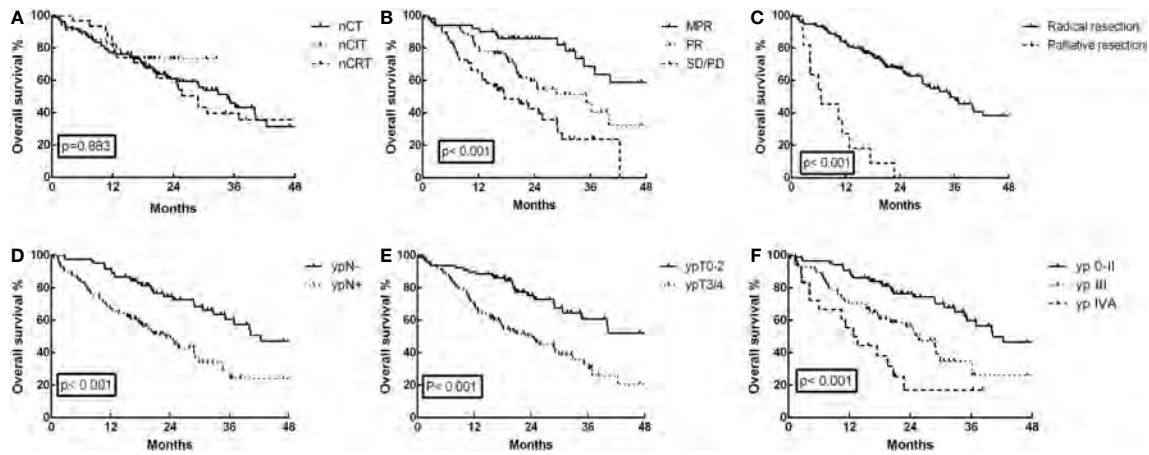
FIGURE 2
Overall survival (OS) curves for the 162 ESCC patients. **(A)** OS was not significantly different in the neoadjuvant chemoimmunotherapy (nCIT) group compared with the neoadjuvant chemotherapy (nCT) and neoadjuvant chemoradiotherapy (nCRT) groups (p=0.883). **(B)** OS was significantly increased for patients who achieved major pathological response (MPR) compared with those who achieved partial response (PR) and stable disease (SD)/progressive disease (PD) (p<0.001). **(C)** OS was increased for patients who achieved radical esophagectomy compared with those who achieved palliative surgery (p<0.001). **(D)** OS was increased in patients with stage ypN- compared with those who had stage ypN+ (p<0.001). **(E)** OS was increased in patients with stage ypT0-2 compared with those who had stage ypT3/4 (p<0.001). **(F)** OS was increased in patients with stage yp0-II compared with those who had stage ypIII and ypIVA (p<0.001).

more resected lymph nodes during surgery, less intraoperative blood loss, and comparable results in other perioperative parameters. Compared with nCRT, nCIT achieved similar pCR and MPR rates, significantly more resected lymph nodes during surgery, shorter operation time, less intraoperative blood loss, and less frequent ICU stays after surgery. Regarding postoperative complications, no

significant statistical difference was detected between the nCIT and the nCT or nCRT groups.

Over the past decade, there have been lingering controversies concerning the effects of neoadjuvant chemotherapy (nCT), chemoradiotherapy (nCRT), and immunotherapy for ESCC. There is still no convincing evidence to prove which neoadjuvant

TABLE 5 Univariate and multivariate analysis of OS for 162 ESCC patients treated with surgery following neoadjuvant therapy.

Characteristics	Univariate		Multivariate	
	HR (95% CI)	P	HR (95% CI)	P
Age (y): < 60 vs ≥ 60	1.039 (0.660-1.634)	0.870		
Gender: Male vs Female	0.564 (0.138-2.299)	0.424		
Weight loss at initial diagnosis: Yes vs No	1.679 (1.047-2.692)	0.032*		
BMI index: < 22 vs ≥ 22	0.870 (0.545-1.390)	0.561		
Tumor length at initial diagnosis: <5 vs ≥5cm	0.981 (0.620-1.553)	0.936		
Tumor location: Lower vs Upper/middle	1.250 (0.793-1.972)	0.337		
Pathological differentiation: Poor/moderate vs Well	1.170 (0.673-2.035)	0.579		
Surgical radicality: Palliative vs Radical	7.415 (3.765-14.605)	<0.001*	5.882 (2.799-12.359)	<0.001
Pathological response: SD(PD) vs PR vs MPR(CR)	2.090 (1.533-2.849)	<0.001*	1.493 (1.040-2.143)	0.030
ypT stage: ypT3-4 vs ypT0-2	2.555 (1.569-4.161)	<0.001*		
ypN stage: ypN+ vs ypN-	2.601 (1.615-4.190)	<0.001*	2.100 (1.245-3.542)	0.005
ypTNM stage: IVA vs III vs 0-II	1.588 (1.300-1.939)	<0.001*		
LVI/perineural invasion: Yes vs No	2.026 (1.105-3.715)	0.022*		
Neoadjuvant therapeutic modality: nCRT vs nCIT vs nCT	0.990 (0.872-1.125)	0.883		
Adjuvant systemic therapy: Yes vs No	0.957(0.606-1.511)	0.849		

*Factors included into multivariate analysis.
ESCC, esophageal squamous cell carcinoma; OS, overall survival; nCIT, neoadjuvant chemotherapy plus Camrelizumab; nCT, neoadjuvant chemotherapy; nCRT, neoadjuvant chemoradiotherapy; ypT, pathological T stage after neoadjuvant therapy; ypN, pathological N stage after neoadjuvant therapy; ypTNM, pathological TNM stage after neoadjuvant therapy; vs, versus; HR, hazard ratio; CI, confidence interval.

therapeutic modality is best for locally advanced resectable ESCC. Pathological responses including pCR and MPR have been considered as principal surrogate endpoints to evaluate the therapeutic efficacy of different neoadjuvant treatments. Previous large-scale randomized clinical trials have reported that nCRT could achieve higher pCR rates (43.2-49%) than nCT (3.8-10.7%) in ESCC, but nCRT might have more postoperative complications and higher postoperative mortality, with no identified overall survival differences (4, 17–24). Therefore, in Western countries, many institutions have adopted nCRT followed by esophagectomy, but globally, many other countries support nCT alone (4, 25).

In this study, the pCR rate for the primary tumor was 26.4%, and the MPR rate was 52.9% after nCIT, consistent with previous reports (9, 11, 12, 26–30). However, after nCT for ESCC, the pCR rate in previous studies is usually between 3.8% and 10.7% (23, 24, 31), which is close to the 4.1% for the primary tumor in this study and significantly lower than the results for nCIT. In contrast, the pCR rate for nCRT has reached approximately 28.9% to 49% in previous studies, which is slightly better than the 25.8% in this study (21, 24, 31–33). Xu et al. demonstrated that the pCR rate was comparable between nCIT and nCRT (29.8% vs 34.0%), with no significant differences in the incidence of postoperative complications and 30-day mortality (34). Thus, this study showed that ESCC might achieve better therapeutic efficacy from nCIT and nCRT on the basis of pCR and MPR results.

Although the pathological efficacy was better for nCIT and nCRT, controversies concerning the long-term survival results remained. Previous prospective trials on esophageal cancer, including JCOG9907, OEO2, CROSS, and NEOCRTEC5010 have demonstrated that nCT or nCRT can achieve better OS results than surgery alone or postoperative chemotherapy (20, 21, 32, 35). Nonetheless, survival differences between different neoadjuvant therapeutic modalities have not been clarified. Klevebro et al. and Wang et al. showed that nCRT could result in a higher pCR rate than nCT, but with no significant survival benefits (24, 31). Another study showed no significant differences in the 5-year OS or the 5-year relapse-free survival (RFS) rates between nCRT and nCT (36). Two separate meta-analyses also reported that nCRT did not show significant long-term survival benefits as nCT (37, 38). In this study, the 1-year OS rate in the nCIT group were 82.4%, consistent with the 1-year OS of between 87.6% and 92.8% in previous reports (29, 39), but not significantly different from nCT (77.3%) and nCRT (83.9%). In a few propensity score matching analyses, the 1-year OS rate in the nCIT group was 94.5-95.7%, slightly better than 84.8% in the nCT group and 86.2% in the nCRT group, but with no significant statistical differences (40, 41). Although no statistically significant difference was observed in our data, the 3-year OS after nCIT was 73.3%, slightly higher than 46.1% after nCT and 39.7% after nCRT. However, the sample size and follow-up time in the present study were too limited to report mature OS results. Therefore, the survival benefit after nCIT in locally advanced resectable ESCC still requires further investigation. Furthermore, as previously reported (4, 36, 42), our further analysis showed that radical esophagectomy, MPR, and ypN0 (no lymph node metastasis) were independent favorable prognostic factors for OS after neoadjuvant therapy. As to adjuvant therapy, approximately half of the patients received adjuvant therapy in each group, and no statistically significant difference was observed among the three groups. No survival difference was observed between patients received adjuvant therapy or not in our analysis.

This study also highlighted advantages for esophagectomy, as nCIT had more lymph nodes resected and less intraoperative blood loss compared with nCT. During our surgery, tumor and metastatic lymph nodes regression was more significant in the nCIT group than in the nCT group, facilitating lymph node clearance and reducing operation times. Qiao et al. also reported that patients who received nCIT had more lymph nodes cleared during surgery than those who received nCT (34 vs. 30, p<0.001), with comparable incidence of complications (23). Furthermore, when compared with nCRT, esophagectomy after nCIT also achieved more resected lymph nodes, shorter operation times, less intraoperative blood loss, and less frequent ICU stays after surgery. Based on our surgical experience, mild or moderate tissue adhesions were more frequently observed in the nCIT group compared to the nCRT group, which might help reduce the intraoperative difficulties. In certain propensity score matching analyses by Hong et al. and Xiao et al, esophagectomy after nCIT required shorter operative times, and dissected more lymph nodes than after nCRT (41, 43). Cheng et al. also reported that the nCIT group had minimal intraoperative blood loss, shorter operative times, and fewer perioperative complications than the nCRT group (37). However, the extent of lymph node resection and positive lymph node numbers after nCIT were similar to after nCT and nCRT in this study. Regarding other perioperative parameters such as radical resection rate and several postoperative recovery parameters, no significant differences were detected among the three groups.

Perioperative morbidity and mortality are the principal concerns in surgical treatment following neoadjuvant therapy. This study detected no significant statistical differences in the CTCAE grade related to neoadjuvant therapy and postoperative complication types among the three groups. Thus, the addition of camrelizumab to nCT did not increase morbidity or mortality. Additionally, another study by Qiao et al. showed that the total incidence of adverse events during nCIT was lower (77.1%) than nCT (91.7%, p=0.003) (23). As reported in previous studies (26, 30), pneumonia was the most prevalent major 30-day postoperative complication in this study. Other common complications included hoarseness, cardiac complication, and anastomotic leakage. Fortunately, no treatment- or surgery-related deaths were observed within 30 days after esophagectomy in this study, except for one sudden death in the nCT group, proving that esophagectomy following nCIT is safe and feasible.

Some limitations are apparent in this study. First, selection biases were inevitable between groups due to the limited sample size and the retrospective design. For example, the cT4 percentage in the nCIT group was 35.3%, which was significantly higher than in the nCT group. Second, the follow-up and recurrences data are insufficient to report mature OS and disease-free survival results. Third, each neoadjuvant therapy might have specific benefits for patient subgroups. The information on predictive biomarkers for therapeutic efficacy, such as PD-L1 expression, was absent in the present study. Therefore, the problem remains with selecting optimal patients who might benefit from different therapeutic modalities. Hence, more prospective phase III clinical trials with larger sample sizes and multiple centers should be conducted to identify the advantages and disadvantages of each neoadjuvant therapy in locally advanced resectable ESCC.

Conclusion

In conclusion, this real-world analysis showed that nCIT is safe and feasible, with satisfactory pCR and MPR rates. Esophagectomy following nCIT achieved several perioperative advantages over nCT and nCRT, with comparable perioperative morbidity and mortality. Although the 3-year OS after nCIT is slightly higher, the long-term survival benefits still require further investigation.

Data availability statement

The original contributions presented in the study are included in the article/supplementary material. Further inquiries can be directed to the corresponding authors.

Ethics statement

The studies involving human participants were reviewed and approved by The Ethics Committee of Hunan Cancer Hospital (No. 2022097). The patients/participants provided their written informed consent to participate in this study.

Author contributions

(I) Conception and design: BZ, QX, W, JW, XW, HZ. (II) Administrative support: BZ, QX. (III) Provision of study materials or patients: BZ, JW, DY, XL, WW, QX, XW, HZ, LG, XC, JL. (IV) Collection and assembly of data: BZ, JW, QX, XW, HZ, LG. (V) Data analysis and interpretation: BZ, QX. (VI) Manuscript writing: all authors. (VII) Final approval of manuscript: all authors. All authors contributed to the article and approved the submitted version.

Conflict of interest

The authors declare that the research was conducted in the absence of any commercial or financial relationships that could be construed as a potential conflict of interest.

Publisher's note

All claims expressed in this article are solely those of the authors and do not necessarily represent those of their affiliated organizations, or those of the publisher, the editors and the reviewers. Any product that may be evaluated in this article, or claim that may be made by its manufacturer, is not guaranteed or endorsed by the publisher.

References

1. Sung H, Ferlay J, Siegel RL, Laversanne M, Soerjomataram I, Jemal A, et al. Global cancer statistics 2020: GLOBOCAN estimates of incidence and mortality worldwide for 36 cancers in 185 countries. *CA: Cancer J Clin* (2021) 71(3):209–49. doi: 10.3322/caac.21660

2. Pennathur A, Gibson MK, Jobe BA, Luketich JD. Oesophageal carcinoma. *Lancet* (2013) 381(9864):400–12. doi: 10.1016/S0140-6736(12)60643-6

3. Arnold M, Ferlay J, van Berge Henegouwen MI, Soerjomataram I. Global burden of oesophageal and gastric cancer by histology and subsite in 2018. *Gut* (2020) 69(9):1564–71. doi: 10.1136/gutjnl-2020-321600

4. Leng XF, Daiko H, Han YT, Mao YS. Optimal preoperative neoadjuvant therapy for resectable locally advanced esophageal squamous cell carcinoma. *Ann New York Acad Sci* (2020) 1482(1):213–24. doi: 10.1111/nyas.14508

5. Demarest CT, Chang AC. The landmark series: Multimodal therapy for esophageal cancer. *Ann Surg Oncol* (2021) 28(6):3375–82. doi: 10.1245/s10434-020-09565-5

6. Yang H, Liu H, Chen Y, Zhu C, Fang W, Yu Z, et al. Long-term efficacy of neoadjuvant chemoradiotherapy plus surgery for the treatment of locally advanced esophageal squamous cell carcinoma: The NEOCRTEC5010 randomized clinical trial. *JAMA Surg* (2021) 156(8):721–9. doi: 10.1001/jamasurg.2021.2373

7. Ge F, Huo Z, Cai X, Hu Q, Chen W, Lin G, et al. Evaluation of clinical and safety outcomes of neoadjuvant immunotherapy combined with chemotherapy for patients with resectable esophageal cancer: A systematic review and meta-analysis. *JAMA Net Open* (2022) 5(11):e2239778. doi: 10.1001/jamanetworkopen.2022.39778

8. Zhu J, Leng X, Gao B, Wang B, Zhang H, Wu L, et al. Efficacy and safety of neoadjuvant immunotherapy in resectable esophageal or gastroesophageal junction carcinoma: A pooled analysis of prospective clinical trials. *Front Immunol* (2022) 13:1041233. doi: 10.3389/fimmu.2022.1041233

9. Yang Y, Tan L, Hu J, Li Y, Mao Y, Tian Z, et al. Safety and efficacy of neoadjuvant treatment with immune checkpoint inhibitors in esophageal cancer: Real-world multicenter retrospective study in China. *Dis esophagus* (2022) 35(11):doac031. doi: 10.1093/dote/doac031

10. Luo H, Lu J, Bai Y, Mao T, Wang J, Fan Q, et al. Effect of camrelizumab vs placebo added to chemotherapy on survival and progression-free survival in patients with advanced or metastatic esophageal squamous cell carcinoma: The ESCORT-1st randomized clinical trial. *Jama* (2021) 326(10):916–25. doi: 10.1001/jama.2021.12836

11. Liu J, Yang Y, Liu Z, Fu X, Cai X, Li H, et al. Multicenter, single-arm, phase II trial of camrelizumab and chemotherapy as neoadjuvant treatment for locally advanced esophageal squamous cell carcinoma. *J immunother Cancer* (2022) 10(3):e004291. doi: 10.1136/jitc-2021-004291

12. Liu J, Li J, Lin W, Shao D, Depypere L, Zhang Z, et al. Neoadjuvant camrelizumab plus chemotherapy for resectable, locally advanced esophageal squamous cell carcinoma (NIC-ESCC2019): A multicenter, phase 2 study. *Int J cancer.* (2022) 151(1):128–37. doi: 10.1002/ijc.33976

13. Yang P, Zhou X, Yang X, Wang Y, Sun T, Feng S, et al. Neoadjuvant camrelizumab plus chemotherapy in treating locally advanced esophageal squamous cell carcinoma patients: a pilot study. *World J Surg Oncol* (2021) 19(1):333. doi: 10.1186/s12957-021-02446-5

14. Yang W, Xing X, Yeung SJ, Wang S, Chen W, Bao Y, et al. Neoadjuvant programmed cell death 1 blockade combined with chemotherapy for resectable esophageal squamous cell carcinoma. *J immunother Cancer* (2022) 10(1):e003497. doi: 10.1136/jitc-2021-003497

15. Zhang B, Xiao H, Pu X, Zhou C, Yang D, Li X, et al. A real-world comparison between neoadjuvant chemoimmunotherapy and chemotherapy alone for resectable non-small cell lung cancer. *Cancer Med* (2022) 12(1):274–86. doi: 10.1002/cam4.4889

16. Cottrell TR, Thompson ED, Forde PM, Stein JE, Duffield AS, Anagnostou V, et al. Pathologic features of response to neoadjuvant anti-PD-1 in resected non-small-cell lung carcinoma: A proposal for quantitative immune-related pathologic response criteria (irPRC). *Ann Oncol* (2018) 29(8):1853–60. doi: 10.1093/annonc/mdy218

17. Mariette C, Dahan L, Mornex F, Maillard E, Thomas PA, Meunier B, et al. Surgery alone versus chemoradiotherapy followed by surgery for stage I and II esophageal cancer: Final analysis of randomized controlled phase III trial FFCD 9901. *J Clin Oncol* (2014) 32 (23):2416–22. doi: 10.1200/JCO.2013.53.6532

18. Chan KKW, Saluja R, Delos Santos K, Lien K, Shah K, Cramarossa GA, et al. Neoadjuvant treatments for locally advanced, resectable esophageal cancer: A network meta-analysis. *Int J cancer.* (2018) 143(2):430–7. doi: 10.1002/ijc.31312

19. Zheng Y, Liu XB, Sun HB, Xu J, Shen S, Ba YF, et al. A phase III study on neoadjuvant chemotherapy versus neoadjuvant toripalimab plus chemotherapy for locally advanced esophageal squamous cell carcinoma: Henan cancer hospital thoracic oncology group 1909 (HCHTOG1909). *Ann Trans Med* (2021) 9(1):73. doi: 10.21037/atm-20-5404

20. Ando N, Kato H, Igaki H, Shinoda M, Ozawa S, Shimizu H, et al. A randomized trial comparing postoperative adjuvant chemotherapy with cisplatin and 5-fluorouracil versus preoperative chemotherapy for localized advanced squamous cell carcinoma of the thoracic esophagus (JCOG9907). *Ann Surg Oncol* (2012) 19(1):68–74. doi: 10.1245/s10434-011-2049-9

21. Yang H, Liu H, Chen Y, Zhu C, Fang W, Yu Z, et al. Neoadjuvant chemoradiotherapy followed by surgery versus surgery alone for locally advanced squamous cell carcinoma of the esophagus (NEOCRTEC5010): A phase III multicenter, randomized, open-label clinical trial. *J Clin Oncol* (2018) 36(27):2796–803. doi: 10.1200/JCO.2018.79.1483

22. van Hagen P, Hulshof MC, van Lanschot JJ, Steyerberg EW, van Berge Henegouwen MI, Wijnhoven BP, et al. Preoperative chemoradiotherapy for esophageal or junctional cancer. *New Engl J Med* (2012) 366(22):2074–84. doi: 10.1056/NEJMoa1112088

23. Qiao Y, Zhao C, Li X, Zhao J, Huang Q, Ding Z, et al. Efficacy and safety of camrelizumab in combination with neoadjuvant chemotherapy for ESCC and its impact on esophagectomy. *Front Immunol* (2022) 13:953229. doi: 10.3389/fimmu.2022.953229

24. Wang H, Tang H, Fang Y, Tan L, Yin J, Shen Y, et al. Morbidity and mortality of patients who underwent minimally invasive esophagectomy after neoadjuvant chemoradiotherapy vs neoadjuvant chemotherapy for locally advanced esophageal squamous cell carcinoma: A randomized clinical trial. *JAMA Surg* (2021) 156(5):444–51. doi: 10.1001/jamasurg.2021.0133

25. Shah MA, Kennedy EB, Catenacci DV, Deighton DC, Goodman KA, Malhotra NK, et al. Treatment of locally advanced esophageal carcinoma: ASCO guideline. *J Clin Oncol* (2020) 38(23):2677–94. doi: 10.1200/JCO.20.00866

26. Zhang Z, Hong ZN, Xie S, Lin W, Lin Y, Zhu J, et al. Neoadjuvant sintilimab plus chemotherapy for locally advanced esophageal squamous cell carcinoma: A single-arm, single-center, phase 2 trial (ESONICT-1). *Ann Trans Med* (2021) 9(21):1623. doi: 10.21037/atm-21-5381

27. Xing W, Zhao L, Zheng Y, Liu B, Liu X, Li T, et al. The sequence of chemotherapy and toripalimab might influence the efficacy of neoadjuvant chemoimmunotherapy in locally advanced esophageal squamous cell cancer-a phase II study. *Front Immunol* (2021) 12:772450. doi: 10.3389/fimmu.2021.772450

28. Yan X, Duan H, Ni Y, Zhou Y, Wang X, Qi H, et al. Tislelizumab combined with chemotherapy as neoadjuvant therapy for surgically resectable esophageal cancer: A prospective, single-arm, phase II study (TD-NICE). *Int J Surg (London England).* (2022) 103:106680. doi: 10.1016/j.ijsu.2022.106680

29. Chen F, Qiu L, Mu Y, Sun S, Yuan Y, Shang P, et al. Neoadjuvant chemoradiotherapy with camrelizumab in patients with locally advanced esophageal squamous cell carcinoma. *Front Surg* (2022) 9:893372. doi: 10.3389/fsurg.2022.893372

30. Gu YM, Shang QX, Zhang HL, Yang YS, Wang WP, Yuan Y, et al. Safety and feasibility of esophagectomy following neoadjuvant immunotherapy combined with chemotherapy for esophageal squamous cell carcinoma. *Front Surg* (2022) 9:851745. doi: 10.3389/fsurg.2022.851745

31. Klevebro F, Alexandersson von Döbeln G, Wang N, Johnsen G, Jacobsen AB, Friesland S, et al. A randomized clinical trial of neoadjuvant chemotherapy versus neoadjuvant chemoradiotherapy for cancer of the oesophagus or gastro-oesophageal junction. *Ann Oncol* (2016) 27(4):660–7. doi: 10.1093/annonc/mdw010

32. Shapiro J, van Lanschot JJB, Hulshof M, van Hagen P, van Berge Henegouwen MI, Wijnhoven BPL, et al. Neoadjuvant chemoradiotherapy plus surgery versus surgery alone for oesophageal or junctional cancer (CROSS): Long-term results of a randomised controlled trial. *Lancet Oncol* (2015) 16(9):1090–8. doi: 10.1016/S1470-2045(15)00040-6

33. Chao YK, Chen HS, Wang BY, Hsu PK, Liu CC, Wu SC. Factors associated with survival in patients with oesophageal cancer who achieve pathological complete response after chemoradiotherapy: A nationwide population-based study. *Eur J cardio-thoracic Surg* (2017) 51(1):155–9. doi: 10.1093/ejcts/ezw246

34. Xu L, Wei XF, Li CJ, Yang ZY, Yu YK, Li HM, et al. Pathologic responses and surgical outcomes after neoadjuvant immunochemotherapy versus neoadjuvant chemoradiotherapy in patients with locally advanced esophageal squamous cell carcinoma. *Front Immunol* (2022) 13:1052542. doi: 10.3389/fimmu.2022.1052542

35. Allum WH, Stenning SP, Bancewicz J, Clark PI, Langley RE. Long-term results of a randomized trial of surgery with or without preoperative chemotherapy in esophageal cancer. *J Clin Oncol* (2009) 27(30):5062–7. doi: 10.1200/JCO.2009.22.2083

36. Zhang G, Zhang C, Sun N, Xue L, Yang Z, Fang L, et al. Neoadjuvant chemoradiotherapy versus neoadjuvant chemotherapy for the treatment of esophageal squamous cell carcinoma: A propensity score-matched study from the national cancer center in China. *J Cancer Res Clin Oncol* (2022) 148(4):943–54. doi: 10.1007/s00432-021-03659-7

37. Jing SW, Qin JJ, Liu Q, Zhai C, Wu YJ, Cheng YJ, et al. Comparison of neoadjuvant chemoradiotherapy and neoadjuvant chemotherapy for esophageal cancer: A meta-analysis. *Future Oncol (London England).* (2019) 15(20):2413–22. doi: 10.2217/fon-2019-0024

38. Han J, Wang Z, Liu C. Survival and complications after neoadjuvant chemotherapy or chemoradiotherapy for esophageal cancer: a meta-analysis. *Future Oncol (London England).* (2021) 17(17):2257–74. doi: 10.2217/fon-2021-0021

39. Yin GQ, Li ZL, Li D. The safety and efficacy of neoadjuvant camrelizumab plus chemotherapy in patients with locally advanced esophageal squamous cell carcinoma: A retrospective study. *Cancer Manage Res* (2022) 14:2133–41. doi: 10.2147/CMAR.S358620

40. Jing SW, Zhai C, Zhang W, He M, Liu QY, Yao JF, et al. Comparison of neoadjuvant immunotherapy plus chemotherapy versus chemotherapy alone for patients with locally advanced esophageal squamous cell carcinoma: A propensity score matching. *Front Immunol* (2022) 13:970534. doi: 10.3389/fimmu.2022.970534

41. Xiao X, Yang YS, Zeng XX, Shang QX, Luan SY, Zhou JF, et al. The comparisons of neoadjuvant chemoimmunotherapy versus chemoradiotherapy for oesophageal squamous cancer. *Eur J cardio-thoracic Surg* (2022) 62(1):ezac341. doi: 10.1093/ejcts/ezac341

42. Leng X, He W, Yang H, Chen Y, Zhu C, Fang W, et al. Prognostic impact of postoperative lymph node metastases after neoadjuvant chemoradiotherapy for locally advanced squamous cell carcinoma of esophagus: From the results of NEOCRTEC5010, a randomized multicenter study. *Ann Surg* (2021) 274(6):e1022–e9. doi: 10.1097/SLA.0000000000003727

43. Hong ZN, Gao L, Weng K, Huang Z, Han W, Kang M. Safety and feasibility of esophagectomy following combined immunotherapy and chemotherapy for locally advanced esophageal squamous cell carcinoma: A propensity score matching analysis. *Front Immunol* (2022) 13:836338. doi: 10.3389/fimmu.2022.836338

日中笹川医学奨学金制度（学位取得コース）中間評価書
課程博士：指導教官用

Supported by 日本財団 THE NIPPON FOUNDATION

第 44 期　　研究者番号：G4407　　　　　　　　　作成日 ： 2023 年 3 月 1 日

氏　名	周　英	ZHOU YING	性別	F	生年月日	1983/11/10
所属機関（役職）	金沢大学大学院人間社会環境研究科（大学院生）					
研究先（指導教官）	金沢大学大学院人間社会環境研究科人間社会環境学専攻（堤 敦朗　教授）					
研究テーマ	日本における精神科医療通訳が受ける心理的影響に関する研究：質的研究 A study of the psychological impact of psychiatric interpreter in Japan: A qualitative study					
専攻種別	☐論文博士			☑課程博士		

研究者評価（指導教官記入欄）

成績状況	優　良　可　不可 学業成績係数=	取得単位数
		取得単位数 14／取得すべき単位総数 16

学生本人が行った研究の概要	日本の外国人医療の現場では医療通訳が存在し、大きな役割を果たすが、彼らがボランティアベースで取り組んでいることが多く、医学アマチュアとして医療現場でどう立ち振る舞い、どういった困難に直面しているかが分からない。心的外傷を受け、仕事に復帰できずに辞めてしまうケースや、精神科の医療通訳が患者と精神科医の間に立ち、ストレスをためているケースがある。本人は日本の医療通訳者、とりわけ精神科医療通訳者が受ける心理的影響から着手して、日本の医療通訳の実態を究明している。
総合評価	【良かった点】 独自性があり、これまでに触れられていないテーマに目をつけている。 意欲的にとりくんでおり、研究方法等について習得している。 【改善すべき点】 海外の関連研究をより多く参考した方が良い。 【今後の展望】 質的研究の調査段階を経て、結果がまとめられたら、結果に基づき、量的研究で検証すると良い。
学位取得見込	このまま進めていけば、学位取得が可能である。

評価者（指導教官名）　堤 敦朗

日中笹川医学奨学金制度(学位取得コース)中間報告書
研究者用

Supported by
日本財団
THE NIPPON
FOUNDATION

第44期　　　　研究者番号：G4407　　　　作成日：2023年3月1日

氏名	周 英	ZHOU YING	性別	F	生年月日　1983/11/10

所属機関(役職)	金沢大学大学院人間社会環境研究科(大学院生)
研究先(指導教官)	金沢大学大学院人間社会環境研究科人間社会環境学専攻(堤 敦朗 教授)
研究テーマ	日本における精神科医療通訳が受ける心理的影響に関する研究：質的研究 A study of the psychological impact of psychiatric interpreter in Japan: A qualitative study

専攻種別	論文博士	□	課程博士	☑

１．研究概要（1）

1）目的（Goal）
　2020年6月末に日本における在留外国人数は288万5904人、日本の総人口のおよそ2％を占めている。在日外国人医療に関する病院や診療所では「言葉・コミュニケーション」「保健・経済的側面」「保健医療システムの違い」「異文化の理解」などの課題を抱えているが、これらの問題解決のために、医療通訳が果たす役割は重要である。しかし、医療の現場では死産や癌の告知、余命の説明や抗がん剤の治療など、精神的に負担の大きい内容の通訳を強いられることがある。時には、患者や家族のやり場のない怒りやストレスのはけ口が医療従事者や通訳士に向けられることもあり、心的外傷を受けた医療通訳は苦しみ、仕事に復帰できずに辞めてしまうケースもあるという。特に、精神科医療における通訳は、様々な精神的症状を呈している患者と精神科医の間に立ち、一般身体の医療通訳以上に心理的な影響を受けていると報告されている。さらに、日本では医療通訳が国家資格として確立されず、多くがボランティアベースで取り組む医学アマチュアであることも、通訳の心理的負担の要因になっている。したがって、本研究は、日本における医療通訳、特に精神科医療通訳者が医療通訳の仕事によって受ける心理的影響について、明らかにすることを目的とする。

2）戦略（Approach）
　構築主義的グランデッドセオリーに基づき、データを収集し、データをLine by lineコード化する。コーディングによって新たなカテゴリーを生成する。カテゴリーを確かめるために、さらにデータを収集する。元々のデータに戻って、読み直し、他に新たなカテゴリーが生まれる余地がないかを確認する。必要に応じて、新たなリサーチクエスチョンを立てる。分析過程で生成したカテゴリーをデータと絶えずに比較をしていく。新しいコード・内容が出てこなくなるまで、調査をしていく。最終的に状況限定理論（その適用が特定の状況に限定される理論）を形成していくのを目的にする。

3）材料と方法（Materials and methods）
　本研究の調査が主に医療通訳者（精神科医療通訳の経験を持つ）を対象とする。候補者はNPO、精神科クリニックおよび大学病院などに所属する通訳者たちとなる。可能な範囲で、対象者の多様性（年齢、性別、言語、所属機関など）を重視する。
　半構造化インタビューの方法を採用する。新型コロナウイルスの影響で、対面方式ではなく、遠隔方式（「ZOOM」または「テンセント会議」）を使用する。時間は一人当たり1-2時間で、インタビューをする際に録音の許可をいただき、録音機2台で録音させていただいた後、文字起こしをし、逐語録を作る。

4）実験結果（Results）
　調査中であり、まだ結果を出していない。現段階で9名の対象者をインタビューした。属性に関しては、女性8名で男性1名；NPO所属7名で大学病院所属2名；通訳8名でコーディネーター1名；50代以上7名で50代以下2名となる。文字起こしとコーディング作業をしているが、現段階では、年齢、雇用形態および性別で違いが見られたため、次の段階では、若い世代、大学病院所属の医療通訳、男性を重点的に探して、調査していく予定である。

5）考察（Discussion）
　結果が出ていないため、考察段階ではないが、質的研究の結果を持って、量的研究を行い、検証していくことも視野に入れている。

１．研究概要（2）

6）参考文献（References）

出入国在留管理庁　在留外国人統計（旧登録外国人統計）統計表
https://www.moj.go.jp/isa/policies/statistics/toukei_ichiran_touroku.html　（アクセス日：2022年3月1日）
中村安秀　「医療通訳士の必要性と重要性　－外国人に対する保健医療の現状と課題－」『医療通訳士という仕事』　大阪：大阪大学出版社：2013：3-19
南谷かおり　「病院における医療通訳士の役割」『医療通訳士という仕事』　大阪：大阪大学出版社：2013：61-68
阿部裕　精神医療におけるコミュニティ通訳の必要性　シリーズ多言語・多文化協働実践研究16　2013：111-112
阿部裕　多文化精神医療　自然、風土、文化、そして、こころ　鹿児島：ラグーナ出版：2019
阿部裕　精神医療におけるコミュニティ通訳の必要性　シリーズ多言語・多文化協働実践研究16　2013：105-113
村松紀子　「コミュニティ活動における医療通訳士の役割」『医療通訳士という仕事』　大阪：大阪大学出版社：2013：69-79
長尾ひろみ　「医療通訳の職業倫理規定」『医療通訳入門』東京：松柏社：2007 29-46
押見貴之　精神医療における医療通訳　こころと文化　2009：8巻：108-113
木原雅子　木原正博　質的研究法：その理論と方法　健康・社会科学分野における展開と展望
Raval H (2006) A systematic perspective on working with refugees. Clinical Child Psychology and Psychiatry
Haenel F (1997) Aspects and problems associated with the use of interpreters in psychotherapy of victims of torture. Torture
Sande H (1998) Supervision of refugee interpreters: five years of experience from northern Norway. Nordic Journal of Psychiatry
Miller KE(2005) The role of interpreters in psychotherapy with refugees: an exploratory study. American Journal of Orthopsychiatry
Butler C(2009) Speaking the unspeakable: female interpreters' responses to working with women who have been raped. Clinical Psychology Forum (supplement)
Loutan L(1999)　Medical interpreters have feelings too. Sozial‐Und Praventivmedizin
Doherty M(2010) How does it feel for you? The emotional impact and specific challenges of mental health interpreting

2. 執筆論文　Publication of thesis　※記載した論文を添付してください。Attach all of the papers listed below.

論文名 1 Title	精神科医療通訳の「患者擁護」について				
掲載誌名 Published journal	日中医学				
	2022　年　　11　月	Vol.37No.3　巻（号）	29　頁　〜　33　頁	言語 Language	日本語と中国語
第1著者名 First author	周英	第2著者名 Second author	堤敦朗	第3著者名 Third author	
その他著者名 Other authors					
論文名 2 Title					
掲載誌名 Published journal					
	年　　　月	巻（号）	頁　〜　頁	言語 Language	
第1著者名 First author		第2著者名 Second author		第3著者名 Third author	
その他著者名 Other authors					
論文名 3 Title					
掲載誌名 Published journal					
	年　　　月	巻（号）	頁　〜　頁	言語 Language	
第1著者名 First author		第2著者名 Second author		第3著者名 Third author	
その他著者名 Other authors					
論文名 4 Title					
掲載誌名 Published journal					
	年　　　月	巻（号）	頁　〜　頁	言語 Language	
第1著者名 First author		第2著者名 Second author		第3著者名 Third author	
その他著者名 Other authors					
論文名 5 Title					
掲載誌名 Published journal					
	年　　　月	巻（号）	頁　〜　頁	言語 Language	
第1著者名 First author		第2著者名 Second author		第3著者名 Third author	
その他著者名 Other authors					

3．学会発表 Conference presentation ※筆頭演者として総会・国際学会を含む主な学会で発表したものを記載してくだ

※Describe your presentation as the principal presenter in major academic meetings including general meetings or international me

学会名 Conference	第29回多文化間精神医学会学術総会				
演 題 Topic	日本における医療通訳（特に精神科医療通訳）が受ける心理的影響に関する研究：質的研究				
開催日 date	2023 年 1 月 20 日	開催地 venue	滋賀県大津市		
形式 method	☑ 口頭発表 Oral □ ポスター発表 Poster	言語 Language	☑ 日本語 □ 英語 □ 中国語		
共同演者名 Co-presenter	堤敦朗、砂子阪将大				
学会名 Conference					
演 題 Topic					
開催日 date	年 月 日	開催地 venue			
形式 method	□ 口頭発表 Oral □ ポスター発表 Poster	言語 Language	□ 日本語 □ 英語 □ 中国語		
共同演者名 Co-presenter					
学会名 Conference					
演 題 Topic					
開催日 date	年 月 日	開催地 venue			
形式 method	□ 口頭発表 Oral □ ポスター発表 Poster	言語 Language	□ 日本語 □ 英語 □ 中国語		
共同演者名 Co-presenter					
学会名 Conference					
演 題 Topic					
開催日 date	年 月 日	開催地 venue			
形式 method	□ 口頭発表 Oral □ ポスター発表 Poster	言語 Language	□ 日本語 □ 英語 □ 中国語		
共同演者名 Co-presenter					

4．受賞（研究業績） Award (Research achievement)

名 称 Award name					
	国名 Country		受賞年 Year of	年	月
名 称 Award name					
	国名 Country		受賞年 Year of	年	月

5．本研究テーマに関わる他の研究助成金受給 Other research grants concerned with your resarch them

受給実績 Receipt record	☐ 有　　■ 無
助成機関名称 Funding agency	
助成金名称 Grant name	
受給期間 Supported period	年　　　　月 ～　　　　　年　　　　月
受給額 Amount received	円
受給実績 Receipt record	☐ 有　　☐ 無
助成機関名称 Funding agency	
助成金名称 Grant name	
受給期間 Supported period	年　　　　月 ～　　　　　年　　　　月
受給額 Amount received	円

6．他の奨学金受給 Another awarded scholarship

受給実績 Receipt record	☐ 有　　■ 無
助成機関名称 Funding agency	
奨学金名称 Scholarship name	
受給期間 Supported period	年　　　　月 ～　　　　　年　　　　月
受給額 Amount received	円

7．研究活動に関する報道発表 Press release concerned with your research activities

※記載した記事を添付してください。Attach a copy of the article described below

報道発表 Press release	☐ 有　　■ 無	発表年月日 Date of release	
発表機関 Released medium			
発表形式 Release method	・新聞　・雑誌　・Web site　・記者発表　・その他（　　　　　　　　　　　）		
発表タイトル Released title			

8．本研究テーマに関する特許出願予定 Patent application concerned with your research theme

出願予定 Scheduled	☐ 有　　■ 無	出願国 Application	
出願内容（概要） Application contents			

9．その他 Others

指導責任者（記名）　　堤 敦朗

精神科医療通訳の「患者擁護」について

"Patient Advocacy" for Psychiatric Interpreters

金沢大学人間社会環境研究科 博士後期課程　周　　英

金沢大学融合研究域 教授　堤　敦朗

【Abstract】

Globalization has facilitated international travel, and the number of non-native patients receiving psychiatric services in Japan is increasing. Consequently, differences in language and culture have become the biggest issues faced by psychiatric institutions. Therefore, psychiatric interpreters are expected to play a major role. Studies have indicated that medical interpreters require advocacy, especially in psychiatric settings. This article clarifies what is meant by the term "advocacy" and why it is required in psychiatric interpretation.

【Key words】

Psychiatric interpreters, Advocacy, Community interpreters

はじめに

世界規模でグローバル化が進み、人々の国境を跨ぐ移動が容易となっている。出入国在留管理庁[1]によると、2020年6月末に日本における在留外国人数は288万5904人で、日本の総人口のおよそ2%を占めている。

日本全国の精神医療機関に対して実施された「精神医療機関における外国人患者受入の現状と課題把握に関する調査」[2]（2020年3月）で、精神医療機関を受診する外国人患者の対応には多くの施設が苦慮していて、その背景に「言語面」や「文化的」背景が存在すること、また日本にいる外国人に対応するために「同意書および告知文書」の多言語版の作成や精神保健福祉法の早急な整備など、精神科医療における外国人患者の受け入れ環境の整備の必要性などが認識された。

このような状況下において、医療通訳が大きな役割を担うことができる。「言葉」の問題に関して、「心の病を患うと、外国語能力が極端に落ちる」「母語以外で自分の内面を語ることは難しい」[3]ことがあるため、医療通訳が間に立つと、患者が母語で病状や心境などを語ることができる。さらに「文化」の問題に関しては、両方の文化を知る医療通訳者がいる場合、文化の違いによる理解の差に気づき、適度な範囲内で補足説明をすることで医師と患者の間の意思疎通がよりスムーズになり、医師の病状把握や患者の安心感につながることが期待できる。

本稿では、精神科の医師と患者の間に立つ医療通訳者のことを「精神科医療通訳」とする。「精神科医療通訳」は「一般身体の医療通訳」と区別をするために名づけたもので、既存の固有名詞ではない。また、医療通訳は「コミュニティ通訳」の一種であるため、医療通訳を論ずるにあたり、まずコミュニティ通訳について論ずる必要がある。

コミュニティ通訳とは

通訳の種類の分類方法には大きく分けて２つある。一つは通訳の手法で分類する方法であり、「同時通訳」「逐次通訳」「ウィスパリング通訳」がある。もう一つは目的によって分類する方法であり、「会議通訳」「エンターテインメント通訳」「ビジネス通訳」「放送通訳」「コミュニティ通訳」「通訳ガイド」などがある[1]。

本稿で取り扱う「コミュニティ通訳」とは、在住外国人が専門職と話す時に使う通訳であり、具体的には「医療通訳」「司法通訳」「行政通訳」「教育通訳」などが挙げられる[4]。これらの異なるタイプの通訳者は異文化の媒介者として意思疎通のための役割を果たす点においては同じだが、通訳者が置かれている環境がそれぞれ異なるため、通訳に求められる「言葉の伝達」以外の要素が異なってくる。例えば、「司法通訳」は中立性が極端に求められる[5]のに対し、医療通訳は医師と患者のつなぎ役として患者の擁護をする必要がある[6]。

精神科医療通訳の特殊性

医療通訳の役割を決定するいくつかの要素の中の一つに「医療科の特質」がある。

精神科医療の特質は、精神科医が患者の「行動・振る舞い」「認知能力」「コミュニケーション能力」を確認して診断をする点にある。これらの要素を判断するために、Turner[7]は患者の話し方の要素、すなわち「構文」「語順」「語彙の整合性」「言葉の

脱落」「文化や宗教との整合性」「母国語での言語能力」の６つに注目すべきだと述べている。

つまり精神科医療における医療通訳では、患者の話す言葉の構文や語順の自然さ、不自然さを再現し、語彙の選択や整合性に問題があればそれも再現し、患者が話す事柄がその所属する文化や宗教において適切なものであるかも説明し、さらには通訳するだけではわからない患者の母国語での言語能力の評価を行うことまでもが求められるのである。精神科医療において医療通訳は、辻褄の合わないものは辻褄の合わないまま通訳して、その説明も求められる[8]。例えば、統合失調症の幻覚妄想状態の患者がいるとする。統合失調症患者の最も重要な障害は思考障害で、精神科医が患者の訴えを聞いても、思考に論理の飛躍があるため、話の脈絡がうまくつかめず、理解不能であったりする。構文や語順の崩れ、語彙の整合性の不具合、言葉の脱落、自分自身で新しい言葉を作るという言語新作もみられる[6]。しかし、通訳者はそのまま通訳し、その内容についても説明しなければならない。

さらに、上述の６つの要素を再現するには「機械的な通訳」では足りないため、事前に医師と通訳者が打ち合わせを行う必要がある。Turner が診察前の打ち合わせ項目として「患者の医療背景」「患者の文化背景」「医療通訳の役割」「異文化問題への対処法」そして「中断方法」を提起している。さらに診察後の確認項目として、「診断に重要な要素の確認」と「通訳者の精神状態の把握」を指摘している[7]。

事前の打ち合わせに関して、精神科医の阿部先生は、通訳者と患者が行うことも必要だと指摘する[6]。診察をスムーズに進めるためには、患者が受

---

[1] 通訳の分類法は国や地域、ひいては通訳派遣会社などによって違うため、上記の分類法は、状況や場面によって呼称が変わる場合がある。

診に至った背景を通訳者が事前に聞き取っておく必要があり、そのため通訳者は、精神科医療に関する医学的知識をある程度有しておく必要がある。また、医師と通訳者の事前打ち合わせと比較して、患者と通訳者の事前打ち合わせは、患者に通訳者が自分の味方であると感じさせやすいため、患者と通訳者の信頼構築につながる可能性がある。

精神科医療において同じ通訳者が担当することがより良いと考えられている。同じ通訳が継続的に担当すると患者と通訳者の間に個人的な関係が生まれ、「中立的」な立場が取りにくくなる懸念もあるが、他方で同じ通訳者が担当することで、前述した6つの要素に精通しやすくなり、患者との信頼関係の構築が容易になるメリットもある。その結果、診断に必要な要素を効率よく、正確に伝えることが可能になる[8]。

したがって、精神科医療以外の医療における通訳は主に身体疾患に関わる医学的な知識が求められるが、精神医療における通訳は、精神疾患の症状、診断名や精神医療制度などに関する専門的知識が求められる。また、精神科医と患者の心をつなぐ理解者として位置づけられなければならないため、語学力以外に文化の理解や患者の擁護が求められる[8]。

精神医療の通訳者に求められる専門性とは、精神疾患名とその疾患の概念、精神症状、診断方法、治療法、薬物の効用と副作用、治療経過、予後と精神医療制度の知識を指す。さらに、診察室で患者と精神科医をつなぐ通訳者として、自分の感情をできるだけ排除し、習得した知識を用いて両者の橋渡しをすることである。そのためには、両者の表情に気を配り、患者の苦悩や文化社会的背景を理解し、それぞれの感情と会話を正確な訳語で適切に伝え、患者と精神科医が通訳内容に対して同じ解釈をしているかを見抜いて、両者のつながりに揺るぎなく位置することが求められる[6]。

精神科医療通訳の「患者擁護」とは

日本看護協会[9]によると、「患者擁護」＝アドボカシー（advocacy）とは権利擁護や代弁などという意味であり、看護実践において看護職は、患者のアドボケーター（権利擁護者、代弁者）として患者の権利を擁護し、患者の価値や信念に最も近い決定ができるように援助し、さらに患者の人間としての尊厳、プライバシーなどを尊重しなければならないという。

通訳の立場での「患者擁護」の定義について、国際的な規定やアメリカ、日本の規定、また専門家の見解を以下に示す。

・ 国際医療通訳者協会[10]（IMIA：International Medical Interpreters Association）は医療通訳者の行動に関する倫理規定を策定した。倫理規程においては「通訳者は、患者の権利を擁護する役割、および情報伝達のために適切かつ必要な場合に限り、専門的な判断力で、異文化間の仲介者として医療提供者と患者に文化の違いや慣行を説明する役割を担う。」との記述がある。

・ 全米医療通訳協議会[11]（NCIHC）は2004年7月に「全米医療通訳倫理規定」を発表した。この規定で「患者擁護」について「患者の健康、福利、あるいは尊厳が危険にさらされている場合、通訳者は、アドボケーター（擁護者）としてふるまうことを正当化されるかもしれない。アドボカシー（擁護的行為）とは、健康上の良い結果を支援するという意図を伴い、コミュニケーション促進の範囲を超えて、個人のために行われる行為であると理解される。擁護は、状況を慎重に思慮深く分析した後に、そして、他のより介入的でない手段によって問題が解決されなかった場合にのみ、行われるべきである。」

と示している。

・ 日本における規程に関して、厚生労働省の「医療通訳」[12] テキストでは、権利擁護（アドボカシー）に関して「権利擁護（アドボカシー）とは患者が生命の尊厳や危機にさらされている場合には、適切な知識と判断によって権利擁護を果たすことである。」と示している。さらに、「通訳者が権利擁護を行うことは、通訳者の役割を超えており、すべきではないと禁止している国もあるが、本基準では、医療通訳においては、適切な状況分析をした上で、患者の安全や生命が脅かされる、危機にさらされている場合に限り、本来の医療通訳者としての役割から外れて、権利擁護のための行動を取ることができる」と付け加えている。

・ 専門家は通訳者の「患者擁護」について、飯田[13] は「医療通訳士は患者と医療従事者の言葉と文化、置かれる状況を理解するから、全ての人に適切な医療サービスが提供されるよう尽力することが求められ、患者擁護ができる。」、また「権利の擁護は医療通訳士が直接的代理や代行を行うことでなく、患者が自らの権利を確保し回復して行くための支援を行うこと」と述べている。

・ エレーラ・ルルデス[14] は「患者擁護」について、「外国人の患者などが言葉の壁によって自分を語れない（自身を代弁できない）場合、通訳士は「救済者」として手を差し伸べる」、「日本に暮らす外国人の社会的・経済的状況を把握したり、患者のわずかな顔の表情から文化的、家族的、個人的な状況を読み取ったりして必要な擁護を行う」、「通訳士は外国人に対する情報提供者（情報源）の役割を担っている。患者は通訳士に対して色々な期待を寄せているが、通訳者は、いつ直接介入すべきか、いつ他者に援助を求めるべきかについて判断しなければならない」、「通訳士という仕事は、良心的で粘り強く、過保護にならない程度の暖かさを持った尊敬されるような対人援助である」と述べている。

以上の倫理規定および専門家の観点を踏まえ、通訳者の立場における「患者擁護」は「患者が危険にさらされ、他の介入的な手段がない場合にのみ行って良いという極めて稀な行為だ」と一部に認識されている一方、「通訳者が患者を観察し、患者が危険にさらされている場合には、患者の権利が尊重されるように患者の代弁者になったり、文化の理解者として患者と医者との間の文化的なギャップを埋めたり、情報提供者になったり、患者のために他の人に助けを求めたりして患者の回復を支援することである」と暫定的に定義づけることもできる。

終わりに

精神科医療通訳の特殊性と「患者擁護」の定義について論じた。しかし、実際の現場で精神科医療通訳をしている医療通訳者たちは「患者擁護」をどのように認識・実行しているのか、また実行する際の課題の有無に関して、引き続き研究をしていきたい。

謝辞

引用文献：
[1] 出入国在留管理庁　在留外国人統計（旧登録外国人統計）統計表　https://www.moj.go.jp/isa/policies/statistics/toukei_ichiran_touroku.html （アクセス日：2022 年 3 月 1 日）
[2] 厚生労働省課題　令和元年度障害者総合福祉推進事業精神医療機関における外国人患者受入の現状と課題把握に関する調査 https://www.mhlw.go.jp/content/12200000/000672477.pdf（アクセス日：2022 年 3 月 1 日）
[3] 阿部裕　多文化精神医療　鹿児島：ラグーナ出版：2019
[4] 村松紀子 「コミュニティ活動における医療通訳士の役割」『医療通訳士という仕事』 大阪：大阪大学出版社：2013：76
[5] 長尾ひろみ 「医療通訳の職業倫理規定」『医療通訳入門』東京：松柏社：2007 29-46
[6] 阿部裕　精神医療におけるコミュニティ通訳の必要性シリーズ多言語・多文化協働実践研究16　2013：105-113
[7] Turner G Onsite Mental Health Interpreting A workshop for Professional Interpreters from MMHA's NT forum
[8] 押見貴之　精神医療における医療通訳　こころと文化 2009：8 巻：108-113
[9] 日本看護協会　看護実践情報　臨床倫理のアプローチ https://www.nurse.or.jp/nursing/practice/rinri/text/basic/approach/index.html（アクセス日：2022 年 3 月 1 日）
[10] IMIA Code of Ethics https://www.imiaweb.org/code/default.asp（アクセス日：2022 年 3 月 1 日）
IMIA 倫理規定（日本語訳）https://www.imiaweb.org/uploads/pages/393.pdf（アクセス日：2022 年 3 月 1 日）
[11] 全米医療通訳倫理規定 https://www.migrationpolicy.org/sites/default/files/language_portal/ANationalCodeofEthicsforInterpretersinHealthCareinJapanese_0.pdf（アクセス日：2022 年 3 月 1 日）
[12] 厚生労働省　医療通訳に関する資料　テキスト「医療通訳」https://www.mhlw.go.jp/content/10800000/000385181.pdf アクセス日：2022 年 3 月 1 日）
[13] 飯田奈美子 「医療通訳士倫理規定を読み解く」『医療通訳士という仕事』 大阪：大阪大学出版社：2013：33-47
[14] エレーラ・ルルデス 「外国人患者から見た医療通訳士の役割」『医療通訳士という仕事』 大阪：大阪大学出版社：2013：89-97

◆━━━━◆著者連絡先◆━━━━◆

周　英

金沢大学人間社会環境研究科 博士後期課程

E-mail：11431984@qq.com

精神科医疗口译的"患者拥护"

"Patient Advocacy" for Psychiatric Interpreters

金泽大学人间社会环境研究科 博士后期课程 ｜ 周　英

金泽大学融合研究域 教授 ｜ 堤　敦朗

【Abstract】

Globalization has facilitated international travel, and the number of non-native patients receiving psychiatric services in Japan is increasing. Consequently, differences in language and culture have become the biggest issues faced by psychiatric institutions. Therefore, psychiatric interpreters are expected to play a major role. Studies have indicated that medical interpreters require advocacy, especially in psychiatric settings. This article clarifies what is meant by the term "advocacy" and why it is required in psychiatric interpretation.

【Key words】

Psychiatric interpreters, Advocacy, Community interpreters

前　言

全球化正在世界范围进行，人们可以更容易的在世界各地移动。根据日本出入国在留管理厅[1]的数据显示，截至 2020 年 6 月底，在日本的外国人人数为 288 万 5904 人，约占日本总人口的 2%。

根据以日本全国范围的精神科医疗机构为对象开展的"精神科医疗机构接收外国人患者的现状和问题把握的相关调查"[2]（2020 年 3 月）显示，许多精神科医疗机构在接诊外国患者时感到困惑，并表示其原因在于"语言"和"文化"的不同。为了更好地应对在日本的外国患者，有必要准备更多种语言版本的"知情同意书和告知文件"，尽早完善精神保健福祉法，以改善对外国患者的接收环境。

在这样的大背景下，医疗口译员可以发挥重要作用。在"语言"的问题上，由于"当一个人患有精神疾病时，他的外语能力会极大降低。""使用母语之外的语言来谈论自己内心感受是很困难的"[3]，所以医疗口译员可以帮助患者使用母语来谈论自己的病情和感受。此外，在"文化"方面，可以预见，了解两种文化的医疗口译员更明白文化差异造成的理解偏差，并能在合理的范围内提供补充说明，从而使医生和患者之间的沟通更加顺畅，使医生更好的了解患者病情并使患者更为放心。

在本文中，将介于精神科医生和患者之间的医疗口译员称为"精神科医疗口译"。它并非固定术语，是为了与"一般身体类医疗口译"区分，才冠以此名。医疗口译是"社区口译"的一种，在探讨医疗口译之前，需要首先认识什么是社区口译。

什么是社区口译

口译主要有两种分类。一种是按照翻译方式，可分为"同声传译"、"交替传译"和"耳语翻译"。另

一种是按照翻译目的划分。主要类别包括"会议口译"、"娱乐口译"、"商务口译"、"广播口译"、"社区口译"和"导游口译"等[1]。

而本文所涉及的"社区口译"是指居住在日本的外国居民与专职人员交谈时所使用的口译。具体包括"医疗口译"、"司法口译"、"行政口译"和"教育口译"[4]。这些不同类型的口译员作为不同文化间的中介，发挥促进沟通的作用方面是相同的，但由于口译员所处的环境不同，所以对他们除了"语言传播"之外的素质要求也不同。比如，"司法口译"被要求必须极为中立[5]，而与此相对，医疗口译则更需要口译员作为医生与患者之间的纽带，对患者进行拥护[6]。

精神科医疗口译的特殊性

有几个要素决定了医疗口译的实际作用，其中之一是"医疗部门的特质"。

精神科医学的特殊性在于医生诊断时需要考虑患者的"行动和行为"、"认知能力"以及"沟通能力"。Turner[7] 认为，精神科医生需要关注患者的表达，即"句法"、"词序"、"词汇的一致性"、"单词的遗漏"、"与文化和宗教的一致性"、"母语的语言能力"这六要素。

也就是说，精神科医疗口译，需要在翻译中再现出患者所表达的语言的句法和词序是否自然，如果词汇的选择和一致性方面出现问题也应将其体现在翻译中，并对患者所说的事由是否与其所属的文化与宗教相契合进行说明。并且，因为仅靠翻译无法评估患者的母语水平，口译员还需要对其母语能力进行评价。也就是说，精神科医疗口译如果遇到患者的话语不合常理不合逻辑，也应该使用不合常理不合逻辑的方式进行翻译[8]。例如，假设有一位精神分裂症的患者出

现幻觉和妄想。由于精神分裂症患者最严重的问题是思维障碍，所以精神科医生即使倾听了患者的主诉，但由于病人的思维具有跳跃性，无法掌握其言语脉络，从而导致患者的话语无法理解。除了句法和词序的混乱之外，还可能出现词汇的不一致以及单词的遗漏和患者自身创造出新语言的语言创新现象[6]。但是，出现这样的情况时，口译员必须如实翻译，并对这些情况进行解释说明。

此外，由于"机械翻译"不足以再现上述六个要素，所以需要医生与口译员进行事前沟通确认。Turner 提出了"患者的就医经历"、"患者的文化背景"、"医疗口译的作用"、"跨文化问题的处理方法"以及"如何打断"来作为检查前的沟通项目。并认为，就诊后应该"确认诊断过程中的重要要素"和"把握口译员的精神状态"[7]。

但是，关于事前沟通确认，精神科的阿部医生认为应该由口译员和患者来进行事前沟通[6]。为使诊疗能够顺利进行，口译员需要事先听取患者的就诊背景，因此，口译员需要具备一定程度的精神科方面的医学知识。此外，与医生和口译员的事前沟通确认相比，患者与口译员的事前沟通确认能让患者更容易产生口译员是站在自己一方的感觉，从而更容易的建立双方之间的信任关系。

在精神科医疗中由同一位口译员来持续负责被认为是更为理想的。但也有人担心，同一位口译员持续负责会使患者和译员之间形成个人关系，从而很难保持"中立"立场。但另一方面，同一位口译员负责的好处在于更容易把握上述六要素，并更容易与患者建立信任关系，从而能够更高效准确的传递诊断所需的要素信息[8]。

因此，精神科医疗之外的医疗口译主要需要掌握与身体疾病相关的医学知识。而精神科医疗口译，则需要具备精神疾病的症状、诊断名称和精神保健系统

---

[1] 由于各国、各地区以及各口译派遣机构对口译员的分类不同，上述分类法在不同的情况和场合下会有不同的叫法。

的专业知识。此外，他们还必须是精神科医生与患者心灵之间的理解纽带。除了语言能力之外，还需要有文化的理解和对患者的拥护[8]。

精神科医疗口译需要具备的专业素质，是指精神疾病的名称及其概念、精神疾病的症状、诊断方法、治疗方法、药物效益和副作用、治疗过程、预后和精神疾病医疗系统的相关知识。此外，作为诊疗室中患者与精神科医生的桥梁，口译员需要尽量不受自己情绪的影响，用所掌握的知识为二者的沟通作出努力。为此，需要既注意双方的面部表情，又理解患者的苦恼和文化社会背景，并用正确的语言恰当地传达每一次情绪和对话，观察患者和精神科医生对翻译内容是否有相同的理解，坚定地置身于两者的沟通之中[6]。

精神科医疗口译的"患者拥护"是什么

根据日本护理协会[9]的说法，"患者拥护"= advocacy 有权利拥护和代言等意思。在护理实践中，护士作为患者的 advocator（权利拥护者、代言人），需要维护患者的权利，帮助患者做出最接近他们价值观和信念的决定，并确保患者作为人的尊严和隐私得到尊重。

从口译员的角度来看，"患者拥护"意味着什么？本节将探讨国际和美国、日本的规定，以及专家的意见。

· 首先，国际医疗口译员协会[10]（IMIA：International Medical Interpreters Association）为医疗口译员的行为制定了一套道德准则。其中，"口译员有责任维护患者的权利，为了传递信息在合适并必须这样做的情况下，利用他们的专业判断，作为跨文化的中介人士来向医疗服务提供者和患者解释文化和习惯差异。"

· 全美医疗口译委员会[11]（NCIHC）于 2004 年 7 月发布了"全美医疗口译道德准则"。准则对"患者拥护"的定义如下。当"病人的健康、福祉或尊严受到威胁时，口译员可以充当 advocator（拥护者）。Advocacy（拥护行为）被理解为，有支持形成积极的健康方面的结果的意图，并超越了促进沟通的范畴，为了个人而发生的行为。这种拥护行为，必须要在对情况深思熟虑之后，并且仅在其他非介入类手段无法解决问题的情况下才能使用。"

· 日本的情况，可以参考厚生劳动省的"医疗口译"[12]教材。该教材中关于权利拥护（Advocacy）提供了如下措辞。"权利拥护（Advocacy）是在患者的生命尊严受到威胁时，使用恰当的知识和判断来保护他们权利的行为。"还进一步指出，"口译员的权利拥护行为，超出了口译员的职责范围，有些国家禁止口译员的这一行为。但本准则中规定，医疗口译在对情况进行恰当分析的基础上，仅在患者的安全和生命受到威胁，处于危险中时，才可以偏离原有的医疗口译的职责，来采取权利拥护的行为。"

· 专家们对口译员的患者拥护的解释则如下所示。饭田[13]认为，"医疗口译员了解患者和医护人员的语言和文化，以及他们所处的环境，因此他们应致力于向所有人提供合适的医疗服务，并能够进行患者拥护行为。"他／她还指出，"权利拥护不是医疗口译员直接代理或代行，而是协助患者争取和恢复自己的权利。"

· Lourdes Herrera[14]对"患者拥护"提出了以下观点。"当外国患者因语言障碍而无法为自己说话（无法为自己代言）时，口译者会像"救援者"一样伸出援手"，"需要通过了解生活在日本的外国人的社会和经济状况，并从患者的细微面部表情来读取其文化、家庭和个人情况，提供必要的拥护行为。""口译员还扮演着向外国人提供信息（信息来源）的角色。患者对口译员有诸多

期待，但口译员必须判断应该何时直接干预，何时寻求他人的帮助。""口译这份工作，应该是善良和坚持的，并且是令人尊重的援助过程，既给予一定程度上的温暖，又不会过度保护。"

总结上述道德规范和专家意见，虽然部分观点认为口译员所做出的"患者拥护"是"只有在患者处于危险境地，并在没有其他可干预的手段时才能采取的及其罕见的行为。"但作者希望暂且将其定义为"口译员观察患者，当患者处于危险境地时，需要成为患者的代言人以确保患者的权利得到尊重，还需要作为文化的理解者来弥补患者和医护之间的文化差异，以及作为信息提供者，或者作为支持者为患者寻求他人的帮助来协助患者康复"。

结　论

本文探讨了精神科医疗口译的特殊性和"患者拥护"的定义。然而，在实际临床中，从事精神科医疗口译的口译员们究竟如何看待和实践"患者拥护"，以及在实践过程中是否有困难之处。这些将会成为作者未来的研究课题。

鸣　谢

引用文献：
[1] 出入国在留管理厅 在留外国人统计（旧登录外国人统计）统计表
https://www.moj.go.jp/isa/policies/statistics/toukei_ichiran_touroku.html （访问时间：2022 年 3 月 1 日）
[2] 厚生劳动省课题 令和元年度残疾人综合福祉推进事业
精神科医疗机构接收外国人患者的现状和问题把握的相关调查 https://www.mhlw.go.jp/content/12200000/000672477.pdf（访问时间：2022 年 3 月 1 日）
[3] 阿部裕 多文化精神医疗 鹿儿岛：Laguna 出版：2019
[4] 村松纪子 "社区活动中医疗口译员的作用"《医疗口译这份工作》大阪：大阪大学出版社：2013：76
[5] 长尾 Hiromi "医疗口译的职业伦理规定"《医疗口译入门》东京：松柏社：2007 29-46
[6] 阿部裕 精神医疗领域中社区口译的必要性 Series 多语言和多文化合作实践研究 16 2013：105-113
[7] Turner G Onsite Mental Health Interpreting A workshop for Professional Interpreters from MMHA's NT forum
[8] 押见贵之　精神医疗中的医疗口译　心与文化　2009：8 卷：108-113
[9] 日本护理协会 护理实践信息 临床伦理方法 https://www.nurse.or.jp/nursing/practice/rinri/text/basic/approach/index.html（访问时间：2022 年 3 月 1 日）
[10] IMIA Code of Ethics https://www.imiaweb.org/code/default.asp（访问时间：2022 年 3 月 1 日）
IMIA 伦理规定（日语翻译版）https://www.imiaweb.org/uploads/pages/393.pdf（访问时间：2022 年 3 月 1 日）
[11] 全美医疗口译伦理规定 https://www.migrationpolicy.org/sites/default/files/language_portal/ANationalCodeofEthicsforInterpretersinHealthCareinJapanese_0.pdf（访问时间：2022 年 3 月 1 日）
[12] 厚生劳动省 与医疗口译相关的资料 课本《医疗口译》https://www.mhlw.go.jp/content/10800000/000385181.pdf（访问时间：2022 年 3 月 1 日）
[13] 饭田奈美子 "医疗口译员伦理规定解读"《论医疗口译这份工作》大阪：大阪大学出版社：2013：33-47
[14] Lourdes Herrera "从外国患者的角度看医疗口译的作用"《论医疗口译这份工作》大阪：大阪大学出版社：2013：89-97

━━━━━━◆ 著者联系方法 ◆━━━━━━
周　英
金泽大学人间社会环境研究科 博士后期课程
E-mail：11431984@qq.com

日中笹川医学奨学金制度（学位取得コース）中間評価書
課程博士：指導教官用

第 44 期　　研究者番号：G4408　　　　　　　　作成日　：2023 年 3 月 7 日

氏　名	劉 天驕	LIU TIANJIAO	性別	M	生年月日　1995/03/10

所属機関（役職）	成都市婦女児童中心医院医務部（幹事）
研究先（指導教官）	京都大学大学院　医学研究科遺伝医学講座分子遺伝学分野（篠原 隆司　教授）
研究テーマ	α-Klotho を要因とする老化過程における精子幹細胞の微小環境制御 The study on the molecular mechanism of α-Klotho's regulation of spermatogonial stem cell niche during aging
専攻種別	☐論文博士　　　　　　☑課程博士

研究者評価（指導教官記入欄）

成績状況	ⓔ　良　可　不可 学業成績係数=90	取得単位数 12／30

学生本人が行った研究の概要	劉さんは現在 Klotho 遺伝子に突然変異を保つために老化が促進されるモデルマウスを用いて老化研究を行なっています。このマウスでは精子幹細胞の自己複製分裂が活性化されており、その原因は未だに明らかになっていません。ところが劉さんは男性ホルモンであるテストステロンと Klotho が関連する可能性を見出しました。現在、特に寿命や老化マーカーのモニタリングや次世代に与える影響について注目して解析を行なっております。これまでのところ概ね順調にデータを出しています。
総合評価	【良かった点】 文章の能力が高く、英語によるコミュニケーションはこれまでの留学生の中でも最も高いと思います。ウェスタンブロッテイングなど生化学実験の技術に優れています。 【改善すべき点】 一方でまだ日本語の習得に苦戦しており、日常会話を日本語で行うとか文章を書くなどの点については一層の努力が必要です。日本で習得した細胞培養や遺伝子操作、組織学的解析の技術についてはまだ十分でなく、練習が必要です。 【今後の展望】 研究については順調に進んでおり問題はありません。今後さらに日本語の能力も高めつつ解析を掘り下げて行く予定です。
学位取得見込	老化を含む研究なので個体老化で表現型が出てくるまでに時間がかかりますが、今のペースで行けば 3 年以内に論文を発表できそうです。

評価者（指導教官名）　　　篠原隆司

第44期　　　研究者番号： G4408　　　作成日：2023年3月　1　日

氏名	刘 天骄	LIU TIANJIAO	性別	M	生年月日　1995/03/10
所属機関(役職)	成都市婦女児童中心医院産婦人科(医師)				
研究先(指導教官)	京都大学大学院　医学研究科遺伝医学講座分子遺伝学分野(篠原 隆司　教授)				
研究テーマ	α-Klothoを要因とする老化過程における精子幹細胞の微小環境の調節メカニズムの研究 The study on the molecular mechanism of α-Klotho's regulation of spermatogonial stem cell niche during aging				
専攻種別	論文博士	□		課程博士	☑

1．研究概要(1)
1）目的(Goal)

　　Aging is an urgent sociomedical issue which greatly threats the fertility of population in many societies, especially in the developed countries and regions. It was reported that advanced paternal age brings higher risks of the pre-mature birth, low Apgar scores or admission to a neonatal intensive care department of newborns. The paternal age also improves the incidence rate of multiple congenital defects such as heart malformations as well as oral, palate and lip cleft. In addition, many mental disorders like autism, schizophrenia, bipolar disorder, low intelligence capacity were also more frequently observed with advanced father's age.1

　　The spermatogonial stem cells (SSCs), a rare subpopulation of the spermatogonia, are tasked to self-renew actively to sustain the SSC reservoir and give rise to progenitors poised for eventually differentiating into sperms2. Spermatogonial stem cell (SSC) transplantation is regarded as a promising technique for treating the infertility of male survivors from cancer therapies before sexual maturation. The SSC transplantation, which reintroduces the SSCs into the seminiferous tubules of recipient's testis, can initiate their spermatogenesis and enable the production of their own biological children. The aging of SSCs is always accompanied by impaired proliferation, epigenetic abnormalities, altered metabolism and even the loss of sperm-forming function3, hampering the scientific utilization of SSCs' versatility a lot. The serial transplantation of SSCs into young testes, which enabled the longer than lifetime proliferation of SSCs and also proved their strong proliferation ability4. This evidence indicated that the SSCs have a unique mode of aging which is likely caused by the deteriorated niche, a protective region for stem cells with surrounding stromal cells.

　　The Klotho gene is a critical gene in regulating phosphate metabolism and senescence. Mice deficient in α-Klotho not only have a phosphate metabolism dysfunction and hyperphosphatasemia due to the impaired urinary phosphate excretion but also show apparent and multiple phenotypes of premature aging, including slower growth, smaller body size, atrophy of multiple organs, vascular calcification, sarcopenia, cardiac hypertrophy and fibrosis, osteopenia, emphysematous lung, hearing impairment, cognitive defects and shortened lifespan.5 Its abnormal expression and functioning was recently found play an essential role in the premature placental senescence and malformation caused by advanced maternal age.6 However, its regulation on the aging of male fertility has not been reported yet. This study aims to investigate the molecular mechanism of Klotho's regulation on the senescence of spermatogonial stem cells and their niche.

2）戦略(Approach)
(1)investigate the spermatogonial stem cell niche of Klotho testis using immunostaining
(2)functional analysis of the blood testicular barrier (BTB) of Klotho testis
(3)exogenous supplement of testosterone of Klotho testis and investigate its spermatogonial stem cell niche and spermatogenesis

3）材料と方法(Materials and methods)
(1)Animal: All the experimental protocols including animals were granted by the Institutional Animal Care and Use Committee of Kyoto University. The Klotho-deficient mice were produced by crossing the heterozygous Klotho +/- male and female mice.
(2)Testosterone implantation: At least 2 days before the implantation surgery, a soft, 1cm-long plastic tube (Clinic medics, Osaka, Japan) in 10mm diameter were filled with testosterone or cholesterol. Both ends of the tube were sealed using Basubondo Q gel (Konishi company, Osaka) and then kept in room temperature for drying. After the opening of tube ends were sealed, the tubes were soaked in sterile saline and incubated overnight in 37-degree incubator one day before the surgery. On the day of surgery, the 8-week-old Klotho deficient male mice were first narcotized using 150ul 2% Avertin and then a 0.5cm wide incision on their back skin was made. The tube was inserted into the subcutaneous space. Finally, the incision was closed by suturing.
(3)Biotin intrusion experiment: A total volume of 10 ul 7.5mg/ml biotin was injected into each testis when the Klotho-deficient mice turned 10-week-old after anesthesia. Half hour after the injection, the mice were sacrificed, and the testes were removed and processed for immunostaining of Biotin.
(4)Macroscopic and histological analysis of testes: Implanted mice were killed at the age of 12 weeks (4 weeks post-implantation). The testes were kept intact in cold PBS and observed under macroscopy. The testes and epididymis were fixed in 10% neutral-buffered formalin and embedded in paraffin blocks. Slides were stained with hematoxylin and eosin and checked for histological analysis

(5)Immunostaining: Testes were fixed in 4% paraformaldehyde for 2 h at 4°C, and embedded in Tissue-Tek OCT compound (Sakura Finetek, Tokyo, Japan) before cryosectioning. Cryo-sections of 6 μm thickness were then prepared. The tissue were then treated with 0.1% Triton-X and sodium citrate in phosphate-buffered saline (PBS) for permeabilization. Donkey serum diluted at 10 fold in PBS were applied onto the slide for blocking. The tissues were treated with first antibodies in 4 degree overnight, then incubated with second antibodies in room temperature for 1 hour after washing with PBS. Hochest were diluted at 1:300 ratio in PBS and then dropped onto the slides and kept for 10 minutes for counter staining.

(6)Serum collection and Enzyme linked immunosorbent assay (ELISA): The blood from the carotid artery of mice will be collected during scarification. The blood would be kept in 4 degree overnight. The serum was collected after centrifugation at 1200rpm for 30min and cryopreserved in -80 degree. The ELISA will be performed for detecting the concentration of testosterone according to producer's protocol.

4）実験結果（Results）

We firstly examined the expression of Claudin 3, 5 and 11, as well as the key enzymes of testosterone synthesis (CYP17A1 and HSD3B) in the testes of Klotho KO and WT mice. We noticed that Cldn3(0.004 ±0.001 vs. 0.045 ±0.008 um2/um, p<0.001), Cldn11(0.006 ±0.017 vs. 0.025 ±0.006 um2/um, p=0.01), and CYP17A1(0.112 ±0.112 vs. 58.27±9.82 um2, p=0.0005) are remarkably lower in Klotho KO testes in comparison with the WT, but the expressions of HSD3B and Cldn5 are comparable in both groups. These results imply the impaired BTB and testosterone metabolism in Klotho-deficient testis. Then we performed the Biotin intrusion experiment on the 10 weeks old Klotho KO mice and WT mice's testes(n=4) to confirm whether there is a functional defect of BTB in Klotho KO testes. A total volume of 10 ul 7.5mg/ml biotin was injected into each testis. We observed that the majority of seminiferous tubules in Klotho KO mice's testes are notably more penetrated by biotin, while almost no biotin intrusion could be found in the WT testes (88.89±4.54% vs. 6.25±3.61%, p<0.0001). We also detected the mRNA level of Klotho-alpha in the testes of CTL and W mice (5 Weeks old, n=3) using qPCR. The result shows that alpha-Klotho's expression in W mice testes is significantly lower than the control group(1.023 ± 0.031 vs. 0.457 ±0.062, p=0.0012).

Previous results showed the impaired testosterone metabolism and tight junction between Sertoli cells in Klotho KO testes. As previous studies showed that testosterone could rescue the incomplete tight junction between Sertoli cells and ameliorated the phenotype of aging, we hypothesized that the malfunctioning and lower expression of cldn3 and cldn11 in Klotho KO testes were caused by the lower level of testosterone. We planned to supplement the testosterone in Klotho-deficient mice via implantation of tiny plastic tubes containing testosterone. To verify the feasibility of such technique, we made 4 testosterone tubes and 4 cholesterol tubes to implant to the 8 weeks female mice. After 8 weeks, we noticed that the external genital organ of the testosterone group became more male-like. As we sacrificed these 8 mice and checked their internal organs and the plastic tubes, we found that the testosterone were completely absorbed and testosterone treated female mice had significantly enlarged uteri, hearts, and kidneys.

We subsequently performed the implantation surgery on the 8-week-old Klotho KO mice. As we investigate the testosterone and cholesterol treated Klotho KO by immunofluorescence, we found that the testosterone-treated Klotho deficient mice not only had a comparable level of Cldn5 as compared with the cholesterol group, but also showed increased level of Cldn3, Cldn11, as well as the GFRA1, Ki67 Positive GFRA1, and PNA, indicating that the testosterone treatment might not only repaired the BTB, but also facilitated its spermatogenesis. In consistent with these findings, the macroscopic and histological investigation of testosterone and cholesterol treated testes and the pathological examination of their epididymis also showed that the testosterone treatment had notably increased the size and weight of Klotho KO testis and facilitated the maturation of sperm in the epididymis compared with the cholesterol group.

5）考察（Discussion）

We previously reported the intrinsic senescence model of SSC via Jnk-mediated glycolysis activation using long-term cultured SSCs. We noticed that aged SSCs proliferate faster than young SSCs and showed enhanced glycolytic activity, but still kept euploidy and exhibited stable androgenetic imprinting patterns with robust SSC activity, though having shortened telomeres. In consistency with this, the investigation of Klotho-deficient mice model also showed hyperactivation of JNK and enhanced glycolysis. We also reported the significantly smaller size, fewer PNA+ tubules, increased proliferation of ZBTB16+ cells, and enhanced level of 53BP1 expression in Klotho KO testis.

Although many phenotypes of Klotho-deficient testis were described in our previous work, the detailed molecular mechanism of Klotho's regulation on the spermatogonial stem cell niche and spermatogenesis has not been clearly elucidated. In present study, we observed the impaired testosterone metabolism, functional and structural defects of blood testicular barrier in the Klotho-KO testis, which could be rescued by the exogenous supplement of testosterone. To our surprise, the 4-week implantation of testosterone (from 8 weeks to 12 weeks) not only repaired the BTB of Klotho-deficient testis but also recovered their spermatogenesis. These findings indicated the potential existence of the Klotho- testosterone-BTB pathway. To verify such hypothesis, we plan to perform western blot in our future study. In addition, we would also endeavor to explore the underlying molecular mechanism in detail.

6）参考文献（References）

1Janeczko, D., Hołowczuk, M., Orzeł, A., Klatka, B. & Semczuk, A. Paternal age is affected by genetic abnormalities, perinatal complications and mental health of the offspring. Biomed Rep 12, 83–88, doi:10.3892/br.2019.1266 (2020).
2Takashima, S. & Shinohara, T. Culture and transplantation of spermatogonial stem cells. Stem Cell Res 29, 46–55, doi:10.1016/j.scr.2018.03.006 (2018).
3Schultz, M. B. & Sinclair, D. A. When stem cells grow old: phenotypes and mechanisms of stem cell aging. Development 143, doi:10.1242/dev.130633 (2016).
4Ryu, B.-Y., Orwig, K. E., Oatley, J. M., Avarbock, M. R. & Brinster, R. L. Effects of aging and niche microenvironment on spermatogonial stem cell self-renewal. Stem Cells 24, 1505–1511 (2006).
5Kuro-O, M. The Klotho proteins in health and disease. Nat Rev Nephrol 15, 27–44, doi:10.1038/s41581-018-0078-3 (2019).
6Chen, Z. et al. Advanced maternal age causes premature placental senescence and malformation via dysregulated α-Klotho expression in trophoblasts. Aging Cell 20, e13417, doi:10.1111/acel.13417 (2021).

2. 執筆論文　Publication of thesis　※記載した論文を添付してください。Attach all of the papers listed below.

論文名 1 Title	Current perception of transvaginal natural orifice translumenal endoscopic surgery among Chinese female gynecological medical staff						
掲載誌名 Published journal	Asian journal of surgery						
	2022　年　　12　月	45　　巻（号）	2947　頁　～　2950　頁		言語 Language		English
第1著者名 First author	Tianjiao Liu	第2著者名 Second author	Dan Feng		第3著者名 Third author		Xin Li
その他著者名 Other authors							
論文名 2 Title	Health QR Code Application in the Novel Containment Strategy and Healthcare Plan for Pregnant Women and Children Under Quarantine During the Summer Outbreak of SARS-CoV-2 Delta Variant in Chengdu, China: An Observational Study						
掲載誌名 Published journal	Risk Management and Healthcare Policy						
	2021　年　　11　月	14　　巻（号）	4499　頁　～　4510　頁		言語 Language		English
第1著者名 First author	Shan Chen	第2著者名 Second author	Tianjiao Liu		第3著者名 Third author		Xin Li
その他著者名 Other authors	Yingjuan Luo, Li Xiao, Libing Zhang, Rongkang Wen, Yonghong Lin						
論文名 3 Title							
掲載誌名 Published journal							
	年　　　月	巻（号）	頁　～　頁		言語 Language		
第1著者名 First author		第2著者名 Second author			第3著者名 Third author		
その他著者名 Other authors							
論文名 4 Title							
掲載誌名 Published journal							
	年　　　月	巻（号）	頁　～　頁		言語 Language		
第1著者名 First author		第2著者名 Second author			第3著者名 Third author		
その他著者名 Other authors							
論文名 5 Title							
掲載誌名 Published journal							
	年　　　月	巻（号）	頁　～　頁		言語 Language		
第1著者名 First author		第2著者名 Second author			第3著者名 Third author		
その他著者名 Other authors							

3. 学会発表 Conference presentation ※筆頭演者として総会・国際学会を含む主な学会で発表したものを記載してくだ

※Describe your presentation as the principal presenter in major academic meetings including general meetings or international me

学会名 Conference	
演　題 Topic	
開催日 date	年　　　　月　　　　日　開催地 venue
形式 method	□ 口頭発表 Oral □ ポスター発表 Poster 言語 Language □ 日本語 □ 英語 □ 中国語
共同演者名 Co-presenter	
学会名 Conference	
演　題 Topic	
開催日 date	年　　　　月　　　　日　開催地 venue
形式 method	□ 口頭発表 Oral □ ポスター発表 Poster 言語 Language □ 日本語 □ 英語 □ 中国語
共同演者名 Co-presenter	
学会名 Conference	
演　題 Topic	
開催日 date	年　　　　月　　　　日　開催地 venue
形式 method	□ 口頭発表 Oral □ ポスター発表 Poster 言語 Language □ 日本語 □ 英語 □ 中国語
共同演者名 Co-presenter	
学会名 Conference	
演　題 Topic	
開催日 date	年　　　　月　　　　日　開催地 venue
形式 method	□ 口頭発表 Oral □ ポスター発表 Poster 言語 Language □ 日本語 □ 英語 □ 中国語
共同演者名 Co-presenter	

4. 受賞（研究業績）Award（Research achievement）

名　称 Award name			受賞年 Year of	年　　　月
名　称 Award name	国名 Country		受賞年 Year of	年　　　月

5．本研究テーマに関わる他の研究助成金受給 Other research grants concerned with your resarch theme

受給実績 Receipt record	□ 有	■ 無			
助成機関名称 Funding agency					
助成金名称 Grant name					
受給期間 Supported period	年	月 ～		年	月
受給額 Amount received	円				
受給実績 Receipt record	□ 有	■ 無			
助成機関名称 Funding agency					
助成金名称 Grant name					
受給期間 Supported period	年	月 ～		年	月
受給額 Amount received	円				

6．他の奨学金受給 Another awarded scholarship

受給実績 Receipt record	□ 有	■ 無			
助成機関名称 Funding agency					
奨学金名称 Scholarship name					
受給期間 Supported period	年	月 ～		年	月
受給額 Amount received	円				

7．研究活動に関する報道発表 Press release concerned with your research activities

※記載した記事を添付してください。Attach a copy of the article described below

報道発表 Press release	□ 有	■ 無	発表年月日 Date of release	
発表機関 Released medium				
発表形式 Release method	・新聞　・雑誌　・Web site　・記者発表　・その他（　　　　　　　　　　）			
発表タイトル Released title				

8．本研究テーマに関する特許出願予定 Patent application concerned with your research theme

出願予定 Scheduled	□ 有	■ 無	出願国 Application	
出願内容（概要） Application contents				

9．その他 Others

指導責任者（記名）　　　篠原　隆司

Letter to Editor

Current perception of transvaginal natural orifice translumenal endoscopic surgery among Chinese female gynecological medical staff

To the editor,

Natural orifice transluminal endoscopic surgery (NOTES) is a novel minimally invasive surgical (MIS) concept for performing endoscopic procedures via natural orifices.[1] Its feasibility for human clinical application was initially proven by transgastric appendicectomy surgery conducted in 2003.[2] Since then, NOTES has developed rapidly, and surgeons have explored its use through other orifices, such as the intestinal tract and vagina. Notably, transvaginal NOTES (vNOTES) has been shown to outperform many other NOTES approaches due to the availability of greater operative space and easier removal of resected tissues, thus it has become increasingly popular for peritoneal surgeries, especially gynecologic laparoendoscopy, despite some reservations regarding the procedure.[3]

Theoretically, the acceptance of and preference for vNOTES can vary remarkably among patients and healthcare workers from different cultural, ethnic, and socioeconomic backgrounds, and it can be also expected to change with the development of endoscopic techniques and instruments. In the Western world, several surveys on patients and medical workers have investigated their

perceptions of the vNOTES procedure and yielded paradoxical results.[4] However, after the introduction of vNOTES in mainland China seven years ago, its familiarity among the public and acceptance among mainland Chinese medical professionals has rarely been reported.[5] Since healthcare workers' perception and awareness of such novel MIS procedures is probably a prerequisite for its recommendation and popularization, and female medical staff can provide insights from gynecological patients' perspective in hypothetical scenarios, we conducted a citywide online questionnaire survey in Chengdu, China, to investigate Chinese female gynecological health workers' current perceptions of vNOTES and to identify potential factors that contribute to their preference for vNOTES.

In our study, 523 gynecologists and 482 nurses completed the questionnaire. The majority (92.6%) had a positive attitude toward vNOTES. The "prefer vNOTES" group included a much lower proportion of respondents finishing postgraduate education than the "did not prefer vNOTES" group (11.0% vs. 25.7%, p = 0.003). They also included significantly more respondents having heard of the vNOTES procedure (83.9% vs. 68.9%, p = 0.001) and a strikingly higher proportion of members who had participated in vNOTES training courses (47.1% vs. 11.8%, p = 0.029). A significantly higher proportion of participants opted for vNOTES for reasons like safety (73.9% vs. 23.0%, p < 0.001), effectiveness (70.8% vs. 25.7%, p < 0.001), postsurgical cosmesis (93.7% vs. 73.0%, p < 0.001) and less postprocedural pain (71.1% vs. 47.3%, p < 0.001) than those in the "did not prefer vNOTES" group (shown in Table 1). Logistic regression revealed that concerns regarding postprocedural cosmesis (odds ratio (OR) = 3.239, p < 0.001) and prior awareness of vNOTES (OR = 2.271, p = 0.004) were significant predictors of preference for vNOTES, whereas those with higher education levels had a negative coefficient for vNOTES preference (OR = 0.549, p = 0.003) (see Fig. 1).


	OR	95%CI	P value
Education	0.549	(0.368, 0.819)	.003**
Postsurgical cosmesis	3.239	(1.757, 5.972)	<.001***
Having heard of vNOTES	2.271	(1.294, 3.984)	.004**
vNOTES is conducted in respondent's hospital	1.356	(0.810, 2.271)	.246
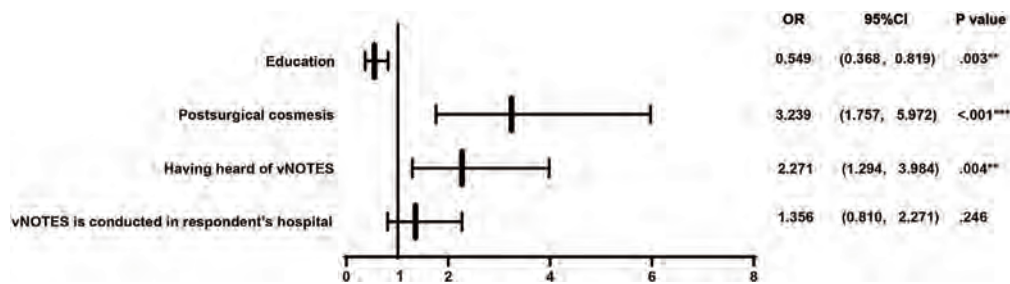
Fig. 1. Logistic regression model for factors that made vNOTES preferable. NOTE: **p < .01, ***p < .001 Abbreviations: vNOTES, transvaginal natural orifice translumenal endoscopic surgery.

Table 1
Subject characteristics and attitudes toward vNOTES in "prefer for vNOTES" group versus "not prefer for vNOTES" group.

Subject characteristics	prefer vNOTES	not prefer vNOTES	X^2	P value
	n = 931(92.6%)	n = 74 (7.4%)		
Age group (years old)			2.871	0.580
20-30	258(27.7%)	22 (29.7%)		
31-40	394(42.3%)	36 (48.6%)		
41-50	204 (21.9%)	13 (17.6%)		
51-60	70 (7.5%)	3 (4.1%)		
≧61	5 (0.5%)	0(0%)		
Occupation			2.462	0.117
Gynecologist	478 (51.3%)	45 (60.8%)		
Nurse	453 (48.7%)	29 (39.2%)		
Educational background			13.762	0.003**
College	203 (21.8%)	14 (18.9%)		
Bachelor	625 (67.1%)	41 (55.4%)		
Master	97 (10.4%)	18 (24.3%)		
Doctoral	6 (0.6%)	1 (1.4%)		
Occupational title			2.271	0.518
Elementary	313 (33.6%)	24 (32.4%)		
Intermediate	354 (38.0%)	27 (36.5%)		
Senior	241 (25.9%)	19 (25.7%)		
Others	23 (2.5%)	4 (5.4%)		
The level of hospital you working for			3.203	0.361
Tertiary A	591 (63.5%)	54 (73.0%)		
Tertiary B	167 (17.9%)	8 (10.8%)		
Secondary A	96 (10.3%)	7 (9.5%)		
Secondary B	77 (8.3%)	5 (6.8%)		
How many years have you practiced medicine?			4.135	0.388
≤3	117 (12.6%)	13 (17.6%)		
3-5	92 (9.9%)	8 (10.8%)		
5-10	200 (21.5%)	16 (21.6%)		
10-20	297 (31.9%)	26 (35.1%)		
≧20	225 (24.2%)	11 (14.9%)		
Have you ever experienced laparoscopic surgery or examination			2.430	0.119
Yes	182 (19.5%)	9(12.2%)		
No	749 (80.5%)	65 (87.8%)		
Have you experienced laparotomy?			2.208	0.137
Yes	397(42.6%)	25 (33.8%)		
No	534 (57.4%)	49 (66.2%)		
Do you have child or children?			1.583	0.208
Yes	804 (93.1%)	60 (81.1%)		
No	127 (13.6%)	14 (18.9%)		
Attitude toward vNOTES				
Do you think postsurgical cosmesis is as important as safety for gynecologic surgery?			21.215	<0.001***
Yes	862 (92.6%)	57 (77.0%)		
No	69 (7.4%)	17 (23.0%)		
Have you ever heard of laparoendoscopic single site surgery?			0.698	0.404
Yes	867 (93.1%)	67 (90.5%)		
No	64 (6.9%)	7 (9.5%)		
(Q10)Have you heard of transvaginal natural orifice translumenal endoscopic surgery (vNOTES)?			10.779	0.001**
Yes	781 (83.9%)	51 (68.9%)		
Never	150(16.1%)	23 (31.1%)		
If your answer to Q10 is yes, how do you know about it?	n = 781	n = 51		
Academic conference	488 (62.5%)	25 (49.0%)	3.671	0.055
Training courses	368 (47.1%)	16 (11.8%)	4.776	0.029*
Reading literatures	413 (52.9%)	29 (56.9%)	0.305	0.580
Heard from colleagues	496 (63.5%)	33 (64.7%)	0.057	0.811
Relatives and friends received vNOTES	119 (15.2%)	6 (11.8%)	0.452	0.501
Is vNOTES conducted in your hospital?			4.014	0.045*
Yes	490 (52.6%)	30 (40.5%)		
No	441 (47.4%)	44 (59.5%)		
What is the acceptable complication incidence rate of vNOTES for you to replace the conventional laparoendoscopic gynecologic surgery? (The incidence rate for surgical complications of laparoendoscopy is 0%–3%)			10.220	0.006**
0%–3%	626 (67.2%)	37 (50.0%)		
3%–6%	200 (21.5%)	27 (36.5%)		
6%–9%	105 (11.3%)	10 (13.5%)		
Are you willing to undergo vNOTES (if diagnosed with indication) or recommend it to relatives/friends/families?			84.902	<0.001***
Yes	688 (73.9%)	17 (23.0%)		
No	243 (26.1%)	57 (77.0%)		
If you are a patient or a family member of a patient, for what reason(s) you would prefer to undergo vNOTES (multiple options)?				
Safe	688 (73.9%)	17 (23.0%)	84.902	<0.001***

Table 1 (*continued*)

Subject characteristics	prefer vNOTES	not prefer vNOTES	X^2	P value
	n = 931(92.6%)	n = 74 (7.4%)		
Effective	659 (70.8%)	19 (25.7%)	63.546	<0.001***
Cosmetic/scarless	874 (93.9%)	54 (73.0%)	42.344	<0.001***
No pain or painless	662 (71.1%)	35 (47.3%)	18.283	<0.001***
Other reasons	6 (0.6%)	9 (12.2%)	61.852	<0.001***
If you are a patient or a family member of a patient, refuse to undergo vNOTES may for (multiple options)?				
Worried about its potential impact on sexual life	210 (22.6%)	27 (36.5%)	7.382	0.007**
Worried about its potential impact on pregnancy and childbirth	193 (20.7%)	29 (39.2%)	13.572	<0.001***
Worried about the failure of the operation	273 (29.3%)	27 (36.5%)	1.680	0.195
Worried about surgical complications	334 (35.9%)	43 (58.1%)	14.455	<0.001***
Other reasons	10 (1.1%)	11 (14.9%)	63.725	<0.001***
Do you think age is a major factor for choosing vNOTES or recommending it to friends and relatives?			3.272	0.070
Yes	330 (35.4%)	34 (45.9%)		
No	601 (64.6%)	40 (54.1%)		
If your answer is yes, what do you think is the most appropriate age for vNOTES	n = 330	n = 34	9.656	0.008**
20-40	227 (68.8%)	16 (47.1%)		
41-55	84 (25.4%)	12 (25.5%)		
>55	19 (5.8%)	6 (17.6%)		
(Q22) Do you think finish childbirth or not is a major factor in the surgical selection of vNOTES or the recommendation of it to your family and friends' choice?			1.002	0.317
Yes	348 (37.4%)	32 (43.2%)		
No	583 (62.6%)	42 (56.8%)		
If your answer to Q22 is yes, do you think you should finish childbirth before undergoing vNOTES?	n = 342	n = 32	0.021	0.885
Yes	265 (77.5%)	24 (75.0%)		
No	83 (22.5%)	8 (25.0%)		
Gynecologists' perspective of vNOTES				
	Prefer vNOTES n = 495	Not prefer vNOTES n = 42	X^2	P value
Would you like to conduct vNOTES in your department?			20.148	<0.001***
Yes	485 (98.0%)	36 (85.7%)		
No	10 (2.0%)	6 (14.3%)		
Do you think the prospect of vNOTES is good?			61.310	<0.001***
Yes	474 (95.8%)	27 (64.3%)		
No	21 (4.2%)	15 (35.7%)		
What do you think make it difficult to popularize vNOTES (multiple options)?				
Difficulty in establishment of surgical platform	294(59.4%)	25(59.5%)	0.002	1.000
Restricted operative visualization	388(78.4%)	38(90.4%)	3.452	0.063
The chopstick effect of single-port laparoscopy makes it difficult to perform vNOTES	376(76.0%)	24(57.1%)	7.213	0.007**
Low acceptance rate among patients	99(20.0%)	12(28.5%)	1.735	0.188
Higher operative cost	201(40.6%)	9(21.4%)	5.979	0.014*
Other————	10(2.0%)	0(0%)	0.865	0.352
Gynecologists' perspective of vNOTES				
	Prefer vNOTES n = 495	Not prefer vNOTES n = 42	X^2	P value
Would you like to conduct vNOTES in your department?			20.148	<0.001***
Yes	485 (98.0%)	36 (85.7%)		
No	10 (2.0%)	6 (14.3%)		
Do you think the prospect of vNOTES is good?			61.310	<0.001***
Yes	474 (95.8%)	27 (64.3%)		
No	21 (4.2%)	15 (35.7%)		
What do you think make it difficult to popularize vNOTES (multiple options)?				
Difficulty in establishment of surgical platform	294(59.4%)	25(59.5%)	0.002	1.000
Restricted operative visualization	388(78.4%)	38(90.4%)	3.452	0.063
The chopstick effect of single-port laparoscopy makes it difficult to perform vNOTES	376(76.0%)	24(57.1%)	7.213	0.007**
Low acceptance rate among patients	99(20.0%)	12(28.5%)	1.735	0.188
Higher operative cost	201(40.6%)	9(21.4%)	5.979	0.014*
Other————	10(2.0%)	0(0%)	0.865	0.352

In conclusion, the majority of surveyed female gynecologic healthcare workers had a supportive attitude toward vNOTES. Prior awareness and evaluation of surgical cosmesis had a positive influence on the surgical preference for vNOTES. However, concerns about its impact on sexual life, pregnancy, and childbirth still exist.

Data availability statement

Data of this study can be obtained from the corresponding author upon reasonable request.

Author contributions

Dan Feng conceptualized the study and formulated the questionnaire. Tianjiao Liu, Dan Feng, and Xin Li drafted and revised the manuscript. Tianjiao Liu and Xin Li also participated in statistical analyses. Li He supervised this study and critically reviewed the manuscript.

Declaration of competing interest

The authors declared no conflicts of interest related to this article.

Acknowledgment

We thank all the gynecologists and nurses who participated in our survey.

Appendix A. Supplementary data

Supplementary data to this article can be found online at https://doi.org/10.1016/j.asjsur.2022.06.117.

References

1. Rattner D, Kalloo A. ASGE/SAGES working group on natural orifice translumenal endoscopic surgery. *Surg Endosc.* 2006;20(2):329—333. October 2005.
2. Rao GV, Reddy DN, Banerjee R. NOTES: human experience. *Gastrointest Endosc Clin N Am.* 2008;18(2).
3. Kho RM. vNOTES: is it the panacea we are all hoping for? *J Minim Invasive Gynecol.* 2021;28(6):1146—1147.
4. Gerntke CI, Kersten JF, Schön G, Mann O, Stark M, Benhidjeb T. Women's perception of transvaginal natural orifice transluminal endoscopic surgery (NOTES): results of a survey of female medical staff and literature review. *Surg Innovat.* 2016;23(2):201—211.
5. Fei YF, Fei L, Salazar M, Renton DB, Hazey JW. Transvaginal surgery: do women want it? *J Laparoendosc Adv Surg Tech.* 2014;24(10):676—683.

Tianjiao Liu[1], Dan Feng[1]
The Department of Gynecology of Chengdu Women's and Children's Central Hospital, School of Medicine, University of Electronic Science and Technology of China, Chengdu, People's Republic of China

Xin Li[1]
The Department of Obstetrics of Chengdu Women's and Children's Central Hospital, School of Medicine, University of Electronic Science and Technology of China, Chengdu, People's Republic of China

Li He[*]
The Department of Gynecology of Chengdu Women's and Children's Central Hospital, School of Medicine, University of Electronic Science and Technology of China, Chengdu, People's Republic of China

[*] Corresponding author. No.1617, Riyue Avenue, Chengdu, Sichuan, 610091, China.
E-mail address: helisichuan@163.com (L. He).

---

[1] These authors contributed equally to this work.

ORIGINAL RESEARCH

Health QR Code Application in the Novel Containment Strategy and Healthcare Plan for Pregnant Women and Children Under Quarantine During the Summer Outbreak of SARS-CoV-2 Delta Variant in Chengdu, China: An Observational Study

Shan Chen [1,*]
Tianjiao Liu [1,2,*]
Xin Li [2,*]
Yingjuan Luo [3]
Li Xiao [1]
Libing Zhang [4]
Rongkang Wen [3]
Yonghong Lin [2]

[1]The Medical Administration Department, Chengdu Women's and Children's Central Hospital, School of Medicine, University of Electronic Science and Technology of China, Chengdu, People's Republic of China; [2]The Department of Obstetrics and Gynecology, Chengdu Women's and Children's Central Hospital, School of Medicine, University of Electronic Science and Technology of China, Chengdu, People's Republic of China; [3]The Healthcare Department, Chengdu Women's and Children's Central Hospital, School of Medicine, University of Electronic Science and Technology of China, Chengdu, People's Republic of China; [4]The Department of Pediatric Surgery, Chengdu Women's and Children's Central Hospital, School of Medicine, University of Electronic Science and Technology of China, Chengdu, People's Republic of China

*These authors contributed equally to this work

Correspondence: Yonghong Lin
Tel +86 13808031895
Fax +86 28 61866003
Email linyh.2007@aliyun.com

Purpose: To report the experience of health QR code application in Chengdu's anti-epidemic measures including circle-layer management, hospital triage system and healthcare plan for quarantined pregnant women and children during the summer outbreak of SARS-CoV-2 Delta strain in 2021 and to evaluate these measures.

Methods: We comprehensively summarized Chengdu's health code application in the circle-layer management (a set of stringent confinement measures of places confirmed cases and close contacts have recently been to and less strict quarantine measures of surrounding areas), hospital triage system, and healthcare plan for quarantined pregnant women and children. We also assessed the effectiveness or efficiency of these measures by analyzing the number of different cases with confirmed COVID-19 infections or epidemiological history, the attitude of quarantined pregnant women toward the summer outbreak and healthcare services, as well as the time needed for obtaining epidemiological history and accuracy of health-code-based hospital triage system.

Results: The circle-layer management lasted 15 days and ended with no community or nosocomial transmission happened. Approximately 70 pregnant women and 600 children below 6-year-old were quarantined. Four home visits and two patient transfers were performed. Online survey indicated that about 80% of quarantined women felt satisfactory about the healthcare service. The novel triage system identified 137/221 (61.99%) patients with epidemiological history from patients with yellow health code, and 71/4504 (1.57%) patients from patients with green health code in our hospital (p < 0.001). The health QR code markedly outperformed the traditional methods in the efficiency experiment of obtaining epidemiological history (3.52 ± 0.98 vs 78.91 ± 23.18 seconds, P < 0.001).

Conclusion: The circle-layer management has successfully and precisely prevented the spread of the summer outbreak of COVID-19 in Chengdu. The health-code-based triage system showed great effectiveness and efficiency in triaging patients with epidemiological history. The healthcare services for quarantined pregnant women has basically met their needs.

Keywords: triage, quarantine, pediatrics, obstetrics, precise prevention and control

Introduction

The global society has experienced an exponential increase in the number of confirmed cases of infection and death of Severe Acute Respiratory Syndrome

Graphical Abstract
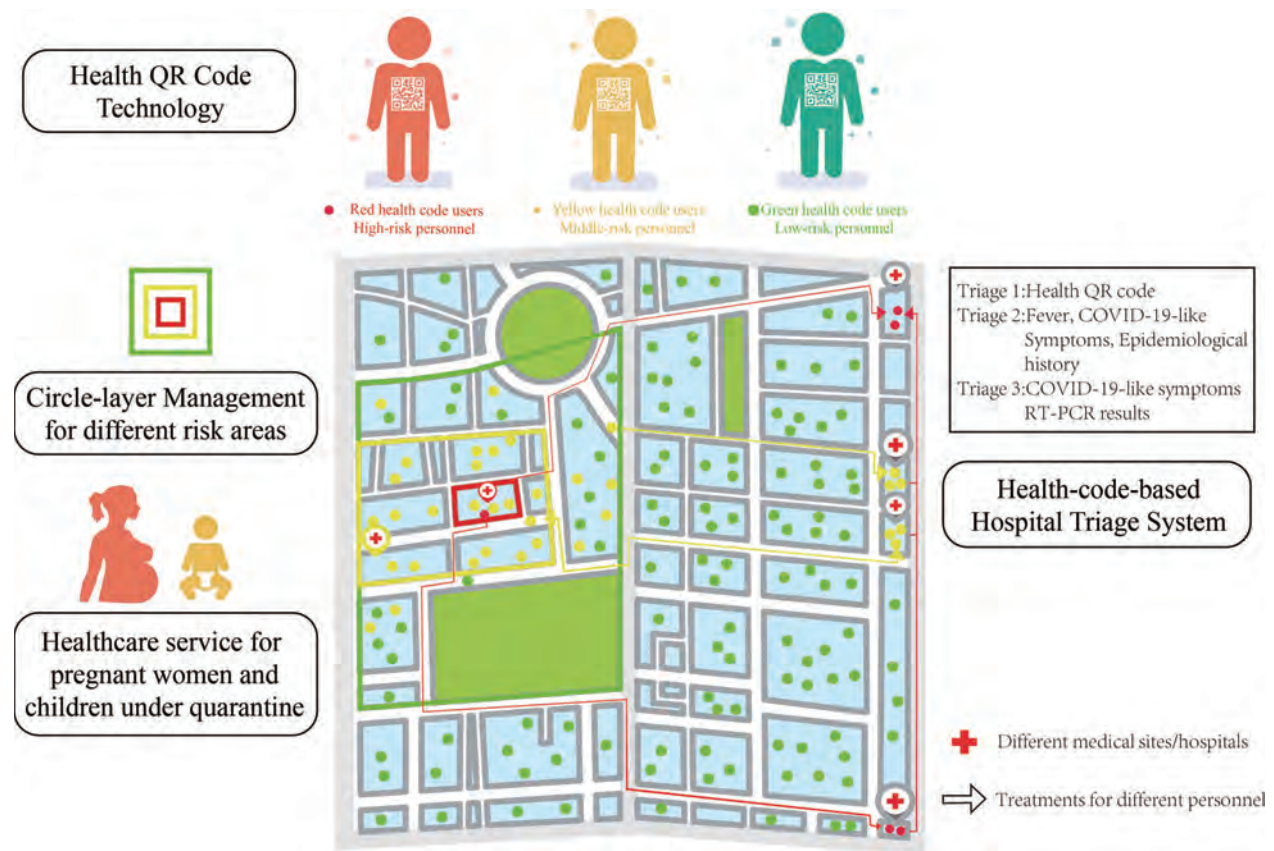
Coronavirus 2 (SARS-CoV-2) since March 2020.[1] Various strategies have been implemented by many countries, including social distancing, lockdown, and nation-wide vaccination,[2–5] but from a global perspective, the pandemic is still rampant. Through the long-term and united efforts of all citizens, especially healthcare workers, China has almost successfully eradicated the domestic epidemic of the Coronavirus Disease 19 (COVID-19) and hence resumed the social and economic orders since April 2020.[6] However, the Nanjing outbreak from mid-July to mid-August 2021 has caused about 1100 correlated confirmed infections in multiple provinces and cities. On 27th July, a family of three in Chengdu were diagnosed as confirmed cases 3 days after their travel to Zhangjiajie, a tourism hotspot that just underwent a clustered outbreak. Another 3 cases were subsequently diagnosed with confirmed infection, including an airport worker, a close contact of the beforementioned family, and a middle-aged female who also traveled to Zhangjiajie several days ago.

Considering that, unlike previous strikes of COVID-19, the summer outbreak in Chengdu was sporadic, small-scale, and traveling-correlated, thus it was unsuitable to be tackled by rigorous measures like city-wide lockdowns and home quarantine. On the other hand, close contacts of confirmed cases and personnel with epidemiological history and COVID-19 manifestations (fever, cough, and dizziness, etc.) should be identified efficiently and effectively in public places, especially hospitals. However, the traditional ways of epidemiological history inquiry were laborious, time-consuming, and unable to screen out misleading information. Noteworthily, the majority of the confirmed cases in the current epidemic were infected by the Delta variant. As described in the previous publications, this mutant strain has a 60% higher risk of community transmission than the ancestral Alpha strain. It is even able to cause asymptomatic breakthrough infections in vaccinated patients,[7,8] making it unfeasible to triage patients simply based on the body temperature and

COVID-19-like clinical manifestations. To address these problems, Chengdu promptly implemented the circle-layer quarantine policy, and widely applied the health QR code in the circle-layer management and the triage system of hospitals.

The circle-layer quarantine policy is a set of risk-level-based containment measures which categorized the potential risk areas into 3 circles or layers: (1) lockdown areas, the areas where the confirmed cases have recently been to; (2) restricted areas, the areas where the close contacts have recently been to; and (3) areas with potential risks, the surrounding areas of the lockdown or restricted areas. Accordingly, this policy implemented stringent confinement measures in lockdown and restricted areas and carried out relatively less strict containment measures in areas with potential risks, aiming to minimize the scale of influenced communities and citizens while stopping the spread of the epidemic.

The health QR code is a plug-in-like mini program running in social media apps like WeChat and online payment platforms like Alipay, which records and updates the users' COVID-19 related health information such as body temperature, clinical symptoms (fever, cough, dizziness, etc.), potential contact with the infected patient and daily itinerary details.[9] The three colors of the QR code match the corresponding risk levels of its user. Only users with a green code are allowed to use public transportation and facilities freely. Smartphone owners with a red or yellow health QR code will be required to be quarantined and/or get RT-PCR tests for SARS-CoV-2.[9]

Pregnant women and children in China are presumably vulnerable to the Delta strain due to their low vaccination rate.[10,11] It was reported that the pregnant women have a significantly higher ICU admission rate if infected by the SARS-Cov-2.[12] Previous publications also indicated that pregnant women and children under quarantine had higher rates of depressive symptoms, anxiety, and other negative effects.[13–15] Therefore, to ensure their mental and physical health of and to avoid difficulties and inconveniences in getting medical care for quarantined pregnant women and children, a healthcare plan for them was made and implemented. In this plan, medics and community workers in quarantine sites would help monitor the health condition of pregnant women and children and do the RT-PCR tests for them. For those needed professional obstetrics and pediatrics services, they can appoint medical home visits by phone call. The patient transfer would also be performed when the patient should be taken care of in the hospital after medical evaluation.

This article aims to summarize, report, and evaluate Chengdu's anti-epidemic measures in the summer outbreak of the Delta variant of SARS-CoV-2, in which the novel anti-epidemic technology, health QR code, played an essential role. We hope our experience could be helpful in providing some novel strategies and inspirations of swiftly containing the small-scale and imported epidemic for domestic or overseas cities and medical institutions confronted with similar situations.

Materials and Methods
Health QR Code System

The Health QR code system applied in the present research was Tianfu Health Code released by Sichuan Provincial Emergency Headquarters for Covid-19.[16,17] It is a mandatory system in all public places and facilities in mainland China during the epidemic, which collects and integrates users' spatial and temporal data using Bluetooth, Global Positioning System (GPS), geolocation information of Network base station, and online transactions.[9] As shown in Supplementary Figure 1, it has a built-in module called Entrance Code required to be shown before entering communities and public places, which can record and upload the users' visit history of public places or communities. Young and senior citizens and other non-smartphone-users can also get their health QR codes once their family applied the Family Health Code for them. Functions like senior mode and voice assistant were also available in the mini program for the elderly. Through a specific algorithm, the health code was able to identify people with epidemiological history, which includes (1) those who have traveled to or lived in the communities with confirmed cases within 14 days before onset; (2) those who have had close contact with confirmed cases and asymptomatic cases within 14 days before onset; (3) those with respiratory symptoms and have had close contact with the people from the communities with confirmed cases within 14 days before onset; (4) those who have been to foreign countries within 14 days.[18] At the very beginning of the summer outbreak, 29th July, a survey on the epidemiological history of confirmed cases and their close contacts was conducted by workers of corresponding communities and local Center of Disease Control through phone calls, surveillance videos checks, and face-to-face

interviews (with personal protective equipment). This information was used to identify the communities and persons at the highest risks of being infected and was uploaded to the Sichuan Big Data Center as the initial information for the circle-layer management and health QR code system.

The Classification and Management of Areas at Different Risk Levels

The classification of areas at different risk levels was based on the numbers of existing confirmed cases: areas with more than 50 existing confirmed cases and clustered onset within 14 days were defined as high-risk areas; areas with less than 50 confirmed cases were defined as middle-risk areas; areas with no confirmed cases were defined as low-risk areas.

The circle-layer management was a set of comprehensive containment measures based on the risk levels of communities with confirmed cases and their surrounding areas. These areas were classified into 3 different layers or circles and were managed accordingly as described below (Figure 1).

Lockdown areas (middle-/high-risk areas): the finding spots, living places, activity places and workplaces of confirmed cases were set as lockdown areas. No citizen would be allowed to enter or leave these areas during the circle-layer management. Citizens living in the lockdown areas were all regarded as potential close contacts thus were required to be quarantined for 14 days. They got RT-PCR tests on the 1st, 4th, 7th, and 14th days of quarantine. Community workers and volunteers were designated to offer life services such as food delivery, express delivery, and daily necessities delivery. If there were no new confirmed cases during these 14 days, the lockdown policy in these areas would be lifted. Additionally, they were still not allowed to do any group activity in the first week after the quarantine.

Restricted areas: the living and working places of the close contacts were set as restricted areas. Citizens in the restricted areas were required to be quarantined for 14 days. Individuals from outside were allowed to get into these areas but could not leave till the end of quarantine. The RT-PCR tests were performed for everyone living in the restricted areas on the 1st, 7th, and 14th days of quarantine.

Areas with potential risks: the surrounding areas of the lockdown or restricted areas were defined as areas with potential risks. Normal life activities, except group activity and mass gathering, were all allowed in these areas. The

RT-PCR tests for people living in these areas were performed on the 1st and 7th day of circle-layer management.

The Classification and Management of People Groups at Different Risk Levels Using Health Code

Close contacts: According to the latest Protocol of COVID-19 Prevention and Control (Edition 8) released by the National Health Commission of the People's Republic of China, close contacts are individuals who have had contact, without effective protection, with one or more suspected or confirmed COVID-19 cases any time starting 2 days before the onset of the suspected or confirmed cases' symptoms or 2 days before sampling for laboratory testing of asymptomatic infected persons.[18]

High-risk personnel: includes confirmed cases, suspected cases, close contacts, secondary close contacts, people from overseas, people who have been to high-risk areas within 14 days.

Middle-risk personnel: includes people with potential contacts with high-risk persons within a week.

Low-risk personnel: includes people without epidemiological history.

There are 3 different colors of Health QR Code matching personnel of corresponding risk levels: red, high-risk personnel; yellow, middle-risk personnel; green, low-risk personnel (Supplementary Table 1). Citizens were managed according to their health code color and living areas during the circle-layer management:

1. Red health code users with confirmed infections: these cases were transferred to infectious disease hospitals for treatment through negative pressure ambulance once identified (Figure 1 Route A&B).
2. Red health code users with close contacts or secondary close contacts, or recently arrived in Chengdu from high-risk areas: these citizens were transferred to centralized isolation sites for medical observation (Figure 1 Route C&D).
3. Yellow health code users in restricted areas without confirmed infections were quarantined in their own apartment.
4. Yellow health code users in areas with potential risks were not allowed to use public transportation or go to public places like malls, supermarkets, movies theaters, bars, etc. Once found in public places, they would be suggested to wear proper

- 327-

Figure 1 The schematic diagram of Chengdu's COVID-19 confinement arrangement (circle-layer policy) during the summer outbreak.
Notes: The medical sites and routes of personnel arrangement were listed as following: Medical sites 1: Infectious disease hospital for treating confirmed or suspected cases; Medical sites 2: Designated nucleic acid testing stations and hospitals for yellow health code users from areas with potential risks; Medical sites 3: Designated hospitals serving for patients from lockdown/restricted area; Medical sites 4: Centralized isolation sites for newly arrived red health code users with epidemiological history. Route A: Routes for transferring confirmed cases from lockdown or restricted areas to infectious disease hospital; Route B: Routes for transferring confirmed cases from centralized isolation sites, designated hospitals or testing sites to infectious disease hospital; Route C: Routes for transferring close contacts or secondary close contacts of confirmed cases from lockdown or restricted areas to infectious disease hospital; Route D: Routes for transferring red health code users with epidemiological history from airports/ freeway toll station to centralized isolation sites; Route E: Routes for yellow health code users to get nucleic acid tests in designated sites or hospitals via private transportation; Route F: Routes for providing medical services to lockdown and restricted areas or transferring patients to hospitals when necessary.

protective equipment and transferred back to their community. They were permitted to go to designated hospitals or RT-PCR testing stations via private or community-arranged vehicles for RT-PCR tests or other medical services (Figure 1 Route E).

The yellow health codes of users from areas with potential risks would be turned into green once they got a negative nucleic acid testing result, while the red and yellow health codes of users in the lockdown and restricted areas would be turned into green only when they finished quarantine and got negative results in each nucleic acid test.

Management and Healthcare for Pregnant Women and Children Under Circle-Layer Management

The characteristics of quarantined pregnant women and children below 6 years old were listed in Supplementary

Tables 2 and 3. We recorded their body temperatures, pregnancy-related clinical features, and epidemiological history. A detailed healthcare plan for them was made (Supplementary Figure 2). Door-to-door medical services were provided for quarantined yellow health code users with mild symptoms. Through phone appointments, pregnant women and children who need medical care would be treated by a standby team of obstetrics, pediatrics, emergency, nosocomial infection specialists. Patients with severe symptoms were transferred into designated hospitals by the negative pressure ambulance and settled in the isolation ward (Figure 1 Route F). Another standby team of obstetrics and pediatrics was arranged to back up the infectious disease hospital whenever necessary. The services we provided include the severity assessment, blood test, electrocardiography, two-dimensional ultrasonic image. For pregnant women, the urine pregnancy test and fetal heart rate monitoring were also provided. On the final day of their quarantine, an online survey about quarantined pregnant women's attitude toward this summer outbreak and our healthcare services and the degree of their worry about being infected with COVID-19 was performed on the WeChat platform. The results are presented in Supplementary Table 2.

The Triage System Based on Health Code

The triage system implemented in this study was an update of our previous strategy with the application of Health QR Code.[19] Only one entrance (hospital gate) and one exit (backdoor) were open for patients during the epidemic. Patients and medical staff had different designated one-way paths for entering and leaving the hospital. As shown in Figure 2, the 3 levels of our preliminary triage system had different tasks based on their locations and medical duties:

Triage 1 (Entrance of outpatient and emergency department): a rapid triage through body temperature detection and health code color checking. The epidemiological history of patients and their attendants were also briefly asked.

Triage 2 (Outpatient inquiries at nurse station): a detailed inquiry of patients and their attendants' epidemiological history was performed in this triage. The health code and body temperature were also checked in case of omitted from the first triage.

Triage 3 (By the physicians who made the first diagnosis in outpatient clinic or in-patient department): a detailed inquiry or examination of patients' chief complaint, COVID-19 correlated symptoms,[19] epidemiological history was performed in this triage. The health code and body temperature would also be checked when necessary.

In this 3-level triage system, the patients were guided to different clinics or nucleic acid testing sites according to the result of the triage assessment:

1. Patients with green health codes and no epidemiological history were guided to outpatient clinic. Those with fever or epidemiological history were referred to the regular fever clinic.
2. Patients with green health codes, fever and epidemiological history, and patients with yellow health codes and fever/epidemiology history/COVID-19 symptoms were guided to the special fever clinic and get nucleic acid test thereby. If they got negative results in two consecutive samplings, their yellow code would turn green. If they got a positive result, they would be managed as suspected cases and get a second test to confirm their infection.[19]
3. Patients with yellow health codes but had no fever, epidemiology history or COVID-19 symptoms were guided to the designated testing zone for yellow code users. Once they got a negative result, their health code would turn green after the result has been updated. If they got a positive result, they would also be managed as suspected cases and get a second test to confirm their infection.

Triage Efficiency Experiment of Health QR Code

An experiment testing the triage efficiency of the Health QR code and traditional face-to-face inquiry was conducted on 28th October 2021. The timing for the health QR code started when users initiated the Health QR code mini-program and ended when their smartphones showed their health QR code and itinerary information. The timing for a face-to-face inquiry began when the nurses in triage system started their first question and ended when they got a clear and satisfactory answer of epidemiological history. Our experiment equally included the results of all the 6 shifts of the triage system on that day. The results of this experiment are presented in Supplementary Table 4.

Data Collection

We collected and analyzed the daily numbers of different personnel with red health codes from the WeChat platform's official account of the Chengdu Municipal Health
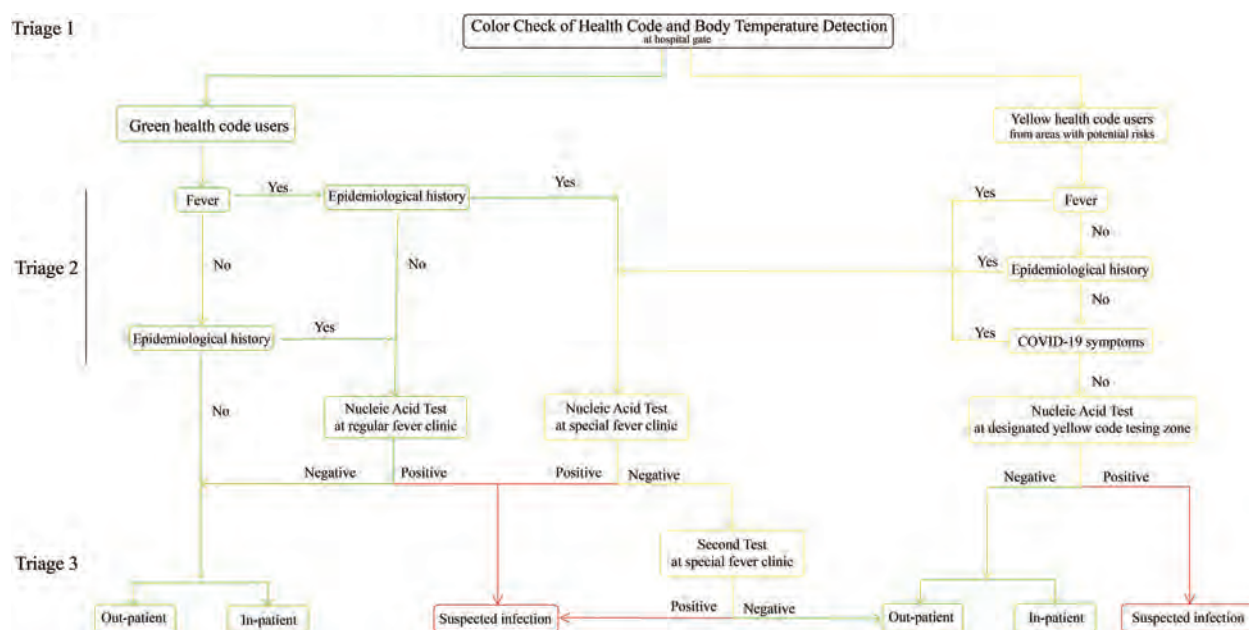
Figure 2 The flowchart of the health-code-based triage system.
Note: Colors of lines and boxes were matched with the color of patients' or attendants' health QR code.

Commission from July 21 to August 13, 2021. During the whole period of the circle-layer management (from July 28 to August 12, 2021), the numbers of pregnant women and children in quarantine were rendered daily by community workers or the medical professionals in the centralized isolation sites and infectious disease hospitals. The results of the online survey were gathered and processed automatically by the WeChat platform. Similarly, the numbers of patients with green and yellow health codes from regular and special fever clinics in Chengdu Women's and Children's Central Hospital were recorded by the doctors on duty during the circle-layer management.

Statistical Analysis

The software SPSS version 23.0 (IBM SPSS Inc., US) was applied for statistical analysis in this research. Categorical variables were all presented in the form of frequencies and percentages, including health QR code colors, age groups, educational background, monthly family income, epidemiological history, etc. Chi-square tests were used for the analysis of categorical variables. The continuous variable in the current study was the time (seconds) needed to obtain epidemiological history through different methods. It was shown in the form of mean ± SD and analyzed by Student's t-test. A p-value < 0.05 was regarded as statistically significant.

Results

As shown in Figure 3A, after 3 indigenous confirmed cases have been identified on 27th July, the circle-layer management in Chengdu has included 3 communities and identified 2 indigenous confirmed cases and 1 asymptomatic case on 28th July. The number of imported confirmed and asymptomatic cases also remained stable during the circle-layer management (from July 28th to August 12th). Since July 29th, as the epidemiological history survey went on, about 1200 citizens have been identified and given red health codes. The circle-layer management ended on August 12th when the lockdowns in all 3 communities were lifted, with no new indigenous cases reported for 15 consecutive days. Only approximately 500 close contacts or imported cases remained, meaning that the circle-layer management controlled the transmission resource within 2 days and have prevented community chain transmission and nosocomial infection during the whole period.

The number of quarantined citizens peaked on August 9, 2021. On that day, 71 pregnant women and 575 children below 6 years old were under quarantine as shown in Figure 3B and C. During the quarantine, the staff from the Chengdu Women's and Children's Central Hospital has performed 4 home visits and 2 patient transfers. From Supplementary Tables 2 and 3, we can notice

- 330-
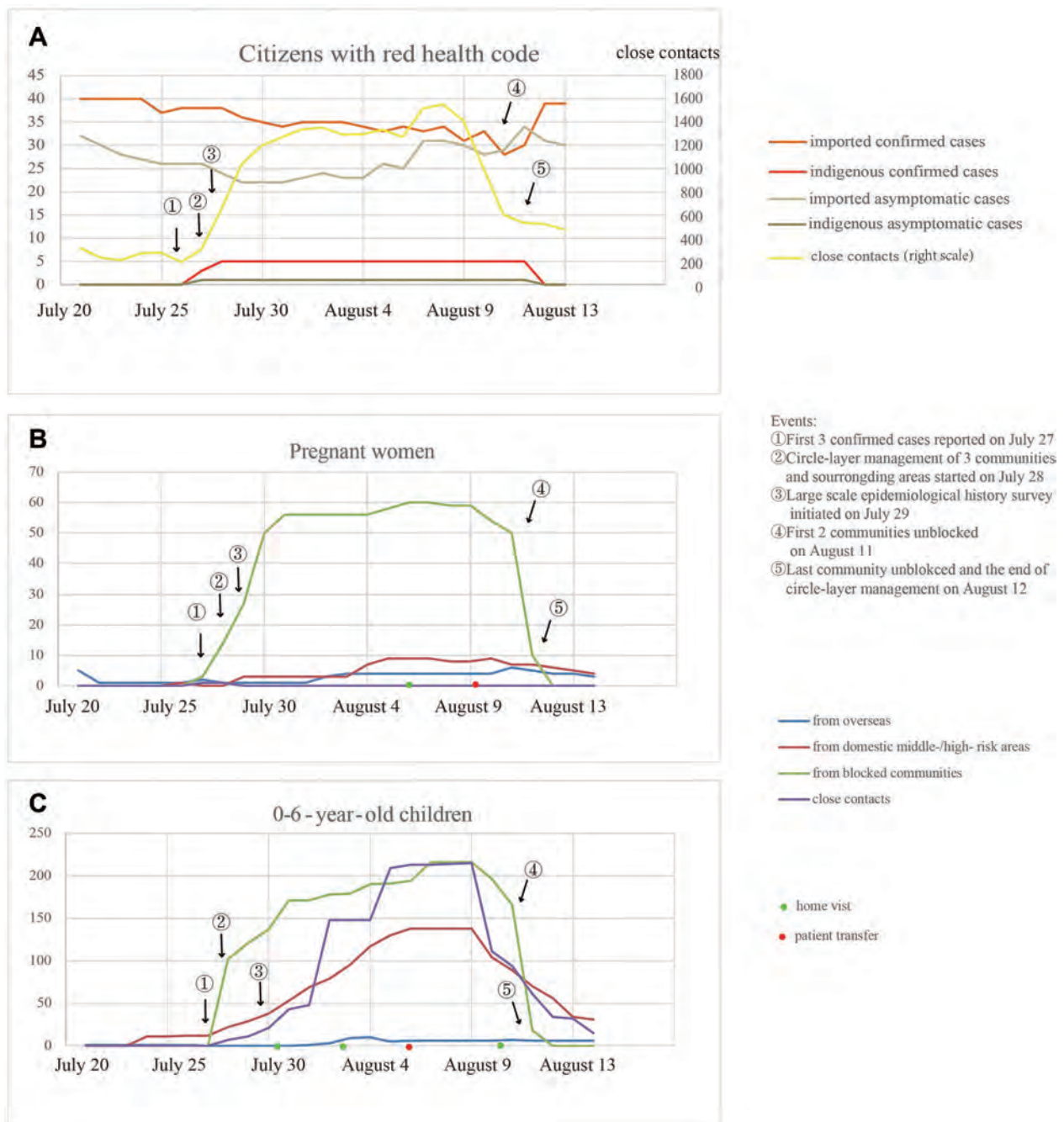
Figure 3 The dynamic change in the number of different personnel under Chengdu's circle-layer management during the summer outbreak of COVID-19. (**A**) The dynamic change in the number of different personnel with red health codes. (**B**) The dynamic change in the number of quarantined pregnant women. (**C**) The dynamic change in the number of children below 6 years old.

that the majority of quarantined pregnant women circle-layer management were from blocked communities while the children under quarantine were from disparate epidemiological history resources. All quarantined pregnant women participated in the online survey. The survey results indicated that about 80% of them did not worry about being infected with COVID-19, held an optimistic view about the summer outbreak in Chengdu, and felt quite satisfactory about the healthcare services we provided.

During the circle-layer management, as shown in Table 1, the health-code-based triage system of the hospital has identified 137 patients with epidemiological history from 211 patients with yellow health code (61.99%) and 71 patients with epidemiological history from 4504 patients with green code (1.57%) in the fever clinic (p < 0.001). As presented in Supplementary Table 4, the triage efficiency experiment showed that the health QR code remarkably outperformed the traditional face-to-face inquiry in the time (seconds) needed to obtain the epidemiological history of patients (3.52 ± 0.98 vs 78.91 ± 23.18, P < 0.001).

Discussion

Our study summarized the policies and measures taken by the local government and hospitals to stop the spread of SARS-CoV-2 Delta variants and serve for the obstetric and pediatric patients, among which the health code and a special quarantine policy (circle-layer management) played an essential role. The "circle-layer" policy had successfully exterminated the indigenous cases and avoided community transmission through widespread application of epidemiological history tracing technology, rigorous containment efforts of the communities where confirmed cases lived, and relatively less strict management of surrounding areas. The health code based 3-level triage system also played an essential role in preventing nosocomial infection. During the whole period of "circle-layer" management, pregnant women and children's healthcare was also ensured by home visits or patient transfers provided from the medical professionals of designated women's and children's hospital.

Plenty of previous studies have proved the positive impact of containment in preventing the epidemic of COVID-19.[5,20–23] Lau indicated that the lockdown measures in Wuhan since late January 2020 had remarkably slowed down the growth rate and extended the doubling time of confirmed cases.[5] Another mathematical model-based research also implicated that the combined non-pharmaceutical interventions could achieve the strongest and quickest effect in containing the epidemic.[21] However, such measures also inevitably lead to many side effects on the daily life, work, physical and mental health of citizens to varying degrees.[24,25] Thus, an ideal strategy to prevent and control the epidemic must minimize the number of impacted citizens and the containment scale while stopping the transmission. The circle-layer policy, was proved precise and feasible to some extent in the scenario of sporadic or small-scale imported outbreaks like the one that occurred in Chengdu. With only 3 communities been lockdown for 2 weeks, the other 20 million inhabitants can still live a normal life and commute to their workplaces without worrying about the spread of transmission. Thus, the whole city could almost exert its full capability of providing life replenishment and medical support to those under confinement and blanketing the reignition of the epidemic at its very beginning.[26,27]

The status quo of the epidemic in China greatly lowered the applicability of the previous triage strategy.[19,28] By mid-August, evidence showed that a quarter of the 2500 confirmed infections in China were defined as asymptomatic cases,[29] suggesting that the epidemiological history is getting more critical and the previous triage systems are no longer reliable, since they heavily relied on the COVID-19 symptoms. However, the inquiry of epidemiological history is hard to be well performed in the 1st and 2nd triages, since it is too laborious and wrong information may be provided by patients and their attendants. Besides, for departments like pediatrics, respiratory, and fever clinic, it is quite impractical for them to perform the previous 3-level triage since a big percentage of their patients have COVID-19-like symptoms. The advent of the health QR code, a contact-tracing, and health surveillance mini program, had perfectly solved these problems, fulfilled the concept of precise epidemic control, and facilitated a variety of other COVID-19 containment

Table 1 The Comparison of COVID-19 Correlated Features in Patients with Green and Yellow Health Code from Regular and Special Fever Clinic in Chengdu Women's and Children's Central Hospital During the Circle-Layer Management

	Patients with Green Code (n = 4504)	Patients with Yellow Code (n = 221)	X2	p
Patients with epidemiological history	71(1.57%)	137 (61.99%)	1827.101	<0.001
Confirmed cases	0(0%)	0(0%)	–	–

measures. It timely and precisely collects and updates the COVID-19 correlated symptoms and itinerary information of most citizens, thus enabled governments' prompt, coherent and accurate decisions on public health policies and the management of citizens with epidemiological history.[9] It also provided a convenient platform for public facilities, especially the hospitals, to quickly identify and reject personnel at high or potential risks.[30]

However, the health code also harbors many hidden troubles regarding data security, accuracy, and government surveillance. For instance, at the beginning of the summer outbreak in Chengdu, quite a few citizens who declared no epidemiological history still received a yellow health code. It led to many inconveniences to those citizens and posed tremendous pressure in the nucleic acid testing capability of medical institutions, for citizens want to turn their health code to green. Other concerns about the health code would be the discrimination toward the red or yellow health code users found in public and their difficulty in getting public services, including the medical care. Moreover, the public is not well acknowledged of who manages the health code, how their information is disposed of or protected, and whether their personal information would be disclosed.[9]

In the present study, the group that we mainly focused on were pregnant women and children. Due to the low vaccination rate of pregnant women and children in China, they are susceptible to the Delta variant.[10,11] Evidence also showed that COVID-19 infected pregnant women had a higher ICU admission rate than those without gestation.[12] Therefore, we formulated a detailed plan for providing healthcare to children and pregnant women in quarantine. They could appoint the medical services they need through phone appointments, and the community workers would also pay several home visits to record their physical and mental health status. The online survey results showed that the majority of quarantined pregnant women were satisfied with the medical services we offered and were optimistic about the summer outbreak. It indicated that though only 4 home visits and 2 patient transfers were performed during the quarantine, such medical cares have basically ensured their accessibility of medical service. Previous publications indicated that pregnant women and children in quarantine had higher rates of depressive symptoms, anxiety, and negative affect.[13–15] However, due to the lack of professionals with psychological backgrounds, no mental counseling was provided for the children and pregnant women in quarantine. Generally speaking, given that no community chain transmission occurred, our healthcare system had basically satisfied their healthcare needs.

Though the proper containment efforts that a city has to make should be proportionate to the epidemic scenario she is in,[31] new variants with high transmissibility and morbidity continuously appear and get prevalent, making the feasibility of coexistence with the SARS-CoV-2 through large-scale vaccination decreasing noticeably.[32–34] As many non-capital Chinese cities and tourism hotspots with limited resources and brittle epidemic prevention systems reported hundreds of confirmed cases in this summer outbreak, the prompt implementation of the circle-layer management of risk areas and the health code based triage system may greatly reduce the resources and efforts it would cost to exterminate the outbreak before the occurrence of medical resources panic squeeze. Chengdu's comprehensive containment strategy had again proved the effectiveness of conservative and rigorous measures, including comprehensive surveillance, strict contact tracing, and most importantly, quarantine. Many factors contributed to the success of fighting against the summer outbreak, including anti-epidemic experience in previous strikes or from other cities, expert suggestions on the arrangement of COVID-19 control and prevention, and the publics' cooperation and fear for the virus. Unlike previous situations, the application of health QR codes has made these efforts less time-wasting, money consuming, and less laborious. The more precise and smaller-scale quarantine policy had also brought novelty to our strategy. The way we provided healthcare to the pregnant and the young also set an example for cities under similar situations.

Conclusion

The circle-layer management successfully and precisely prevented the spread of summer outbreaks of COVID-19 in Chengdu, China in 2021. The health code-based triage system was efficient and effective in triaging patients with epidemiological history. The healthcare services had basically met quarantined pregnant women's needs.

Data Sharing Statement

The data is available upon reasonable request to the corresponding author.

Ethics Approval and Informed Consent

This study was approved by the Ethics Committee of Chengdu Women's and Children's Central Hospital (WCCH-202124) and conducted with the written informed consent of the participants.

Acknowledgments

Author Contributions

All authors made a significant contribution to the work reported, whether that is in the conception, study design, execution, acquisition of data, analysis and interpretation, or in all these areas; took part in drafting, revising or critically reviewing the article; gave final approval of the version to be published; have agreed on the journal to which the article has been submitted; and agree to be accountable for all aspects of the work.

Funding

Disclosure

The authors declare no conflicts of interest in this work.

References

1. Wu Z, McGoogan JM. Characteristics of and important lessons from the Coronavirus Disease 2019 (COVID-19) outbreak in China: summary of a report of 72 314 cases from the Chinese Center for Disease Control and Prevention. *JAMA*. 2020;323(13):1239–1242. doi:10.1001/jama.2020.2648

2. Hodgson SH, Mansatta K, Mallett G, Harris V, Emary KRW, Pollard AJ. What defines an efficacious COVID-19 vaccine? A review of the challenges assessing the clinical efficacy of vaccines against SARS-CoV-2. *Lancet Infect Dis*. 2021;21(2):e26–e35. doi:10.1016/S1473-3099(20)30773-8

3. Habas K, Nganwuchu C, Shahzad F, et al. Resolution of coronavirus disease 2019 (COVID-19). *Expert Rev Anti Infect Ther*. 2020;18 (12):1201–1211. doi:10.1080/14787210.2020.1797487

4. Ang YY. When COVID-19 meets centralized, personalized power. *Nat Hum Behav*. 2020;4(5):445–447. doi:10.1038/s41562-020-0872-3

5. Lau H, Khosrawipour V, Kocbach P, et al. The positive impact of lockdown in Wuhan on containing the COVID-19 outbreak in China. *J Travel Med*. 2020;27(3). doi:10.1093/jtm/taaa037

6. Tu H, Tu S, Gao S, Shao A, Sheng J. Current epidemiological and clinical features of COVID-19; a global perspective from China. *J Infect*. 2020;81(1):1–9. doi:10.1016/j.jinf.2020.04.011

7. Lopez Bernal J, Andrews N, Gower C, et al. Effectiveness of Covid-19 vaccines against the B.1.617.2 (Delta) variant. *N Engl J Med*. 2021;385(7):585–594. doi:10.1056/NEJMoa2108891

8. Dyer O. Covid-19: delta infections threaten herd immunity vaccine strategy. *BMJ*. 2021;374:n1933. doi:10.1136/bmj.n1933

9. Liang F. COVID-19 and health code: how digital platforms tackle the pandemic in China. *Soc Media Soc*. 2020;6(3):20563051 20947657.

10. Liu S, Yuan C, Lin J, et al. Association between vaccinations and clinical manifestations in children with COVID-19. *Transl Pediatr*. 2021;10(1):17–25. doi:10.21037/tp-20-225

11. Transcript of the Press Conference on March 21st, 2021 by the Joint Prevention and Control Mechanism of the State Council; 2021. Available from: http://www.nhc.gov.cn/xcs/s3574/202103/b3b8103da9104fc58d7ce8f5189e9be2.shtml. Accessed March 21, 2021.

12. Pirjani R, Hosseini R, Soori T, et al. Maternal and neonatal outcomes in COVID-19 infected pregnancies: a prospective cohort study. *J Travel Med*. 2020;27(7). doi:10.1093/jtm/taaa158

13. Xie X, Xue Q, Zhou Y, et al. Mental health status among children in home confinement during the Coronavirus disease 2019 outbreak in Hubei Province, China. *JAMA Pediatr*. 2020;174(9):898–900. doi:10.1001/jamapediatrics.2020.1619

14. López-Morales H, Del Valle MV, Canet-Juric L, et al. Mental health of pregnant women during the COVID-19 pandemic: a longitudinal study. *Psychiatry Res*. 2021;295:113567. doi:10.1016/j.psychres.2020.113567

15. Almeida M, Shrestha AD, Stojanac D, Miller LJ. The impact of the COVID-19 pandemic on women's mental health. *Arch Womens Ment Health*. 2020;23(6):741–748. doi:10.1007/s00737-020-01092-2

16. "Sichuan Tianfu Health Code" health QR code was launched across the province; 2021. Available from: http://www.sc.gov.cn/10462/12771/2021/1/13/9387f1c13bf54c2cb8cc9346e35a2380.shtml. Accessed January 13, 2021.

17. Tianfu Health Code; 2021. Available from: https://www.tfjkt.cn/. Accessed 2021.

18. Council JPaCMotS. Notice on the issuance of the protocol for prevention and control of COVID-19 (Edition 8). National Health Commission of China; 2021 [updated May 21]. Available from: http://www.gov.cn/xinwen/2021-05/14/content_5606469.htm. Accessed May 21, 2021.

19. Li C, Tang L, Luo L, et al. The prevention and control experience of maternal health care from Chengu, China During the COVID-19 epidemic. *Risk Manag Healthc Policy*. 2020;13:2213–2217. doi:10.2147/RMHP.S261821

20. Li X, Liu M, Zhou R, Zhang Y, Wu C, Xu L. Centralized medical quarantine for imported COVID-19 in Shanghai, China. *J Travel Med*. 2020;27(5). doi:10.1093/jtm/taaa109

21. Lai S, Ruktanonchai NW, Zhou L, et al. Effect of non-pharmaceutical interventions to contain COVID-19 in China. *Nature*. 2020;585 (7825):410–413. doi:10.1038/s41586-020-2293-x

22. Wilder-Smith A, Freedman DO. Isolation, quarantine, social distancing and community containment: pivotal role for old-style public health measures in the novel coronavirus (2019-nCoV) outbreak. *J Travel Med*. 2020;27(2). doi:10.1093/jtm/taaa020

23. Kang C, Meng F, Feng Q, et al. Implementation of quarantine in China during the outbreak of COVID-19. *Psychiatry Res*. 2020;289:113038. doi:10.1016/j.psychres.2020.113038

24. Brooks SK, Webster RK, Smith LE, et al. The psychological impact of quarantine and how to reduce it: rapid review of the evidence. *Lancet*. 2020;395(10227):912–920. doi:10.1016/S0140-6736(20) 30460-8

25. Xin M, Luo S, She R, et al. Negative cognitive and psychological correlates of mandatory quarantine during the initial COVID-19 outbreak in China. *Am Psychol*. 2020;75(5):607–617. doi:10.1037/amp0000692

- 334-

26. Wen J Life of blocked communities in Chengdu during the summer outbreak of COVID-19; 2021. Available from: https://m.thepaper.cn/baijiahao_13995382. Accessed August 11, 2021.

27. Fight against the Delta Variant in Chengdu; 2021. Available from: https://m.thepaper.cn/baijiahao_14017839. Accessed August 12, 2021.

28. Wang Q, Wang X, Lin H. The role of triage in the prevention and control of COVID-19. *Infect Control Hosp Epidemiol*. 2020;41 (7):772–776. doi:10.1017/ice.2020.185

29. Council JPaCMotS. Notice on the issuance of the protocol for prevention and control of COVID-19 (Edition 6). National Health Commission of China; 2021. Available from: http://www.gov.cn/xinwen/2021-05/14/content_5606469.htm. Accessed May 14, 2021.

30. Zhu R, Cui Y, Guo L, et al. Application of QR code in three-level previewing triage system in a hospital's response to Beijing Xinfadi wholesale market COVID-19 epidemic. *Chin J Nosocomiol*. 2021;31 (08):1267–1271.

31. Lee VJ, Chiew CJ, Khong WX. Interrupting transmission of COVID-19: lessons from containment efforts in Singapore. *J Travel Med*. 2020;27(3). doi:10.1093/jtm/taaa039

32. Callaway E. Could new COVID variants undermine vaccines? Labs scramble to find out. *Nature*. 2021;589(7841):177–178. doi:10.1038/d41586-021-00031-0

33. Tang JW, Tambyah PA, Hui DS. Emergence of a new SARS-CoV-2 variant in the UK. *J Infect*. 2021;82(4):e27–e28. doi:10.1016/j.jinf.2020.12.024

34. Rubin EJ, Baden LR, Farrar JJ, Morrissey S. Audio interview: viral variants and Covid-19. *N Engl J Med*. 2021;384(7):e38. doi:10.1056/NEJMe2102882

Supported by
日本財団
THE NIPPON
FOUNDATION

第 44 期　　研究者番号：G4409　　　　　　　　　作成日　：2023 年 3 月 6 日

氏　名	馬　快	MA KUAI	性別	F	生年月日　1993/08/25
所属機関（役職）	大阪大学大学院医学系研究科（大学院生）				
研究先（指導教官）	大阪大学大学院医学系研究科腎臓内科学（猪阪 善隆　教授） 国立成育医療研究センター研究所 RI 管理室/移植免疫研究室（李 小康　室長）				
研究テーマ	腎移植における腎臓線維化発生機序の解明と新規治療法の開発に関する研究 Elucidation of the mechanism and development of new therapeutic methods for renal fibrosis after kidney transplantation				
専攻種別	☐論文博士		☑課程博士		

研究者評価（指導教官記入欄）

成績状況	優 学業成績係数=90	取得単位数
		20／30

学生本人が行った研究の概要	腎臓の線維化は、ほとんどの進行性腎臓病の特徴である。腎線維化の動物モデルでは、マウスの左尿管を結紮する一側尿管閉塞（UUO）より確立され、広く基礎研究に使用されている。一方、5-アミノアセチルアクリル酸（5-ALA）は、ヘムやプロトポルフィリンIX（PpIX）の重要な前駆体である。我々これまでの研究で、ヘムオキシゲナーゼ（HO）-1 の発現が 5-ALA とクエン酸第一鉄（SFC）により増強されることが今までの研究で明らかにした。本研究では、UUO によって誘発されたマウスの腎線維化および炎症に対する 5-ALA および SFC の保護効果を検証することを目的とした。
総合評価	【良かった点】 短い期間内で、腎線維化のマウスモデルを確立することができた。評価項目として、病理学、血清学と関連遺伝子の mRNA 発現の実験系も併せて確立した。また、5-ALA および SFC マウスへ投与の予備実験として、その効果が示された。 【改善すべき点】 5-ALA および SFC を用いたマウスへ投与後の効果について、その機序がまだ不明な点が沢山あるため、引き続き、検証する必要がある。 【今後の展望】 上記腎線維化のマウスモデルを用いて、5-ALA および SFC の投与での治療評価及びその作用機序を解明することで、将来臨床への応用に目指したい。
学位取得見込	学位取得見込み

評価者（指導教官名）　　李　小康

第44期　　　研究者番号：　G4409　　　作成日：2023年3月3日

氏名	马 快	MA KUAI	性別	F	生年月日　1993/08/25

所属機関（役職）	大阪大学大学院医学系研究科（大学院生）
研究先（指導教官）	大阪大学大学院医学系研究科腎臓内科学（猪阪 善隆　教授） 国立成育医療研究センター研究所RI管理室/移植免疫研究室（李 小康　室長）
研究テーマ	腎移植における腎臓線維化発生機序の解明と新規治療法の開発に関する研究 Elucidation of the mechanism and development of new therapeutic methods for renal fibrosis after kidney transplantation

専攻種別	論文博士	□	課程博士	☑

１．研究概要

1）目的（Goal）

Renal fibrosis is the hallmark of most progressive kidney diseases. Unilateral ureteral obstruction (UUO), the ligation of the ureter, most commonly the left ureter, has been widely used to establish animal models of renal fibrosis [1]. 5-aminoacetylacrylic acid (5-ALA), a key precursor of heme and protoporphyrin IX (PpIX), is catalyzed in animal cells by mitochondrial aminoacetylacrylic synthetase using glycine and succinyl-coA [2]. Previous studies demonstrated that heme oxygenase (HO)-1 expression was up-regulated by 5-ALA and sodium ferrous citrate (SFC) [2-5]. HO-1 is known to be a rate-determining enzyme in heme metabolism that produces bilirubin and carbon monoxide, which were demonstrated to act as anti-inflammatory factors. The present study aimed to investigate the protective effect of 5-ALA and SFC against UUO-induced renal fibrosis and inflammation in mice.

2）戦略（Approach）

In present study, we used 5-ALA and SFC to treat UUO-induced renal fibrosis and inflammation. For that purpose, mice were randomly divided into five treatment groups: Naive group, 7d UUO model group, 7d UUO + 5ALA/SFC group, 14d UUO model group, 14d UUO + 5ALA/SFC group. 5ALA/SFC was administered to the mice for 7 or 14 days following UUO. At the sampling days, blood and kidney tissue samples were collected for evaluation. Renal tissue was harvested and fixed in 10% formalin or optimal cutting temperature compound for histological examination. For the biochemical and molecular expression assessments, kidney tissues were immediately frozen and stored at 80°C until analysis.

3）材料と方法（Materials and methods）

(1) Animals:

Eight-week-old male C57BL/6JJmsSlc mice were purchased from Shizuoka Laboratory Animal Center (Shizuoka, Japan) and housed in a feeding room with automatically controlled light and temperature according to the guidelines of the Institutional Animal Care and Use Committee. All animal procedures were authorized by the National Research Institute for Child Health and Development.

(2) Serum biochemical analyses:

Serum was collected from whole-blood samples after standing for 30 minutes at 37°C and centrifuged at 3000 g for 20 minutes at 4°C. The samples were then measured for blood urea nitrogen (BUN) and serum creatinine (Cr) were detected with a commercially available kit (Fujifilm, Tokyo, Japan) and an automatic biochemical analyzer (DRI-CHEM 3500i; Fujifilm) according to the manufacturer's instructions.

(3) Histology and histopathological analyses:

The paraffin-embedded sections were stained with hematoxylin and eosin (HE), Sirus red and Masson's trichrome to evaluate histological change and fibrosis. Ten non-repeating fields were randomly selected. Tubular lesions were scored from 0 to 4. 0: normal; 1: mild (<25% of the cortex); 2: moderate (25~50%); 3: severe (50~75%); 4: extensive damage (>75%). The positive area of Sirus red (red) and Masson's trichrome staining (blue) were quantified using the WinRoof 7.4 software program (Mitani Corporation, Tokyo, Japan).

(4)Cell preparation and the flow cytometry analysis

Lymphocytes from spleen and kidney tissues were detected by the LSRFortessa system (BD Biosciences, Franklin Lakes, NJ). The stained cells were analyzed with the FlowJo software program (Version 10.5.0; BD Biosciences).

1．研究概要（2）

(6) Western blot analyses

In brief, frozen renal tissues were homogenized in RIPA buffer containing 1% protease inhibitor cocktail-1 and 1% protease inhibitor cocktail-2 (Sigma–Aldrich) followed by centrifugation in a microfuge at top speed for 30 min. Protein concentrations were assayed using Bio-Rad Protein Assay (Bio-Rad, Hercules, CA). Samples were separated by electrophoresis on 10% polyacrylamide gels and transferred to Immobilon-PVDF (Bio-Rad). After brief incubation with 5% non-fat milk to block non-specific binding, membranes were exposed overnight at 4 °C. Protein activity was quantified by a laser densitometric analysis of the radiographic film using the ImageJ software program (NIH, Bethesda, MD).

(7) Statistical analyses

The GraphPad Prism 9 software program (GraphPad, San Diego, CA) was used to calculate statistical significance. Student T test method and one-way ANOVA method were used to compare the three groups. Data are expressed as the mean $\pm$ SD. A value of $P < 0.05$ was considered to be statistically significant (*$P < 0.05$; **$P < 0.01$; ***$P < 0.001$; ****$P < 0.0001$).

3）実験結果（Results）

(1)5-ALA/SFC treatment alleviates renal damage of UUO-induced mouse model of renal fibrosis. Compared with naive group, serum BUN in UUO model group on day7 and day14 increased significantly ($p<0.001$ and $p<0.0001$, respectively). 5-ALA/SFC treatment did not decrease the levels of BUN on day7, but decreased significantly on day14 ($p<0.01$). The levels of Cr also down-regulated markedly by 5-ALA/SFC administration on day14 ($p<0.05$).

Expected results:

(2)5-ALA/SFC treatment inhibits inflammatory responses

(3)5-ALA/SFC reduces renal fibroblast activation and ameliorates ECM deposition

4）考察（Discussion）

Not available.

6）参考文献（References）

1 Bai Y, Wang W, Yin P, Gao J, Na L, Sun Y, Wang Z, Zhang Z, Zhao C. Ruxolitinib Alleviates Renal Interstitial Fibrosis in UUO Mice. INT J BIOL SCI 2020 2020-01-20; 16(2): 194-203.

2 Fujino M, Nishio Y, Ito H, Tanaka T, Li XK. 5-Aminolevulinic acid regulates the inflammatory response and alloimmune reaction. INT IMMUNOPHARMACOL 2016 2016-08-01; 37: 71-78.

3 Liu C, Zhu P, Fujino M, Zhu S, Ito H, Takahashi K, Nakajima M, Tanaka T, Zhuang J, Li XK. 5-ALA/SFC Attenuated Binge Alcohol-Induced Gut Leakiness and Inflammatory Liver Disease in HIV Transgenic Rats. ALCOHOL CLIN EXP RES 2019 2019-08-01; 43(8): 1651-1661.

4 Hu X, Que W, Hirano H, Wang Z, Nozawa N, Ishii T, Ishizuka M, Ito H, Takahashi K, Nakajima M, Tanaka T, Zhu P, Guo WZ, Li XK. 5-Aminolevulinic acid/sodium ferrous citrate enhanced the antitumor effects of programmed cell death-ligand 1 blockade by regulation of exhausted T cell metabolism in a melanoma model. CANCER SCI 2021 2021-07-01; 112(7): 2652-2663.

5 Negoro H, Chatziantonio C, Razzaque MS. Therapeutic potential of 5-aminolevulinic acid and sodium-ferrous citrate for viral insults: relevance to the COVID-19 crisis. EXPERT REV ANTI-INFE 2022 2022-05-01; 20(5): 657-661.

2．執筆論文　Publication of thesis　※記載した論文を添付してください。Attach all of the papers listed below.

論文名 1 Title	Combinations of anti-GITR antibody and CD28 superagonist ameliorated dextran sodium sulfate-induced mouse colitis						
掲載誌名 Published journal	Clinical and Experimental Immunology						
	2022 年　6 月	208（3） 巻（号）	340 頁 ～　350 頁		言語 Language	英語	
第1著者名 First author	Kuai Ma	第2著者名 Second author	Weitao Que	第3著者名 Third author		Xin Hu	
その他著者名 Other authors	Wen-Zhi Guo, Liang Zhong, Daisuke Ueda, Er-Li Gu, Xiao-Kang Li						
論文名 2 Title	Combinations of anti-GITR antibody and CD28 superagonist induce permanent allograft acceptance by generating type 1 regulatory T cells						
掲載誌名 Published journal	SCIENCE ADVANCES						
	2022 年　8 月	8（31） 巻（号）	頁 ～ 頁		言語 Language	英語	
第1著者名 First author	Weitao Que	第2著者名 Second author	Kuai Ma	第3著者名 Third author		Xin Hu	
その他著者名 Other authors	Wen-Zhi Guo, Xiao-Kang Li						
論文名 3 Title							
掲載誌名 Published journal							
	年　月	巻（号）	頁 ～ 頁		言語 Language		
第1著者名 First author		第2著者名 Second author		第3著者名 Third author			
その他著者名 Other authors							
論文名 4 Title							
掲載誌名 Published journal							
	年　月	巻（号）	頁 ～ 頁		言語 Language		
第1著者名 First author		第2著者名 Second author		第3著者名 Third author			
その他著者名 Other authors							
論文名 5 Title							
掲載誌名 Published journal							
	年　月	巻（号）	頁 ～ 頁		言語 Language		
第1著者名 First author		第2著者名 Second author		第3著者名 Third author			
その他著者名 Other authors							

3．学会発表　Conference presentation　※筆頭演者として総会・国際学会を含む主な学会で発表したものを記載し

※Describe your presentation as the principal presenter in major academic meetings including general meetings or international meetings.

学会名 Conference	第58回日本移植学会総会
演　題 Topic	Combinations of anti-GITR antibody and CD28 superagonist generated type 1 regulatory T cells
開催日 date	2022　年　　10　月　　14　日　　開催地 venue　名古屋
形式　method	☑　口頭発表　Oral　□　ポスター発表　Poste　言語　Language　□　日本語　☑　英語　□　中国語
共同演者名 Co-presenter	Weitao Que, Xin Hu, Xiao-Kang Li
学会名 Conference	
演　題 Topic	
開催日 date	年　　　月　　　日　　開催地 venue
形式　method	□　口頭発表　Oral　□　ポスター発表　Poste　言語　Language　□　日本語　□　英語　□　中国語
共同演者名 Co-presenter	
学会名 Conference	
演　題 Topic	
開催日 date	年　　　月　　　日　　開催地 venue
形式　method	□　口頭発表　Oral　□　ポスター発表　Poste　言語　Language　□　日本語　□　英語　□　中国語
共同演者名 Co-presenter	
学会名 Conference	
演　題 Topic	
開催日 date	年　　　月　　　日　　開催地 venue
形式　method	□　口頭発表　Oral　□　ポスター発表　Poste　言語　Language　□　日本語　□　英語　□　中国語
共同演者名 Co-presenter	

4．受賞（研究業績）Award (Research achievement)

名　称 Award name					
	国名 Country		受賞年 Year of	年	月
名　称 Award name					
	国名 Country		受賞年 Year of	年	月

5．本研究テーマに関わる他の研究助成金受給 Other research grants concerned with your resarch theme

受給実績 Receipt record	□ 有　　■ 無			
助成機関名称 Funding agency				
助成金名称 Grant name				
受給期間 Supported	年　　　　月 ～ 　　　　年　　　　月			
受給額 Amount received	円			
受給実績 Receipt record	□ 有　　■ 無			
助成機関名称 Funding agency				
助成金名称 Grant name				
受給期間 Supported	年　　　　月 ～ 　　　　年　　　　月			
受給額 Amount received	円			

6．他の奨学金受給 Another awarded scholarship

受給実績 Receipt record	■ 有　　□ 無
助成機関名称 Funding agency	中国国家留学基金管理委員会
奨学金名称 Scholarship	国家建設高水平大学公派研究生項目
受給期間 Supported	2020　年　12　月 ～　2024　年　12　月
受給額 Amount received	8,160,000　　　円

7．研究活動に関する報道発表 Press release concerned with your research activities

　　※記載した記事を添付してください。 Attach a copy of the article described below

報道発表 Press release	□ 有　　■ 無	発表年月日 Date of release	
発表機関 Released medium			
発表形式 Release method	・新聞　・雑誌　・Web site　・記者発表　・その他（　　　　　　　　　　　　　　　）		
発表タイトル Released title			

8．本研究テーマに関する特許出願予定 Patent application concerned with your research them

出願予定 Scheduled	□ 有　　■ 無	出願国 Application	
出願内容（概要） Application contents			

9．その他 Others

指導責任者（記名）　　　*Li Xiaokang*

Research Article

Combinations of anti-GITR antibody and CD28 superagonist ameliorated dextran sodium sulfate-induced mouse colitis

Kuai Ma[1,2], Weitao Que[2], Xin Hu[2], Wen-Zhi Guo[3], Liang Zhong[4], Daisuke Ueda[5], Er-li Gu[1], and Xiao-Kang Li[*,2,3], iD

[1]Department of Gastroenterology and Hepatology, Jing'an District Central Hospital, Jing'an Branch of Huashan Hospital, Fudan University, Shanghai, China

[2]Division of Transplantation Immunology, National Research Institute for Child Health and Development, Tokyo, Japan

[3]Department of Hepatobiliary and Pancreatic Surgery, The First Affiliated Hospital of Zhengzhou University, Zhengzhou, China

[4]Department of Gastroenterology, Huashan Hospital, Fudan University, Shanghai, China

[5]Division of Hepato-Pancreato-Biliary Surgery and Transplantation, Department of Surgery, Kyoto University Graduate School of Medicine, Kyoto, Japan

*Correspondence: Xiao-Kang Li, Division of Transplantation Immunology, National Research Institute for Child Health and Development, 2-10-1 Okura, Setagaya-ku, Tokyo 157-8535 Japan. Tel: +81 3 3416 0181; Fax: +81 3 3417 2864; E-mail: ri-k@ncchd.go.jp

Abstract

Ulcerative colitis (UC) is one of the two main forms of inflammatory bowel disease (IBD) and is an idiopathic, chronic inflammatory disease of the colonic mucosa with an unclear etiology. Interleukin (IL)-10 has been reported to play a crucial role in the maintenance of immune homeostasis in the intestinal environment. Type 1 regulatory T (Tr1) cells are a subset of CD4+Foxp3− T cells able to secrete high amounts of IL-10 with potent immunosuppressive properties. In this study, we found that the combination of anti-GITR antibody (G3c) and CD28 superagonist (D665) treatment stimulated the generation of a large amount of Tr1 cells. Furthermore, G3c/D665 treatment not only significantly relieved severe mucosal damage but also reduced the incidence of colonic shortening, weight loss, and hematochezia. Dextran sodium sulfate (DSS) upregulated the mRNA levels of IL-6, IL-1β, IL-17, IL-12, tumor necrosis factor-alpha, C-C chemokine receptor type 5, and Bax in splenic lymphocytes (SPLs) and colon tissues, while G3c/D665 treatment conversely inhibited the increase in mRNA levels of these genes. In addition, G3c/D665 treatment altered the proportion of CD4+ and CD8+ T cells and increased CD4+CD25+Foxp3+ regulatory T cells in SPLs, mesenteric lymph nodes (MLNs), and lamina propria lymphocytes (LPLs). Thus, the combination of G3c and D665 treatment showed efficacy against DSS-induced UC in mice by inducing a large amount of Tr1 cell generation via the musculoaponeurotic fibrosarcoma pathways *in vivo* and relieving inflammatory responses both systematically and locally.

Keywords: anti-GITR antibody, CD28 superagonist, dextran sulfate sodium, inflammatory bowel disease, type 1 regulatory T cells

Abbreviations: Ahr: Aryl hydrocarbon receptors; APCs: activated antigen-presenting cells; CTLs: cytotoxic T cells; CTLA-4: cytotoxic T lymphocyte antigen 4; DSS: dextran sodium sulfate; Ebi3: EBV-induced gene 3; Egr2: early growth response 2; Eomes: eomesodermin; FCM: flow cytometry; GITR: glucocorticoid-induced tumor necrosis factor receptor-related protein; IBD: inflammatory bowel disease; IL: Interleukin; Irf4: Interferon regulatory factor 4; LPLs: lamina propria lymphocytes; Maf: musculoaponeurotic fibrosarcoma; MLNs: mesenteric lymph nodes; PBS: phosphate-buffered saline; Prdm1: PR domain zinc finger protein 1; RT-PCR: real-time polymerase chain reaction; SPLs: splenic lymphocytes; Tbx21: T-box transcription factor 21; TCR: T-cell receptor; Teff: effector T cell; TGF-β: transforming growth factor beta; TLR: Toll-like receptor; Tregs: regulatory T cells; Tr1: Type 1 regulatory T; UC: ulcerative colitis.

Introduction

Ulcerative colitis (UC) is a type of inflammatory bowel disease (IBD) characterized by chronic and repeated episodes of enteropatia with symptoms of abdominal pain, severe diarrhea, rectal bleeding, tenesmus, and extraintestinal manifestation [1]. Although the etiology and pathogenesis of UC are complicated and remain uncertain, studies have demonstrated that UC is closely related to the imbalance in mucosal immunity and changes in the colonic barrier [2]. Previous studies showed that the oral administration of dextran sodium sulfate (DSS) in mice induced colitis with clinical symptoms

and histopathological features markedly similar to those of human UC [3]. Therefore, the DSS-induced mouse model has been widely used to assess the effects of therapeutic manipulation of UC. At present, there is no cure for UC, and the main treatments for this disorder remain glucocorticosteroids and immunosuppressive agents. More effective and viable therapies with fewer side effects are thus urgently needed [4].

In recent years, cellular therapies have been explored in various immune-mediated inflammatory diseases (IMIDs), including IBD [5, 6]. The immune system maintains peripheral tolerance and downregulates unwanted inflammatory

responses through specialized subpopulations of T cells, namely regulatory T cells (Tregs). The two best-characterized subsets of CD4^{+} Tregs are CD25^{+}Foxp3^{+}CD4^{+} T cells and IL-10-producing Foxp3^{-}CD4^{+} T cells, Type 1 regulatory T (Tr1) cells [7]. Foxp3^{+} Tregs are characterized by the constitutive expression of the transcription factor forkhead box protein 3 (Foxp3) and the expression of the IL-2 receptor a-chain (CD25) [8]. Tr1 cells represent a subset of CD4^{+}Foxp3^{-} T cells able to suppress colitogenic T cell responses mainly through the production of high amounts of the cytokine IL-10 with potent immunosuppressive properties [9]. IL-10 has been reported to play a crucial role in the maintenance of the intestinal microbe-immune homeostasis [10]. In addition to CD25^{+}Foxp3^{+} Tregs, Tr1 cells are potential candidates for cellular therapy in mucosal diseases [5]. Previous studies have reported that Tr1 cells can be generated from murine and human CD4^{+} T cells *in vitro* [11, 12], but no effective pharmacological approaches have been able to expand antigen-specific or disease-specific Tr1 cells *in vivo*. In the present study, we found that combinations of anti-GITR antibody (G3c) and CD28 superagonist (D665) treatment induced large amounts of IL-10/IFN-γ-co-producing CD4^{+}Foxp3^{-} Tr1 cells in mice. Furthermore, Tr1 cells contribute to the immunomodulatory effect of protecting against colitis via the high production of IL-10.

In the present study, we determined the protective role of the combinations of G3c and D665 treatment on DSS-induced UC in mice by evaluating the disease activity index (DAI), colon lengths, and pathological changes. To clarify the variation in the proportion and phenotype of immune cells after G3c/D665 treatment, we performed a flow cytometry (FCM) analysis with splenic lymphocytes (SPLs), mesenteric lymph nodes (MLNs), and colon lamina propria lymphocytes (LPLs). Furthermore, cytokine levels were detected by real-time polymerase chain reaction (RT-PCR). The key role of Tr1 cells in G3c/D665 treatment against UC was further elucidated.

Materials and methods

Animal model

Male C57BL/6JJmsSLc (B6/J; H-2k[b]) mice 8–10 weeks old, purchased from Shizuoka Laboratory Animal Center (Shizuoka, Japan), were maintained under specific-pathogen-free conditions in a feeding room with automatically controlled light and temperature according to the guidelines of the Institutional Animal Care and Use Committee. All animal procedures were authorized by the National Research Institute for Child Health and Development (permission no. A2009-010-C12).

Mice were randomized into three groups: a naïve group, a 3.5% DSS-control group and a 3.5% DSS + G3c/D665-treated group. Acute colitis of mice was induced with 3.5% DSS (molecular weight, 36 000–50 000; MP Biomedicals, Irvine, CA) for 5 days followed by *ad libitum* drinking water for 3 days. The DSS solutions were dissolved in sterile, distilled water, and prepared fresh every other day. Mice were given a single dose of D665, 1 mg/mice on day 0 and a single dose of G3c, 1 mg/mice on day 3 via intraperitoneal injection as a treated group. G3c and D665 antibodies were purified from the supernatant of hybridomas, gifts from J. Shimizu, Kyoto University, Japan and Dr T. Hunig, University of Wurzburg, respectively. Naïve mice received free water during the study period. Body weight and the DAI were evaluated daily during the colitis induction and recovery phases of the experiment [13]. After mice were sacrificed on day 8, the entire colon was removed from the caecum to the anus, and the colon length was measured as an indirect marker of inflammation.

The DAI

The body weight of mice in each group was recorded daily, as well as the stool consistency and the presence of occult or gross blood per rectum during the experimental period. These parameters were respectively scored by one trained observer blinded to the protocol, and the DAI was calculated as reported previously (Table 1) [14].

Histology and histological scoring

The entire colon was washed with phosphate-buffered saline (PBS), and the distal colon was fixed in 10% formaldehyde solution for 48 h and embedded in paraffin for histological analyses. Sections of the colon (4-mm thick) were prepared and subjected to staining with hematoxylin and eosin (H&E; Muto Pure Chemicals, Osaka, Japan) for morphological analyses. Slides were then examined by light microscopy (OLYMPUS, Tokyo, Japan) in a blinded fashion to assess the inflammation state and blindly scored using a previously published grading system (Table 2) [15].

Table 1: Disease activity index (DAI) scoring.

Score	Weight loss (%)	Stool consistency	Rectal bleeding
0	< 1	Normal	Negative hemoccult test
1	1-5		
2	5-10	Loose stools	Positive hemoccult test
3	10-20		
4	>20	Diarrhea	Gross bleeding

Table 2: Histological injury scoring.

Score	Severity of inflammation	Depth of injury	Crypt damage
0	None	None	None
1	Slight	Mucosal	Basal 1/3 damaged
2	Moderate	Mucosal and submucosal	Basal 2/3 damaged
3	Severe	Transmural	Only surface epithelium intact
4			Entire crypt and epithelium lost

Cell preparation and the flow cytometry analysis

Lymphocyte types among SPLs, MLNs, and LPLs were detected by the LSRFortessa system (BD Biosciences, Franklin Lakes, NJ). Cells were subjected to live/dead staining (Thermo Fisher Scientific, Cleveland, OH) for labeling dead cells and blocked with anti-CD16/CD32 Fc Block antibody to prevent non-specific antibody binding. The following antibodies were purchased from BioLegend (San Diego, CA) and used in the flow cytometry analysis: BV405 anti-mouse CD45 mAb, PE/CF594 anti-mouse CD3 mAb, AF700 anti-mouse CD4 mAb, APC/Cy7 anti-mouse CD4 mAb, AF700 anti-mouse CD8 mAb, and APC/Cy7 anti-mouse CD25 mAb. For intracellular staining, cells were fixed and permeabilized using the transcription factor staining buffer set (eBioscience, San Diego, CA), and then intracellular Foxp3 staining was performed using FITC anti-mouse Foxp3 mAb (eBioscience), PE/Cy7 anti-mouse IFN-γ mAb, APC anti-mouse CTLA-4 mAb, and PE anti-mouse IL-10 mAb purchased from BioLegend. For intracellular cytokine staining, cells were stimulated with 50 ng/ml phorbol 12-myristate 13-acetate (BD Golgi Plug™), 1 mM ionomycin (Sigma–Aldrich, St. Louis, MO), and Brefeldin A (eBioscience) in complete medium for 4 h, followed by surface and intracellular staining. The stained cells were analyzed with the FlowJo software program (Version 10.5.0; BD Biosciences).

Total mRNA preparation and quantitative RT-PCR (qRT-PCR)

Total mRNA was extracted from frozen SPLs, MLNs, and colon tissues using a RNeasy Mini Kit (Qiagen, Valencia, CA). Each 0.8-μg aliquot of mRNA was reverse-transcribed to cDNA using a Prime Script RT reagent Kit (RR037A; Takara, Shiga, Japan). qRT-PCR was performed by the SYBR® Green system using an Applied Biosystem PRISM7900 apparatus (Thermo Fisher Scientific). The PCR cycle conditions for the SYBR® Green system were 50 °C for 2 min, 95 °C for 2 min, 45 cycles of 95 °C for 15 s, and 60 °C for 60 s. The comparative cycle threshold (Ct) method was used to determine the relative gene expression, and the results of target genes (Table 3) were normalized by subtracting the Ct value of 18S rRNA, with the fold change calculated by comparative CT.

Western blot analyses

In brief, frozen SPLs in three groups were homogenized in RIPA buffer containing 1% protease inhibitor cocktail-1 and 1% protease inhibitor cocktail-2 (Sigma–Aldrich) followed by centrifugation in a microfuge at top speed for 30 min. Protein concentrations were assayed using Bio-Rad Protein Assay (Bio-Rad, Hercules, CA). Samples were separated by electrophoresis on 10% polyacrylamide gels and transferred to Immobilon-PVDF (Bio-Rad). After brief incubation with 5% non-fat milk to block non-specific binding, membranes were exposed overnight at 4 °C to specific musculoaponeurotic fibrosarcoma (Maf) (Cell Signaling Technology, Danvers, MA). Maf activity was quantified by a laser densitometric analysis of the radiographic film using the ImageJ software program (NIH, Bethesda, MD).

Statistical analyses

The GraphPad Prism 9 software program (GraphPad, San Diego, CA) was used to calculate statistical significance. A two-way analysis of variance (ANOVA) method and one-way ANOVA method were used to compare the three groups. Data are expressed as the mean ± SD. A value of $P < 0.05$ was considered to be statistically significant (*$P < 0.05$; **$P < 0.01$; ***$P < 0.001$; ****$P < 0.0001$).

Results

G3c/D665 treatment exhibited the potential to attenuate DSS-induced colitis in mice

We evaluated the potential therapeutic effect of G3c/D665 on a DSS-induced mouse colitis model that had been established by orally feeding 3.5% DSS for 5 consecutive days and water

Table 3: Primer sequences for real-time qPCR.

Gene	Forward Primer (5′~3′)	Reverse Primer (3′~5′)
Prdm1	CCCTCATCGGTGAAGTCTA	ACGTAGCGCATCCAGTTG
Eomes	GCGCATGTTTCCTTTCTTGAG	GGTCGGCCAGAACCACTTC
Egr2	GCCAAGGCCGTAGACAAAATC	CCACTCCGTTCATCTGGTCA
Tbx21	AGCAAGGACGGCGAATGTT	GGGTGGACATATAAGCGGTTC
Ahr	AGCCGGTGCAGAAAACAGTAA	AGGCGGTCTAACTCTGTGTTC
TGF-β	ATCCTGTCCAAACTAAGGCTCG	ACCTCTTTAGCATAGTAGTCCGC
Foxp3	CACCCAGGAAAGACAGCAACC	GCAAGAGCTCTTGTCCATTGA
Maf	GCAGAGACACGTCCTGGAGTCG	CGAGCTTGGCCCTGCAACTAGC
TNF-α	AAGCCTGTAGCCCACGTCGTA	GGCACCACTAGTTGGTTGTCTTTG
IL-1β	ACCTTCCAGGATGAGGACATGA	AACGTCACACACCAGCAGGTTA
Bax	GGCTGCTTGTCTGGATCCAA	ATGGTCACTGTCTGCCATGTG
CCR-5	GACATCCGTTCCCCCTACAAG	TCACGCTCTTCAGCTTTTTGCAG
IL-6	GGCGGATCGGATGTTGTGAT	GGACCCCAGACAATCGGTTG
IL-12	AGCACGGCAGCAGAATAAA	CTCCACCTGTGAGTTCTTCAAA
IL-17	CAGCAGCGATCATCCCTCAAAG	CAGGACCAGGATCTCTTGCTG
IL-10	GCTCTTACTGACTGGCATGAG	CGCAGCTCTAGGAGCATGTG
18S	ACATCGACCTCACCAAGAGG	TCCCATCCTTCACATCCTTC

for 3 days. As expected, mice in the 3.5% DSS-control group lost more body weight and exhibited shorter colon lengths and higher DAI scores than the naïve and G3c/D665-treated groups. The improvement of symptoms, such as colonic shortening, weight loss, and hematochezia, in mice treated with G3c/D665 was significant. The colon tissue sections in naïve mice showed no signs of inflammation, while those in the control group showed distortion of crypts, loss of goblet cells, inflammatory cell infiltration, and severe mucosal damage. In contrast, G3c/D665 treatment obviously improved the pathological changes (Fig. 1A). The colons from G3c/D665-treated DSS-colitis mice were relatively normal, exhibiting only slight evidence of inflammatory cell infiltration. These findings were also quantitatively evaluated by a histopathological analysis and scored using a previously published grading system (Fig. 1B). Taken together, these findings indicate that the combination of G3c/D665 treatment effectively attenuated DSS-induced colitis in mice.

G3c/D665 treatment substantially suppressed inflammatory and apoptotic responses in colitis mice

To understand the anti-inflammatory effect of the combinations of G3c/D665 treatment in DSS-induced colitis in mice, we measured the mRNA levels of pro-inflammatory and apoptotic cytokines and chemokines in colon tissues and spleen lymphocytes. The results show that the mRNA levels

of pro-inflammatory cytokines (such as TNF-α, IL-6, IL-1β, IL-17, and IL-12), pro-inflammatory chemokines (such as CCR-5) and apoptotic factors (such as Bax) were significantly increased in mice in the control group. However, the increase in these cytokines and chemokines was reduced by G3c/D665 treatment in colon tissues (Fig. 2A). In spleen lymphocytes, the mRNA levels of pro-inflammatory cytokines, such as TNF-α, IL-6, IL-1β, and IL-12, were significantly reduced in the G3c/D665-treated group as well (Fig. 2B). Our data indicated that G3c/D665 treatment conferred profound protection against DSS-induced colitis in association with reduced inflammatory and apoptotic responses, alleviated tissue damage, and the maintenance of intestinal integrity and functionality.

G3c/D665 treatment altered the proportion of CD4+ and CD8+ T cells in SPLs, MLNs, and LPLs.

To clarify the variation in the number and/or phenotype of immune cells after G3c/D665 treatment, we performed an FCM analysis with SPLs, MLNs, and LPLs. Previous studies have shown that CD8+ cytotoxic T cells play a vital role in inducing relapsing colitis [16]. As shown in Fig. 3, in the present study, the proportion of CD8+ cytotoxic T cells among SPLs ($P < 0.0001$) and MLNs ($P < 0.05$) was significantly downregulated by the combinations of G3c and D665 treatment compared to the control group, whereas there was no significant change in the LPLs. Furthermore, SPLs, MLNs,
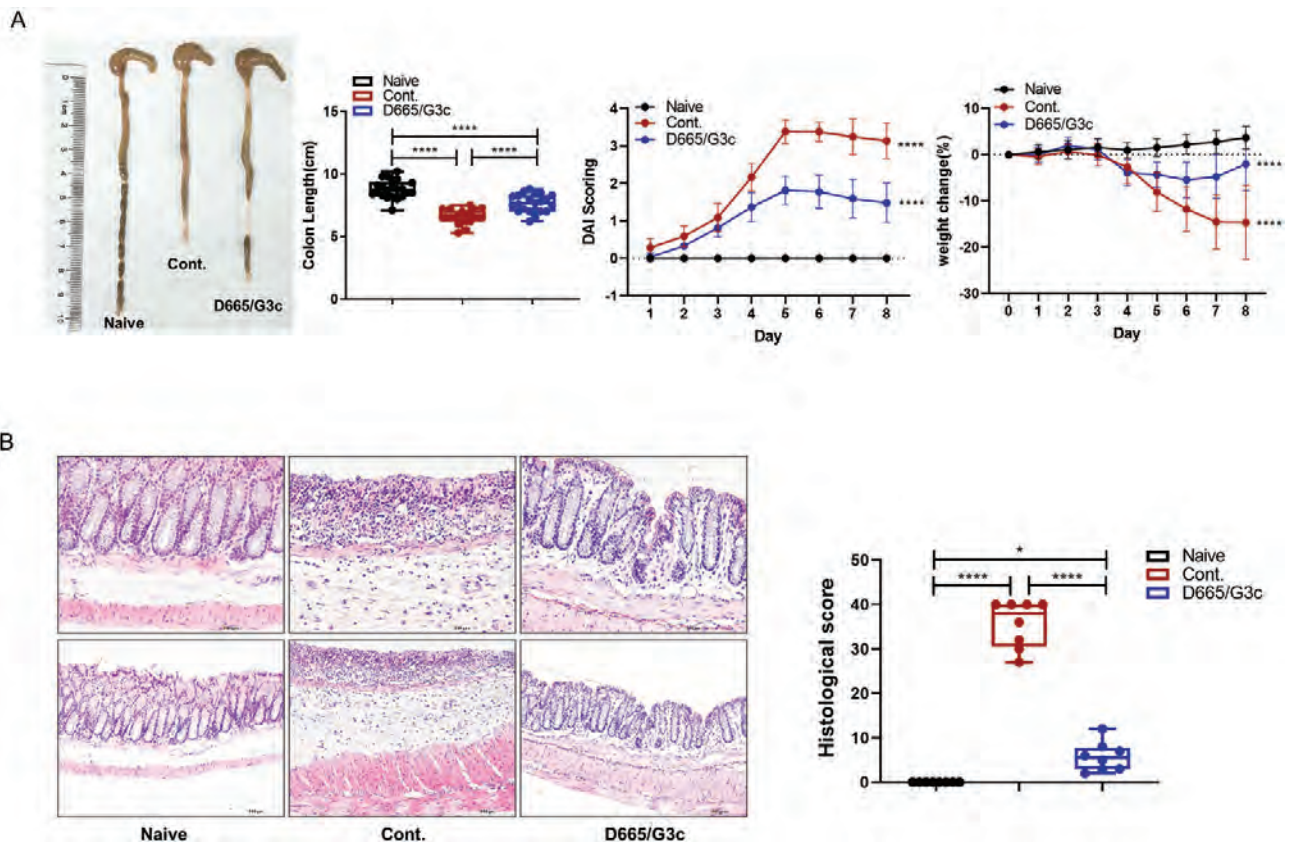
Figure 1: G3c/D665 treatment attenuated DSS-induced damage of colon. (A) The colon gross appearance and length analysis of mice are shown. The DAI of mice and the weight change (%) of mice are also presented. (B) Hematoxylin and eosin (HE) staining of colon specimens in the three groups. Substantial monocyte infiltration, mucosa erosion, goblet cell arrangement disorder, and reduction were seen in the colon specimens of the 3.5% DSS-control group. A Hematoxylin and eosin (HE) analysis of the colon specimens is shown (scale bars = 100 and 200 μm). Each bar represents the mean ± SD. *$P < 0.05$, ****$P < 0.0001$.
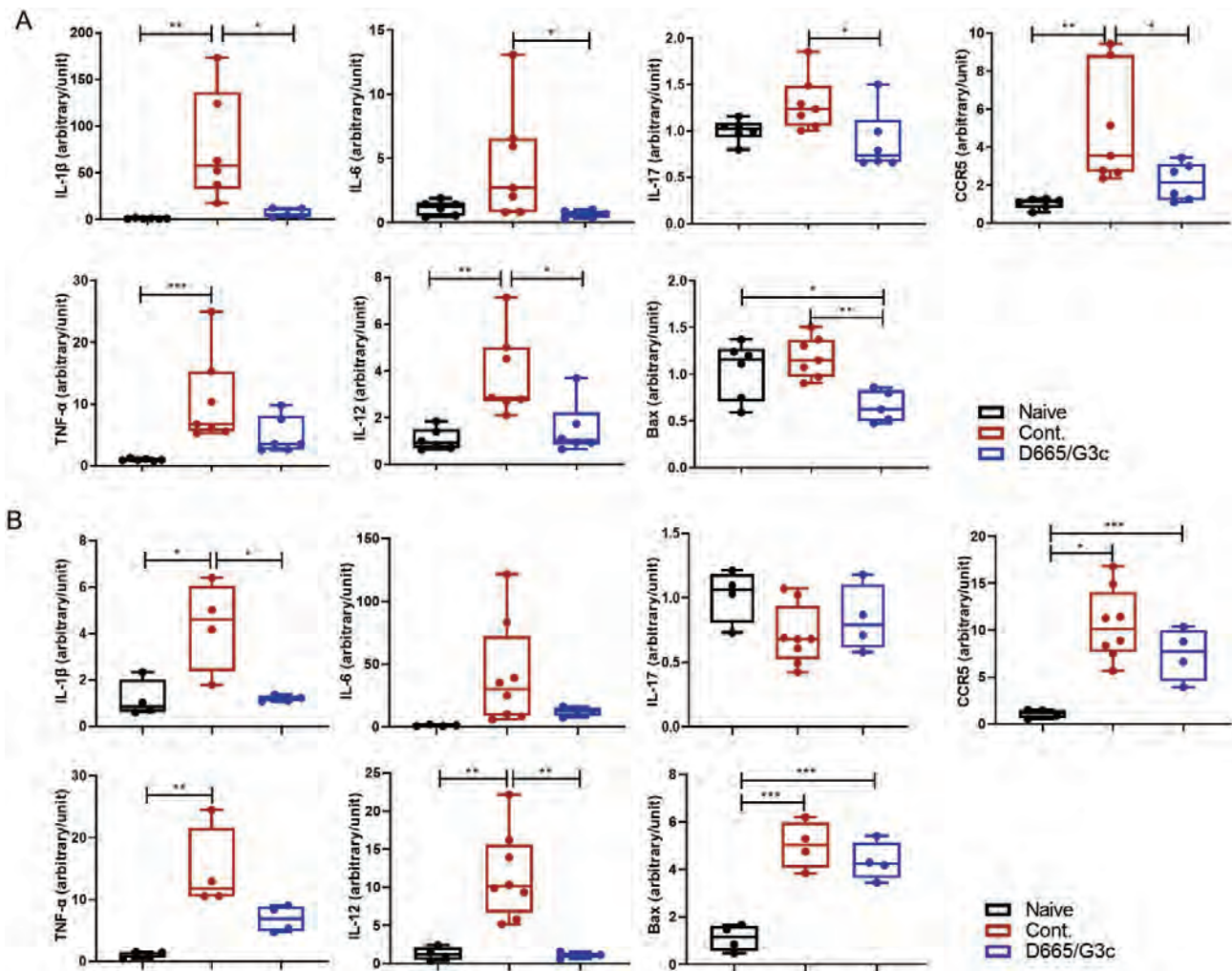
Figure 2: G3c/D665 treatment reduced the mRNA expression of inflammatory and apoptosis cytokine-related genes. (A) Homogenates of colon tissues were analyzed by qRT-PCR as described in the materials and methods. The mRNA expression of inflammatory cytokines-related genes, particularly IL-1β, IL-6, IL-12, IL-17, and CCR-5, was significantly lower in the G3c/D665-treated group than in the control group. The mRNA expression of apoptosis-related gene, such as Bax, was reduced in the G3c/D665-treated group. (B) SPLs were analyzed by qRT-PCR as well. Compared with the control group, the mRNA expression of inflammatory and apoptosis cytokine-related genes, such as IL-1β, IL-12, and Bcl-2, was reduced in the G3c/D665-treated group. Values are expressed as arbitrary units (mean ± SD). *$P < 0.05$, **$P < 0.01$, ***$P < 0.001$.

and LPLs in the G3c/D665 group showed an apparent increase in the proportion of CD4+ T cells compared with the control group.

G3c/D665 treatment led to CD4+CD25+Foxp3+ Treg expansion in DSS-induced colitis

Tregs are a unique subpopulation of CD4+ T cells that play pivotal roles in maintaining immune tolerance, improving the inflammatory intestinal environment, and conferring therapeutic benefits for colitis [17, 18], so we evaluated the population of CD4+CD25+Foxp3+ Tregs in SPLs, MLNs, and LPLs among the three groups.

Our analysis showed that the percentage of CD4+CD25+Foxp3+ Tregs in the G3c/D665-treated group was markedly higher than in the other two groups (Fig. 4A, B). Although the combination of G3c and D665 treatment generated a large number of CD4+CD25+Foxp3+ Tregs according to the FCM analysis, the mRNA expression of Foxp3 gene was not significantly increased in the G3c/D665 group (Supplementary Fig. S1). Both the T cell

protein cytotoxic T lymphocyte antigen 4 (CTLA-4) pathway and CD4+CD25+Foxp3+ Tregs are essential for maintaining control of immune homeostasis [19]. We further analyzed CTLA-4 and found that CD4+CD25+Foxp3+ Tregs significantly expressed CTLA-4 in the SPLs, MLNs, and LPLs of the three groups (Fig. 4C, D).

G3c/D665 treatment increased the proportion of Tr1 cells in DSS-induced mouse colitis

Tr1 cells are characterized by their high IL-10-producing capacity and the ability to inhibit T cell responses and colitis [11]. Therefore, we performed an FCM analysis to gain insight into the expression of IL-10+Foxp3- Tr1 cells and IL-10+IFN-γ+ Tr1 cells gated from CD4+ T cells. Our result showed that the combinations of G3c and D665 treatment generated large amounts of IL-10+Foxp3- Tr1 cells and IL-10+IFN-γ+ Tr1 cells in the three different lymphocyte types (Fig. 5). To identify the expression of Tr1-related transcription factors (TFs), we extracted TFs known to regulate Tr1 differentiation, including early growth response 2 (Egr2), Aryl hydrocarbon receptors
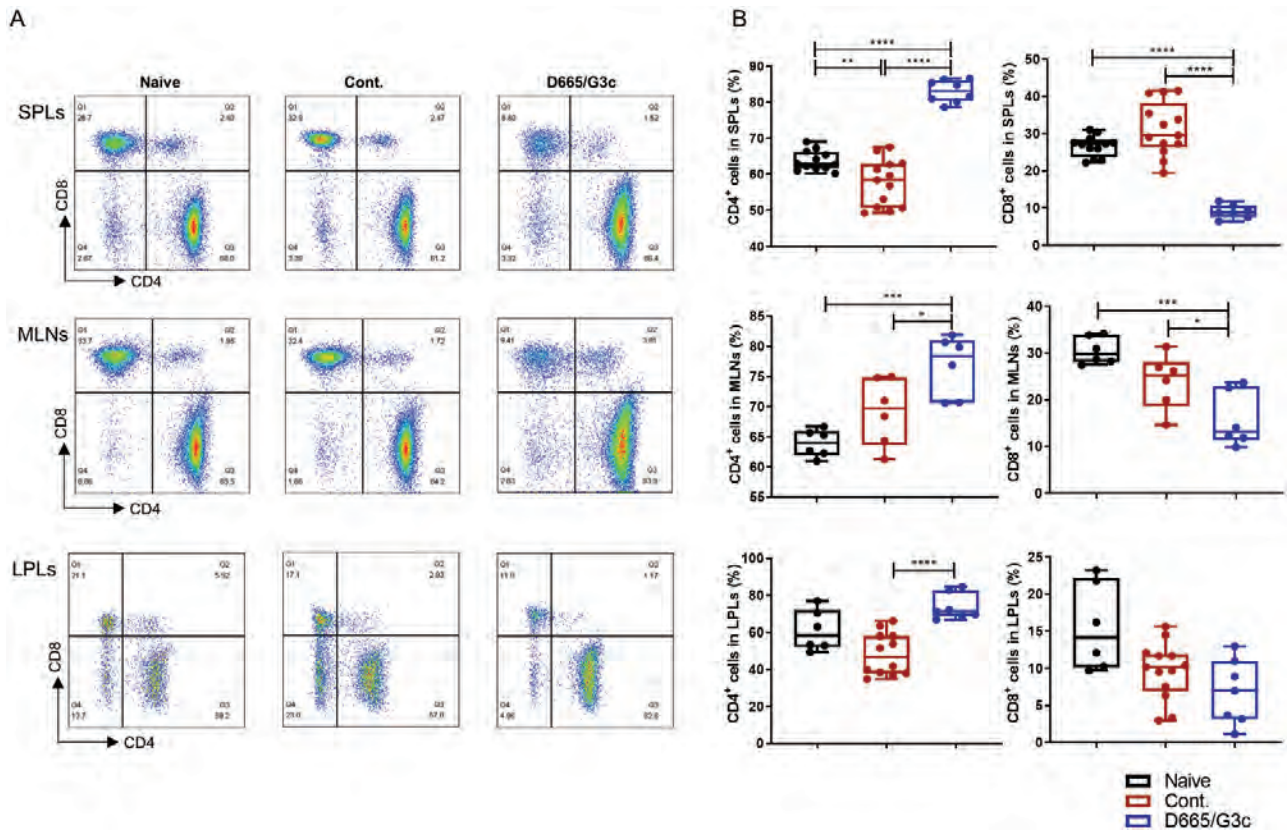
Figure 3: G3c/D665 treatment increased the proportion of CD4$^+$ T cells in SPLs, MLNs, and LPLs. (A) A representative FCM analysis assessing the expression of CD8$^+$ and CD4$^+$ T cells gated on CD3$^+$ T cells in SPLs, MLNs, and LPLs of three groups. (B) The proportion of CD4$^+$ T cells was significantly increased in the G3c/D665-treated group compared to the control group in SPLs, MLNs, and LPLs. The proportion of CD8$^+$ T cells was significantly reduced in the G3c/D665-treated group compared to the 3.5% DSS group in SPLs and MLNs. Data are expressed as the mean ± SD. *$P <$ 0.05, **$P <$ 0.01, ***$P <$ 0.001, ****$P <$ 0.0001.

(Ahr), T-box transcription factor 21 (Tbx21), Eomesodermin (Eomes), PR domain zinc finger protein 1 (Prdm1), transforming growth factor beta (TGF-β), and Maf (Fig. 6, Supplementary Fig. S1). Of these, the mRNA expression of the Prdm1 and Eomes genes was markedly upregulated in the MLNs of the G3c/D665-treated group but showed no significant difference in SPLs or LPLs. In contrast, the mRNA expression of the Ahr gene was shown to be downregulated in MLNs, SPLs, and LPLs of the G3c/D665-treated group, while the Tbx21, Egr2, and TGF-β mRNA expression did not increase as well Supplementary (Fig. S1). The mRNA expression of IL-10 was significantly increased in the SPLs of the G3c/D665-treated group but did not differ markedly among the three groups in MLNs or LPLs. Interestingly, the protein expression of Maf was increased in the SPLs of the G3c/D665-treated group (Fig. 6D) according to Western blotting, but its mRNA expression was not upregulated in any of the three lymphocyte species according to RT-PCR (Supplementary Fig. S1).

Discussion

UC has become a global public health threat, UC patients suffer from a poor quality of life, increased risk of colorectal cancer, and morbidity/mortality associated with colectomy performed for possible symptomatic relief [20]. Despite recent advances and the development of biological therapies, no drugs provide sustained remission of UC at present [21].

Due to substantial advances in our understanding of the biology of regulatory immune cells, novel cell-based therapies to dampen or prevent undesired immune responses in multiple immune diseases, including UC, have been developed. In previous studies on cell therapies for IBD, increased attention has been paid to the use of Foxp3$^+$ Tregs, but there have been few studies on Tr1 cells. Our study showed that Tr1 cells also have several functional properties that may make them particularly well-suited for treating UC or other inflammatory intestinal diseases.

D665 is a unique class of CD28-superagonist monoclonal antibody that has been reported to be capable of activating T cells without overt stimulation of the T-cell receptor (TCR) and selectively activating Tregs in rodents, suggesting an option for the treatment of autoimmune and inflammatory diseases [22]. Glucocorticoid-induced tumor necrosis factor receptor-related protein (GITR) is a transmembrane protein expressed on the surface of multiple types of immune cells and acts as a co-activating molecule that promotes the function of effector T cells and the expansion of Tregs, making it an attractive target for immunotherapy [23, 24]. The important role of GITR in immune system regulation has attracted a lot of attention for immunotherapeutic treatment of cancers and autoimmune diseases and resulted in the development of anti-GITR antibodies [25, 26]. G3c is an anti-GITR antibody that can recognize GITR and have strong co-stimulatory activity for both Tregs and responder T cells [27]. In our previous trials, we found that the use of D665 alone expanded Foxp3$^+$
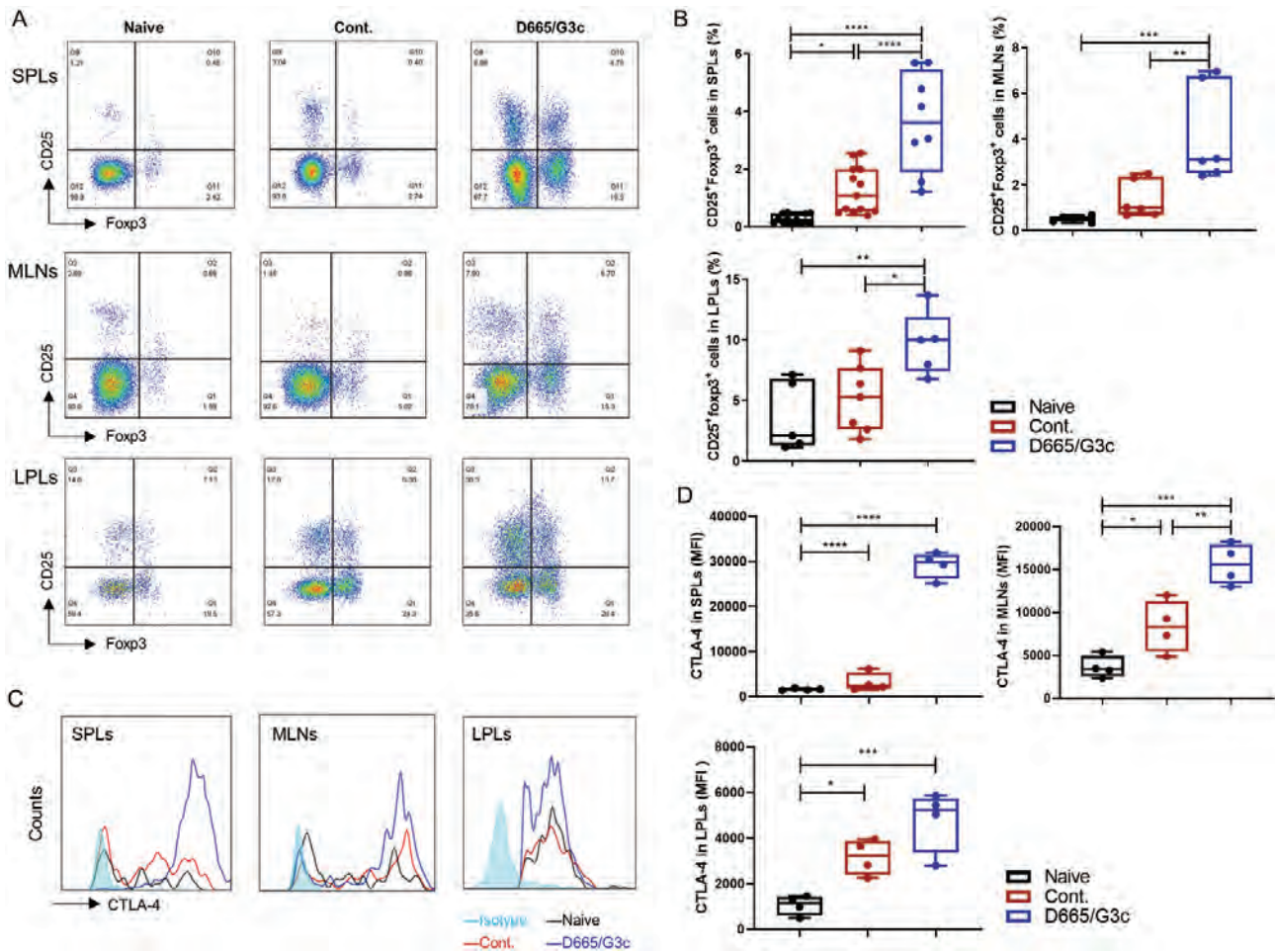
Figure 4: G3c/D665 treatment increased the proportion of CD4$^+$CD25$^+$Foxp3$^+$ Tregs in SPLs, MLNs, and LPLs. (A) A representative FCM analysis assessing the expression of CD4$^+$CD25$^+$Foxp3$^+$ Tregs gated on CD4$^+$ T cells in the SPLs, MLNs, and LPLs of the three groups. (B) The proportion of Tregs was significantly increased in the G3c/D665-treated group compared to the control group among SPLs, MLNs, and LPLs. (C–D). A representative FCM analysis assessing the MFI of CTLA-4 expression in the SPLs, MLNs, and LPLs of the three groups gated from CD4$^+$CD25$^+$Foxp3$^+$ Tregs. Data are expressed as the mean ± SD. *$P < 0.05$, **$P < 0.01$, ***$P < 0.001$, ****$P < 0.0001$.

Tregs, whereas the single-use of G3c could not generate Tregs. In our data, D665 potently expanded Tregs, and the GITR-targeting G3c application further enforced the expansion of Tregs. Large amounts of Tr1 cells were generated after D665 and G3c treatments. G3c played an important role in the induction of Tr1 cells based on D665 treatment. Interestingly, injecting G3c before D665 did not have this effect as well.

To understand the protective effects of G3c/D665 on DSS-induced colitis, mice that had received DSS were given a single dose of D665 1 mg/mice on day 0 and a single dose of G3c 1 mg/mice on day 3 by intraperitoneal injection. This G3c/D665 treatment markedly ameliorated the severity of DSS-induced colitis by inhibiting various pathological manifestations, such as colonic shortening, weight loss, intestinal bleeding, and diarrhea, resulting in a significant reduction in the DAI of the treatment group compared with the non-treated group (Fig. 1A). Furthermore, the degree of mucosal inflammation was markedly improved in mice given G3c/D665 treatment, with observations of decreased mucosal lesions, decreased inflammatory infiltration, and crypt damage microscopically (Fig. 1B).

A hallmark of UC is the dysregulated activation of inflammatory cytokines and components of signaling pathways [28]. Aberrant activation of the immune response and uncontrolled production of inflammatory cytokines has been proven to cause disruption of intestinal barriers, disturbance of intestinal homeostasis, and extensive mucosal injury and inflammation, leading to the development of UC. In response to the commensal microbiota and Toll-like receptor (TLR) signaling, activated antigen-presenting cells (APCs) in the inflamed mucosa of UC produce large amounts of pro-inflammatory cytokines, such as IL-1β, IL-6, IL-12, and TNF-α [28–30]. CCR-5 is a chemokine receptor predominantly expressed on the surface of Th1 polarized T cells and plays an important role in T cell-mediated tissue damage [31]. IL-17 was reported to mediate pro-inflammatory functions including the upregulation of TNF-α, IL-1β, and IL-6 and the recruitment of neutrophils to induce tissue destruction in IBD [28]. In our study, the mRNA levels of pro-inflammatory cytokines (such as TNF-α, IL-6, IL-1β, IL-17, and IL-12), pro-inflammatory chemokines (such as CCR-5), and apoptotic factors (such as Bax) were significantly upregulated in mice in the DSS-control group, as expected (Fig. 2). These indicators were downregulated after treatment, suggesting that G3c/D665 has a significant inhibitory effect on intestinal inflammation and cell necrosis.
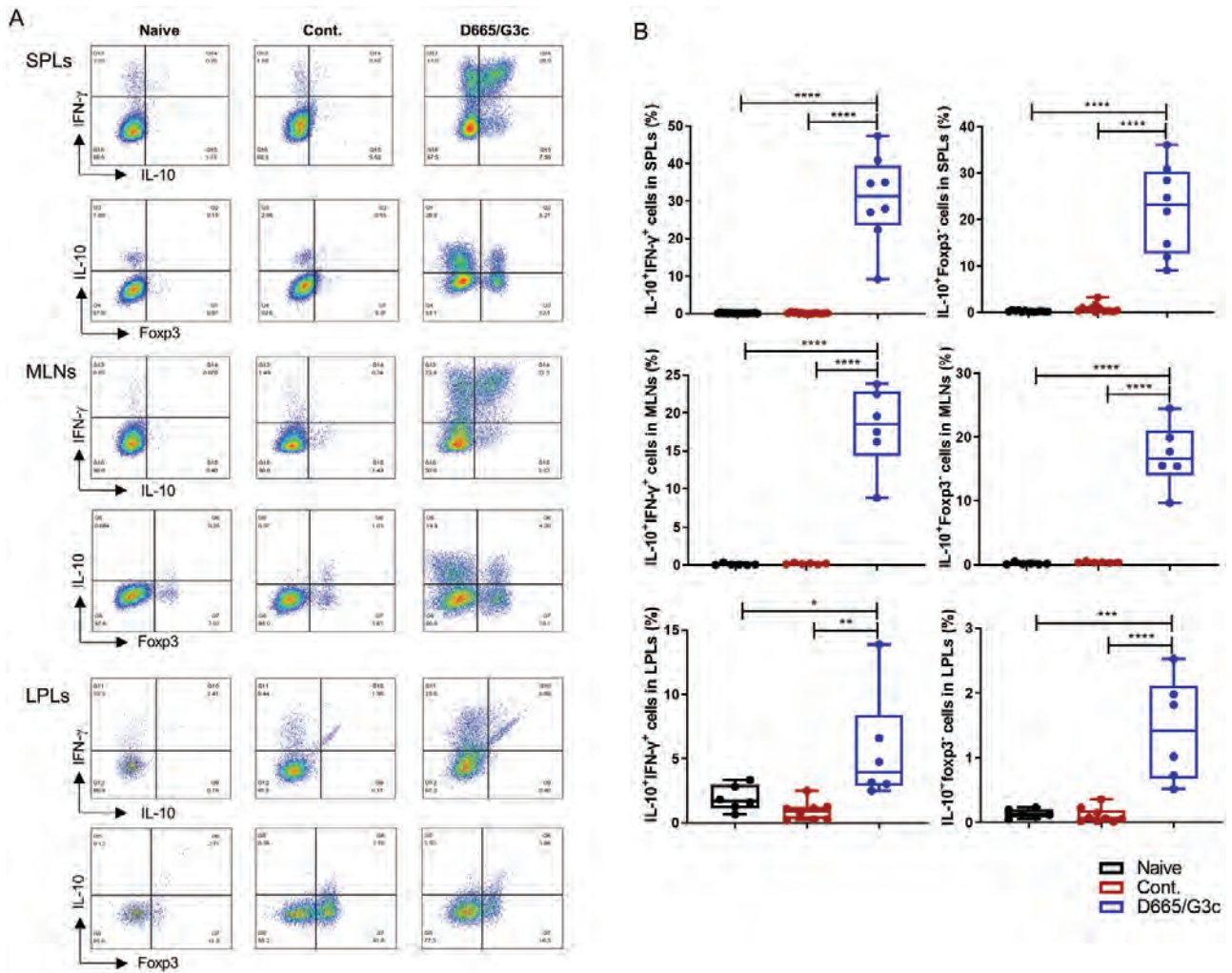
Figure 5: G3c/D665 treatment increased the proportion of IL-10+IFN-g+Tr1 cells and IL-10+Foxp3- Tr1 cells in SPLs, MLNs, and LPLs. (A) A representative FCM analysis assessing the proportion of IL-10+IFN-g+ Tr1 and IL-10+Foxp3- Tr1 cells gated on CD4+ T cells among the SPLs, MLNs, and LPLs of the three groups. (B) The proportion of IL-10+IFN-g+ Tr1 cells and IL-10+Foxp3- Tr1 cells was significantly increased in the G3c/D665-treated group compared to the control group among SPLs, MLNs, and LPLs. Data are expressed as the mean ± SD. *$P < 0.05$, **$P < 0.01$, ***$P < 0.001$, ****$P < 0.0001$.

Previous studies have reported that colitis was prevented by *in vivo* antibody depletion of CD8+ T cells but not by that of CD4+ T cells. CD8+ cytotoxic T cells (CTLs) induce relapsing colitis in normal mice, and the cytolytic function of CD8+ CTLs against epithelial cells may initiate the intestinal inflammatory process [16]. Our FCM data showed that CD8+ CTLs were significantly downregulated by G3c/D665 treatment in SPLs and MLNs, whereas there were no significant differences between these two groups in LPLs (Fig. 3). G3c/D665 treatment obviously altered the proportion of CD8+ CTLs and CD4+ T cells, and the proportion of CD4+ T cells in SPLs, MLNs, and LPLs of G3c/D665 group was significantly higher than that in the control group. These results suggest an important role of CD8+ CTLs as initiators of colitis and that G3c/D665 treatment can improve colitis by modulating CD4+ T cell and CD8+ CTL production by modulating systemic or local immunity.

Intestinal mucosal damage caused by UC is associated with mucosal T-cell dysfunction, the imbalance between pro-inflammatory and anti-inflammatory cytokines, and cellular inflammation [28, 32, 33]. CD4+CD25+Foxp3+ Tregs play a critical role in the maintenance of self-tolerance and control

of autoimmune diseases and offer a therapeutic option in cases of inflammatory colitis [17, 34, 35]. To clarify the protective activity of G3c/D665 treatment in DSS-colitis, the CD4+CD25+Foxp3+ Treg population was evaluated by FCM. In our study, the combination of G3c and D665 treatment led to the expansion of CD4+CD25+Foxp3+ Tregs in the spleen and MLNs and LPLs of DSS-induced colitis mice (Fig. 4A, B). Cytotoxic T lymphocyte antigen 4 (CTLA-4) (also called CD152) is a key regulator of adaptive immune responses and an inhibitory relative of the T cell co-stimulatory molecule CD28, which has an immunoregulatory function of suppressing the T cell response [36, 37]. Tregs and CTLA-4 have complementary and largely overlapping mechanisms of immune tolerance, and Tregs commonly use CTLA-4 to effect suppression [19]. Our results showed that CD4+CD25+Foxp3+ Tregs significantly expressed CTLA-4 in both SPLs and MLNs, with increased CTLA-4 levels in LPLs, but there was no statistical significance (Fig. 4C, D), indicating that the combination therapy of G3c and D665 partly played a role in the treatment of colitis through Foxp3+ Tregs and CTLA-4.

Tr1 cells regulate responses of both naïve and memory T cells and control inflammasome activity *in vivo* and *in*
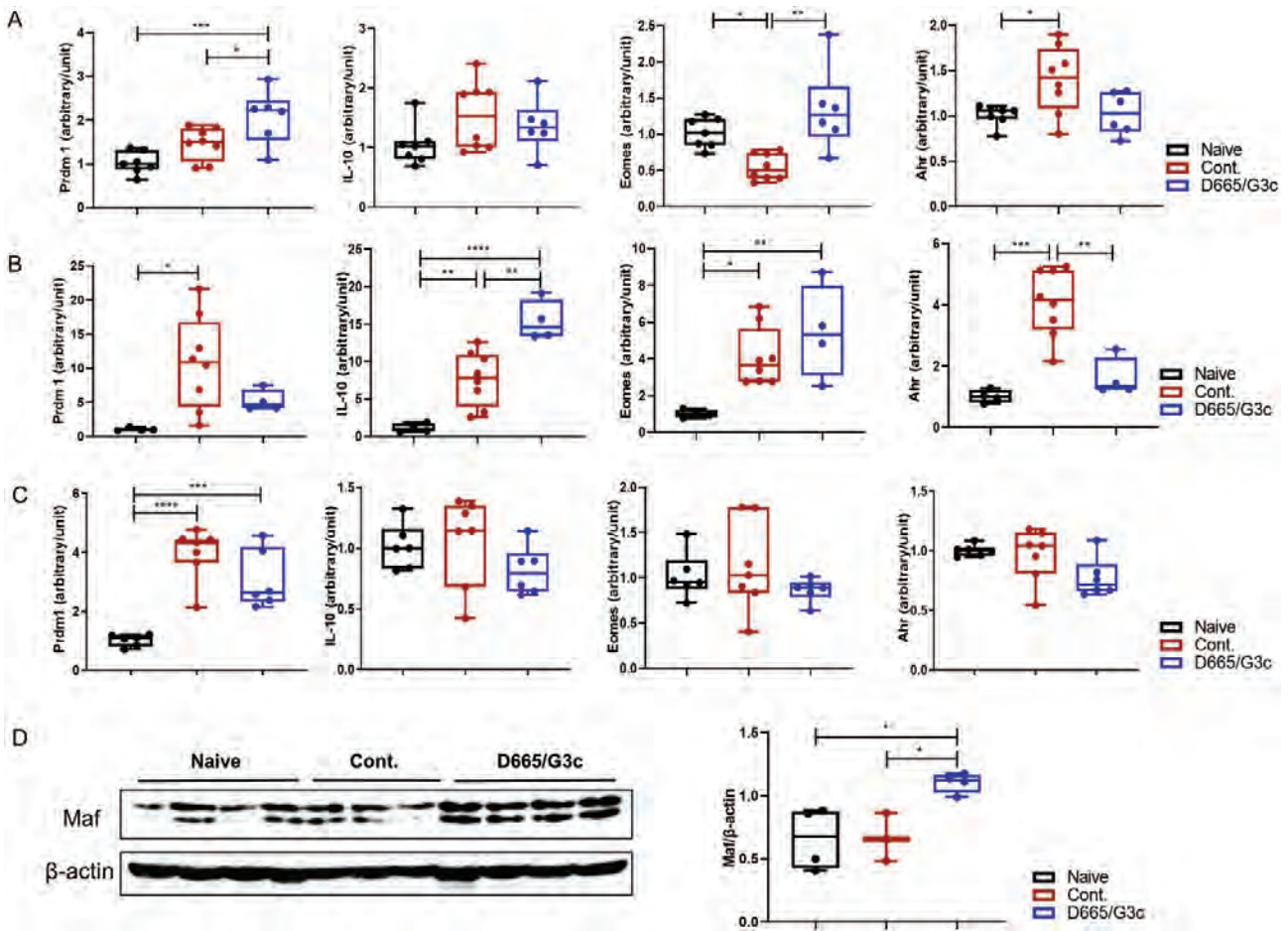
Figure 6: G3c/D665 treatment altered the mRNA expression and protein levels of Tr1 cell-related genes. MLNs (A), SPLs (B) and colon tissues (C) were analyzed by qRT-PCR as described in the materials and methods. The mRNA expression of Tr1 cell-related genes, particularly Prdm1, IL-10, Eomes, and Ahr is shown. (D). A Western blot analysis of the Maf of the SPLs in the three group is shown. Data are expressed as the mean ± SD. *$P < 0.05$, **$P < 0.01$, ***$P < 0.001$, ****$P < 0.0001$.

vitro, mainly through the secretion of the immunosuppressive cytokine IL-10 [12]. IL-10 is an anti-inflammatory and immune regulatory cytokine that plays a key role in maintaining immune homeostasis in the gut environment [11, 38]. Furthermore, Tr1 cells have been reported to have a unique ability to promote the development of intestinal goblet cells and repair the epithelial cell barrier function, supporting their use as a cell-based therapy for modulating intestinal inflammation [11]. Previous studies have reported that D665 was able to induce the expansion of CD4+Foxp3+ Tregs *in vivo*, but it has not been reported to induce Tr1 cells thus far [22, 34, 39]. The application of G3c following D665 in our study mediated the expansion of Tregs and the generation of a large number of Tr1 cells. Based on these findings, along with the evidence that aberrant Tregs function and dysregulated control of epithelial homeostasis induce spontaneous intestinal inflammation in gene-knockout mice deficient for IL-10 [40], we hypothesized that Tr1 cells might have unique advantages over CD4+Foxp3+ Tregs in controlling colitis. Our studies showed that the combination of G3c and D665 induced the generation of large amounts of IL-10/IFN-γ-co-producing CD4+Foxp3- Tr1 cells *in vivo*, and the proliferation of Tr1 cells was much greater than that of CD4+CD25+Foxp3+ Tregs (Fig. 4). Human Tr1-like

cells reportedly express the Eomes gene, a T-box transcription factor that controls the cytotoxic functions of CD8+ CTLs and NK cells [41]. Another important transcriptional regulator, Prdm1, has also been shown to promote IL-10 production by Tr1 cells [42]. We assessed the expression of these Tr1 cell-related TFs and found that the mRNA expression of the Prdm1 and Eomes genes was markedly upregulated in MLNs of the G3c/D665-treated group (Fig. 6). A previous study revealed that Maf acted as a growth factor for Tr1 cell development and was critical for IL-10 secretion since IL-27-induced Tr1 cell differentiation was defective in Maf−/− mice [43, 44]. The protein expression of Maf was significantly increased in the SPLs of the G3c/ D665-treated group, suggesting that G3c/D665 treatment may promote the generation of Tr1 cells through the Maf pathway.

In a clinical trial in 2006, CD28 superagonist (TGN1412) was reported to result in the instantaneous arrest and uncontrolled T cell activation with cytokine storm [45], but it was later clear that dose-reduction could preferentially address Tregs in humans [46]. The further development of CD28 superagonist (TAB08) has been resumed and is now being evaluated in a phase II study. A previous study has reported that using D665 alone on DSS-induced colitis weakly induced
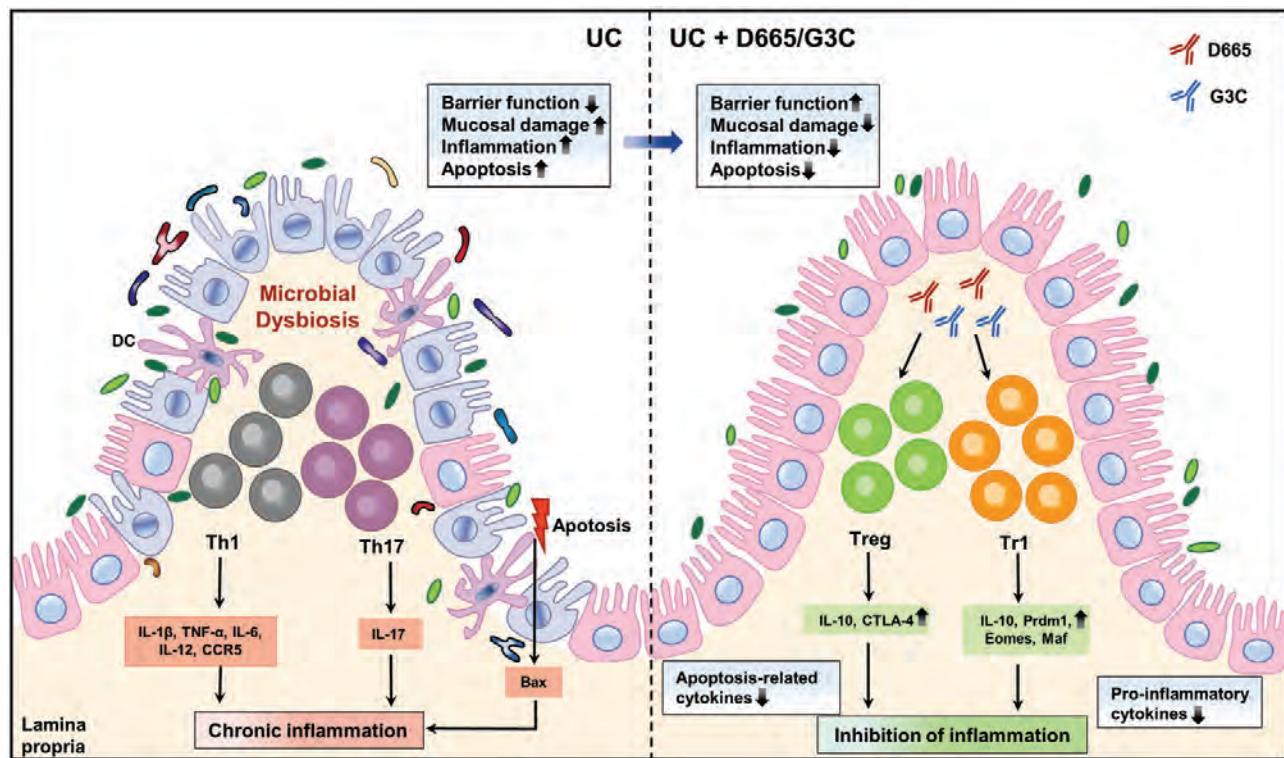
Figure 7: Immune mechanism of G3c/D665 in the treatment of UC. In UC, the intestinal barrier is disrupted, the mucosa is severely damaged, and the balance of intestinal microflora is dysregulated. In the colonic lamina propria, Th1 cells release many pro-inflammatory cytokines, such as IL-1β, TNF-α, IL-6, IL-12, and CCR-5, while Th17 cells release IL-17. The release of apoptotic factor, such as Bax, is also increased in UC. G3c and D665 treatment expands Tregs and Tr1 cells, thereby increasing the release of anti-inflammatory cytokines and decreasing the release of pro-inflammatory cytokines and apoptotic factors. Tregs release IL-10 and CTLA-4, while Tr1 cells release IL-10, Prdm1, Eomes, and Maf. After the administration of G3c and D665, the intestinal barrier is restored, mucosal damage is repaired, and colitis is improved.

the levels of IL-2 and IFN-γ in the spleen and colon but did not result in pathophysiologically relevant levels of cytokine storm [34]. we have not observed any signs of the disorders in the G3c/D665 treated mice with DSS-induced colitis.

Taken together, our data demonstrated that the combination of G3c and D665 treatment targets Tr1 cell generation *in vivo* to reduce the colon damage in DSS-induced mouse colitis by secreting a large amount of IL-10, maintaining and enhancing their regulatory functions (Fig. 7). This represents a major advance towards the therapeutic use of Tr1 cells as cellular therapy and supports the potential of the combination of G3c and D665 as a new auspicious therapeutic option for treating UC in the clinic. Furthermore, harnessing the suppressive potential of Tr1 cells may have important implications for cell therapy of autoimmune, autoinflammatory, and transplantation-related diseases.

Supplementary data

Supplementary data is available at *Clinical and Experimental Immunology* online.

Acknowledgements

Conflicts of interest

All authors of this manuscript have no conflicts of interest to disclose as described by Clinical and Experimental Immunology.

Author contributions

KM, WTQ, XH, WZG, LZ, DU, ELG, and XKL conceived and designed the project; KM acquired the data; KM, WTQ, XH, WZG, LZ, DU, ELG, and XKL analyzed and interpreted the data; KM and XKL wrote the paper. All authors read and approved the final manuscript.

Clinical trial registration

Not applicable.

Ethical approval

Mice were cared for in accordance with the National Research Institute for Child Health and Development guidelines on laboratory animal welfare (permission no. A2009-010-C12). The animal research adheres to the ARRIVE guidelines.

Data availability

Data are available upon reasonable request.

References

1. Ordas I, Eckmann L, Talamini M, et al. Ulcerative colitis. *Lancet* 2012, 380, 1606–19.

2. Geremia A, Biancheri P, Allan P, et al. Innate and adaptive immunity in inflammatory bowel disease. *Autoimmun Rev* 2014, 13, 3–10.

3. Chassaing B, Aitken JD, Malleshappa M, et al. Dextran sulfate sodium (DSS)-induced colitis in mice. *Curr Protoc Immunol* 2014, 104, 15–25.

4. Cao H, Liu J, Shen P, et al. Protective effect of naringin on DSS-induced ulcerative colitis in mice. *J Agric Food Chem* 2018, 66, 13133–40.

5. Cassinotti A, Passamonti F, Segato S. Cell therapy in inflammatory bowel disease. *Pharmacol Res* 2021, 163, 105247.

6. Negi S, Saini S, Tandel N, et al. Translating treg therapy for inflammatory bowel disease in humanized mice. *Cells-Basel* 2021, 10, 1847.

7. Roncarolo MG, Gregori S, Bacchetta R, et al. The biology of T regulatory type 1 cells and their therapeutic application in immune-mediated diseases. *Immunity* 2018, 49, 1004–19.

8. Rudensky AY. Regulatory T cells and Foxp3. *Immunol Rev* 2011, 241, 260–8.

9. Andolfi G, Fousteri G, Rossetti M, et al. Enforced IL-10 expression confers type 1 regulatory T cell (Tr1) phenotype and function to human CD4(+) T cells. *Mol Ther* 2012, 20, 1778–90.

10. Neumann C, Scheffold A, Rutz S. Functions and regulation of T cell-derived interleukin-10. *Semin Immunol* 2019, 44, 101344.

11. Cook L, Stahl M, Han X, et al. Suppressive and gut-reparative functions of human type 1 T regulatory cells. *Gastroenterology* 2019, 157, 1584–98.

12. Battaglia M, Gregori S, Bacchetta R, et al. Tr1 cells: from discovery to their clinical application. *Semin Immunol* 2006, 18, 120–7.

13. Hidalgo-Cantabrana C, Algieri F, Rodriguez-Nogales A, et al. Effect of a ropy exopolysaccharide-producing Bifidobacterium animalis subsp. lactis strain orally administered on DSS-induced colitis mice model. *Front Microbiol* 2016, 7, 868.

14. Cooper HS, Murthy SN, Shah RS, et al. Clinicopathologic study of dextran sulfate sodium experimental murine colitis. *Lab Invest* 1993, 69, 238–49.

15. Dieleman LA, Palmen MJ, Akol H, et al. Chronic experimental colitis induced by dextran sulphate sodium (DSS) is characterized by Th1 and Th2 cytokines. *Clin Exp Immunol* 1998, 114, 385–91.

16. Nancey S, Holvoet S, Graber I, et al. CD8+ cytotoxic T cells induce relapsing colitis in normal mice. *Gastroenterology* 2006, 131, 485–96.

17. Fan L, Qi Y, Qu S, et al. *B*. adolescentis ameliorates chronic colitis by regulating Treg/Th2 response and gut microbiota remodeling. *Gut Microbes* 2021, 13, 1–17.

18. Clough JN, Omer OS, Tasker S, et al. Regulatory T-cell therapy in Crohn's disease: challenges and advances. *Gut* 2020, 69, 942–52.

19. Walker LS. Treg and CTLA-4: two intertwining pathways to immune tolerance. *J Autoimmun* 2013, 45, 49–57.

20. Miao Z, Chen L, Feng H, et al. Baitouweng decoction ameliorates ulcerative colitis in mice partially attributed to regulating Th17/Treg balance and restoring intestinal epithelial barrier. *Front Pharmacol* 2020, 11, 531117.

21. Nunes NS, Chandran P, Sundby M, et al. Therapeutic ultrasound attenuates DSS-induced colitis through the cholinergic anti-inflammatory pathway. *EBioMedicine* 2019, 45, 495–510.

22. Langenhorst D, Tabares P, Gulde T, et al. Self-recognition sensitizes mouse and human regulatory T cells to low-dose CD28 superagonist stimulation. *Front Immunol* 2017, 8, 1985.

23. Riccardi C, Ronchetti S, Nocentini G. Glucocorticoid-induced TNFR-related gene (GITR) as a therapeutic target for immunotherapy. *Expert Opin Ther Targets* 2018, 22, 783–97.

24. Zappasodi R, Sirard C, Li Y, et al. Rational design of anti-GITR-based combination immunotherapy. *Nat Med* 2019, 25, 759–66.

25. He C, Maniyar RR, Avraham Y, et al. . Therapeutic antibody activation of the glucocorticoid-induced TNF receptor by a clustering mechanism. *Sci Adv* 2022, 8, m4552.

26. Petrillo MG, Ronchetti S, Ricci E, et al. . GITR+ regulatory T cells in the treatment of autoimmune diseases. *Autoimmun Rev* 2015, 14, 117–26.

27. Nishioka T, Nishida E, Iida R, et al. In vivo expansion of CD4+Foxp3+ regulatory T cells mediated by GITR molecules. *Immunol Lett* 2008, 121, 97–104.

28. Neurath MF. Cytokines in inflammatory bowel disease. *Nat Rev Immunol* 2014, 14, 329–42.

29. Ng SC, Benjamin JL, McCarthy NE, et al. Relationship between human intestinal dendritic cells, gut microbiota, and disease activity in Crohn's disease. *Inflamm Bowel Dis* 2011, 17, 2027–37.

30. Moschen AR, Tilg H, Raine T. IL-12, IL-23 and IL-17 in IBD: immunobiology and therapeutic targeting. *Nat Rev Gastroenterol Hepatol* 2019, 16, 185–96.

31. Turner JE, Steinmetz OM, Stahl RA, et al. Targeting of Th1-associated chemokine receptors CXCR3 and CCR5 as therapeutic strategy for inflammatory diseases. *Mini Rev Med Chem* 2007, 7, 1089–96.

32. Maynard CL, Weaver CT. Intestinal effector T cells in health and disease. *Immunity* 2009, 31, 389–400.

33. Larabi A, Barnich N, Nguyen H. New insights into the interplay between autophagy, gut microbiota and inflammatory responses in IBD. *Autophagy* 2020, 16, 38–51.

34. Chen J, Xie L, Toyama S, et al. The effects of Foxp3-expressing regulatory T cells expanded with CD28 superagonist antibody in DSS-induced mice colitis. *Int Immunopharmacol* 2011, 11, 610–7.

35. Xu M, Duan XY, Chen QY, et al. Effect of compound sophorae decoction on dextran sodium sulfate (DSS)-induced colitis in mice by regulating Th17/Treg cell balance. *Biomed Pharmacother* 2019, 109, 2396–408.

36. Rowshanravan B, Halliday N, Sansom DM. CTLA-4: a moving target in immunotherapy. *Blood* 2018, 131, 58–67.

37. Hansel TT, Kropshofer H, Singer T, et al. The safety and side effects of monoclonal antibodies. *Nat Rev Drug Discov* 2010, 9, 325–38.

38. Schmitt H, Ulmschneider J, Billmeier U, et al. The TLR9 agonist cobitolimod induces IL10-producing wound healing macrophages and regulatory T cells in ulcerative colitis. *J Crohns Colitis* 2020, 14, 508–24.

39. Schmidt T, Willenborg S, Hunig T, et al. Induction of T regulatory cells by the superagonistic anti-CD28 antibody D665 leads to decreased pathogenic IgG autoantibodies against desmoglein 3 in a HLA-transgenic mouse model of pemphigus vulgaris. *Exp Dermatol* 2016, 25, 293–8.

40. Matharu KS, Mizoguchi E, Cotoner CA, et al. Toll-like receptor 4-mediated regulation of spontaneous Helicobacter-dependent colitis in IL-10-deficient mice. *Gastroenterology* 2009, 137, 1380–90.e1.

41. Gruarin P, Maglie S, De Simone M, et al. Eomesodermin controls a unique differentiation program in human IL-10 and IFN-gamma coproducing regulatory T cells. *Eur J Immunol* 2019, 49, 96–111.

42. Montes DOM, Kumar R, de Labastida RF, et al. Blimp-1-dependent IL-10 production by Tr1 cells regulates TNF-mediated tissue pathology. *PLoS Pathog* 2016, 12, e1005398.

43. Pot C, Jin H, Awasthi A, et al. Cutting edge: IL-27 induces the transcription factor c-Maf, cytokine IL-21, and the costimulatory receptor ICOS that coordinately act together to promote differentiation of IL-10-producing Tr1 cells. *J Immunol* 2009, 183, 797–801.

44. Pot C, Apetoh L, Kuchroo VK. Type 1 regulatory T cells (Tr1) in autoimmunity. *Semin Immunol* 2011, 23, 202–8.

45. Sundqvist KG. CD28 Superagonist shock and blockage of motogenic T cell cascade. *Front Immunol* 2021, 12, 670864.

46. Hunig T. The rise and fall of the CD28 superagonist TGN1412 and its return as TAB08: a personal account. *FEBS J* 2016, 283, 3325–34.

Combinations of anti-GITR antibody and CD28 superagonist induce permanent allograft acceptance by generating type 1 regulatory T cells

Weitao Que[1,2,3], Kuai Ma[2], Xin Hu[1,2], Wen-Zhi Guo[1], Xiao-Kang Li[1,2]*

Type 1 regulatory T (Tr1) cells represent a subset of IL-10–producing CD4+Foxp3− T cells and play key roles in promoting transplant tolerance. However, no effective pharmacological approaches have been able to induce Tr1 cells in vivo. We herein report the combined use of a CD28 superagonist (D665) and anti–glucocorticoid-induced tumor necrosis factor receptor–related protein monoclonal antibody (G3c) to induce Tr1 cells in vivo. Large amounts of IL-10/interferon-γ–co-producing CD4+Foxp3− Tr1 cells were generated by D665-G3c sequential treatment in mice. Mechanistic studies suggested that D665-G3c induced Tr1 cells via transcription factors *Prdm1* and *Maf*. G3c contributed to Tr1 cell generation via the activation of mitogen-activated protein kinase–signal transducer and activator of transcription 3 signaling. Tr1 cells suppressed dendritic cell maturation and T cell responses and mediated permanent allograft acceptance in fully major histocompatibility complex–mismatched mice in an IL-10–dependent manner. In vivo Tr1 cell induction is a promising strategy for achieving transplant tolerance.

INTRODUCTION

Organ transplantation is considered the optimal treatment for a variety of end-stage organ diseases. However, the life-long, systemic immune suppression required after transplantation severely compromises host immune defense and is associated with adverse effects, including organ toxicity, infections, and malignancies. Operational tolerance has long been the ultimate goal in the field of transplantation, which would enable transplant recipients to maintain a stable and acceptable graft function without the need for immunosuppression therapy, thus avoiding undesirable side effects (*1*).

Allograft immunity is a complex process that results from the interplay of multiple different cell types, including lymphocytes, monocytes, macrophages, and dendritic cells (DCs). Recipient alloreactive T cells recognize non–self-donor alloantigens presented by donor or recipient antigen-presenting cells and initiate the adaptive inflammatory immune response, leading to allograft rejection. Regulatory immune cells regulate or suppress immune responses of other cells and help prevent anti-donor immune responses. Regulatory immune cell–based therapies, via inducing or adoptively transferring regulatory immune cells, are emerging as promising strategies for achieving permanent donor-specific immune tolerance, thus minimizing or even obviating immunosuppressants after organ transplantation.

CD4+ T cells coordinate immune responses by helping to activate and regulate other immune cells and are critical in determining transplantation rejection or tolerance. Type 1 regulatory T (Tr1) cells represent a subset of CD4+Foxp3− T cells and secrete high amounts of interleukin-10 (IL-10), their signature cytokine, with potent immunosuppressive properties. The potent immunosuppressive function of Tr1 cells has been implicated both in vitro and in vivo

(*2*). Tr1 cells have been proven to play key regulatory roles in peripheral immune tolerance and are considered an emerging therapeutic target for improving transplant tolerance (*3*). However, as with Foxp3+ regulatory T (Treg) cells, in vivo effective pharmacological approaches to induce Tr1 cells are largely lacking.

CD28 superagonist is a monoclonal antibody (mAb) that engages CD28 costimulatory receptors, which laterally bind to the CD28 homodimer, thus allowing its clustering via lattice formation (*4*, *5*). The particular binding topology of CD28 superagonist confers its superagonist properties, resulting in potent T cell activation and expansion independent of concomitant T cell receptor (TCR) engagement (*6*). CD28 superagonist was shown to expand Treg cells preferentially over effector T (Teff) cells both in vitro and in vivo, a characteristic that was used to prevent autoimmune disease, graft-versus-host disease (GvHD), and allograft rejection (*6*–*8*). Glucocorticoid-induced tumor necrosis factor receptor–related protein (GITR), also referred to as TNFRSF18, is a type I transmembrane protein of the tumor necrosis factor receptor (TNFR) superfamily, characterized by three cysteine-rich domain pseudorepeats in its extracellular domain (*9*). GITR is constitutively expressed at high levels on Treg cells and at low levels on naïve and memory T cells (*9*–*11*). Its expression is rapidly up-regulated upon TCR activation on both Treg and Teff cells (*11*, *12*). GITR serves as a costimulatory molecule that exerts multiple distinct effects on T cells. GITR engagement results in the proliferation and cytokine production of activated T cells but abrogates the suppressive activity of Treg cells (*10*, *11*, *13*, *14*). Targeting GITR has been evaluated for its utility in the treatment of cancers, autoimmune diseases, and organ rejection in both animal models and clinical trials (*15*–*19*). However, the effects of GITR agonism on T cells, which is cell specific and context dependent, remain controversial (*20*, *21*).

We herein report the combined use of CD28 superagonist D665 and anti-GITR mAb G3c to induce Tr1 cells in vivo. Large amounts of IL-10/interferon-γ (IFN-γ)–co-producing CD4+Foxp3− Tr1 cells were generated by D665-G3c sequential treatment in mice. Tr1 cells suppressed DC maturation and T cell responses in an IL-10–dependent

[1]Department of Hepatobiliary and Pancreatic Surgery, The First Affiliated Hospital of Zhengzhou University, Zhengzhou, China. [2]Division of Transplantation Immunology, National Research Institute for Child Health and Development, Tokyo, Japan. [3]Department of General Surgery, Shanghai General Hospital, Shanghai Jiao Tong University School of Medicine, Shanghai, China.
*Corresponding author. Email: ri-k@ncchd.go.jp

manner. Further mechanical studies suggested that D665-G3c induced Tr1 cells via the positive regulatory domain zinc finger protein 1 (*Prdm1*), and musculoaponeurotic fibrosarcoma (*Maf*) pathways. G3c contributed to Tr1 cell generation via the activation of mitogen-activated protein kinase–signal transducer and activator of transcription 3 (MAPK-STAT3) signaling. The combined use of D665 and G3c induced permanent allograft acceptance in a Tr1-dependent manner. Our study presented an effective pharmacological approach to generate Tr1 cells in vivo by D665-G3c sequential treatment and demonstrated their therapeutic potential in transplantation.

RESULTS

Induction of Tr1 cells in vivo

Foxp3-GFP mice [expressing green fluorescent protein (GFP) under the control of the mouse Foxp3 promoter] and IL-10–Venus mice [expressing yellow fluorescent protein (Venus) under the control of the mouse IL-10 promoter] were treated with D665 (250 μg per mouse) and G3c (250 μg per mouse) on days −3 and 0 sequentially (Fig. 1A). On day 0, before G3c administration, D665 induced a robust expansion of T_{reg} cells over Teff cells (Fig. 1B), consistent with previous reports (*22–25*). The GITR expression was significantly up-regulated on the surface of both T_{reg} and Teff cells (Fig. 1, C and D).
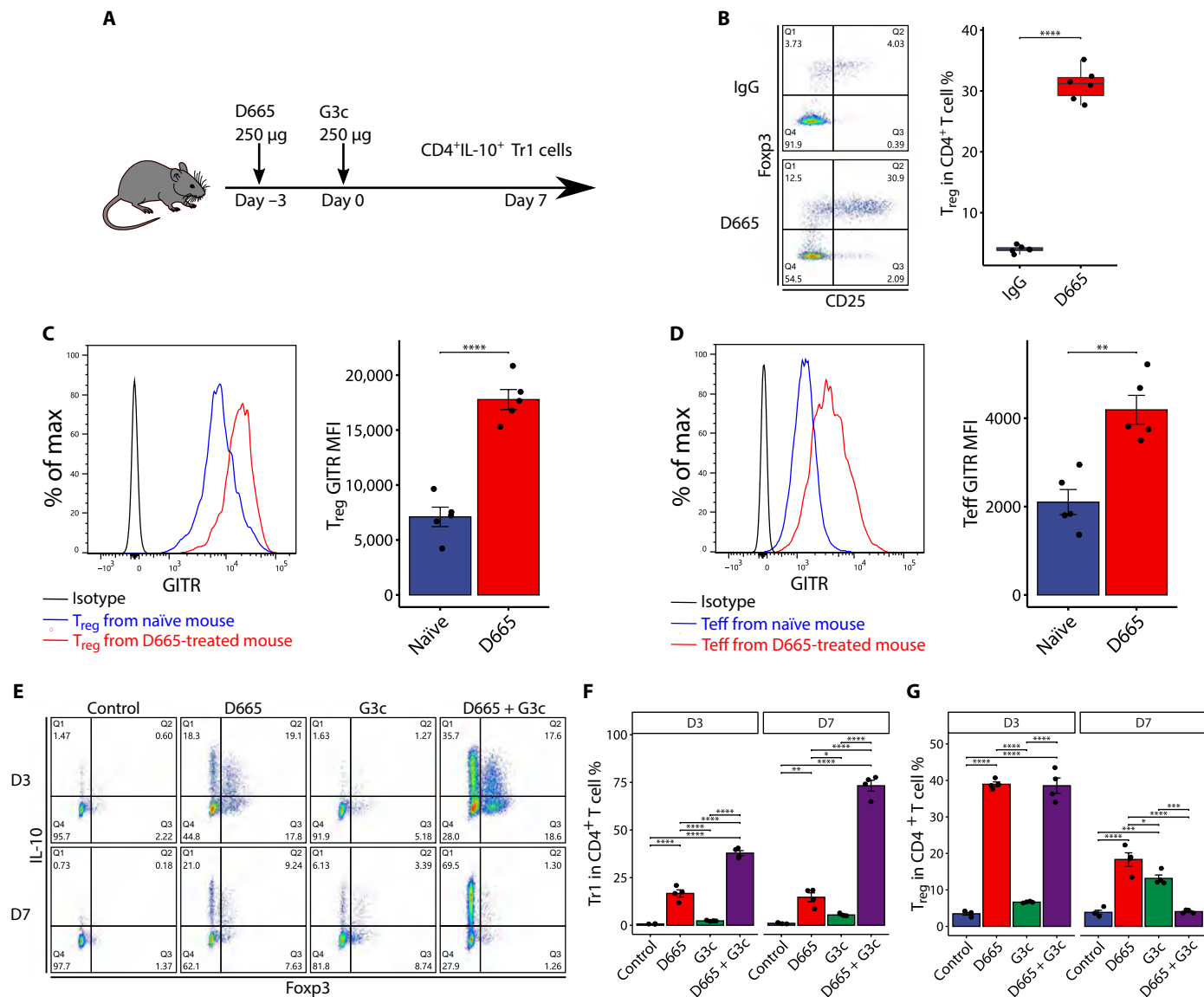
Fig. 1. Protocol for the induction of IL-10/IFN-γ–co-producing CD4⁺Foxp3⁻ Tr1 cells. (**A**) D665 (250 μg per mouse) and G3c (250 μg per mouse) were intraperitoneally injected on days −3 and 0 sequentially. (**B**) Representative flow cytometry (FCM) analysis and frequency of T_{reg} cells in the splenocytes of D665- and immunoglobulin G (IgG)–treated mice on day 0 ($n = 6$ for each group). ****$P < 0.0001$. (**C** and **D**) The median fluorescence intensity (MFI) of the GITR on CD4⁺Foxp3⁺ T_{reg} cells and CD4⁺Foxp3⁻ Teff cells in the splenocytes of D665- and IgG-treated mice on day 0 ($n = 5$ for each group). **$P < 0.01$ and ****$P < 0.0001$. (**E**) Representative FCM analysis of CD4⁺Foxp3⁺ T_{reg} cells and CD4⁺Foxp3⁻IL-10⁺ Tr1 cells in the splenocytes of each treatment group day 3 (D3) and D7 ($n = 4$ for each group). (**F**) Frequency of CD4⁺Foxp3⁻IL-10⁺ Tr1 cells in the splenocytes of each treatment group on day 3 and day 7 ($n = 4$ for each group). *$P < 0.05$, **$P < 0.01$, and ****$P < 0.0001$. (**G**) Frequency of CD4⁺Foxp3⁺ T_{reg} cells in the splenocytes of each treatment group on day 3 and day 7 ($n = 4$ for each group). *$P < 0.05$, ***$P < 0.001$, and ****$P < 0.0001$. Values are shown as the mean ± SEM.

-354-

When targeting GITR with G3c, large amounts of CD4+Foxp3−IL-10+ Tr1 cells were generated on days 3 and 7 (Fig. 1, E and F). Although T_{reg} cells were also potently expanded, they were obviously decreased on day 7 in the combination treatment group (Fig. 1, E and G). On day 7, most of the CD4+ IL-10+ T cells were IL-10/IFN-γ–co-producing CD4+Foxp3− Tr1 cells (Fig. 1E and fig. S1A). The gene expression of *IL-10* and *Ifng* exhibited a consistent trend with flow cytometry (FCM) results (fig. S1B). The numbers of splenocytes obtained in each group are shown in fig. S1C.

We further analyzed the phenotype of T_{reg} and Tr1 cells. T_{reg} cells showed a central memory phenotype and strongly expressed the activation markers CD25 and CD69, coinhibitory markers programmed cell death protein 1 (PD-1), inducible costimulatory molecule (ICOS), T cell immunoglobulin and mucin-domain containing-3 (TIM-3), T cell protein cytotoxic T lymphocyte antigen 4 (CTLA-4), lymphocyte activation gene 3 (LAG3), and T cell immunoreceptor with immunoglobulin (Ig) and ITIM domains (TIGIT). The detected GITR expression was slightly lower compared to that in naïve CD4+ T cells because of blockade of FCM antibody binding to GITR by G3c (Fig. 2A and fig. S2A). Tr1 cells comprised both central and effector memory phenotypes and strongly expressed coinhibitory markers PD-1, ICOS, CTLA-4, and LAG3 but weakly expressed activation markers CD25 and CD69 (Fig. 2B and fig. S2B). The coexpression of CD49b and LAG3, identified as biomarkers for a population of murine and human memory Tr1 cells, was not observed (*26*).

Function of induced Tr1 cells in vitro

Tr1 cells are characterized by the production of high amounts of IL-10, which has a potent immunosuppressive function. IL-10 exerts its major suppressive effects on the DC maturation and accessory functions (*27*, *28*). To determine the suppressive function of Tr1 cells on DCs, we isolated CD4+IL-10+ T cell, CD4+IL-10− T cells, and naïve CD4+ T cells and cocultured them with bone marrow–derived DCs (BMDCs) stimulated with lipopolysaccharide (LPS) on day 5. CD11b+CD11c+ population cells were identified as BMDCs to assess maturation state on day 7 (fig. S3). Tr1 cells prevented LPS-mediated BMDC maturation, as measured by the decreased median fluorescence intensity of surface CD40, CD80, CD86, and major histocompatibility complex class II (MHC-II) molecules (Fig. 3, A and B). Furthermore, the addition of anti–IL-10–neutralizing antibody diminished the Tr1 cell–mediated prevention of BMDC maturation.

IL-10 also exerts inhibitory effects by suppressing T cell proliferation (*29*, *30*). Cytotoxic CD8+ T cells are the principal driving force of allograft destruction and regulated by helper CD4+ T cells. We therefore next investigated the suppressive effects of Tr1 cells on CD8+ T cells using a one-way mixed lymphocyte reaction (MLR) system, where purified B6/J mice CD8+ T cells were labeled with carboxyfluorescein diacetate succinimidyl ester (CFSE) as responders and cocultured with BALB/c BMDC stimulators. FCM-sorted CD4+IL-10+ T cells, CD4+IL-10− T cells, and naïve CD4+ T cells were added to the MLR systems as regulators and cocultured for 3 days. As shown in Fig. 3 (C and D), CD8+ T cell proliferation was significantly suppressed in the presence of CD4+IL-10+ Tr1 cells, whereas the addition of an anti–IL-10 antibody restored the CD8+ T cell proliferation. These data indicated that Tr1 cells mediated the suppressive function mainly dependent on IL-10 signaling.

Mechanism underlying Tr1 cell generation

To investigate the mechanism underlying the generation of Tr1 cells by D665-G3c sequential treatment, we isolated CD4+IL-10+
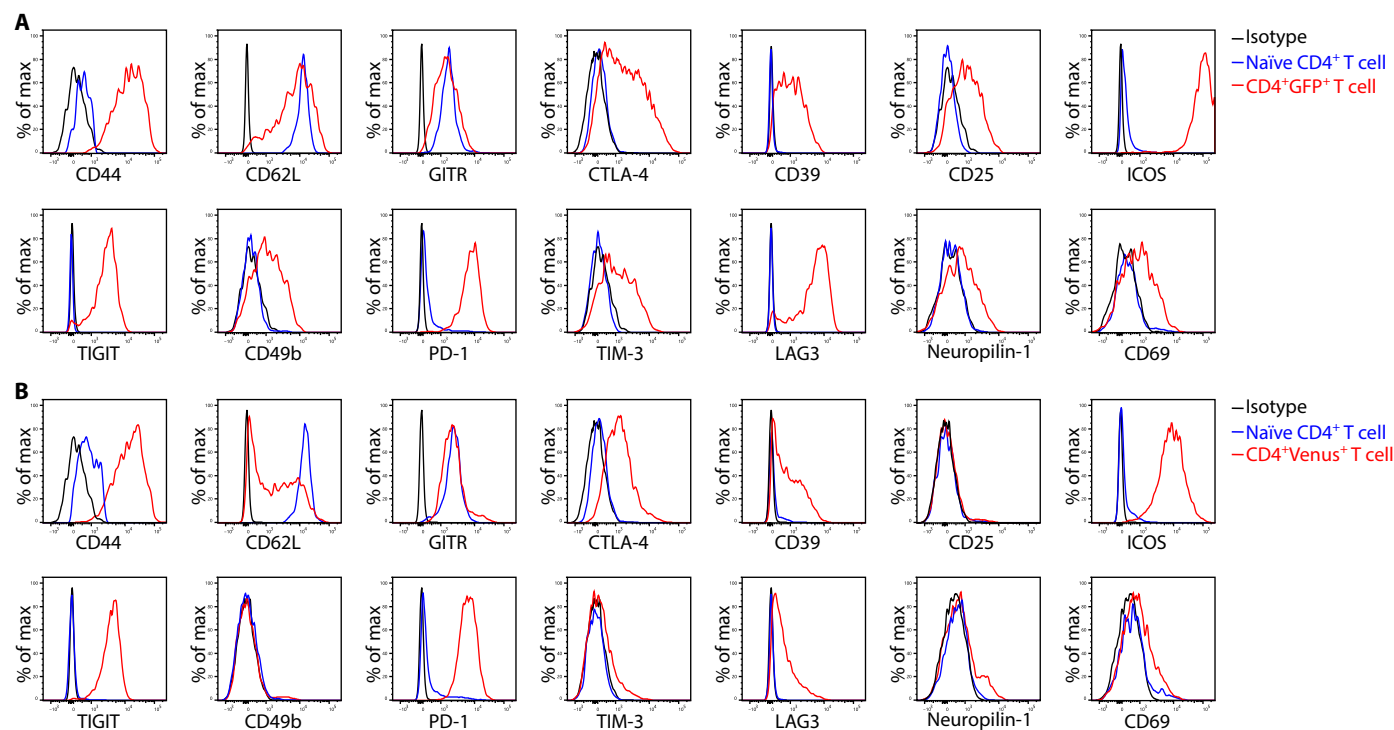

Fig. 2. The phenotype of T_{reg} and Tr1 cells. (A) Representative histogram of molecule markers on CD4+Foxp3(GFP)+ T_{reg} cells as evaluated by FCM (*n* = 4 for each group). **(B)** Representative histogram of molecule markers on CD4+Foxp3−IL-10(Venus)+ Tr1 cells as evaluated by FCM (*n* = 4 for each group).

-355-
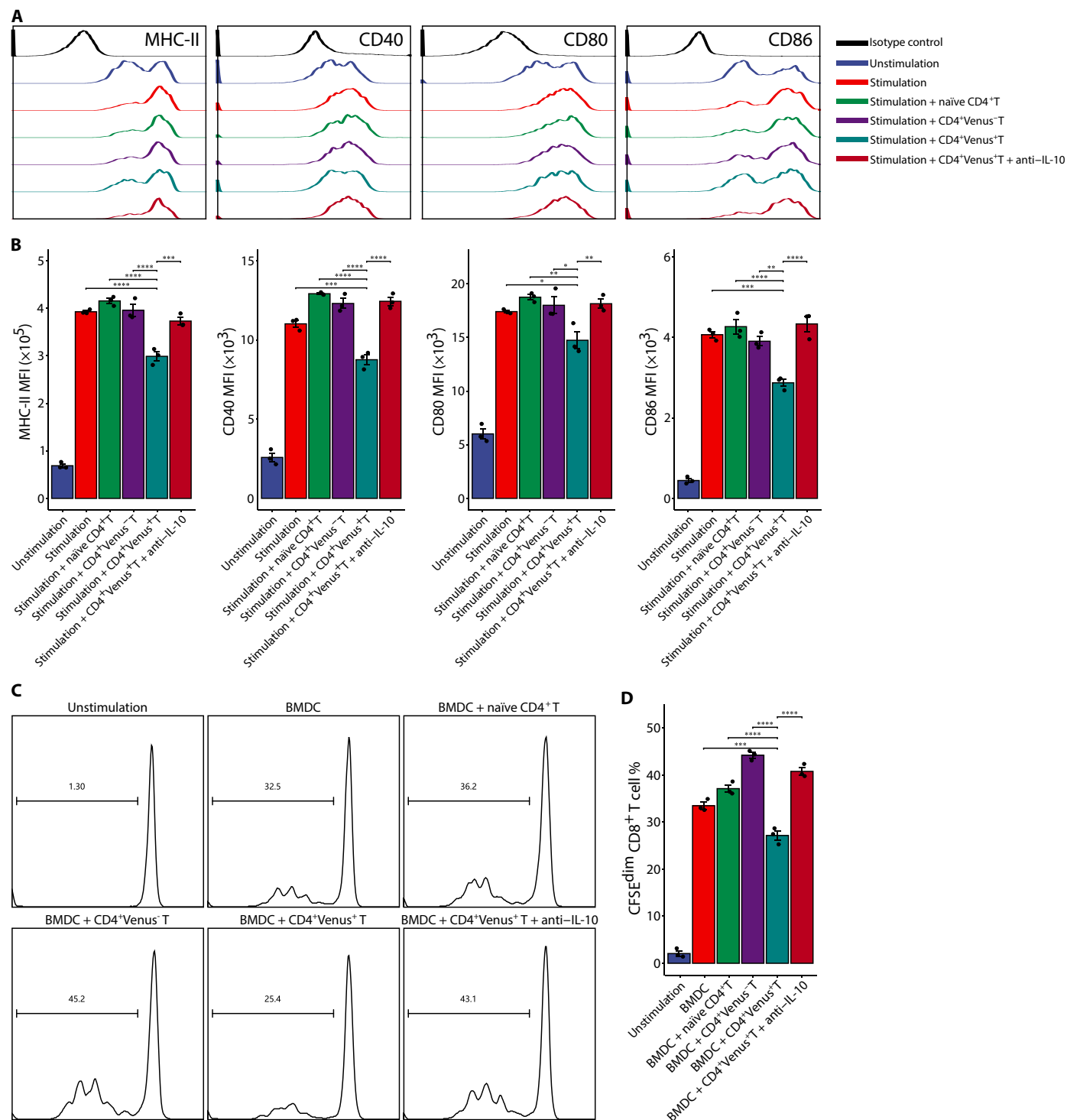
Fig. 3. Tr1 cells suppress immune responses via IL-10 signaling. (**A**) Representative histogram of surface MHC-II, CD40, CD80, and CD86 on BMDCs in each group ($n = 4$ for each group). (**B**) Quantitative data of the MFI of surface MHC-II, CD40, CD80, and CD86 on BMDCs in each group ($n = 4$ for each group). *$P < 0.05$, **$P < 0.01$, ***$P < 0.001$, and ****$P < 0.0001$. (**C**) Representative histogram of CFSE dilution of CD8+ T cells in each group ($n = 4$ for each group). (**D**) Quantitative data of the proportion of CFSE^{dim} proliferating CD8+ T cells in each group ($n = 4$ for each group). Values are shown as the mean ± SEM; ***$P < 0.001$ and ****$P < 0.0001$.

Tr1 cells and CD4+IL-10− T cells from D665-G3c–treated IL-10–Venus mice on day 7 and conducted a transcriptome RNA sequencing (RNA-seq) analysis (Fig. 4A). The gene expression of *IL-10* and *Ifng* in both cell populations was confirmed by real-time quantitative

reverse transcription polymerase chain reaction (qRT-PCR) (Fig. 4B). Following the RNA-seq analysis, a magnitude component (principal component #1) separated samples by cell type, explaining 83% of the total variation (fig. S4). Compared to CD4+IL-10− T cells, 1963
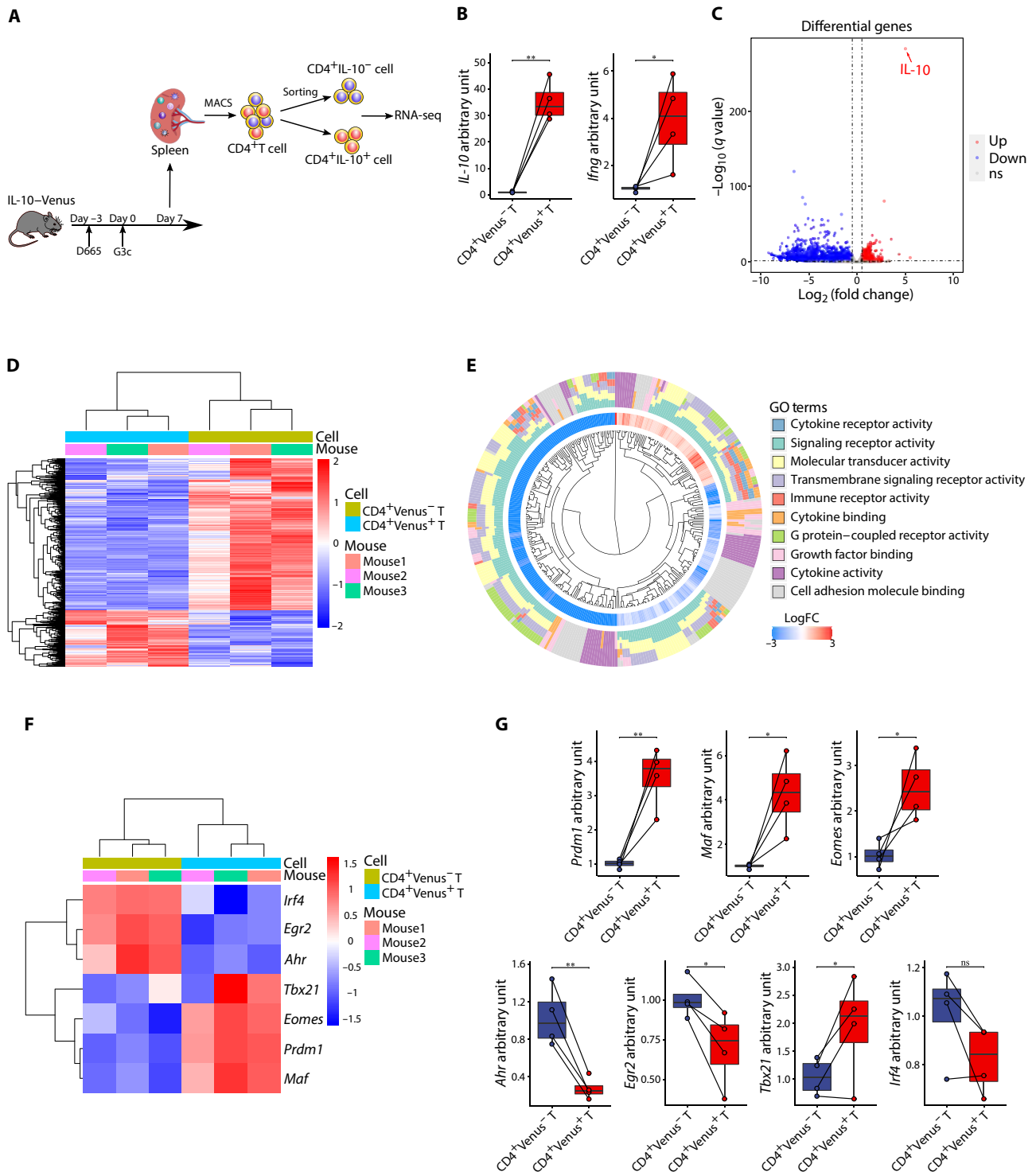
Fig. 4. Results of an RNA-seq analysis of CD4+IL-10+ and CD4+IL-10− T cells. (**A**) Total CD4+ T cells were purified by magnetic-activated cell sorting (MACS) from the splenocytes of D665-G3c–treated IL-10–Venus mice on day 7 and then subjected to CD4+IL-10+ and CD4+IL-10− T cell sorting based on the Venus expression. The isolated CD4+IL-10+ and CD4+IL-10− T cell samples were prepared in three duplicates for the subsequent transcriptome RNA-seq analysis. (**B**) The relative mRNA expression of *IL-10* and *Ifng* in CD4+IL-10+ and CD4+IL-10− T cells, detected by qRT-PCR, normalized with 18S for each sample (n = 4 for each group). Paired Student's t test; *P < 0.05 and **P < 0.01. (**C**) The volcano plot shows the DEGs, with a threshold of absolute log2FC of >0.5 and adjusted P value of <0.05, between CD4+IL-10+ T cells versus CD4+IL-10− T cells. ns, not significant. (**D**) The heatmap shows 1963 DEGs, among which 525 were up-regulated and 1438 were down-regulated, between CD4+IL-10+ cells versus CD4+IL-10− cells. (**E**) GO cluster plot displaying a circular dendrogram of the clustering of the DEGs with color-coded log2FC (inner ring) and the assigned functional terms (outer ring). (**F**) Heatmap of differentially expressed TFs known to regulate Tr1 differentiation. (**G**) The relative mRNA expression of differentially expressed TFs identified in (F), validated by qRT-PCR, and normalized with 18S for each sample (n = 4 for each group). Paired Student's t test; *P < 0.05 and **P < 0.01. Values are shown as the mean ± SEM.

differentially expressed genes (DEGs) were obtained in CD4$^+$IL-10$^+$ Tr1 cells, with a threshold of absolute log$_2$ fold change (log$_2$FC) > 0.5 and adjusted P value of <0.05, including 525 genes that were up-regulated and 1438 that were down-regulated (Fig. 4, C and D). Consistent with the cell-sorting strategy, IL-10 was the most up-regulated gene compared to the CD4$^+$IL-10$^-$ T cells (Fig. 4C).

We then performed a gene ontology (GO) enrichment analysis to gain insight into the molecular functions of the DEGs that were enriched in CD4$^+$IL-10$^+$ Tr1 cells (Fig. 4E). The most enriched GO terms were those involving signaling receptor activity, molecular transducer activity, transmembrane signaling activity, cell adhesion molecular binding, immune receptor activity, cytokine binding, G protein–coupled receptor activity, growth factor binding, cytokine receptor activity, and cytokine activity. To identify transcription factors (TFs) that might be responsible for IL-10 production, we extracted TFs known to regulate Tr1 differentiation from DEGs, including interferon regulatory factor 4 (*Irf4*), early growth response 2 (*Egr2*), aryl hydrocarbon receptors (*Ahr*), T-box transcription factor 21 (*Tbx21*), Eomesodermin (*Eomes*), *Prdm1*, and *Maf*. Of these, *Prdm1*, *Maf*, *Eomes*, and *Tbx21* were up-regulated with IL-10, whereas *Irf4*, *Egr2*, and *Ahr* were down-regulated in CD4$^+$IL-10$^+$ Tr1 cells (Fig. 4F). The gene expression of the TFs was further validated by qRT-PCR. *Prdm1*, *Maf*, *Eomes*, and *Tbx21* were verified to be significantly up-regulated in CD4$^+$IL-10$^+$ Tr1 cells (Fig. 4G).

To further explore the role of D665 and G3c in Tr1 cell generation, we examined the expression of TFs in different treatment groups on days 3 and 7 (Fig. 5A). Single-D665 treatment induced *Prdm1* and *Maf* up-regulation, and the combination treatment further increased their expression. We also observed an elevated *Prdm1* expression in the single-G3c treatment group compared to the naïve group on day 7. The *Eomes* expression was only up-regulated in the combination treatment group. Next, we detected the Blimp1 (encoded by the *Prdm1* gene) and c-Maf (encoded by the *Maf* gene) protein expression by Western blotting (Fig. 5, B and C). The expression of both Blimp1 and c-Maf protein was significantly up-regulated in the combination treatment group. It has been shown that STAT3 plays a critical role in Tr1 cell generation and is a potent inducer of both Blimp1 and c-Maf expression during Tr1 cell differentiation (*31–33*). In our study, high STAT3 phosphorylation was observed in the single-G3c treatment group as well as the combination treatment group (Fig. 5, B and C), possibly hinting at the essential role of GITR signaling in Tr1 cell generation. Extracellular signal–related kinase (ERK) MAPK, as downstream signaling of GITR activation, have been shown to induce and maintain IL-10 production in Tr1 cells (*34*). Our results revealed that the phosphorylation of ERK was significantly increased in the single-G3c treatment group as well as the combination treatment group (Fig. 5, B and C). In addition, although IL-27 was highlighted as an important driver of Tr1 cell in previous studies (*35*, *36*), we only observed a slightly increased expression of *IL-27p28* in the combination treatment group on day 7 (Fig. 5D). The level of Epstein-Barr virus–induced gene 3 (*Ebi3*), a subunit of IL-27 heterodimer, was comparable among groups.

Generation of Tr1 cells for permanent allograft acceptance

Previous studies have shown that Tr1 cells play a critical role in promoting and maintaining tolerance (*3*). We therefore next determined whether or not Tr1 cells generated by the combination of D665 and G3c treatment could induce permanent allograft acceptance.

By using a fully MHC-mismatched (donor: BALB/c, H-2k^d; recipient: B6/J, H-2k^b) mouse model of heterotopic heart transplantation (Fig. 6A), we found that the use of D665 alone prolonged the survival of heart allograft, whereas the single use of G3c showed a minimal effect on the heart allograft survival. Unexpectedly, combinations of D665 and G3c treatments induced permanent allograft acceptance (Fig. 6B). A histological analysis of the heart allograft on postoperative day 7 (POD7) indicated pronounced inflammatory infiltration and severe myocyte damage in the no-treatment control transplantation group, effects that were markedly ameliorated in the D665-G3c–treated group (Fig. 6C and fig. S5A). D665 potently expanded T$_{reg}$ cells, and G3c further enforced the expansion of T$_{reg}$ cells on POD3. However, on POD7, T$_{reg}$ cells were largely diminished in the combined treatment group (Fig. 6D and fig. S5B). Large amounts of IL-10/IFN-γ–co-producing CD4$^+$Foxp3$^-$ Tr1 cells were observed both in the cardiac graft-infiltrating lymphocytes (GILs) and splenocytes in the D665-G3c–treated group on POD7 (Fig. 6E and fig. S5C).

Further FCM analyses revealed that the CD4$^+$/CD8$^+$ T cell ratio were significantly increased in both the graft and spleen in the combination treatment group on POD7 (Fig. 6F and fig. S5D). The numbers of splenocytes and GILs obtained in each group are shown in fig. S5E. Consistently, myocardial infiltration of both of cytotoxic CD8$^+$ T cell and proliferating cytotoxic CD8$^+$ T cells, considered the major executor of transplantation rejection, were notably decreased in the combination treatment group on POD7 detected by immunohistochemical staining (Fig. 6G).

Because Foxp3$^+$ T$_{reg}$ cells were also transiently expanded in our model, we next examined the contribution of T$_{reg}$ and Tr1 cells to the induction of heart allograft acceptance. As shown in Fig. 6H, depletion of T$_{reg}$ cells on POD−1, POD3, and POD7, respectively, using anti-CD25 treatment did not disrupt heart tolerance, whereas the neutralization of IL-10 by anti–IL-10 or IL-10 knockout resulted in heart rejection. These results indicated that the combination of D665 and G3c treatment induced permanent allograft acceptance in a Tr1 cell–dependent rather than T$_{reg}$ cell–dependent manner.

DISCUSSION

Tr1 cells are potent IL-10–producing cells capable of suppressing immune responses to self, foreign, and allogeneic antigens. We found in the present study that combinations of CD28 superagonist D665 and anti-GITR antibody G3c could generate large amounts of IL-10/IFN-γ–co-producing CD4$^+$Foxp3$^-$ Tr1 cells in vivo. Mechanistic studies suggested that D665 and G3c treatment induced Tr1 cells via TFs *Prdm1* and *Maf*. G3c contribute to Tr1 cell generation via the activation of MAPK-STAT3 signaling. Tr1 cells suppressed DC maturation and T cell proliferation in an IL-10–dependent manner. Furthermore, in a mouse heart transplantation model, combinations of D665 and G3c treatments induced permanent allograft acceptance in fully MHC-mismatched mice in a Tr1 cell–dependent manner rather than a T$_{reg}$ cell–dependent manner.

CD28 superagonist bivalently binds to the laterally exposed C″D loop of the extracellular Ig-like domains of the CD28 homodimer and forms a stable lattice on the T cell membrane, which provides strong activating signals and leads to potent polyclonal T cell expansion (*4*, *5*, *37*). The CD28 superagonist D665 has been shown to preferentially expand T$_{reg}$ cells over Teff cells in various rodent models for T$_{reg}$-based interference with autoimmune and inflammatory
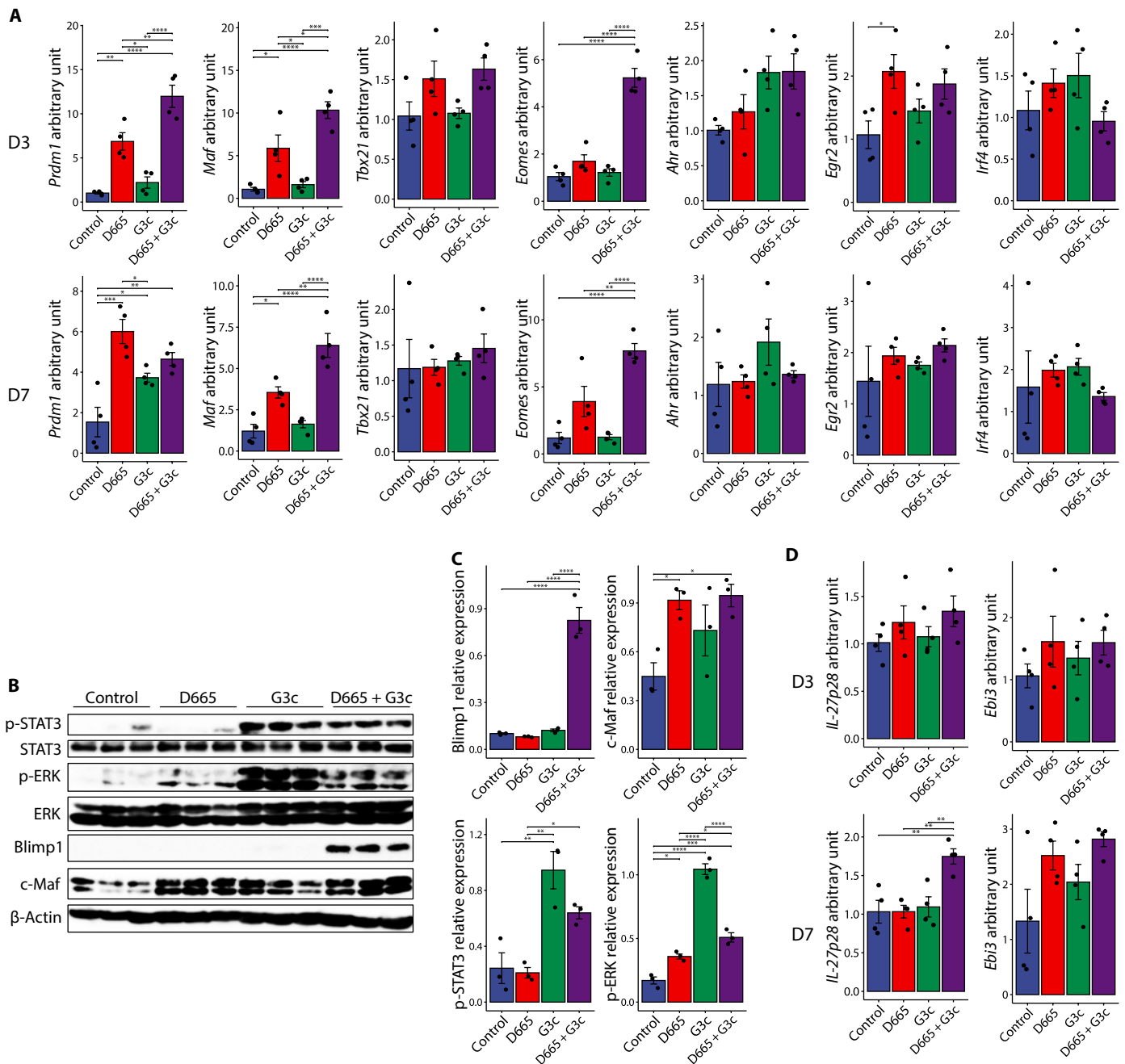
Fig. 5. The mechanism underlying the Tr1 cell functions. (**A**) The relative mRNA expression of differentially expressed TFs identified in Fig. 4F on day 3 and day 7, normalized with 18*S* for each sample (*n* = 4 for each group). *$P < 0.05$, **$P < 0.01$, ***$P < 0.001$, and ****$P < 0.0001$. (**B**) Results of a Western blot analysis of the phosphorylated STAT3 (p-STAT3), STAT3, p-ERK, ERK, Blimp1, c-Maf, and β-actin protein expression in each group on day 7. Data are representative of three independent experiments. (**C**) Quantitative data for the expression of p-STAT3 relative to STAT3, p-ERK relative to ERK, and Blimp1 and c-Maf relative to β-actin in each group on day 7 (*n* = 3 for each group). *$P < 0.05$, **$P < 0.01$, ***$P < 0.001$, and ****$P < 0.0001$. (**D**) The relative mRNA expression of *IL-27p28* and *Ebi3* on day 3 and day 7, normalized with 18*S* for each sample (*n* = 4 for each group). **$P < 0.01$. Values are shown as the mean ± SEM.

disease (*22–25*). We also observed robust T_reg cell expansion consistent with previously published data (Fig. 1). However, use of D665 alone resulted in a prolonged cardiac allograft survival rather than permanent allograft acceptance in the BALB/c to B6/J strain combination with strong rejection responses (Fig. 6). Following D665 treatment, the GITR expression was strongly up-regulated on both T_reg and Teff cells. GITR signaling is complicated, and its functions are cell

specific and context dependent (*21*). The conventional anti-GITR antibody DTA-1 has been reported to activate Teff lymphocytes while depleting GITR-expressing T_reg cells, thereby promoting antitumor immune responses. G3c, another agonist anti-GITR antibody, showed a stronger costimulatory activity than DTA-1 for both Teff and T_reg cells but failed to remove T_reg cells in vivo and cure tumorbearing mice (*38*). The application of G3c targeting GITR following

- 359-
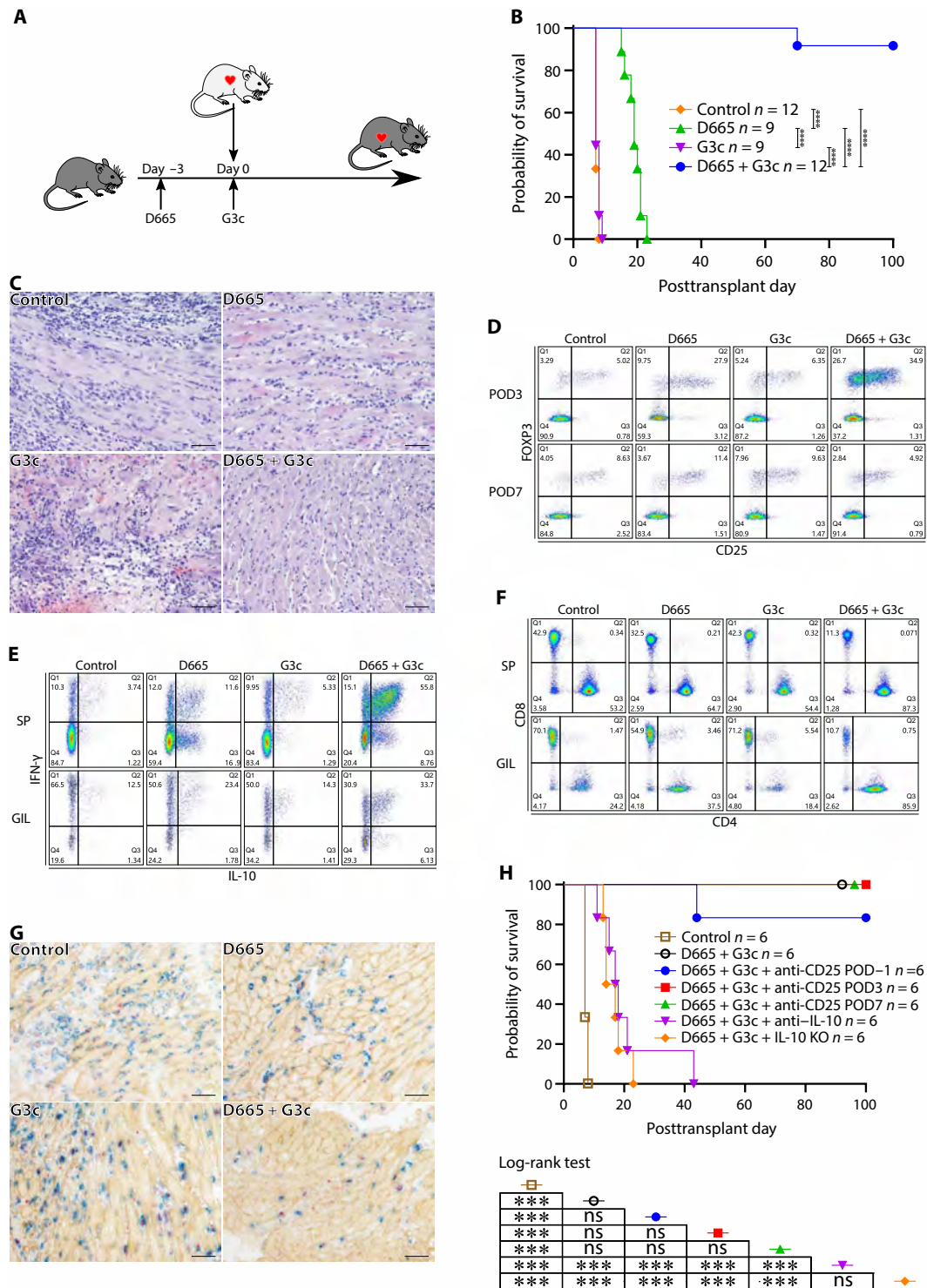
Fig. 6. D665-G3c treatment induced permanent allograft acceptance. (**A**) Treatment protocol of D665 and G3c in mouse heart transplantation. D665 (250 μg per mouse) and G3c (250 μg per mouse) were intraperitoneally injected on days −3 and 0 sequentially. Heart transplantation was performed on day 0. (**B**) The survival of cardiac allografts in each group ($n = 9$ to 12 for each group). The graft survival of each group was evaluated using Kaplan-Meier curves and log-rank tests. ****$P < 0.0001$. (**C**) Representative hematoxylin and eosin staining of cardiac grafts in each treatment group on POD7 ($n = 6$ for each group). Scale bars, 100 μm. (**D**) A representative FCM analysis of CD4+CD25+Foxp3+ T_{reg} cells in the splenocytes of each treatment group on POD3 and POD7. (**E**) A representative FCM analysis of IL-10/IFN-γ–co-producing CD4+ Tr1 cells in the splenocytes (SPs) and GILs of each treatment group on POD7 ($n = 4$ for each group). (**F**) A representative FCM analysis of CD4+ T and CD8+ T cells in the splenocytes and GILs of each treatment group on POD7 ($n = 4$ for each group). (**G**) Representative CD8 (blue), 5-bromo-2'-deoxyuridine (BrdU) (red), and type IV collagen (yellow) triple immunohistochemistry staining of heart grafts in each group on POD7 ($n = 4$ for each group). Scale bars, 100 μm. (**H**) Survival of cardiac allografts in each group ($n = 6$ for each group). The graft survival of each group was evaluated using Kaplan-Meier curves and log-rank tests. ***$P < 0.001$.

D665 generated large amounts of Tr1 cells. G3c played an important role in the induction of Tr1 cells based on D665 treatment.

The strong synthesis of IL-10 is a hallmark of Tr1 cells. Over the past few years, many studies have explored the mechanism underlying the IL-10 expression in Tr1 cells. While the molecular mechanisms underlying the development of Tr1 cells are still unclear, a plethora of TFs have been identified as being involved in IL-10 production (*2*). Notably, several TFs have been identified that contribute to the development of Tr1 cells activated by IL-27 signaling (*35*). *Prdm1* and *Maf* were identified as two central regulators that cooperatively drive the expression of IL-10 expression and Tr1 signature genes induced by IL-27 (*36*). IL-27 induced potent *Egr2* expression via *STAT3* signaling, which is required for IL-27–induced *Prdm1*-mediated IL-10 production in CD4$^+$ T cells (*32*). Furthermore, *Ahr* and *Maf*, which are located downstream of IL-27 signaling, collaboratively promoted the development of Tr1 cells (*39*). In addition, *Eomes* and *Prdm1* cooperated to generate Tr1 cells and mediated the expression of granzyme B, which is another feature of Tr1 cells (*40*). The induction of *Eomes* in Tr1 cells requires *Tbx21* and IL-27 signaling. Recently, *Eomes* has been reported as a lineage-defining TF of the unique granzyme K$^+$ Tr1 cells (*41*). In the present study, *Prdm1*, *Maf*, *Tbx21*, and *Eomes* were up-regulated in Tr1 cells (Fig. 4), accompanied by strong phosphorylation of STAT3 (Fig. 5), whereas *Egr2* and *Ahr* were down-regulated in Tr1 cells (Fig. 4). Of these, *Egr2* was reported to be essential for IL-27–induced Blimp-1–dependent IL-10 induction. A slightly elevated IL-27 expression was only observed in the combination treatment group on day 7, whereas a considerable amount of Tr1 cells had been generated on day 3. We suspect that the cell-intrinsic function of GITR signaling may be responsible for the development of Tr1 cells. GITR induced activation of ERK via TNFR-associated factor 5, which is an adaptor protein and signal transducer of TNFRs (*42*). The ERK/MAPK signaling pathways were able to induce IL-10 production through STAT3 activation (*43*). We therefore proposed that GITR signaling might contribute to Tr1 cell generation via MAPK-STAT3 signaling (Fig. 7). The high expression of *Tbx21*, the lineage-defining TF of T helper type 1 (T$_H$1) cells, and IFN-γ, the signature T$_H$1 cytokine, suggested that T$_H$1 cells might be the origin of Tr1 cells. Switching of IFN-γ–secreting T$_H$1 cells into IL-10/IFN-γ–co-producing Tr1 cells manifest the self-regulation of T$_H$1 immune response, which represent a mechanism of Tr1 generation (*44*).

IL-10 is an important pleiotropic cytokine with broad immuno-modulatory functions. Both immunosuppressive and immuno-stimulatory effects of IL-10 have been reported, the discrepancy in which may be due to differences in diseases, microenvironments, cell status, or other factors in these studies (*45*). In general, the potent anti-inflammatory and immunosuppressive effects represent the primary roles of IL-10 in immune regulation (*46*). One key function of Tr1 cells is to inhibit the DC maturation and function, which is critical for the initiation and determining the magnitude of an immune response (*47*). Coculture of BMDCs with Tr1 cells down-regulated the expression of MHC-II and costimulatory molecules, thereby reducing the magnitude of adaptive immune responses. Tr1 cells also inhibit the DC function by directly killing DCs via granzyme B and perforin secretion (*48*). Tr1 cells can regulate adaptive immune responses by directly suppressing T cells. We showed in the present study that Tr1 cells suppressed alloantigen-driven T cell proliferation in an IL-10–dependent manner (Fig. 3). Furthermore, Tr1 can also suppress T cells via cell contact–dependent
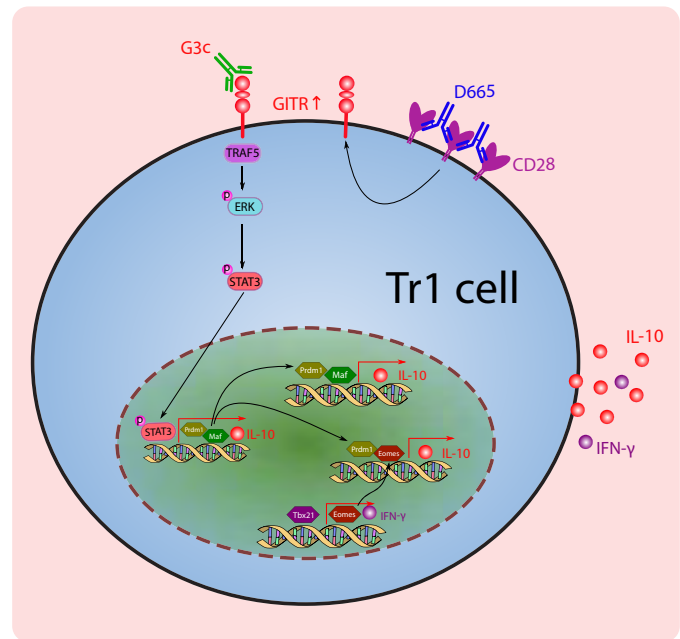

Fig. 7. The proposed cellular and transcriptional regulation of Tr1 cell development in D665-G3c–treated mice. The CD28 superagonist D665 induced up-regulation of GITR along with activation and expansion of T$_H$1 cells. The application of G3c targeting GITR contributes the conversion of T$_H$1 cells into IL-10/IFN-γ–co-producing CD4$^+$Foxp3$^-$ Tr1 cells via the activation of MAPK-STAT3 signaling. TF Blimp1, c-Maf, Eomes, and Tbx21 are responsible for IL-10/IFN-γ production in D665-G3c–induced Tr1 cells. TRAF5, TNFR-associated factor 5.

mechanisms mediated by CTLA-4 or PD-1 and CD39-mediated metabolic disruption (*49*, *50*).

The therapeutic effects of Tr1 cells have been investigated in many preclinical models of immune-mediated diseases, including autoimmune diseases, allergic diseases, GvHD, and transplantation (*40*, *51*–*54*). Tr1 cells, via de novo induction or adoptive transfer, promote pancreatic islet graft tolerance in mouse transplantation models (*51*, *52*). An increased number of circulating Tr1 cells was associated with a stable graft function and operational tolerance in renal transplant patients (*55*). Several good manufacturing practices and clinical-grade compatible protocols have been established to generate human antigen-specific Tr1 cells in vitro (*56*, *57*). We demonstrated that D665-G3c–induced Tr1 cells mediated permanent cardiac allograft acceptance. D665-G3c induced both T$_{reg}$ and Tr1 cells, but the T$_{reg}$ cells were only transiently elevated, and the heart transplantation tolerance was dependent on Tr1 rather than T$_{reg}$ cells (Fig. 6). Further translational studies concerning donor specificity and the safety of Tr1 cells generated by the D665-G3c induction strategy are needed.

In the present study, we found that the combination of D665 and G3c treatment generated large amounts of Tr1 cells, resulting in permanent cardiac allograft acceptance. We proposed that D665-G3c induced Tr1 cells via TFs *Prdm1* and *Maf*. G3c contributed to Tr1 cell generation via the activation of MAPK-STAT3 signaling. Tr1 cells suppressed both innate and adaptive immunity, thus causing permanent cardiac allograft acceptance in an IL-10–dependent manner. Further studies should focus on the associated molecular mechanisms and clinical translation of Tr1 cells. We believe that the in vivo pharmaco-logical induction of Tr1 cells opens up possibilities for transplantation tolerance and can be successfully translated to the clinical setting.

MATERIALS AND METHODS

Animals

Specific pathogen–free inbred male C57BL/6J (B6/J; H-2k[b]) and BALB/c mice (H-2k[d]), 8 to 12 weeks old, were purchased from Japan SLC Inc. (Shizuoka, Japan). Foxp3-GFP mice were purchased from the Jackson Laboratory (Bar Harbor, ME). IL-10–Venus mice were provided by K. Takeda (Graduate School of Medicine, Osaka University, Osaka, Japan) (58), and IL-10^{−/−} mice were provided by T. Yoshimoto (Tokyo Medical University, Tokyo, Japan). All mice received humane care in accordance with the guidelines of the Animal Use and Care Committee of the National Research Institute for Child Health and Development, Tokyo, Japan (permission number: A2008-004-C10). All mouse experiments conformed to the National Institutes of Health guidelines for the care and use of laboratory animals.

Heterotopic heart transplantation

Mouse heterotopic heart transplantation was performed as previously described (59). Fully vascularized hearts from donor BALB/c mice were heterotopically transplanted to the abdomen of recipient B6/J mice. The graft survival was monitored by daily abdominal palpation of the heart impulse. Total cessation of heartbeat was considered to indicate heart allograft rejection and confirmed by direct laparotomy. D665 and G3c antibodies were purified from supernatant of hybridomas, gifts from T. Hunig (University of Würzburg, Würzburg, Germany) and J. Shimizu (Kyoto University, Kyoto, Japan), respectively. For IL-10 neutralization, mice were intraperitoneally injected with 250 μg of anti–IL-10 (Bio X Cell, Lebanon, NH, catalog no. BE0049) on pre- and posttransplantation days −1, 1, 3, 6, 9, and 12. For T$_{reg}$ cell depletion, mice were intraperitoneally injected with 250 μg of anti-CD25 (Bio X Cell, catalog no. BE0012) on pre- and posttransplantation days −1, 3, and 7, respectively. For the in situ immunoproliferative response analysis, recipient mice received a single intravenous injection of 5-bromo-2′-deoxyuridine (BrdU) (0.6 mg per mouse; Sigma-Aldrich, St. Louis, MO) 1 hour before sampling.

Cell preparation and cell sorting

Total CD4^{+} and CD8^{+} T cells were purified from the mouse splenocytes using magnetic-activated cell sorting (MACS) mouse CD4^{+} (Miltenyi Biotec, Bergisch Gladbach, Germany, catalog no. 130-104-454) and CD8^{+} (Miltenyi Biotec, catalog no. 130-095-236) T cell isolation kits according to the manufacturer's instructions. For CD4^{+}IL-10^{+} cells and CD4^{+}IL-10^{−} cell preparation, CD4^{+} T cells were isolated from D665- and G3c-treated IL-10–Venus mice on day 7 using MACS and then subjected to cell sorting for CD4^{+}Venus^{+} and CD4^{+}Venus^{−} populations using a FACSAria (BD Biosciences, Franklin Lakes, NJ). Because most CD4^{+}Venus^{+} T cells (>95%) were IL-10/IFN-γ–co-producing CD4^{+}Foxp3^{−} Tr1 cells (Fig. 1E and fig. S1A), the sorted CD4^{+}Venus^{+} T cells were considered Tr1 cells.

BMDC culture

Bone marrow cells were obtained from the femur and tibia of male BALB/c mice, and then, erythrocytes were removed by lysis. To generate BMDCs, bone marrow cells (1 × 10^{6} per well) were cultured in RPMI 1640 medium supplemented with 10% fetal calf serum (FCS) (Thermo Fisher Scientific, Waltham, MA), granulocyte macrophage colony-stimulating factor (10 ng/ml; PeproTech, Cranbury, NJ), IL-4 (10 ng/ml; PeproTech), and 50 μM β-mercaptoethanol (Wako,

Osaka, Japan) in 24-well tissue culture plates. On day 2, floating granulocyte clusters were drained away, and half of the medium was refreshed. On day 5, for maturation, cells were collected and reseeded (1 × 10^{5} per well) in a 96-well flat-bottom plate with 100 μl per well of fresh medium in the presence of LPS (10 ng/ml; Sigma-Aldrich) and stimulated for 2 days. Different-sorted CD4^{+} T cells (1 × 10^{5} per well) were also added to the medium to test their effect on BMDC maturation. On day 7, different groups of BMDCs were harvested for subsequent analyses.

Mixed lymphocyte reaction

In the one-way MLR, MACS-isolated CD8^{+} T cells from B6/J mouse splenocytes were labeled with CellTrace CFSE (Thermo Fisher Scientific) as responders. BALB/c-derived BMDCs were irradiated with 20-Gy x-ray and used as stimulators. Naïve CD4^{+} T cells, CD4^{+}IL-10^{+} cells, and CD4^{+}IL-10^{−} cells were seeded to serve as regulators. Stimulator BMDCs (1 × 10^{4} per well), responder CD8^{+} T cells (1 × 10^{5} per well), and regulators CD4^{+} T cells (1 × 10^{5} per well) were cocultured in a 96-well U-bottom plate with 100 μl per well of complete RPMI 1640 medium at 37°C for 3 days. For neutralization of secreted cytokines, anti–IL-10 (20 ng/ml; Bio X Cell, catalog no. BE0049) mAb was added at the start of the culture. At the end of the assay, cells were collected for measurement of CFSE dilution by FCM.

Isolation of mouse cardiac GILs

Cardiac grafts were harvested on POD7 and cut into 1- to 2-mm pieces on ice. The tissue was then mechanically disrupted and digested at 37°C for 20 min in 10 ml of digestion solution, which included collagenase IV (0.5 mg/ml; Sigma-Aldrich) and deoxyribonuclease I (50 U/ml; Thermo Fisher Scientific) in phosphate-buffered saline (PBS). Subsequently, 10 ml of iced RPMI 1640 with 5% FCS was added to stop digestion. The digested material was filtered through a nylon mesh (100 μm) to remove aggregates and centrifuged at 200g for 10 min to pellet the cells. The pellet was then suspended in 5 ml of PBS, loaded onto 5 ml of Lympholyte-M (Cedarlane, Ontario, Canada), and centrifuged at 1500g for 25 min at room temperature. GILs were collected from the Lympholyte-M interface and washed twice in PBS before staining.

Flow cytometry

Cells were stained with LIVE/DEAD staining (Thermo Fisher Scientific) for labeling dead cells and blocked with anti-CD16/CD32 (BioLegend, San Diego, CA; catalog no. 101302) Fc Block antibody to prevent nonspecific antibody binding. For cell surface staining, the cells were incubated with different combinations of fluorochrome-conjugated antibodies against mouse CD45 (BioLegend, catalog no. 103136), CD3 (BioLegend, catalog no. 100328), CD4 (BioLegend, catalog no. 100526), CD8α (BioLegend, catalog no. 100730), CD11b (BioLegend, catalog no. 101216), CD11c (BioLegend, catalog no. 117310), CD40 (BioLegend, catalog no. 124610), CD80 (BioLegend, catalog no. 104722), CD86 (BioLegend, catalog no. 105030), MHC-II (BioLegend, catalog no. 107606), CD44 (BioLegend, catalog no. 103012), CD62L (BioLegend, catalog no. 104408), GITR (BioLegend, catalog no. 126310), CD39 (BioLegend, catalog no. 143804), CD25 (BioLegend, catalog no. 102012), ICOS (BioLegend, catalog no. 313508), TIGIT (BioLegend, catalog no. 142104), CD49b (BioLegend, catalog no. 103515), PD-1 (BioLegend, catalog no. 109104), TIM-3 (BioLegend, catalog no. 119718), Neuropilin-1 (BioLegend, catalog

- 362-

no. 145212), and CD69 (BioLegend, catalog no. 104512). For intracellular staining, cells were fixed and permeabilized using the Transcription Factor Staining Buffer Set (eBioscience, San Diego, CA) according to the manufacturer's instructions and then stained with fluorochrome-conjugated antibodies against the following: IL-10 (BioLegend, catalog no. 505008), IFN-γ (BioLegend, catalog no. 505826), CTLA-4 (BioLegend, catalog no. 106306), and Foxp3 (eBioscience, catalog no. 11-5773-82). For intracellular cytokine staining, cells were stimulated with phorbol 12-myristate 13-acetate (50 ng/ml; BD Golgi Plug), 1 mM ionomycin (Sigma-Aldrich), and brefeldin A (eBioscience) in complete medium for 4 hours, followed by surface and intracellular staining. The isotype- and fluorochrome-matched IgG was used as a negative control. Flow data were acquired with an LSRFortessa Cell Analyzer (BD Biosciences) and analyzed using the FlowJo v10 software program (BD Biosciences).

RNA-seq analyses
CD4$^+$IL-10$^+$ and CD4$^+$IL-10$^-$ T cell samples were prepared in three duplicates. Total RNA extraction and DNA removal were performed as described above. These RNA samples were then subjected to preprocessing, DNA nanoball-based library construction, and high-throughput sequencing by BGI Japan (Kobe, Japan) on the DNBseq sequencing platform. The raw sequencing reads were checked for their quality with FastQC (v0.11.8), trimmed with TrimGalore (v0.5.0), and aligned to the GRCm38 reference genome using the RNA-seq aligner HISAT2 (v2.1.0). Read counts for each gene were calculated with Feature Counts. DEGs were identified by DESeq2 (v1.32.0) with the following criteria: absolute log$_2$FC of ≥0.5 and adjusted P value of ≤0.05. Variance stabilization–transformed expression data were Z-transferred and used to generate a heatmap by pheatmap (v1.0.12). A GO enrichment analysis was performed using ClusterProfiler (v4.0.5). The top 10 enriched clusters were visualized with GOplot (v1.0.2).

RNA purification and qRT-PCR
Total RNA from heart grafts was extracted using reagent Sepasol-RNA I Super G (Nacalai Tesque, Kyoto, Japan). Total RNA from the cell suspension was extracted using the RNeasy Mini Kit (Qiagen, Valencia, CA) according to the manufacturer's protocol. After treating samples with a DNA-free kit (Ambion, Life Technologies, Carlsbad, CA), total RNA was reverse-transcribed to generate complementary DNA using a PrimeScript RT Reagent Kit (Takara Bio, Shiga, Japan). qRT-PCR was performed in an Applied Biosystem PRISM 7700 instrument (Applied Biosystems, Foster City, CA) using the SYBR Green system. The threshold cycle (Ct) values of the target genes were normalized to the Ct value of 18S ribosomal RNA. The relative gene expression was calculated by the $\Delta\Delta Ct$ calculation method. The sequences of 18S and target gene primers used in this research are shown in Table 1.

Western blotting
Total cell protein was extracted with radioimmunoprecipitation assay lysis buffer (Wako) containing 1% protease inhibitor cocktail, 1% phosphatase inhibitor cocktail 1, and 1% phosphatase inhibitor cocktail 2 (Sigma-Aldrich), measured concentrations with the BCA Protein Assay (Thermo Fisher Scientific). Twenty micrograms of protein was resolved on 10% SDS–polyacrylamide gel electrophoresis gels and transferred onto polyvinylidene difluoride membranes (Bio-Rad, Hercules, CA). After blocking, the membranes were incubated with primary antibodies containing phosphorylated STAT3 (p-STAT3) (Cell Signaling Technology, Danvers, MA, catalog no. 9131), STAT3 (Cell Signaling Technology, catalog no. 4904), p-ERK (Cell Signaling Technology, catalog no. 4370), ERK (Cell Signaling Technology, catalog no. 4695), Blimp1 (Cell Signaling Technology, catalog no. 9115), c-Maf (Bethyl Laboratories, Montgomery, TX; catalog no. A300-613A-M), and β-actin (Cell Signaling Technology, catalog no. 4970) overnight at 4°C, followed by horseradish peroxidase–linked anti-rabbit IgG secondary antibody (Cell Signaling Technology, catalog no. 7074) probing for 1 hour at room temperature. The chemiluminescence signal intensity of protein bands were detected with enhanced chemiluminescence (GE Healthcare, Piscataway, NJ) and the ImageQuant LAS4000 System (GE Healthcare). The protein expression was quantitated with the ImageJ software program (National Institutes of Health, Bethesda, MD).

Histological analyses
Heart grafts were fixed in 10% neutral buffered formalin (Wako), dehydrated, and then embedded in paraffin. Paraffin sections (4 μm

Table 1. Primer sequences for qRT-PCR.

Gene	Forward primer (5′ to 3′)	Reverse primer (3′ to 5′)
Prdm1	CCCTCATCGGTGAAGTCTA	ACGTAGCGCATCCAGTTG
Maf	GCAGAGACACGTCCTGGAGTCG	CGAGCTTGGCCCTGCAACTAGC
Eomes	GCGCATGTTTCCTTTCTTGAG	GGTCGGCCAGAACCACTTC
Ahr	AGCCGGTGCAGAAAACAGTAA	AGGCGGTCTAACTCTGTGTTC
Egr2	GCCAAGGCCGTAGACAAAATC	CCACTCCGTTCATCTGGTCA
Tbx21	AGCAAGGACGGCGAATGTT	GGGTGGACATATAAGCGGTTC
Irf4	TCCGACAGTGGTTGATCGAC	CCTCACGATTGTAGTCCTGCTT
Il-27p28	CCTGACATGGGCCAGGTGACAGGAGACC	TCACTCGAGTTAGGAATCCCAGGCTGAG
Ebi3	CTTACAGGCTCGGTGTGGC	GTGACATTTAGCATGTAGGGCA
IL-10	GCTCTTACTGACTGGCATGAG	CGCAGCTCTAGGAGCATGTG
Ifng	AAGCGTCATTGAATCACACCTGA	ACCTGTGGGTTGTTGACCTCAA
18S	ACATCGACCTCACCAAGAGG	TCCCATCCTTCACATCCTTC

-363-

thick) were stained with hematoxylin and eosin stain. Heart allograft rejection was graded by two investigators blinded to the group and labeling allocation during the experiment, according to the International Society for Heart and Lung Transplantation criteria (*60*).

Immunohistochemistry

Heart grafts were frozen in Tissue-Tek optimal cutting temperature compound (Sakura Finetek, Torrance, CA) and then cut into 4-μm-thick cryosections. Cryosections were rehydrated, fixed with formaldehyde calcium solution, and then blocked using block ace for 10 min. For CD8α T cell staining, the sections were immunostained with CD8α (BioLegend, catalog no. 100777) as the primary antibody and then incubated with alkaline phosphatase (ALP)-conjugated donkey anti-rat IgG (Jackson ImmunoResearch, West Grove, PA; catalog no. 712-055-153) as the secondary antibody. The positive antigens were visualized with the Vector Blue Alkaline Phosphatase Substrate Kit (Vector Laboratories, Burlingame, CA) according to the manufacturer's instructions. For type IV collagen staining, the sections were immunostained with rabbit–anti-mouse type IV collagen polyclonal antibody (Cosmo Bio, Tokyo, Japan, catalog no. LSL-LB-1403) and then incubated with POD-conjugated goat–anti-rabbit Ig (Jackson ImmunoResearch, catalog no. 111-036-144) as the secondary antibody. The positive antigens were visualized with diaminobenzidine (DAB) (Dojindo, Kumamoto, Japan) substrate reaction. For BrdU staining, the sections were digested with a pepsin (Sigma-Aldrich) solution, immunostained with anti-BrdU (Bio-Rad Laboratories, catalog no. OBT0030CX) as the primary antibody, and then incubated with ALP-conjugated donkey anti-rat IgG (Jackson ImmunoResearch, catalog no. 712-055-153) as the secondary antibody. The positive antigens were visualized with New Fuchsin (Dako, Santa Clara, CA) in a substrate reaction. Last, the sections were fixed in formaldehyde calcium solution and mounted with Aquatex (Merck, Whitehouse Station, NJ).

All of the sections were imaged with a DP70 camera (Olympus, Osaka, Japan). The images were processed and analyzed using the ImageJ software program. Positive cells were determined by counting nine random 400× high-power fields on each slide.

Statistical analyses

All data were analyzed using the GraphPad Prism software program (v7.0, GraphPad Software, San Diego, CA). The results were presented as the mean ± SEM. Student's *t* test (normal distribution data) was used for comparisons between the two groups. A one-way analysis of variance (ANOVA), followed by a post hoc test was used for comparisons between multiple groups. A log-rank (Mantel-Cox) test was used for the survival data. In all experiments, differences were considered statistically significant at $*P < 0.05$, $**P < 0.01$, $***P < 0.001$, and $****P < 0.0001$.

SUPPLEMENTARY MATERIALS

Supplementary material for this article is available at https://science.org/doi/10.1126/sciadv.abo4413

View/request a protocol for this paper from *Bio-protocol*.

REFERENCES AND NOTES

1. J. R. Leventhal, J. M. Mathew, Outstanding questions in transplantation: Tolerance. *Am. J. Transplant* **20**, 348–354 (2020).
2. M. G. Roncarolo, S. Gregori, R. Bacchetta, M. Battaglia, N. Gagliani, The biology of T regulatory type 1 cells and their therapeutic application in immune-mediated diseases. *Immunity* **49**, 1004–1019 (2018).
3. Y. Song, N. Wang, L. Chen, L. Fang, Tr1 cells as a key regulator for maintaining immune homeostasis in transplantation. *Front. Immunol.* **12**, 671579 (2021).
4. F. Lühder, Y. Huang, K. M. Dennehy, C. Guntermann, I. Müller, E. Winkler, T. Kerkau, S. Ikemizu, S. J. Davis, T. Hanke, T. Hünig, Topological requirements and signaling properties of T cell–Activating, anti-CD28 antibody superagonists. *J. Exp. Med.* **197**, 955–966 (2003).
5. E. J. Evans, R. M. Esnouf, R. Manso-Sancho, R. J. C. Gilbert, J. R. James, C. Yu, J. A. Fennelly, C. Vowles, T. Hanke, B. Walse, T. Hünig, P. Sørensen, D. I. Stuart, S. J. Davis, Crystal structure of a soluble CD28-Fab complex. *Nat. Immunol.* **6**, 271–279 (2005).
6. N. Beyersdorf, T. Hanke, T. Kerkau, T. Hünig, Superagonistic anti-CD28 antibodies: Potent activators of regulatory T cells for the therapy of autoimmune diseases. *Ann. Rheum. Dis.* **64**, iv91–iv95 (2005).
7. N. Beyersdorf, S. Werner, N. Wolf, T. Hünig, T. Kerkau, In vitro polyclonal activation of conventional T cells with a CD28 superagonist protects mice from acute graft versus host disease. *Eur. J. Immunol.* **45**, 1997–2007 (2015).
8. Y. Kitazawa, M. Fujino, X.-K. Li, L. Xie, N. Ichimaru, M. Okumi, N. Nonomura, A. Tsujimura, Y. Isaka, H. Kimura, T. Hünig, S. Takahara, Superagonist CD28 antibody preferentially expanded Foxp3-expressing nTreg cells and prevented graft-versus-host diseases. *Cell Transplant* **18**, 627–638 (2009).
9. G. Nocentini, L. Giunchi, S. Ronchetti, L. T. Krausz, A. Bartoli, R. Moraca, G. Migliorati, C. Riccardi, A new member of the tumor necrosis factor/nerve growth factor receptor family inhibits T cell receptor-induced apoptosis. *Proc. Natl. Acad. Sci. U.S.A.* **94**, 6216–6221 (1997).
10. R. S. McHugh, M. J. Whitters, C. A. Piccirillo, D. A. Young, E. M. Shevach, M. Collins, M. C. Byrne, CD4⁺CD25⁺ immunoregulatory T cells: Gene expression analysis reveals a functional role for the glucocorticoid-induced TNF receptor. *Immunity* **16**, 311–323 (2002).
11. J. Shimizu, S. Yamazaki, T. Takahashi, Y. Ishida, S. Sakaguchi, Stimulation of CD25⁺CD4⁺ regulatory T cells through GITR breaks immunological self-tolerance. *Nat. Immunol.* **3**, 135–142 (2002).
12. F. Kanamaru, P. Youngnak, M. Hashiguchi, T. Nishioka, T. Takahashi, S. Sakaguchi, I. Ishikawa, M. Azuma, Costimulation via glucocorticoid-induced TNF receptor in both conventional and CD25⁺ regulatory CD4⁺ T cells. *J. Immunol.* **172**, 7306–7314 (2004).
13. M. Tone, Y. Tone, E. Adams, S. F. Yates, M. R. Frewin, S. P. Cobbold, H. Waldmann, Mouse glucocorticoid-induced tumor necrosis factor receptor ligand is costimulatory for T cells. *Proc. Natl. Acad. Sci. U.S.A.* **100**, 15059–15064 (2003).
14. G. L. Stephens, R. S. McHugh, M. J. Whitters, D. A. Young, D. Luxenberg, B. M. Carreno, M. Collins, E. M. Shevach, Engagement of glucocorticoid-induced TNFR family-related receptor on effector T cells by its ligand mediates resistance to suppression by CD4⁺CD25⁺ T cells. *J. Immunol.* **173**, 5008–5020 (2004).
15. J. I. Kim, S. B. Sonawane, M. K. Lee, S.-H. Lee, P. E. Duff, D. J. Moore, M. R. O'Connor, M.-M. Lian, S. Deng, Y. Choi, H. Yeh, A. J. Caton, J. F. Markmann, Blockade of GITR–GITRL interaction maintains Treg function to prolong allograft survival. *Eur. J. Immunol.* **40**, 1369–1374 (2010).
16. A. Bushell, K. Wood, GITR ligation blocks allograft protection by induced CD25⁺CD4⁺ regulatory T cells without enhancing effector T-cell function. *Am. J. Transplant.* **7**, 759–768 (2007).
17. S. Sukumar, D. C. Wilson, Y. Yu, J. Wong, S. Naravula, G. Ermakov, R. Riener, B. Bhagwat, A. S. Necheva, J. Grein, T. Churakova, R. Mangadu, P. Georgiev, D. Manfra, E. M. Pinheiro, V. Sriram, W. J. Bailey, D. Herzyk, T. K. McClanahan, A. Willingham, A. M. Beebe, S. Sadekova, Characterization of MK-4166, a clinical agonistic antibody that targets human GITR and inhibits the generation and suppressive effects of T regulatory cells. *Cancer Res.* **77**, 4378–4388 (2017).
18. M. G. Petrillo, S. Ronchetti, E. Ricci, A. Alunno, R. Gerli, G. Nocentini, C. Riccardi, GITR⁺ regulatory T cells in the treatment of autoimmune diseases. *Autoimmun. Rev.* **14**, 117–126 (2015).
19. J. Mitsui, H. Nishikawa, D. Muraoka, L. Wang, T. Noguchi, E. Sato, S. Kondo, J. P. Allison, S. Sakaguchi, L. J. Old, T. Kato, H. Shiku, Two distinct mechanisms of augmented antitumor activity by modulation of immunostimulatory/inhibitory signals. *Clin. Cancer Res.* **16**, 2781–2791 (2010).
20. A. Ephrem, A. L. Epstein, G. L. Stephens, A. M. Thornton, D. Glass, E. M. Shevach, Modulation of Treg cells/T effector function by GITR signaling is context-dependent. *Eur. J. Immunol.* **43**, 2421–2429 (2013).
21. D. L. Clouthier, T. H. Watts, Cell-specific and context-dependent effects of GITR in cancer, autoimmunity, and infection. *Cytokine Growth Factor Rev.* **25**, 91–106 (2014).
22. J. Chen, L. Xie, S. Toyama, T. Hünig, S. Takahara, X.-K. Li, L. Zhong, The effects of Foxp3-expressing regulatory T cells expanded with CD28 superagonist antibody in DSS-induced mice colitis. *Int. Immunopharmacol.* **11**, 610–617 (2011).
23. J. C. Wagner, S. Leicht, S. Hofmann, F. Seifert, S. Gahn, C.-T. Germer, N. Beyersdorf, C. Otto, I. Klein, CD28 superagonist D665-mediated activation of mouse regulatory T cells maintains their phenotype without loss of suppressive quality. *Immunobiology* **226**, 152144 (2021).

24. S. Copsel, D. Wolf, K. V. Komanduri, R. B. Levy, The promise of CD4+FoxP3+ regulatory T-cell manipulation in vivo: Applications for allogeneic hematopoietic stem cell transplantation. *Haematologica* **104**, 1309–1321 (2019).

25. M. Guilliams, T. Bosschaerts, M. Hérin, P. Loi, V. Flamand, P. De Baetselier, A. Beschin, Experimental expansion of the regulatory T cell population increases resistance to african trypanosomiasis. *J. Infect Dis.* **198**, 781–791 (2008).

26. N. Gagliani, C. F. Magnani, S. Huber, M. E. Gianolini, M. Pala, P. Licona-Limon, B. Guo, D. R. Herbert, A. Bulfone, F. Trentini, C. Di Serio, R. Bacchetta, M. Andreani, L. Brockmann, S. Gregori, R. A. Flavell, M.-G. Roncarolo, Coexpression of CD49b and LAG-3 identifies human and mouse T regulatory type 1 cells. *Nat. Med.* **19**, 739–746 (2013).

27. C. Haase, T. N. Jørgensen, B. K. Michelsen, Both exogenous and endogenous interleukin-10 affects the maturation of bone-marrow-derived dendritic cells in vitro and strongly influences T-cell priming in vivo. *Immunology* **107**, 489–499 (2002).

28. S. Corinti, C. Albanesi, A. la Sala, S. Pastore, G. Girolomoni, Regulatory activity of autocrine IL-10 on dendritic cell functions. *J. Immunol.* **166**, 4312–4318 (2001).

29. L. K. Smith, G. M. Boukhaled, S. A. Condotta, S. Mazouz, J. J. Guthmiller, R. Vijay, N. S. Butler, J. Bruneau, N. H. Shoukry, C. M. Krawczyk, M. J. Richer, Interleukin-10 directly inhibits CD8+ T cell function by enhancing N-glycan branching to decrease antigen sensitivity. *Immunity* **48**, 299–312.e5 (2018).

30. H. Groux, M. Bigler, J. E. de Vries, M.-G. Roncarolo, Inhibitory and stimulatory effects of IL-10 on human CD8+ T cells. *J. Immunol.* **160**, 3188–3193 (1998).

31. K. G. Schmetterer, W. F. Pickl, The IL–10/STAT3 axis: Contributions to immune tolerance by thymus and peripherally derived regulatory T-cells. *Eur. J. Immunol.* **47**, 1256–1265 (2017).

32. Y. Iwasaki, K. Fujio, T. Okamura, A. Yanai, S. Sumitomo, H. Shoda, T. Tamura, H. Yoshida, P. Charnay, K. Yamamoto, Egr-2 transcription factor is required for Blimp-1-mediated IL-10 production in IL-27-stimulated CD4+ T cells. *Eur. J. Immunol.* **43**, 1063–1073 (2013).

33. Y. Yang, J. Ochando, A. Yopp, J. S. Bromberg, Y. Ding, IL-6 plays a unique role in initiating c-Maf expression during early stage of CD4 T cell activation. *J. Immunol.* **174**, 2720–2729 (2005).

34. M. F. Farez, I. D. Mascanfroni, S. P. Méndez-Huergo, A. Yeste, G. Murugaiyan, L. P. Garo, M. E. B. Aguirre, B. Patel, M. C. Ysrraelit, C. Zhu, V. K. Kuchroo, G. A. Rabinovich, F. J. Quintana, J. Correale, Melatonin contributes to the seasonality of multiple sclerosis relapses. *Cell* **162**, 1338–1352 (2015).

35. A. Vasanthakumar, A. Kallies, IL-27 paves different roads to Tr1. *Eur. J. Immunol.* **43**, 882–885 (2013).

36. H. Zhang, A. Madi, N. Yosef, N. Chihara, A. Awasthi, C. Pot, C. Lambden, A. Srivastava, P. R. Burkett, J. Nyman, E. Christian, A. Lee, H. Stroh, J. Xia, K. Karwacz, P. I. Thakore, N. Acharya, A. Schnell, C. Wang, L. Apetoh, O. Rozenblatt-Rosen, A. C. Anderson, A. Regev, V. K. Kuchroo, An IL-27-driven transcriptional network identifies regulators of IL-10 expression across T helper cell subsets. *Cell Rep.* **33**, 108433 (2020).

37. T. Hünig, K. Dennehy, CD28 superagonists: Mode of action and therapeutic potential. *Immunol. Lett.* **100**, 21–28 (2005).

38. T. Nishioka, E. Nishida, R. Iida, A. Morita, J. Shimizu, In vivo expansion of CD4+Foxp3+ regulatory T cells mediated by GITR molecules. *Immunol. Lett.* **121**, 97–104 (2008).

39. L. Apetoh, F. J. Quintana, C. Pot, N. Joller, S. Xiao, D. Kumar, E. J. Burns, D. H. Sherr, H. L. Weiner, V. K. Kuchroo, The aryl hydrocarbon receptor interacts with c-Maf to promote the differentiation of type 1 regulatory T cells induced by IL-27. *Nat. Immunol.* **11**, 854–861 (2010).

40. P. Zhang, J. S. Lee, K. H. Gartlan, I. S. Schuster, I. Comerford, A. Varelias, M. A. Ullah, S. Vuckovic, M. Koyama, R. D. Kuns, K. R. Locke, K. J. Beckett, S. D. Olver, L. D. Samson, M. M. de Oca, F. de L. Rivera, A. D. Clouston, G. T. Belz, B. R. Blazar, K. P. MacDonald, S. R. McColl, R. Thomas, C. R. Engwerda, M. A. Degli-Esposti, A. Kallies, S.-K. Tey, G. R. Hill, Eomesodermin promotes the development of type 1 regulatory T (TR1) cells. *Sci. Immunol.* **2**, eaah7152 (2017).

41. P. Gruarin, S. Maglie, M. De Simone, B. Häringer, C. Vasco, V. Ranzani, R. Bosotti, J. S. Noddings, P. Larghi, F. Facciotti, M. L. Sarnicola, M. Martinovic, M. Crosti, M. Moro, R. L. Rossi, M. E. Bernardo, F. Caprioli, F. Locatelli, G. Rossetti, S. Abrignani, M. Pagani, J. Geginat, Eomesodermin controls a unique differentiation program in human IL-10 and IFN-γ coproducing regulatory T cells. *Eur. J. Immunol.* **49**, 96–111 (2019).

42. E. M. Esparza, T. Lindsten, J. M. Stockhausen, R. H. Arch, Tumor necrosis factor receptor (TNFR)-associated factor 5 is a critical intermediate of costimulatory signaling pathways triggered by glucocorticoid-induced TNFR in T cells. *J. Biol. Chem.* **281**, 8559–8564 (2006).

43. M. Lucas, X. Zhang, V. Prasanna, D. M. Mosser, ERK activation following macrophage FcγR ligation leads to chromatin modifications at the IL-10 locus. *J. Immunol.* **175**, 469–477 (2005).

44. A. Cope, G. L. Friec, J. Cardone, C. Kemper, The Th1 life cycle: Molecular control of IFN-γ to IL-10 switching. *Trends Immunol.* **32**, 278–286 (2011).

45. W. Ouyang, A. O'Garra, IL-10 family cytokines IL-10 and IL-22: From basic science to clinical translation. *Immunity* **50**, 871–891 (2019).

46. M. Saraiva, P. Vieira, A. O'Garra, Biology and therapeutic potential of interleukin-10. *J. Exp. Med.* **217**, e20190418 (2019).

47. T. De Smedt, M. Van Mechelen, G. De Becker, J. Urbain, O. Leo, M. Moser, Effect of interleukin-10 on dendritic cell maturation and function. *Eur. J. Immunol.* **27**, 1229–1235 (1997).

48. C. F. Magnani, G. Alberigo, R. Bacchetta, G. Serafini, M. Andreani, M. G. Roncarolo, S. Gregori, Killing of myeloid APCs via HLA class I, CD2 and CD226 defines a novel mechanism of suppression by human Tr1 cells. *Eur. J. Immunol.* **41**, 1652–1662 (2011).

49. M. Akdis, J. Verhagen, A. Taylor, F. Karamloo, C. Karagiannidis, R. Crameri, S. Thunberg, G. Deniz, R. Valenta, H. Fiebig, C. Kegel, R. Disch, C. B. Schmidt-Weber, K. Blaser, C. A. Akdis, Immune responses in healthy and allergic individuals are characterized by a fine balance between allergen-specific T regulatory 1 and T helper 2 cells. *J. Exp. Med.* **199**, 1567–1575 (2004).

50. I. D. Mascanfroni, M. C. Takenaka, A. Yeste, B. Patel, Y. Wu, J. E. Kenison, S. Siddiqui, A. S. Basso, L. E. Otterbein, D. M. Pardoll, F. Pan, A. Priel, C. B. Clish, S. C. Robson, F. J. Quintana, Metabolic control of type 1 regulatory T cell differentiation by AHR and HIF1-α. *Nat. Med.* **21**, 638–646 (2015).

51. T. Jofra, R. Di Fonte, G. Galvani, M. Kuka, M. Iannacone, M. Battaglia, G. Fousteri, Tr1 cell immunotherapy promotes transplant tolerance via de novo Tr1 cell induction in mice and is safe and effective during acute viral infection. *Eur. J. Immunol.* **48**, 1389–1399 (2018).

52. N. Gagliani, T. Jofra, A. Stabilini, A. Valle, M. Atkinson, M.-G. Roncarolo, M. Battaglia, Antigen-specific dependence of Tr1-cell therapy in preclinical models of islet transplant. *Diabetes* **59**, 433–439 (2010).

53. H. Yu, N. Gagliani, H. Ishigame, S. Huber, S. Zhu, E. Esplugues, K. C. Herold, L. Wen, R. A. Flavell, Intestinal type 1 regulatory T cells migrate to periphery to suppress diabetogenic T cells and prevent diabetes development. *Proc. Natl. Acad. Sci. U.S.A.* **114**, 10443–10448 (2017).

54. M. Matsuda, K. Doi, T. Tsutsumi, M. Inaba, J. Hamaguchi, T. Terada, R. Kawata, K. Kitatani, T. Nabe, Adoptive transfer of type 1 regulatory T cells suppressed the development of airway hyperresponsiveness in ovalbumin-induced airway inflammation model mice. *J. Pharmacol. Sci.* **141**, 139–145 (2019).

55. D. E. M. van den Boogaardt, P. P. M. C. van Miert, Y. J. H. de Vaal, J. W. de Fijter, F. H. J. Claas, D. L. Roelen, The ratio of interferon-gamma and interleukin-10 producing donor-specific cells as an in vitro monitoring tool for renal transplant patients. *Transplantation* **82**, 844–848 (2006).

56. S. Gregori, M. G. Roncarolo, Engineered T regulatory Type 1 cells for clinical application. *Front. Immunol.* **9**, 233 (2018).

57. B. Mfarrej, E. Tresoldi, A. Stabilini, A. Paganelli, R. Caldara, A. Secchi, M. Battaglia, Generation of donor-specific Tr1 cells to be used after kidney transplantation and definition of the timing of their in vivo infusion in the presence of immunosuppression. *J. Transl. Med.* **15**, 40 (2017).

58. K. Atarashi, T. Tanoue, T. Shima, A. Imaoka, T. Kuwahara, Y. Momose, G. Cheng, S. Yamasaki, T. Saito, Y. Ohba, T. Taniguchi, K. Takeda, S. Hori, I. I. Ivanov, Y. Umesaki, K. Itoh, K. Honda, Induction of colonic regulatory T cells by indigenous *Clostridium* species. *Science* **331**, 337–341 (2011).

59. W. Que, X. Hu, M. Fujino, H. Terayama, K. Sakabe, N. Fukunishi, P. Zhu, S.-Q. Yi, Y. Yamada, L. Zhong, X.-K. Li, Prolonged cold ischemia time in mouse heart transplantation using supercooling preservation. *Transplantation* **104**, 1879–1889 (2020).

60. S. Stewart, G. L. Winters, M. C. Fishbein, H. D. Tazelaar, J. Kobashigawa, J. Abrams, C. B. Andersen, A. Angelini, G. J. Berry, M. M. Burke, A. J. Demetris, E. Hammond, S. Itescu, C. C. Marboe, B. McManus, E. F. Reed, N. L. Reinsmoen, E. R. Rodriguez, A. G. Rose, M. Rose, N. Suciu-Focia, A. Zeevi, M. E. Billingham, Revision of the 1990 working formulation for the standardization of nomenclature in the diagnosis of heart rejection. *J. Heart Lung Transplant.* **24**, 1710–1720 (2005).

ScienceAdvances

Combinations of anti-GITR antibody and CD28 superagonist induce permanent allograft acceptance by generating type 1 regulatory T cells

Weitao QueKuai MaXin HuWen-Zhi GuoXiao-Kang Li

View the article online
https://www.science.org/doi/10.1126/sciadv.abo4413
Permissions
https://www.science.org/help/reprints-and-permissions

Supported by
日本財団
THE NIPPON
FOUNDATION

第 44 期　　研究者番号：G4410　　　　　　　　　作成日　：2023 年 3 月 6 日

氏　名	徐　勇	XU YONG	性別	M	生年月日　1990/05/04

所属機関（役職）	長崎大学大学院医歯薬学総合研究科（大学院生）
研究先（指導教官）	長崎大学原爆後障害医療研究所幹細胞生物学研究分野(原研幹細胞)(李 桃生　教授)
研究テーマ	ニカラベンによる間葉系幹細胞の放射線損傷の軽減 Nicaraven for attenuating the radiation-induced damage of Mesenchymal stem(stromal) cells
専攻種別	□論文博士　　　　　　　　　☑課程博士

研究者評価（指導教官記入欄）

成績状況	優	取得単位数
		取得単位数／取得すべき単位総数

学生本人が行った研究の概要	胸部の放射線がん治療に伴う肺傷害のメカニズムを解明し、新たな予防・治療の開発である。また、人工呼吸管理について、酸素吸入や換気量が肺傷害に与える影響を動物実験で調べている。

総合評価	【良かった点】 　ものことを真摯に取り組み、研究も順調に進んでいる。 　既に研究成果を出し、第一著者として論文２本を国際学術誌に採択・掲載され、もう１報が投稿中である。また、昨年に１回の学会発表もできた。現在も新たな研究テーマを取り組もうとしているところである。 【改善すべき点】 　特にない。 【今後の展望】 　今投稿中の論文を Revise し、また新たな研究テーマも来年度中に本格的に開始できると思われ、良い研究成果を期待したい。

学位取得見込	現在博士課程２年生であるが、既に多くの研究成果を出している。学位取得見込みは早期になる見通しで、2024 年 3 月になる予定である。

評価者（指導教官名）　　　李　桃生

第44期　　　　　研究者番号： G4410　　　　　作成日：2023年3月6日

氏名	徐 勇	XU YONG	性別	M	生年月日 1990/05/04
所属機関(役職)	長崎大学大学院医歯薬学総合研究科(大学院生)				
研究先(指導教官)	長崎大学原爆後障害医療研究所幹細胞生物学研究分野(原研幹細胞)(李 桃生 教授)				
研究テーマ	ニカラベンによる間葉系幹細胞の放射線損傷の軽減 Nicaraven for attenuating the radiation-induced injury of mesenchymal stromal cells				
専攻種別	論文博士		□	課程博士	☑

1．研究概要(1)

1）目的（Goal）
i. To investigate whether nicaraven can attenuate radiation-induced injury of MSCs.
ii.To understand the relevant molecular mechanisms on Nicaraven for attenuating radiation-induced injury of MSCs.
2）戦略（Approach）
　Adult C57BL/6 mice were exposed to 6 Gy X-ray thoracic radiation per day for 5 days (cumulative dose of 30 Gy) and nicaraven (50 mg/kg) or placebo was injected intraperitoneally in 5 min after each radiation exposure. We isolated mesenchymal stromal cells from lung tissue "explants" among groups on the day 1 and day 9 after treatments.Then we investigated whether niaraven can attenuate radiation-induced injury of MSCs.
3）材料と方法（Materials and methods）
1. Ex vivo expansion of MSCs from mouse lung tissue "explants".
　MSCs were expanded using a method as previously desrcibed (Ref.Figure 1B).
2. Detection of characterization of MSCs.
　IF stainging was performed to detect the expression levels of CD90,CD105,Pro-SPC,F4/80 in MSCs.
3. Evaluation of DNA damage of MSCs.
　To evaluate the DNA damage of MSCs,the expression levels of γ-H2AX and CD90 were estimated by immunostaining.
4. Evaluation of paracrine mechanisms of MSCs.
　ELISA was used to detect the growth factors of HGF,VEGF,SDF-1a and inflammatory factors of TGF-β1, CCL2, TNF-1a, IL-6 in conditioned medium from the supernatents of one passaged MSCs.

4）実験結果（Results）
1. Nicaraven administrations significantly restored the decreased outgrowth of MSCs and altered phenotypes caused by radiation exposure.
　At about day5 after the inition of culture, a layer of fibroblast-like cells started to outgrow from the tissue "explants"(Figure 1B). Our data showed that radiation exposure significantly decreased the outgrowth and numbers of MSCs, compared with CON group (P<0.01, Figure 1B). However, nicaraven administration slightly restored the outgrowth and numbers of MSCs (p<0.01, Figure 1B).
　MSCs expanded from lung tissues had been shown to be a mixed population. To examine whether radiation exposure would also change the phenotypic characterization of MSCs, we stained the one-passaged MSCs with a common lung stem cell marker of Pro-SPC, mesenchymal stem cell markers of CD90 and CD105, macrophages marker of F4/80. Compared with CON group, MSCs from the lung tissues of irradiated mice expressed significantly lower Pro-SPC, CD90, CD105 but higher F4/80 (P<0.01, Figure 2). However, the phenotype of lung cells in nicaraven administration groups were restored, which showed higher Pro-SPC, CD90, CD105 but lower F4/80 compared with S group (P < 0.01, Figure 2).
2. Nicaraven significantly attenuated radiation-induced DNA damage of mesenchymal stromal cells.
　Double staining was performed to detect the expression of DNA damage in lung cells, especially CD90-positive mesenchymal stromal cells. Compared to CON group, radiation exposure can not increase the formation of γ-H2AX foci in nuclei of lung cells (Figure 3A). Quanititative data also showed that the percentage of γ-H2AX-positive cells was not significantly changed in S group than CON group. Besides these, the perentage of γ-H2AX-positive cells was slightly increased after nicaraven administration (Figure 3). We then tried to evaluate the formation of γ-H2AX foci in CD90-positive mesenchymal stromal cells. Interestingly, the number of CD90-positive mesenchymal stromal cells with γ-H2AX foci was more effectively decreased in N group compared to IR+S group (Figure 3B,C). These results indicate that nicaraven administration can reduce the radiation-induced DNA damage in lung cells, especially in CD90-positive mesenchymal stromal cells (Figure 3).

3. Nicaraven administration significantly increased the production of growth factors in conditioned medium.

   The implantation of mesenchymal stromal cells for lung injury repair was generally thought to occur mainly through the paracrine mechanism. Therefore, we also examined whether the production of hepatocyte growth factor (HGF), vascular endothelial growth factor (VEGF), and stromal cell-derived factor 1a (SDF-1a) are secreted by mesenchymal stromal cells in conditioned medium, these important beneficial factors for lung tissue repair released by MSCs. Compared with CON group, MSCs isolated from the irradiated mice showed a significant decrease in the production of HGF, VEGF, and SDF-1a. However, nicaraven administration significantly increased the production of HGF, VEGF, and SDF-1a (Figure 3).

4. Nicaraven adminiatrion significantly decreased inflammatory factors levels in conditioned medium.

   MSCs are reported to secrete chemokines, cytokines, which appears to play a key role in repairing injured tissue caused by different pathological conditions. Therefore, we detected the changes of inflammatory factors in conditioned medium. Our data showed a significant increase in the production of TNF-a and CCL2 in the conditioned medium, which was decreased by nicaraven administration. Interestingly, nicaraven administration significantly increased the production of IL-6 in the conditioned medium. However, we cannot examine the significant changes in the production of TGF-β1 in the conditioned medium.
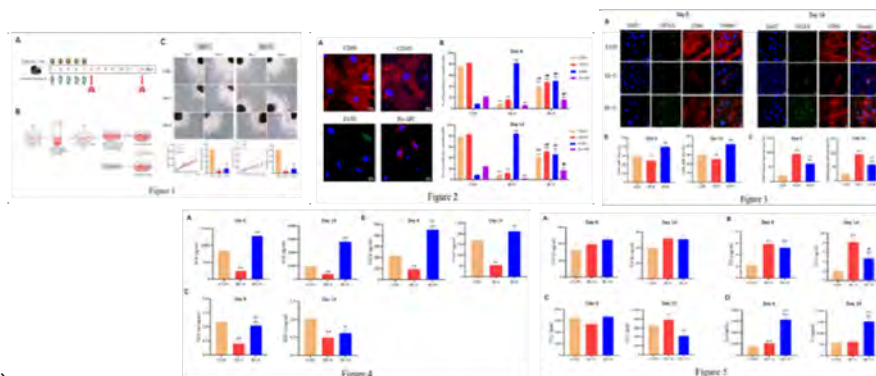
5）考察（Discussion）

   The use of radiation therapy to treat cancer inevitably involves exposure of normal tissues. Which can damage tissue homeostasis. Mesenchymal stromal cells (MSCs) residing in the lung are highly susceptible to radiation and are known to play critical roles in tissue homeostasis. In this study, we tried to primarily MSCs from lung tissues "explants" and then investigated whether nicaraven can attenuate the radiation-induced injury of MSCs, mainly focusing the quantity and quality of MSCs after nicaraven administrations. Our data indicated that nicaraven administration significantly restored the outgrowth of MSCs and their altered phenotypes caused by radiation exposure, clearly attenuated the radiation-induced DNA damage of MSCs. Besides these, nicaraven administration significantly increased the production of HGF,VEGF, SDF-1a, IL-6 and decreased the levels of TNF-a, CCL2 in the conditioned medium, suggesting the effectiveness of nicaraven for attenuating radiation-induced injury of MSCs.

   High ionizing radiation induces directly DNA double-strand breaks and triggers the release of ROS. The level of ROS overwhelms can cause DNA damage. Nicaraven has been well recognized on radical-specific scavenging properties and can attenuate radiation-induced DNA damage of lung tissue cells. we herein found that nicaraven can attenuate DNA damage of lung cells, especially the CD90-positive mesenchymal stromal cells.

   Repair of damaged tissues is a fundamental biological mechanism that allows the ordered replacement of dead or damaged cells after injury. Over the last few decades, advances have been reported in the use of mesenchymal stromal cells (MSCs) for lung tissue repair and regeneration. MSCs are highly metabolically active and their secretome gives rise to the same effects commonly described for the cells themselves. MSCs not only replace damaged lung epithelial cells but also promote tissue repair through the secretion of chemokines, cytokines, growth factors and paracrine molecules.

6）参考文献（References）

1. Henry E, Cores J, Hensley MT, Anthony S et.al. Adult Lung Spheroid Cells Contain Progenitor Cells and Mediate Regeneration in Rodents With Bleomycin-Induced Pulmonary Fibrosis. Stem Cells Transl Med. 2015 Nov;4(11):1265-74.
2. Sveiven SN, Nordgren TM. Lung-resident mesenchymal stromal cells are tissue-specific regulators of lung homeostasis. Am J Physiol Lung Cell Mol Physiol. 2020 Aug 1;319(2):L197-L210.
3. Wynn TA. Integrating mechanisms of pulmonary fibrosis. J Exp Med. 2011 Jul 4;208(7):1339-50.
4. Chen Y, Liu X, Tong Z. Mesenchymal Stem Cells in Radiation-Induced Pulmonary Fibrosis: Future Prospects. Cells. 2022 Dec 20;12(1):6.
5. Wang LK, Wu TJ, Hong JH et.al. Radiation Induces Pulmonary Fibrosis by Promoting the Fibrogenic Differentiation of Alveolar Stem Cells. Stem Cells Int. 2020 Sep 29;2020:6312053.
6. Zanoni M, Cortesi M, Zamagni A et.al. The Role of Mesenchymal Stem Cells in Radiation-Induced Lung Fibrosis. Int J Mol Sci. 2019 Aug 8;20(16):3876.

2. 執筆論文　Publication of thesis　※記載した論文を添付してください。Attach all of the papers listed below.

論文名 1 Title	Optimization on the dose and time of nicaraven administration for mitigating the side effects of radiotherapy in a preclinical tumor-bearing mouse model						
掲載誌名 Published journal	Theraputic Advances Respiratory Research						
	2022 年　12 月	16 巻(号)		頁 ～	頁	言語 Language	English
第1著者名 First author	Yong Xu	第2著者名 Second author		Lina Abdelghany	第3著者名 Third author		Reiko Sekiya
その他著者名 Other authors	Da Zhai, Keiichi Jingu, Tao-Sheng Li						
論文名 2 Title							
掲載誌名 Published journal							
	年　　月	巻(号)		頁 ～	頁	言語 Language	
第1著者名 First author		第2著者名 Second author			第3著者名 Third author		
その他著者名 Other authors							
論文名 3 Title							
掲載誌名 Published journal							
	年　　月	巻(号)		頁 ～	頁	言語 Language	
第1著者名 First author		第2著者名 Second author			第3著者名 Third author		
その他著者名 Other authors							
論文名 4 Title							
掲載誌名 Published journal							
	年　　月	巻(号)		頁 ～	頁	言語 Language	
第1著者名 First author		第2著者名 Second author			第3著者名 Third author		
その他著者名 Other authors							
論文名 5 Title							
掲載誌名 Published journal							
	年　　月	巻(号)		頁 ～	頁	言語 Language	
第1著者名 First author		第2著者名 Second author			第3著者名 Third author		
その他著者名 Other authors							

3. 学会発表 Conference presentation ※筆頭演者として総会・国際学会を含む主な学会で発表したものを記載してください

※Describe your presentation as the principal presenter in major academic meetings including general meetings or international meetin

学会名 Conference	日本放射線影響学会第65回大会							
演 題 Topic	Nicaraven attenuates radiation-induced lung injury by suppressing inflammatory response. Nicaravenは、炎症抑制により放射線肺損傷を軽減する							
開催日 date	2022 年 9 月 16 日		開催地 venue	大阪公立大学				
形式 method	☐ 口頭発表 Oral ☑ ポスター発表 Poster		言語 Language	☐ 日本語 ☑ 英語 ☐ 中国語				
共同演者名 Co-presenter	Taosheng Li							
学会名 Conference								
演 題 Topic								
開催日 date	年 月 日		開催地 venue					
形式 method	☐ 口頭発表 Oral ☐ ポスター発表 Poster		言語 Language	☐ 日本語 ☐ 英語 ☐ 中国語				
共同演者名 Co-presenter								
学会名 Conference								
演 題 Topic								
開催日 date	年 月 日		開催地 venue					
形式 method	☐ 口頭発表 Oral ☐ ポスター発表 Poster		言語 Language	☐ 日本語 ☐ 英語 ☐ 中国語				
共同演者名 Co-presenter								

4. 受賞（研究業績） Award (Research achievement)

名 称 Award name					
	国名 Country		受賞年 Year of award	年	月
名 称 Award name					
	国名 Country		受賞年 Year of award	年	月

5．本研究テーマに関わる他の研究助成金受給 Other research grants concerned with your resarch theme

受給実績 Receipt record	□ 有　　■ 無		
助成機関名称 Funding agency			
助成金名称 Grant name			
受給期間 Supported period	年　　　　　月 ～　　　　　年　　　　　月		
受給額 Amount received	円		
受給実績 Receipt record	□ 有　　■ 無		
助成機関名称 Funding agency			
助成金名称 Grant name			
受給期間 Supported period	年　　　　　月 ～　　　　　年　　　　　月		
受給額 Amount received	円		

6．他の奨学金受給 Another awarded scholarship

受給実績 Receipt record	□ 有　　■ 無
助成機関名称 Funding agency	
奨学金名称 Scholarship name	
受給期間 Supported period	年　　　　　月 ～　　　　　年　　　　　月
受給額 Amount received	円

7．研究活動に関する報道発表 Press release concerned with your research activities

※記載した記事を添付してください。Attach a copy of the article described below

報道発表 Press release	□ 有　　■ 無	発表年月日 Date of release	
発表機関 Released medium			
発表形式 Release method	・新聞　・雑誌　・Web site　・記者発表　・その他（　　　　　　　　　　　）		
発表タイトル Released title			

8．本研究テーマに関する特許出願予定 Patent application concerned with your research theme

出願予定 Scheduled	□ 有　　■ 無	出願国 Application	
出願内容（概要） Application contents			

9．その他 Others

指導責任者（記名）　李　桃生

Optimization on the dose and time of nicaraven administration for mitigating the side effects of radiotherapy in a preclinical tumor-bearing mouse model

Yong Xu, Lina Abdelghany, Reiko Sekiya, Da Zhai, Keiichi Jingu and Tao-Sheng Li [ID]

Abstract

Objective: Radiation-induced lung injury (RILI) is one of the serious complications of radiotherapy. We have recently demonstrated that nicaraven can effectively mitigate RILI in healthy mice. Here, we further tried to optimize the dose and time of nicaraven administration for alleviating the side effects of radiotherapy in tumor-bearing mice.

Methods and results: A subcutaneous tumor model was established in the back of the chest in C57BL/6N mice by injecting Lewis lung cancer cells. Therapeutic thoracic irradiations were done, and placebo or different doses of nicaraven (20, 50, 100 mg/kg) were administrated intraperitoneally pre-irradiation (at almost 5–10 min before irradiation) or post-irradiation (within 5 min after irradiation). Mice that received radiotherapy and nicaraven were sacrificed on the 30th day, but control mice were sacrificed on the 15th day. Serum and lung tissues were collected for evaluation. Nicaraven significantly decreased the level of CCL8, but did not clearly change the levels of 8-OHdG, TGF-β, IL-1β, and IL-6 in serum. Besides these, nicaraven effectively decreased the levels of TGF-β, IL-1β, and SOD2 in the lungs, especially by post-irradiation administration with the dose of 20 mg/kg. Although there was no significant difference, the expression of SOD1, 53BP1, and caspase 3 was detected lower in the lungs of mice received nicaraven post-irradiation than that of pre-irradiation.

Conclusion: According to our data, the administration of nicaraven at a relatively low dose soon after radiotherapy will be recommended for attenuating the side effects of radiotherapy.

Keywords: DNA damage, fibrosis, inflammatory response, lung injury, radiation

Correspondence to:
Tao-Sheng Li
Department of Stem Cell Biology, Atomic Bomb Disease Institute, Nagasaki University, 1-12-4 Sakamoto, Nagasaki 852-8523, Japan.

Department of Stem Cell Biology, Graduate School of Biomedical Sciences, Nagasaki University, Nagasaki, Japan
litaoshe@nagasaki-u.ac.jp

Yong Xu
Lina Abdelghany
Da Zhai
Department of Stem Cell Biology, Atomic Bomb Disease Institute, Nagasaki University, Nagasaki, Japan

Department of Stem Cell Biology, Graduate School of Biomedical Sciences, Nagasaki University, Nagasaki, Japan

Reiko Sekiya
Department of Stem Cell Biology, Atomic Bomb Disease Institute, Nagasaki University, Nagasaki, Japan

Keiichi Jingu
Department of Radiation Oncology, Graduate School of Medicine, Tohoku University, Sendai, Japan

Introduction

Radiotherapy is an essential tool for the treatment of intrathoracic malignancies, including lung, breast, and esophageal cancers.[1,2] Exposure of healthy tissues to radiation and the toxicity it causes often limits its effectiveness and decreases the survival benefit of radiotherapy. Beyond the systemic side effects, radiation-induced lung injury (RILI) is a serious obstacle to patients receiving radiotherapy for thoracic malignant tumors.[3,4] RILI occurs in 5–20% of lung cancer patients receiving radiotherapy, which may lead to the discontinuation of treatment. However, there are still no effective drugs and protective strategies to prevent radiation side effects in cancer patients undergoing radiotherapy.

It is well known that ionizing radiation induces directly DNA double-strand breaks and triggers the release of ROS.[5] The level of ROS overwhelms can cause oxidative damage to DNA, lipids, and proteins.[6] Although radiotherapy is a local therapy, it has systemic effects mainly influencing immune and inflammation processes.[7] Moreover, it has been demonstrated that radiation-induced injuries to tissue cells can promote

the release of a multitude of inflammatory cytokines and chemokines, which indirectly contribute to the consequent damage to cells and tissues and eventually culminate in fibrotic changes.[8–10] Therefore, the scavenging of ROS and the suppression of the inflammatory response are thought to be potential pharmacological interventions for mitigating the side effects of radiotherapy.

Many past studies have challenged to develop radioprotective agents. Thiol-synthetic compounds, such as amifostine has been approved to use clinically for protecting against radiation injury, however, amifostine has the disadvantages of toxicity and limited route of administration in the clinic.[11] Nitrogen oxides, such as Tempol, have also been tested as a radioprotectant, but its application is limited due to problems on producing hypotension and increasing heart rate.[12] Some natural antioxidants, such as vitamin E and selenium have also shown radioprotective effects, but the benefit of antioxidants for cancer radiotherapy is asked to be further confirmed because of the probable effect on radiosensitivity of cancer cells.[12,13] Therefore, there is still required to develop an ideal agent for mitigating the side effects of radiotherapy for cancer patients.

Nicaraven, a chemically synthesized hydroxyl radical-specific scavenger,[14] has previously been reported to protect against radiation-induced cell death.[14,15] Nicaraven can also reduce the radiation-induced recruitment of macrophages and neutrophils into irradiated lungs.[16] Moreover, we have recently demonstrated that nicaraven can also effectively protect against RILI by suppressing the inflammatory response.[17] To further develop for clinical application, we herein aim to optimize the dose and time of nicaraven administration for attenuating the side effects of radiotherapy.

Using a preclinical tumor-bearing mice model, we administered different doses of nicaraven, before or soon after thoracic irradiations. We then evaluated the systemic side effects and RILI, mainly by focusing on oxidative stress and inflammatory responses. According to our experimental data, the administration of nicaraven at a relatively low dose soon after radiotherapy will be recommended for attenuating the side effects of radiotherapy.

Materials and methods

Cancer cells and animals
Mouse Lewis lung cancer (LLC) cells were used for the experiments. The cells were maintained in DMEM (FUJIFILM Wako Pure Chemical Corporation), supplemented with 10% fetal bovine serum (Cytiva) and 1% penicillin/streptomycin (Gibco; Thermo Fisher Scientific, Inc.), and cultured at 37°C in a humidified incubator with 5% CO_2.

Male C57BL/6N mice (8 weeks old) were used for the study. Mice were housed in a pathogen-free room with a controlled environment under a 12-h light-dark cycle and maintained on laboratory chow, with free access to food and water. This study was approved by the Institutional Animal Care and Use Committee of Nagasaki University (No.1608251335-12). All animal procedures were performed in accordance with institutional and national guidelines.

Tumor-bearing mouse model, radiotherapy, and nicaraven administration
To match the pathological status of cancer patients, we used a preclinical tumor-bearing model for the experiment. Briefly, mice were subcutaneously inoculated with 5×10^5 LLC cells/0.1 ml of saline in the back of the chest. At 10 days after cancer cell inoculation, mice had randomly received radiotherapy and nicaraven administration as indicated in Figure 1(a). Considering the common clinical radiotherapy regimen for lung cancer and breast cancer,[18,19] thoracic irradiations (including the heart and lungs) were delivered to mice at a dosage rate of 1.0084 Gy/min (200 kV, 15 mA, 5 mm Al filtration, ISOVOLT TITAN320, General Electric Company, United States). Mice were intraperitoneally injected with 0 (placebo), 20, 50, 100 mg/kg nicaraven pre-irradiation (almost 5–10 min before irradiation) or post-irradiation (within 5 min after irradiation), respectively. Six mice without irradiation exposure were used as control ($n = 6$, Control group).

We measured the body weights of mice every other day. Mice that received radiotherapy and nicaraven were sacrificed on the 30th day, but the control mice were sacrificed on the 15th day. To collect serum, we took the blood from the inferior vena cava of mice under general anesthesia before

- 374-

sacrifice. Lung tissues were then excised and weighed. The collected serum and lung tissue samples were stored under −80°C, and used for experimental evaluations as follows.

ELISA
We measured the concentrations of 8-oxo-29-deoxyguanosine (8-OHdG), a marker of DNA oxidation in serum using an ELISA kit (Nikken SEIL Corporation, Shizuoka, Japan) according to the manufacturer's instructions. The mean values of duplicate assays with each sample were used for the statistical analyses.

ELISA kits (R&D Systems) were used to detect the contents of transforming growth factor β (TGF-β), interleukin-1beta (IL-1β), interleukin-6 (IL-6), C-C Motif Chemokine Ligand 8 (CCL8) in serum and lung tissues according to the manufacturer's instructions. Briefly, the lung tissues were homogenized using Multi-beads shocker® and added to the T-PER reagent (Thermo Fisher Scientific) consisting of proteinase and dephosphorylation inhibitors (Thermo Fisher Scientific). Then, lung lysates and serum were added to each well and measured per the manufacturer's instructions. The optical density of each well was measured at 450 nm using a microplate reader (Multiskan Fc, Thermo Fisher Scientific).

Western blot
Western blot was performed as previously described.[20] Briefly, total protein from the lung tissues was separated by SDS-PAGE gels and then transferred to 0.22-μm PVDF membranes (Bio-Rad). After blocking, the membranes were incubated with primary antibodies against SOD1 (1:500 dilution; cat. no. sc11407; Santa Cruz), SOD2 (1:500 dilution; cat. no. sc30080; Santa Cruz), β-actin (1:1,000 dilution; cat. no. 8457S; CST), 53BP1 (1:1,000 dilution; cat. no. ab36823; Abcam), caspase 3 (1:1,000 dilution; cat. no. 9662; CST), α-SMA (1:1,000 dilution; cat. no. 19245S; CST), collagen Ⅰ (1:1,000 dilution; cat. no. ab34710; Abcam), or α-Tubulin (1:1,000 dilution; cat. no. 3873S; CST) overnight at 4°C, respectively, followed by the appropriate horseradish peroxidase-conjugated secondary antibodies (Dako). The expression was visualized using an enhanced chemiluminescence detection kit (Thermo Scientific). Semiquantitative analysis was done using ImageQuant LAS 4000 mini (GE Healthcare Life Sciences).

Statistical analysis
All the values were presented as the mean ± SD. For comparison of multiple sets of data, one-way analysis of variance (ANOVA) followed by Tukey's test (Dr. SPSS II, Chicago, IL) was used for statistical analyses. All analyses were carried out with the SPSS19.0 statistical software (IBM SPSS Co., USA). A *p*-value less than 0.05 was accepted as significant.

Results

Nicaraven for mitigating the systemic side effects of radiotherapy is not very clearly detectable in tumor-bearing mice under our experimental treatment regimens
Mice had well tolerated the therapeutic regimens, but two mice in the post-irradiation administration with the dose of 20 mL/kg group died on the 9th and 10th days, and one mouse in the placebo group died on the 19th day during the follow-period (Figure 1(a)). Thoracic irradiation was delivered to mice using lead shielding sheets, and we found the death of mice at the next morning after radiation exposure. Radiation exposure to the brain stem may happen even only 1-mm positioning error. As a single 6 Gy exposure to the brain stem can kill some mice,[21] we speculated the death of mice should be an error exposure to the brain due to some positioning or shadowing problems of mice during thoracic exposure. The body weights of mice in all groups were decreased temporarily during radiotherapy, but tended to increase a few days after the stopping of irradiation exposures (Figure 1(b)). There was no significant difference on the body weight changes of mice among groups. Compared with the control mice, the lung weights were slightly increased in mice received placebo treatment after radiotherapy. However, the lung weights showed significantly lower in mice received nicaraven post-irradiation than that of placebo treatment (*p* < 0.05, Figure 1(c)).

ELISA was performed to detect the levels of 8-OHdG, TGF-β, IL-1β, IL-6, CCL8 in serum. The level of 8-OHdG in serum was not significantly different among groups (Figure 2(a)). However, the serum level of 8-OHdG was
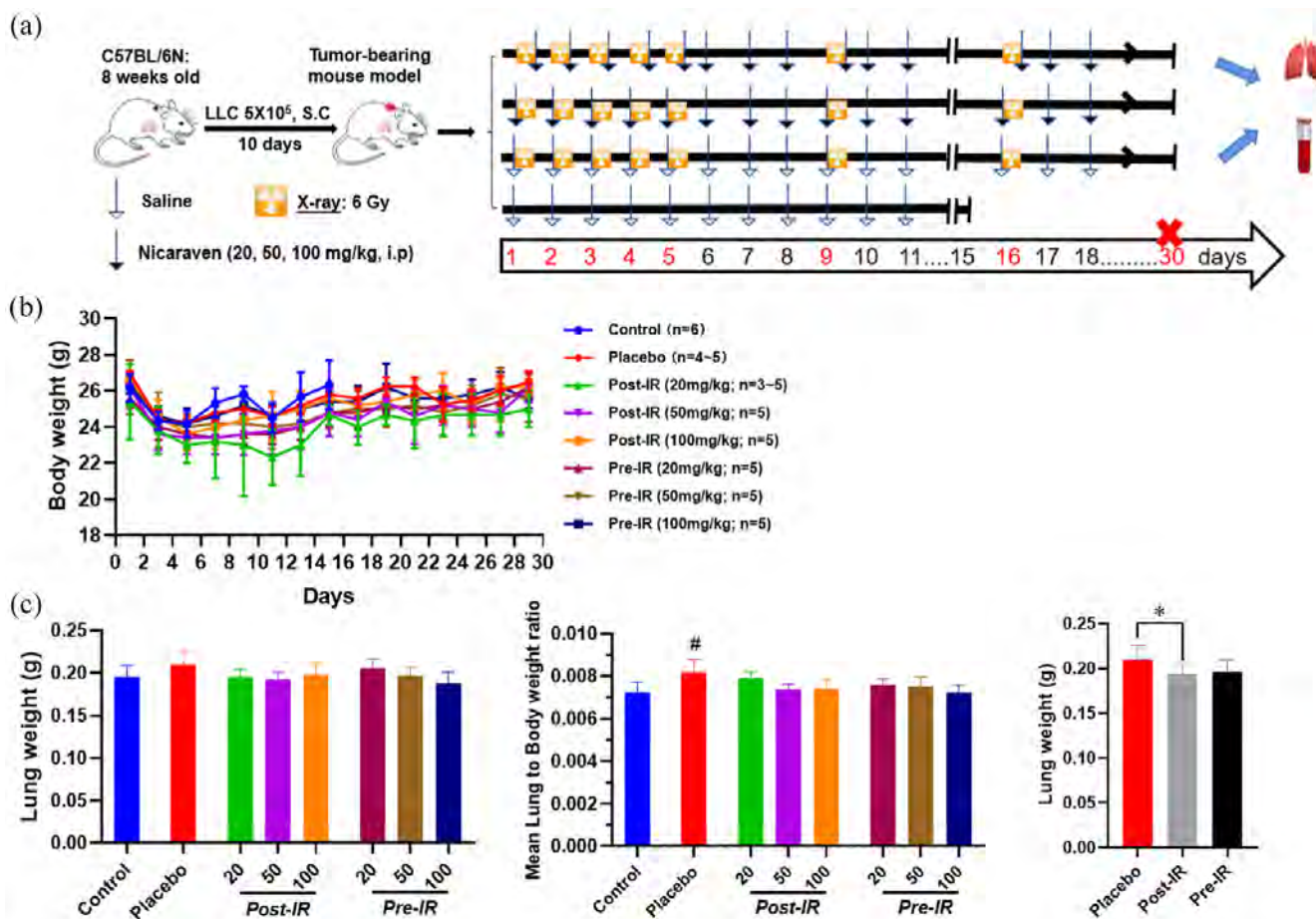
Figure 1. Changes of body weight and lung weight in mice. (a) Schematic diagram about the experimental timeline and protocol. (b) Quantitative data on the changes of body weights through 30 days. (c) Quantitative data on the changes of lung weight and lung to body weight ratio in mice. Data are represented as the means ± SD, $n=3\sim6$ in per group. $^{\#}p<0.05$ *versus* Control group, $*p<0.05$ *versus* Placebo group. IR, irradiation; Post-IR, post-irradiation; Pre-IR, pre-irradiation.

detected significantly lower in mice received nicaraven post-irradiation than that of pre-irradiation ($p<0.05$, Figure 2(a)). Our results also showed that the administration of nicaraven with any dose before or after irradiation did not clearly change the levels of TGF-β, IL-1β, IL-6 in serum. However, the level of CCL8 in serum was significantly lower in mice received nicaraven either post-irradiation or pre-irradiation when compared with mice received placebo treatment ($p<0.05$, Figure 2(e)).

The administration of nicaraven at a relatively low dose after radiotherapy shows partial attenuation of RILI in a preclinical tumor-bearing mouse model
To evaluate the inflammatory responses in lungs, ELISA analysis indicated that the TGF-β level in

lungs was slightly increased in mice received placebo treatment after thoracic radiation, but was effectively attenuated by post-irradiation administration with 20 mg/kg nicaraven ($p<0.05$, Figure 3(a)). Similarly, the IL-1β level in the lungs was also increased in mice that received placebo treatment after thoracic radiation, but significantly decreased by post-irradiation administration with 20 or 50 mg/kg nicaraven ($p<0.05$, Figure 3(b)). Strangely, it seems that post-irradiation administration with relatively lower doses of nicaraven more effectively alleviates the enhancement of TGF-β and IL-1β in lung tissues. However, the levels of IL-6 and CCL8 in the lungs were not significantly different among all groups (Figure 3(c), (d)).

The expression of SOD1 in lungs was detected higher by Western blot in the placebo group than
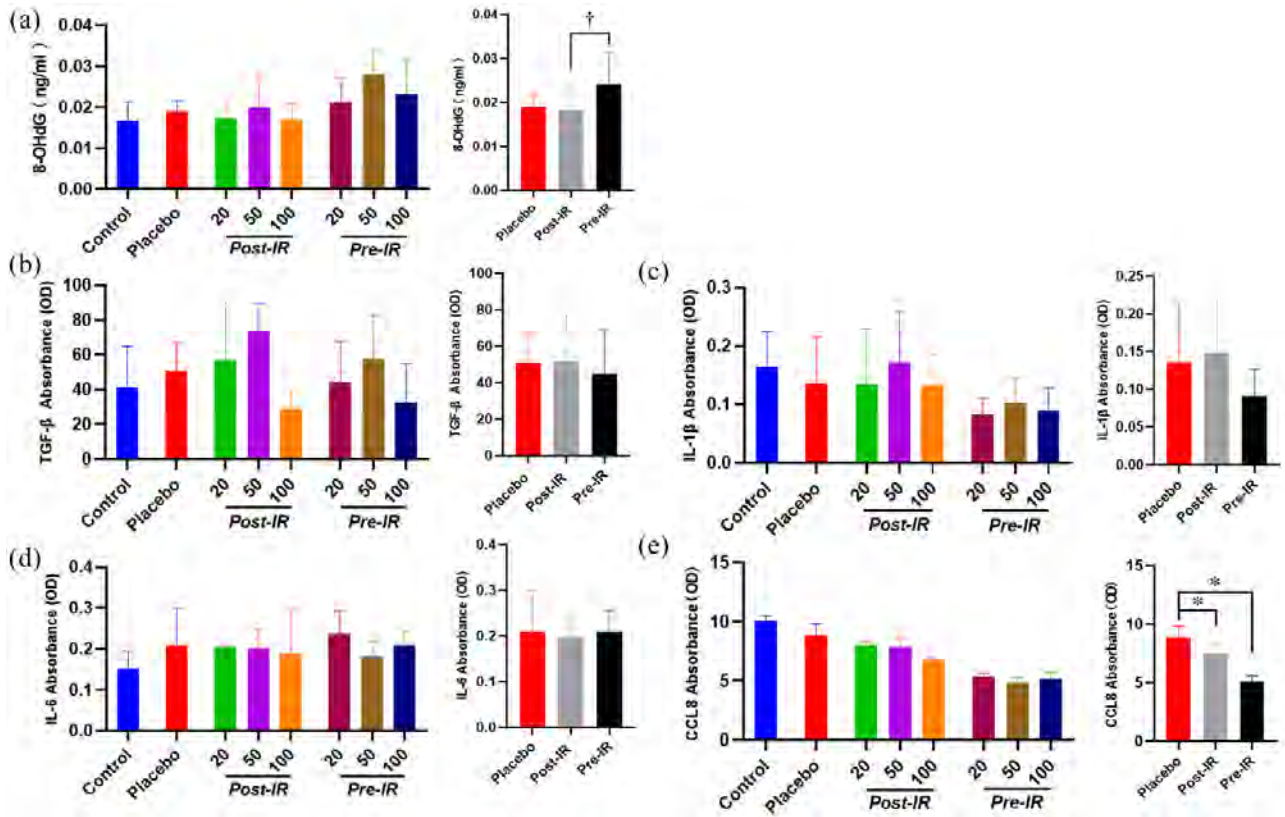
Figure 2. The effect of nicaraven on levels of 8-OHdG and inflammatory factors in serum.
Quantitative data on the levels of 8-OHdG (a), TGF-β (b), IL-1β (c), IL-6 (d), CCL8 (e). Data are represented as the means ± SD, *n*=3~6 in per group.
*$p<0.05$ *versus* Placebo group, †$p<0.05$ *versus* post-IR group.
IR: irradiation; Post-IR: post-irradiation; Pre-IR: pre-irradiation.
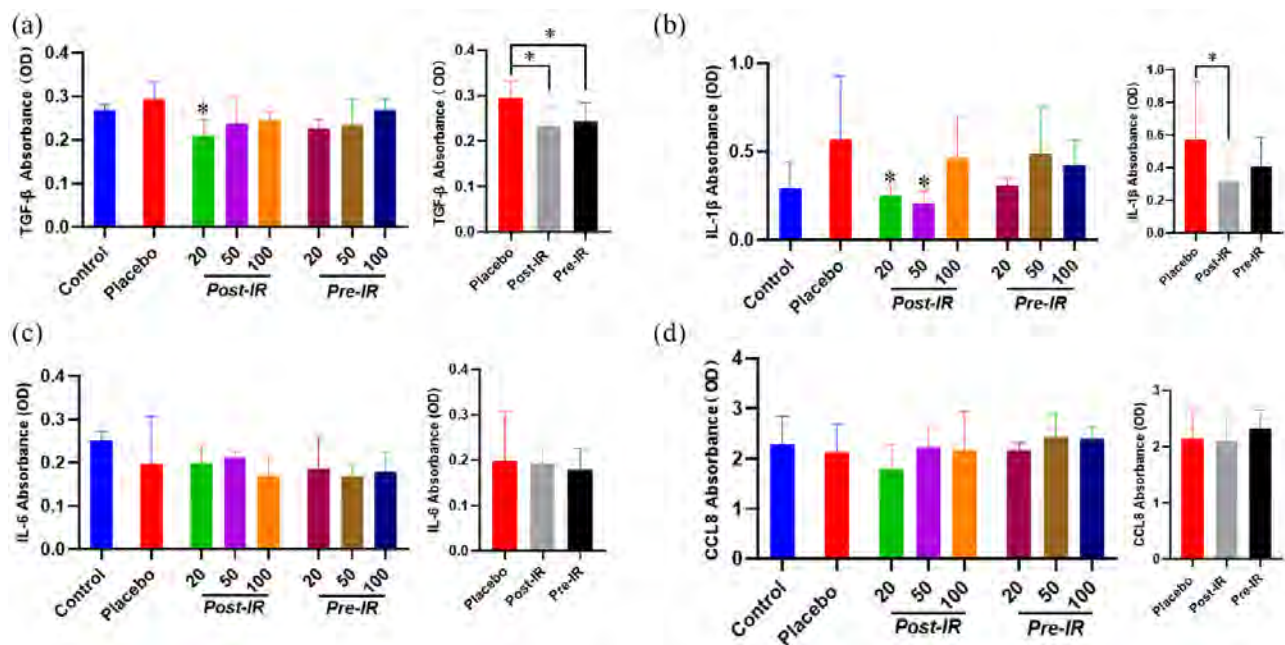
Figure 3. ELISA analysis on the inflammatory response in irradiated lungs. Quantitative data on the levels of TGF-β (a), IL-1β (b), IL-6 (c), CCL8 (d) in irradiated lung tissues were shown. Data are represented as the means ± SD, *n*=3~6 in per group. *$p<0.05$ *versus* Placebo group.
IR: irradiation; Post-IR: post-irradiation; Pre-IR: pre-irradiation.
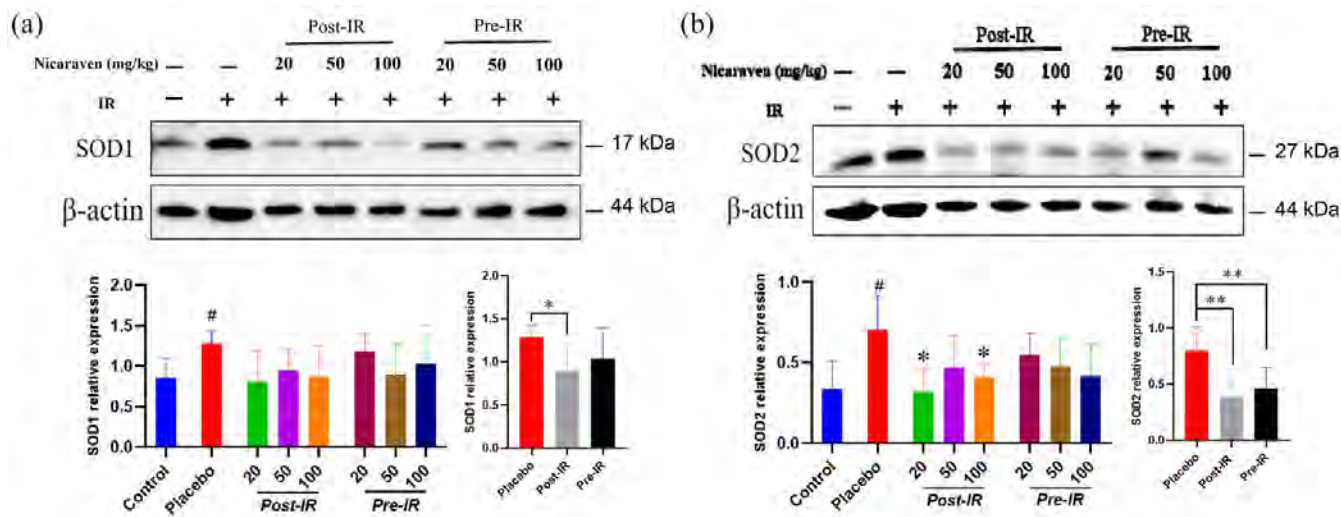
Figure 4. Nicaraven on attenuating oxidative response in irradiated lungs. Representative blots (up), and quantitative data (down) on the expression of SOD1 (a), SOD2 (b). Data are represented as the means ± SD, $n = 3$~6 in per group. #$p < 0.05$ *versus* Control group, *$p < 0.05$, **$p < 0.01$ *versus* Placebo group.
IR: irradiation; Post-IR: post-irradiation; Pre-IR: pre-irradiation.

the control group ($p < 0.05$, Figure 4(a)). Although there was no significant difference among all groups (Figure 4(a)), the increased expression of SOD1 in the lungs was effectively attenuated by post-irradiation administration ($p < 0.05$, Figure 4(a)). The expression of SOD2 was also significantly increased in the placebo group, but the increased expression of SOD2 was clearly decreased by post-irradiation administration with 20 or 100 mg/kg nicaraven ($p < 0.05$, Figure 4(b)). The enhanced expression of SOD2 in the lungs was effectively decreased by either post-irradiation or pre-irradiation administration ($p < 0.01$, Figure 4(b)).

We also measured the expression of 53BP1, a marker for DNA damage in lungs by Western blot. Post-irradiation administration of nicaraven showed to slightly decrease the 53BP1 expression in lungs (Figure 5(a)). Caspase 3 has been considered a key effector in inducing cell apoptosis. Compared with the control group without irradiation, Western blot analysis showed a significant enhancement on the expression of caspase 3 in lungs of mice from the placebo group ($p < 0.05$, Figure 5(b)), but the enhanced expression of caspase 3 in irradiated lungs was effectively attenuated only by post-irradiation administration of nicaraven ($p < 0.05$, Figure 5(b)).

We finally investigated the expression of α-SMA and collagen Ⅰ, the common markers of fibrosis in lungs. Compared with the control group, Western blot analysis showed higher expression of α-SMA and collagen Ⅰ in lungs of mice from the placebo group (Figure 6). Although there was no significant difference among groups, the enhanced expression of α-SMA and collagen Ⅰ in irradiated lungs was partially attenuated in mice that received post-irradiation administration of nicaraven (Figure 6).

Discussion

Radiotherapy for cancer is known to accompany side effects, which may lead to the discontinuation of treatment and decrease the quality of life of patients.[22] In this study, we investigated the optimal dose and time of nicaraven administration for attenuating the side effects of radiotherapy in tumor-bearing mice. We could not clearly detect significant changes on body weight and the levels of inflammatory cytokines in serum. However, nicaraven administration, especially with a relatively lower dose at the time soon after thoracic irradiations partially decreased the levels of TGF-β, IL-1β, SOD1, SOD2, and caspase 3 in lungs, suggesting the effectiveness of nicaraven for attenuating the side effects of radiotherapy.
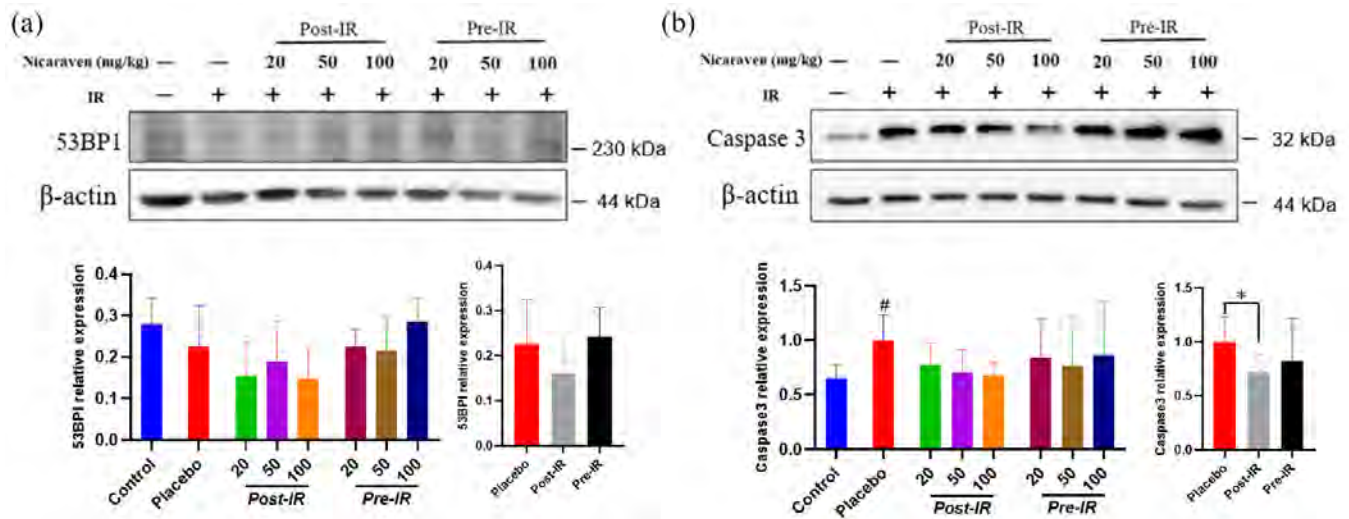
Figure 5. Western blot analysis on the expression of the DNA damage and cell apoptosis in irradiated lungs. Representative blots (up) and quantitative data (down) on the expression of 53BP1 (a), caspase 3 (b). Data are normalized to β-actin. Data are represented as the means ± SD, $n = 3{\sim}6$ in per group. #$p < 0.05$ *versus* Control group, *$p < 0.05$ *versus* Placebo group.
IR: irradiation; Post-IR: post-irradiation; Pre-IR: pre-irradiation.
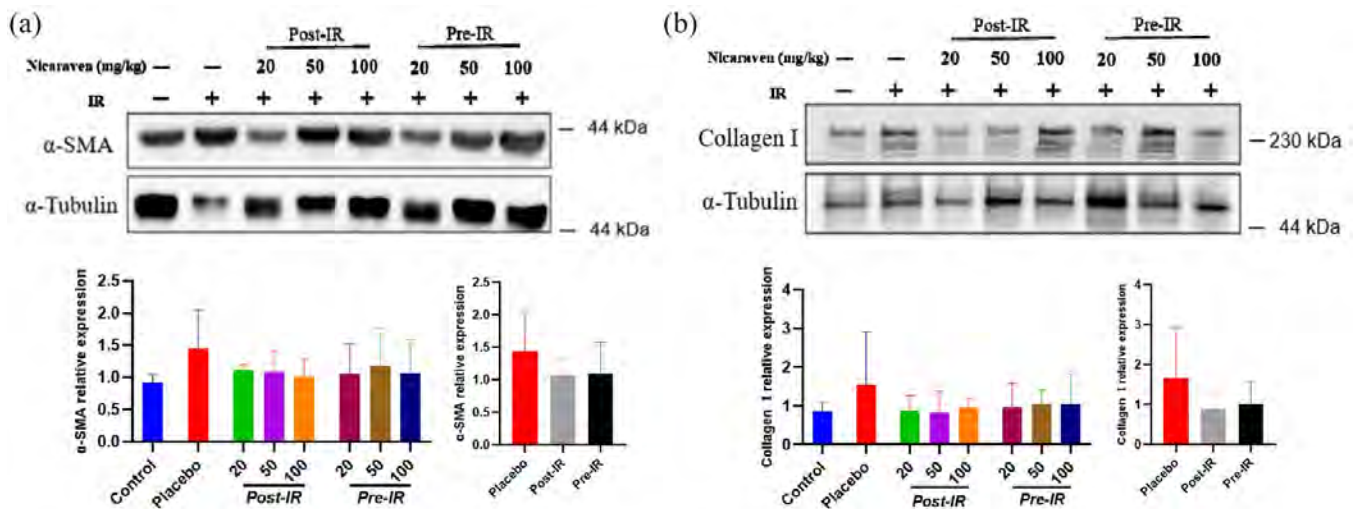
Figure 6. The fibrotic changes in irradiated lungs.
Representative blots (up) and quantitative data (down) on the expression of α-SMA (a), collagen Ⅰ (b) were shown. Data are normalized to α-Tubulin. Data are represented as the means ± SD, $n = 3{\sim}6$ in per group.
IR: irradiation; Post-IR: post-irradiation; Pre-IR: pre-irradiation.

Nicaraven has been well recognized on radical-specific scavenging property.[14] The 8-OHdG, an oxidized nucleoside of DNA has been frequently used as a marker for detecting oxidative stress.[23] However, consistent with our previous study,[24] nicaraven administration did not effectively decrease the level of 8-OHdG in serum in this study.

Radiation exposure results in the release of pro-inflammatory cytokines and chemokines.[8–10] Radiation-induced systemic and local inflammatory responses can be detected in the blood by an increased level of circulatory cytokines and the activation of immune cells.[7,25] However, we found that nicaraven administration did not significantly change the levels of TGF-β, IL-1β, and IL-6 in

serum. Several reasons can be considered for it. First, the sample number in each group was too small to detect a statistical significance. Second, the initial sizes of tumors were widely varied among animals and groups, which also resulted in large variations in measuring data. Third, we collected lungs and serum at 14 days after the last irradiation, which will be not a suitable time window for sensitive detection about the changes of 8-OHdG and inflammatory factors in serum. Otherwise, tumor-secreted factors might also be considered to affect the levels of cytokines and chemokines in serum,[26] but we did not find significant correlations between tumor weights and the levels of systemic inflammatory factors (data not shown).

Increasing evidence has shown that the release of a multitude of cytokines in response to radiation exposure can contribute to the damage to the cells/tissues.[22] Previous studies have demonstrated that RILI could be alleviated by blocking pro-inflammatory factors.[27,28] In this study, we observed that nicaraven partially attenuated the enhanced expression of TGF-β and IL-1β in the lungs, especially by post-irradiation administration with relatively low doses. We have not yet found a clear reason why post-irradiation administration with relatively lower doses of nicaraven even more effectively alleviates the enhancement of TGF-β and IL-1β in the irradiated lungs. Previous studies have well documented the harmless of nicaraven at the dose of 100 mg/kg in mice.[29] As VEGF level may increase in tumor-bearing mice, it is a possibility that a high dose of nicaraven increases the permeability of alveolar capillaries and cause edema of lungs in these tumor-bearing mice.

SOD1 and SOD2 are antioxidant enzymes, but their expression generally increases in response to oxidative stresses and various types of injuries.[6] Nicaraven partially attenuated the enhanced expression of SOD1 and SOD2 in irradiated lungs, especially by post-irradiation administration. Radiation can directly lead to cell death and apoptosis.[4,17] Nicaraven also partially decreased the expression of 53BP1 and caspase 3 in irradiated lungs, especially by post-irradiation administration. The main manifestations of the late stage of RILI are fibroblast proliferation and collagen deposition.[25] Post-irradiation administration of nicaraven partially decreased the expression of α-SMA and collagen Ⅰ in irradiated lungs.

This study has several limitations. First, we did not perform histopathological analysis on lungs. Second, we only used male mice for the experiment, but gender difference may affect radiation-induced outcomes.[30,31] Third, we could not provide data on the 8-OHdG level in lungs because of our technical mistake. Otherwise, due to the small sample size and large individual variation, there was no statistically significance on the expression of α-SMA and collagen I in lungs among groups. Although we have already planned a phase I-II clinical trial in esophageal cancer patients who receiving radiotherapy, the benefit of nicaraven administration will be needed to be further confirmed before clinical application for cancer radiotherapy.

According to our experimental evaluations in a preclinical tumor-bearing mouse model, nicaraven seems to effectively attenuate the side effects of radiotherapy. As nicaraven has a very limited effect on the growth of established tumors,[16] nicaraven may be useful for mitigating the side effects of radiotherapy in cancer patients, and post-irradiation administration with a relatively low dose will be highly recommended.

Declarations

Author contributions
Yong Xu: Data curation; Investigation; Methodology; Writing – original draft; Writing – review & editing.

Lina Abdelghany: Data curation; Investigation; Writing – review & editing.

Reiko Sekiya: Data curation; Investigation.

Da Zhai: Data curation; Writing – review & editing.

Keiichi Jingu: Conceptualization.

Tao-Sheng Li: Conceptualization; Data curation; Investigation; Methodology; Resources; Supervision; Writing – review & editing.

ORCID iD
Tao-Sheng Li [iD] https://orcid.org/0000-0002-7653-8873

References

1. Giuranno L, Ient J, De Ruysscher D, *et al.* Radiation-induced lung injury (RILI). *Front Oncol* 2019; 9: 877.

2. Kim H, Park SH, Han SY, *et al.* LXA4-FPR2 signaling regulates radiation-induced pulmonary fibrosis via crosstalk with TGF-β/Smad signaling. *Cell Death Dis* 2020; 11: 653.

3. Bickelhaupt S, Erbel C, Timke C, *et al.* Effects of CTGF blockade on attenuation and reversal of radiation-induced pulmonary fibrosis. *J Natl Cancer Inst* 2017; 109: 8.

4. McBride WH and Schaue D. Radiation-induced tissue damage and response. *J Pathol* 2020; 250: 647–655.

5. Huang L, Snyder AR and Morgan WF. Radiation-induced genomic instability and its implications for radiation carcinogenesis. *Oncogene* 2003; 22: 5848–5854.

6. Nakane M. Biological effects of the oxygen molecule in critically ill patients. *J Intensive Care* 2020; 8: 95.

7. Formenti SC and Demaria S. Systemic effects of local radiotherapy. *Lancet Oncol* 2009; 10: 718–726.

8. Jin H, Yoo Y, Kim Y, *et al.* Radiation-induced lung fibrosis: preclinical animal models and therapeutic strategies. *Cancers (Basel)* 2020; 12: 1561.

9. Kainthola A, Haritwal T, Tiwari M, *et al.* Immunological aspect of radiation-induced pneumonitis, current treatment strategies, and future prospects. *Front Immunol* 2017; 8: 506.

10. Im J, Lawrence J, Seelig D, *et al.* FoxM1-dependent RAD51 and BRCA2 signaling protects idiopathic pulmonary fibrosis fibroblasts from radiation-induced cell death. *Cell Death Dis* 2018; 9: 584.

11. Weiss JF and Landauer MR. History and development of radiation-protective agents. *Int J Radiat Biol* 2009; 85: 539–573.

12. Hahn SM, Krishna MC, DeLuca AM, *et al.* Evaluation of the hydroxylamine Tempol-H as an in vivo radioprotector. *Free Radic Biol Med* 2000; 28: 953–958.

13. Hosseinimehr SJ. Trends in the development of radioprotective agents. *Drug Discov Today* 2007; 12: 794–805.

14. Akimoto T. Quantitative analysis of the kinetic constant of the reaction of N, N -propylenedini-cotinamide with the hydroxyl radical using dimethyl sulfoxide and deduction of its structure in chloroform. *Chem Pharm Bull (Tokyo)* 2000; 48: 467–476.

15. Watanabe M, Akiyama N, Sekine H, *et al.* Inhibition of poly (ADP-ribose) polymerase as a protective effect of nicaraven in ionizing radiation- and ara-C-induced cell death. *Anticancer Res* 2006; 26(5A): 3421–3427.

16. Yan C, Luo L, Urata Y, *et al.* Nicaraven reduces cancer metastasis to irradiated lungs by decreasing CCL8 and macrophage recruitment. *Cancer Lett* 2018; 418: 204–210.

17. Xu Y, Zhai D, Goto S, *et al.* Nicaraven mitigates radiation-induced lung injury by downregulating the NF-κB and TGF-β/Smad pathways to suppress the inflammatory response. *J Radiat Res* 2022; 2022; rrab112.

18. Kepka L and Socha J. Dose and fractionation schedules in radiotherapy for non-small cell lung cancer. *Transl Lung Cancer Res* 2021; 10: 1969–1982.

19. Shah BA, Xiao J, Oh C, *et al.* Five-fraction prone accelerated partial breast irradiation: long-term

oncologic, dosimetric, and cosmetic outcome. *Pract Radiat Oncol* 2022; 12: 106–112.

20. Doi H, Kitajima Y, Luo L, *et al*. Potency of umbilical cord blood- and Wharton's jelly-derived mesenchymal stem cells for scarless wound healing. *Sci Rep* 2016; 6: 18844.

21. Yang L, Yang J, Li G, *et al*. Pathophysiological responses in rat and mouse models of radiation-induced brain injury. *Mol Neurobiol* 2017; 54: 1022–1032.

22. Hanania AN, Mainwaring W, Ghebre YT, *et al*. Radiation-induced lung injury: assessment and management. *Chest* 2019; 156: 150–162.

23. Valavanidis A, Vlachogianni T and Fiotakis C. 8-hydroxy-2′-deoxyguanosine (8-OHdG): a critical biomarker of oxidative stress and carcinogenesis. *J Environ Sci Health C Environ Carcinog Ecotoxicol Rev* 2009; 27: 120–139.

24. Kawakatsu M, Urata Y, Imai R, *et al*. Nicaraven attenuates radiation-induced injury in hematopoietic stem/progenitor cells in mice. *PLoS ONE* 2013; 8: e60023.

25. Mavragani IV, Laskaratou DA, Frey B, *et al*. Key mechanisms involved in ionizing radiation-induced systemic effects. A current review. *Toxicol Res (Camb)* 2015; 5: 12–33.

26. Singh M, Tian XJ, Donnenberg VS, *et al*. Targeting the temporal dynamics of hypoxia-induced tumor-secreted factors halts tumor migration. *Cancer Res* 2019; 79: 2962–2977.

27. Li W, Lu L, Liu B, *et al*. Effects of phycocyanin on pulmonary and gut microbiota in a radiation-induced pulmonary fibrosis model. *Biomed Pharmacother* 2020; 132: 110826.

28. Chen B, Na F, Yang H, *et al*. Ethyl pyruvate alleviates radiation-induced lung injury in mice. *Biomed Pharmacother* 2017; 92: 468–478.

29. Zhang X, Moriwaki T, Kawabata T, *et al*. Nicaraven attenuates postoperative systemic inflammatory responses-induced tumor metastasis. *Ann Surg Oncol* 2020; 27: 1068–1074.

30. Özdemir BC, Csajka C, Dotto GP, *et al*. Sex differences in efficacy and toxicity of systemic treatments: an undervalued issue in the era of precision oncology. *J Clin Oncol* 2018; 36: 2680–2683.

31. Narendran N, Luzhna L and Kovalchuk O. Sex difference of radiation response in occupational and accidental exposure. *Front Genet* 2019; 10: 260.

日中笹川医学奨学金制度（学位取得コース）中間評価書
課程博士：指導教官用

Supported by
THE NIPPON FOUNDATION

氏　名	李 佩霖	LI PEILIN	性別	M	生年月日	1994/08/21
所属機関（役職）	長崎大学大学院医歯薬学総合研究科（大学院生）					
研究先（指導教官）	長崎大学大学院医歯薬学総合研究科医療学専攻移植・消化器外科学（江口 晋　教授）					
研究テーマ	小分子誘導肝前駆細胞（CLiP）からの 3D 胆管形成 3D bile duct formation from small molecule induced liver progenitor cells(CLiPs)					
専攻種別	☐論文博士			☑課程博士		

研究者評価（指導教官記入欄）

成績状況	㊥　良　可　不可 学業成績係数=	取得単位数 6 ／ 30

<table>
<tr>
<td>学生本人が行った
研究の概要</td>
<td>

Summary:

we formed the functional bile duct from hCLiPs induced from hMHs by molecules combination with FBS. These hCLiPs expressed typical HPCs markers EpCAM, KRT-19, SOX-9, CD133 and gradually downregulated hMHs markers ALB, CYP7A1, and HNF4A during induction. These purified hCLiPs were then used to induce the generation of a 3D bile duct-like structure with lumens in a 3D culture environment with MEF. The bile duct expressed typical biliary epithelial cell markers CK-7, GGT1, CFTR and EpCAM and it had the ability to transport the bile-like substance rhodamine 123 into the lumen of the bile duct. Subsequently, bile ducts were co-cultured with hMHs for two days and bile salt analogues,CLF, were transported into bile duct and aggregate within the lumen from culture medium through the hMHs. The integrated tissue expressed the bile bile canaliculi marker and transporter protein.

</td>
</tr>
<tr>
<td>総合評価</td>
<td>

【良かった点】
　与えられたテーマに沿って、研究プロトコルを作成し、ロードマップに沿って研究を実行できている。
　実験のための手技獲得もしっかりとできている。
　また、英語、日本語を通じて、指導教官と良好なコミュニケーションもとることができる。
　現在の研究進捗を英語と用いてプレゼンテーションを行なうことができる。

【改善すべき点】
　日本語によるコミュニケーション、もしくはプレゼンテーションの工場があれば、尚よろしいかと考える。

【今後の展望】
Next step:
1.　　　To finish and revise the manuscript and then submit.
2.　　　Construction of a drug assay system combined with inhibitors.

</td>
</tr>
<tr>
<td>学位取得見込</td>
<td>

2025 年 10 月あたり
十分に期間内に取得可能と考える。

</td>
</tr>
</table>

評価者（指導教官名）　江口　晋

日中笹川医学奨学金制度(学位取得コース)中間報告書
研究者用

Supported by
日本財団
THE NIPPON
FOUNDATION

第44期		研究者番号： G4411		作成日：2023年3月6日	
氏名	李 佩霖	LI PEILIN	性別	M	生年月日 1994/08/21
所属機関(役職)	長崎大学大学院医歯薬学総合研究科（大学院生）				
研究先(指導教官)	長崎大学大学院医歯薬学総合研究科医療学専攻移植・消化器外科学（江口 晋 教授）				
研究テーマ	小分子誘導肝前駆細胞（CLiP）からの3D胆管形成 3D bile duct formation from small molecule induced liver progenitor cells(CLiPs)				
専攻種別	論文博士		□	課程博士	☑

1．研究概要(1)

1）目的（Goal）
The intrahepatic bile ducts (BDs) play an important role in the modification and transport of bile, and the integration between the bile duct and hepatocytes is the basis of liver function. However, the lack of a source of cholangiocytes limits in vitro research. The aim of the present study was to establish three-dimensional BDs combined with hMHs in vitro using chemically induced human liver progenitor cells (hCLiPs) derived from human mature hepatocytes (hMHs).

2）戦略（Approach）
After using human-derived mature liver cell small molecule compounds to induce hepatic progenitor cells (hCLiPs), seed hCLiPs on mouse-derived MEF cells, use induction medium to induce hCLiPs into bile duct epithelial-like cells, and culture in 3D induction Induced culture into 3D bile duct structure. Subsequently, mature liver cells were inoculated to verify the bile collection and excretion functions of the bile ducts.

3）材料と方法（Materials and methods）
Cell culture and conversion
Human Cryo-Hepatocytes (CHHs) (Lot.416, Corning) were seeded into collagen type-I-coated dishes (Asahi Techno Glass, Tokyo, Japan) at a density of 2×10^4 cells/cm2 in STIM medium for promoting attaching to the plate surface. The STIM medium was a hepatocyte culture media kit with 10 10 ng/μL epidermal growth factor (EGF) containing 1x penicillin-streptomycin-glutamine (100X) (Gibco™) and 10% fetal bovine serum (FBS, Gibco™). 4 hours later, the culture medium was changed to the small chemically reprogramming culture medium. The small chemical reprogramming culture medium was DMEM/F12 containing 2.4g/L NaHCO3 and L-glutamine (Life Technologies) and supplemented with 5 mM HEPES, 30 mg/L L-proline, 0.05% BSA, 10 ng/mL EGF (all from Sigma-Aldrich Japan, Tokyo, Japan), insulin-transferrin-serine (ITS)-X (Life Technologies), $10-7$ M dexamethasone (Dex) (Fuji Pharma Co. Ltd., Tokyo, Japan), 10mM nicotinamide (Sigma-Aldrich Japan), 1mM ascorbic acid-2 phosphate (Wako Pure Chemical), 100 U/mL penicillin, and 100 mg/mL streptomycin (Life Technologies) in addition to two small chemical molecules of 0.5 μM A-83-01 (Wako Pure Chemical), 3 μM CHIR99021 (AdooQ BioScience) and 10% FBS, which would be called FAC medium. The culture medium was changed 1 day after seeding and every two/three day thereafter. It takes 14-16 days to generate hCLiPs up to 90% conference from CHHs.
Human bile duct formation from hCLiPs
The BDs were differentiated and formation from hCLiPs as reported [20]. Briefly, 1-2 days before collecting the hCLiPs suspension, we used embryonic fibroblast feeder cells (MEF) (Cat #PMEF-N, Merck Millipore) to form a MEF feeder layer by seeding $1-2 \times 10^5$ cells on collagen-coated 12-well-plates (around 3×10^4 cells/cm2) in DMEM containing 10% FBS. We plated the dissociated hCLiPs suspension onto the MEF feeder layer at a density of $4-5 \times 10^5$ cells/well (1.2×10^5 cells/cm2) in FAC medium for cell attachment for 1 day. Thereafter, we replaced the medium with BECs induction medium (BIM), which was mTeSR™1 Complete Kit (Catalog #85850, STEMCELL Technologies) included mTeSR™1 basal medium supplemented with TeSR™1 5X supplement, and in addition three small chemical molecules of 10 μM Y-27632, 0.5 μM A-83-01, 3 μM CHIR99021, and probably hepatocyte grow factor (HGF, Sigma-Aldrich Japan, Tokyo, Japan) and EGF, every 2 days for 6 days, followed by BIM supplemented with 2% growth factor reduced Matrigel (Catlog 354230, Corning, Bedford, USA) for an additional 6-10 days, to facilitate the maturation of BECs and the formation of the biliary structures.
Integrated bile duct structure to human hepatocytes
We plated CHHs onto the three-dimensional BDs at a density of 1×10^5 cells/12-well plate (2.5×10^4 cells/cm2) for 1 day in hepatocyte-defined medium (Catlog 05449, Corning, Bedford, USA) supplemented with 10 μg/ml EGF and 10% FBS. We then replaced it with BIM supplemented with 2% Matrigel for another 2-4 days. The bile duct was automatically attached with hepatocytes with bile canaliculi to the biliary cells.

4）実験結果（Results）

Here, we formed the functional BDs from the hCLiPs using hepatocyte growth factor and extracellular matrix. The BDs expressed the typical biliary markers CK-7, GGT1, CFTR and EpCAM and were able to transport the bile-like substance rhodamine 123 into the lumen. The established three-dimensional BDs were co-cultured with hMHs. These cells were able to bind to the bile ducts and the bile acid analogue CLF was transported from the culture medium through the hMHs and accumulated into the lumen of the BDs. The BDs generated from the hCLiPs showed the function of the bile ducts and a physiological system such as the transport of bile within the liver when they were connected to the hMHs.

1.Phase image and RT-qPCR showed that the FAC can successfully induce cryohepatocytes to human CLiPs.

2.Inducing human CLiPs to cholangiocytes and formation of the 3D bile duct structures：the combination of MEF feeder cells and Matrigel can induce the human CLiPs to cholangiocytes and form some 3D bile duct structure, which had positive expressions of biliary genes and concentration of Rhodamine123 in BIM medium with HGF.

3.The BIM+HGF had higher efficiency for the formation of the bile duct from hCLiPs compared with the other conditions.

4.The integrated bile-hepatocyte tissue expressed the bile acid transporter proteins and accumulated CLF into biliary lumen from the culture medium via hepatocytes canaliculi.

5）考察（Discussion）

The small molecule combination could convert the MHs into the LPCs, which had resemble unlimited self-renewal capacity and could be induced to differentiate into both MHs and BECs [25-27]. In the present study, we established functional BDs from hCLiPs induced hMHs by the application of small molecule compounds and FBS. These hCLiPs expressed key markers of LPCs such as EpCAM, KRT-19, SOX-9 and CD133, and gradually decreased the expression of hepatocyte markers such as ALB, CYP7A1 and HNF4A during the induction process. The purified hCLiPs were then used to form the three-dimensional structure with lumens in a three-dimensional culture environment in the presence of MEF. The established BDs expressed characteristic biliary markers such as CK-7, GGT1, CFTR and EpCAM and were able to transport the bile substance rhodamine 123 into the lumen of the BDs. When co-cultured with hMHs for two days, BDs were able to transport bile salt analogues CLF from the culture medium into the lumen of the bile ducts through the MHs. These results demonstrate the functional properties of BECs and the physiological nature of bile transport in the liver, providing a valuable tool for the study of bile transport and metabolism and related diseases. In addition, this tissue-engineered model holds promise for the development of in vitro disease models and drug screening.

Previous studies have explored the use of human BECs in vitro, however, their practical application has been limited by a number of factors. The low proportion of BECs in the liver, difficulties in isolation, scarcity of donors, and ethical concerns have all acted as hindrances to direct utilization of BECs [8, 15, 40]. The use of small molecules to induce mature cell dedifferentiation has gained increased attention in recent times. Unlike iPSCs, small molecule combinations do not alter the genetic sequence of the cell, but instead manipulate cell fate through alterations in the cell's epigenetics, offering a straightforward and highly controllable approach [41-44]. Induction of totipotent or pluripotent stem cells using small molecules has significantly advanced the field of regenerative medicine. The hCLiPs, derived from patients' primary human hepatocytes, display regenerative and metabolic capabilities and hold potential for cell therapy in cases of end-stage liver disease. This not only alleviates the shortage of organs and reduces the risk of immune rejection, but also overcomes the limitation of cell availability in regenerative medicine research. For instance, the three-dimensional BDs generated from the hCLiPs demonstrated in vitro properties that resemble the intrahepatic bile ducts, including the transport of the bile analogs CLF and rhodamine-123. Ramli et al. demonstrated the generation of a human hepatic organoid from iPSCs, in which the cells underwent progressive differentiation into hepatocytes and cholangiocytes within approximately 50 days of culture [17]. While their approach required a long culture period and the use of a complex medium containing multiple growth factors, our method for generating functional BDs from hCLiPs is more straightforward, cost-effective, and safe, requiring only two weeks from the hCLiPs stage and minimal medium adjustments.

6）参考文献（References）

1.O'Hara, S.P., et al., The dynamic biliary epithelia: Molecules, pathways, and disease. Journal of Hepatology, 2013. 58(3): p. 575–582.

2.Tanimizu, N., et al., Hepatic biliary epithelial cells acquire epithelial integrity but lose plasticity to differentiate into hepatocytes in vitro during development. Journal of Cell Science, 2013. 126(22): p. 5239–5246.

3.Alpini, G., J.M. McGill, and N.F. LaRusso, The pathobiology of biliary epithelia. Hepatology, 2002. 35(5): p. 1256–1268.

4.Vroman, B. and N.F. LaRusso, Development and characterization of polarized primary cultures of rat intrahepatic bile duct epithelial cells. Laboratory Investigation, 1996. 74(1): p. 303–313.

5.Itoh, T., Stem/progenitor cells in liver regeneration. Hepatology, 2016. 64(2): p. 663–8.

6.Yoon, Y.B., et al., Effect of side-chain shortening on the physiologic properties of bile acids: hepatic transport and effect on biliary secretion of 23-nor-ursodeoxycholate in rodents. Gastroenterology, 1986. 90(4): p. 837–52.

7.Lazaridis, K.N. and N.F. LaRusso, The Cholangiopathies. Mayo Clinic Proceedings, 2015. 90(6): p. 791–800.

8.Katayanagi, K., N. Kono, and Y. Nakanuma, Isolation, culture and characterization of biliary epithelial cells from different anatomical levels of the intrahepatic and extrahepatic biliary tree from a mouse. Liver, 1998. 18(2): p. 90–8.

9.Xu, X., et al., High-throughput bioengineering of homogenous and functional human-induced pluripotent stem cells-derived liver organoids via micropatterning technique. Front Bioeng Biotechnol, 2022. 10: p. 937595.

10.Park, Y., et al., Three-Dimensional Organoids as a Model to Study Nonalcoholic Fatty Liver Disease. Semin Liver Dis, 2022. 42(4): p. 423–433.

11.Kim, H., et al., Development of human pluripotent stem cell-derived hepatic organoids as an alternative model for drug safety assessment. Biomaterials, 2022. 286: p. 121575.

12.Olgasi, C., A. Cucci, and A. Follenzi, iPSC-Derived Liver Organoids: A Journey from Drug Screening, to Disease Modeling, Arriving to Regenerative Medicine. Int J Mol Sci, 2020. 21(17).

13.Wang, X., et al., Generation of liver bipotential organoids with a small-molecule cocktail. J Mol Cell Biol, 2020. 12(8): p. 618–629.

14.Aizarani, N., et al., A human liver cell atlas reveals heterogeneity and epithelial progenitors. Nature, 2019. 572(7768): p. 199–204.

15.Chen, C., et al., Bioengineered bile ducts recapitulate key cholangiocyte functions. Biofabrication, 2018. 10(3): p. 034103.

16.Carberry, C.K., et al., Using liver models generated from human-induced pluripotent stem cells (iPSCs) for evaluating chemical-induced modifications and disease across liver developmental stages. Toxicol In Vitro, 2022. 83: p. 105412.

17.Ramli, M.N.B., et al., Human Pluripotent Stem Cell-Derived Organoids as Models of Liver Disease. Gastroenterology, 2020. 159(4): p. 1471–1486 e12.

18.Si-Tayeb, K., F.P. Lemaigre, and S.A. Duncan, Organogenesis and development of the liver. Dev Cell, 2010. 18(2): p. 175–89.

19.Huang, Y., et al., Differentiation of chemically induced liver progenitor cells to cholangiocytes: Investigation of the optimal conditions. Journal of Bioscience and Bioengineering, 2020. 130(5): p. 545–552.

20.Huang, Y., et al., Bioengineering of a CLiP-derived tubular biliary-duct-like structure for bile transport in vitro. Biotechnology and Bioengineering, 2021. 118(7): p. 2572–2584.

21.Tian, L., et al., Efficient and Controlled Generation of 2D and 3D Bile Duct Tissue from Human Pluripotent Stem Cell-Derived Spheroids. Stem Cell Rev Rep, 2016. 12(4): p. 500–8.

22.Tanimizu, N., A. Miyajima, and K.E. Mostov, Liver progenitor cells develop cholangiocyte-type epithelial polarity in three-dimensional culture. Mol Biol Cell, 2007. 18(4): p. 1472–9.

23.Velazquez, J.J. and M.R. Ebrahimkhani, Cholangiocyte organoids as a cell source for biliary repair. Transpl Int, 2021. 34(6): p. 999–1001.

24.Sampaziotis, F., et al., Cholangiocyte organoids can repair bile ducts after transplantation in the human liver. Science, 2021. 371(6531): p. 839–846.

25.Katsuda, T., et al., Conversion of Terminally Committed Hepatocytes to Culturable Bipotent Progenitor Cells with Regenerative Capacity. Cell Stem Cell, 2017. 20(1): p. 41–55.

26.Katsuda, T., et al., Generation of human hepatic progenitor cells with regenerative and metabolic capacities from primary hepatocytes. Elife, 2019. 8.

27.Kim, Y., et al., Small molecule-mediated reprogramming of human hepatocytes into bipotent progenitor cells. Journal of Hepatology, 2019. 70(1): p. 97–107.

28.Sakai, Y., et al., Vascularized subcutaneous human liver tissue from engineered hepatocyte/fibroblast sheets in mice. Biomaterials, 2015. 65: p. 66–75.

29.Huang, Y., et al., Bioengineering of a CLiP-derived tubular biliary-duct-like structure for bile transport in vitro. Biotechnol Bioeng, 2021. 118(7): p. 2572–2584.

30.Tanimizu, N., A. Miyajima, and K.E. Mostov, Liver Progenitor Cells Develop Cholangiocyte-Type Epithelial Polarity in Three-dimensional Culture. Molecular Biology of the Cell, 2007. 18(4): p. 1472–1479.

31.Anzai, K., et al., Foetal hepatic progenitor cells assume a cholangiocytic cell phenotype during two-dimensional pre-culture. Scientific Reports, 2016. 6(1): p. 28283.

32.Singh, A., et al., Adhesion strength-based, label-free isolation of human pluripotent stem cells. Nature Methods, 2013. 10(5): p. 438-444.
33.Miyoshi, T., et al., Successful induction of human chemically induced liver progenitors with small molecules from damaged liver. Journal of Gastroenterology, 2022. 57(6): p. 441-452.
34.Gigliozzi, A., et al., Molecular identification and functional characterization of Mdr1a in rat cholangiocytes. Gastroenterology, 2000. 119(4): p. 1113-1122.
35.Webb, M., et al., The detection of rhodamine 123 efflux at low levels of drug resistance. British Journal of Haematology, 1996. 93(3): p. 650-655.
36.Forster, S., et al., Characterization of Rhodamine-123 as a Tracer Dye for Use In In vitro Drug Transport Assays. PLOS ONE, 2012. 7(3): p. e33253.
37.Hirsch-Ernst, K.I., et al., Inhibitors of mdr1-dependent transport activity delay accumulation of the mdr1 substrate rhodamine 123 in primary rat hepatocyte cultures. Toxicology, 2001. 167(1): p. 47-57.
38.de Waart, D.R., et al., Hepatic Transport Mechanisms of Cholyl-l-Lysyl-Fluorescein. Journal of Pharmacology and Experimental Therapeutics, 2010. 334(1): p. 78.
39.Milkiewicz, P., et al., Plasma elimination of cholyl-lysyl-fluorescein (CLF): a pilot study in patients with liver cirrhosis. Liver, 2000. 20(4): p. 330-4.
40.Huang, Y., et al., Differentiation of chemically induced liver progenitor cells to cholangiocytes: Investigation of the optimal conditions. J Biosci Bioeng, 2020. 130(5): p. 545-552.
41.Guan, J., et al., Chemical reprogramming of human somatic cells to pluripotent stem cells. Nature, 2022. 605(7909): p. 325-331.
42.Hou, X., et al., Chemically defined and small molecules-based generation of sinoatrial node-like cells. Stem Cell Res Ther, 2022. 13(1): p. 158.
43.Pan, T., et al., Efficiently generate functional hepatic cells from human pluripotent stem cells by complete small-molecule strategy. Stem Cell Res Ther, 2022. 13(1): p. 159.
44.Knyazer, A., et al., Small molecules for cell reprogramming: a systems biology analysis. Aging (Albany NY), 2021. 13(24): p. 25739-25762.

Backgrounds:
The integrity of liver cell function depends on the integrity of the total triad. Portal triads are composed of three major tubes. Branches of the hepatic artery carry oxygenated blood to the hepatocytes, while branches of the portal vein carry blood with nutrients from the small intestine. The bile duct carries bile products away from the hepatocytes to the larger ducts and gall bladder. Therefore, it is necessary to form the structure including the material supply and metabolic waste discharge in regenerative liver tissue so that the hepatic tissue can maintain completed hepatic function for a long term. Herein, we have been able to successfully use rat CLiPs (a small chemical-induced liver progenitor cells developed by Dr. Katsuda) to induce 3D bile duct structure. If we want to form human liver tissue including bile duct and vascular, we have to establish the human 3D bile duct, but we have not yet completed the differentiation of human CLiPs into 3D bile duct structure. Therefore, we need to use human CLIP to induce 3D bile duct.
Purpose:
To form the three-dimensional bile duct structure and integrated duct-hepatocyte tissue from human CLiPs.
Method:
1.Human CLIPs were induced to form 3D bile duct structure in 3D culture system: MEF cell as feeder cell and Matrigel provides with 3D environment.
2.BIM (bile duct induced medium) combinate with growth factors (HGF and EGF) would be investigated.
Result:
1.Phase image and RT-qPCR showed that the FAC can successfully induce cryohepatocytes to human CLiPs.
2.Inducing human CLiPs to cholangiocytes and formation of the 3D bile duct structures：the combination of MEF feeder cells and Matrigel can induce the human CLiPs to cholangiocytes and form some 3D bile duct structure, which had positive expressions of biliary genes and concentration of Rhodamine123 in BIM medium with HGF.
3.The BIM+HGF had higher efficiency for the formation of the bile duct from hCLiPs compared with the other conditions.
4.The integrated bile-hepatocyte tissue expressed the bile acid transporter proteins and accumulated CLF into biliary lumen from the culture medium via hepatocytes canaliculi.
Summary:
we formed the functional bile duct from hCLiPs induced from hMHs by molecules combination with FBS. These hCLiPs expressed typical HPCs markers EpCAM, KRT-19, SOX-9, CD133 and gradually downregulated hMHs markers ALB, CYP7A1, and HNF4A during induction. These purified hCLiPs were then used to induce the generation of a 3D bile duct-like structure with lumens in a 3D culture environment with MEF. The bile duct expressed typical biliary epithelial cell markers CK-7, GGT1, CFTR and EpCAM and it had the ability to transport the bile-like substance rhodamine 123 into the lumen of the bile duct. Subsequently, bile ducts were co-cultured with hMHs for two days and bile salt analogues,CLF, were transported into bile duct and aggregate within the lumen from culture medium through the hMHs. The integrated tissue expressed the bile bile canaliculi marker and transporter protein.
Next step:
1.To finish and revise the manuscript and then submit.
2.Construction of a drug assay system combined with inhibitors.

2．執筆論文　Publication of thesis　※記載した論文を添付してください。Attach all of the papers listed below.

論文名 1 Title						
掲載誌名 Published journal						
	年　　　　月		巻（号）	頁　～　　　頁		言語 Language
第1著者名 First author		第2著者名 Second author		第3著者名 Third author		
その他著者名 Other authors						
論文名 2 Title						
掲載誌名 Published journal						
	年　　　　月		巻（号）	頁　～　　　頁		言語 Language
第1著者名 First author		第2著者名 Second author		第3著者名 Third author		
その他著者名 Other authors						
論文名 3 Title						
掲載誌名 Published journal						
	年　　　　月		巻（号）	頁　～　　　頁		言語 Language
第1著者名 First author		第2著者名 Second author		第3著者名 Third author		
その他著者名 Other authors						
論文名 4 Title						
掲載誌名 Published journal						
	年　　　　月		巻（号）	頁　～　　　頁		言語 Language
第1著者名 First author		第2著者名 Second author		第3著者名 Third author		
その他著者名 Other authors						
論文名 5 Title						
掲載誌名 Published journal						
	年　　　　月		巻（号）	頁　～　　　頁		言語 Language
第1著者名 First author		第2著者名 Second author		第3著者名 Third author		
その他著者名 Other authors						

3．学会発表 Conference presentation ※筆頭演者として総会・国際学会を含む主な学会で発表したものを記載してくだ

※Describe your presentation as the principal presenter in major academic meetings including general meetings or international me

学会名 Conference	The 67th Annual Congress of International College of Surgeons Japan Section					
演　題 Topic	An animal model of methotrexate-induced acute intestinal mucositis for drug therapy research					
開催日 date	2022　　年　　6　　月　　4　　日	開催地 venue	千葉県千葉市			
形式　method	☑　口頭発表 Oral　　□　ポスター発表 Poster	言語 Language	□　日本語　☑　英語　　□　中国語			
共同演者名 Co-presenter	Peilin Li, Inoue Yusuke, Masaaki Hidaka, Akihiko Soyama, Takanobu Hara, Takayuki Tanaka, Kengo Kanetaka, Susumu Eguchi					
学会名 Conference						
演　題 Topic						
開催日 date	年　　　月　　　日	開催地 venue				
形式　method	□　口頭発表 Oral　　□　ポスター発表 Poster	言語 Language	□　日本語　□　英語　　□　中国語			
共同演者名 Co-presenter						
学会名 Conference						
演　題 Topic						
開催日 date	年　　　月　　　日	開催地 venue				
形式　method	□　口頭発表 Oral　　□　ポスター発表 Poster	言語 Language	□　日本語　□　英語　　□　中国語			
共同演者名 Co-presenter						
学会名 Conference						
演　題 Topic						
開催日 date	年　　　月　　　日	開催地 venue				
形式　method	□　口頭発表 Oral　　□　ポスター発表 Poster	言語 Language	□　日本語　□　英語　　□　中国語			
共同演者名 Co-presenter						

4．受賞（研究業績）Award（Research achievement）

名　称 Award name						
	国名 Country		受賞年 Year of		年	月
名　称 Award name						
	国名 Country		受賞年 Year of		年	月

5．本研究テーマに関わる他の研究助成金受給 Other research grants concerned with your research theme

受給実績 Receipt record	□ 有　　■ 無
助成機関名称 Funding agency	
助成金名称 Grant name	
受給期間 Supported period	年　　　　月 ～ 　　　　年　　　　月
受給額 Amount received	円
受給実績 Receipt record	□ 有　　■ 無
助成機関名称 Funding agency	
助成金名称 Grant name	
受給期間 Supported period	年　　　　月 ～ 　　　　年　　　　月
受給額 Amount received	円

6．他の奨学金受給 Another awarded scholarship

受給実績 Receipt record	□ 有　　■ 無
助成機関名称 Funding agency	
奨学金名称 Scholarship name	
受給期間 Supported period	年　　　　月 ～ 　　　　年　　　　月
受給額 Amount received	円

7．研究活動に関する報道発表 Press release concerned with your research activities

※記載した記事を添付してください。Attach a copy of the article described below

報道発表 Press release	□ 有　　■ 無	発表年月日 Date of release	
発表機関 Released medium			
発表形式 Release method	・新聞　・雑誌　・Web site　・記者発表　・その他（　　　　　　　　　　　　　）		
発表タイトル Released title			

8．本研究テーマに関する特許出願予定 Patent application concerned with your research theme

出願予定 Scheduled	□ 有　　■ 無	出願国 Application	
出願内容（概要） Application contents			

9．その他 Others

指導責任者（記名）江口　晋